

DISCOVERY AND DESIGN OF NOVEL 20S PROTEASOME ACTIVATORS FOR
TARGETED PROTEIN DEGRADATION AND THEIR EVALUATION IN
NEURODEGENERATION MODELS

By

Sophia Dorothea Staerz

A DISSERTATION

Submitted to
Michigan State University
in partial fulfillment of the requirement
for the degree of

Chemistry-Doctor of Philosophy
Pharmacology and Toxicology-Dual Major

2024

ABSTRACT

In cells, proteostasis is a constant and highly choreographed process that maintains a balance between the synthesis and degradation of proteins. The ubiquitin-proteasome system is a critical player in this orchestration through both ubiquitin-dependent and ubiquitin-independent pathways. The former pathway is mainly responsible for the degradation of folded proteins, or proteins with a stable 3D conformation, by using ubiquitin tags to flag proteins for degradation. Conversely, the ubiquitin-independent pathway targets proteins that lack stable 3D conformations, including intrinsically disordered proteins (IDPs). Proteostasis can become perturbed when the synthesis of proteins outpaces their degradation, leading to the accumulation of proteins within a cell. IDP accumulation is linked to various disorders, including neurodegenerative diseases. The small molecule enhancement of the ubiquitin-independent pathway represents a promising therapeutic target to modify protein degradation pathways for treating human diseases. The chemical space of small molecule proteasome enhancers is small, with only a few promising candidates. A significant reason for this lack of progress is the need for cellular systems that easily evaluate levels of IDPs and efficiently screen candidate compounds on a large scale. Two of the projects described in this dissertation directly address these problems. My first project focused on the development of a cell-based high throughput assay and its utilization to screen 30,000 compounds to identify novel small molecule proteasome enhancers. The second project focused on designing and synthesizing a library of 32 small molecules that enhance the ubiquitin-independent proteasomal pathway. Herein, the utilization of *in silico* molecular docking studies to refine structure-activity relationships is discussed. This approach led to the identification

and synthesis of a new small molecule class that includes some of the most potent enhancers of the ubiquitin-independent pathway. In parallel, cellular disease models were developed that allowed for scoring the small molecules' therapeutic potential in treating waste protein accumulation in neurogenerative diseases.

For Erika, thank you for all your help and guidance! For Oma Irene, I have missed you immensely.

ACKNOWLEDGEMENTS

It is bewildering to me that I am at the end of my Ph.D. journey. A journey that would not have been possible without the aid and support of numerous people. First, I would like to thank Prof. Jetze Tepe, who has supported me in many ways throughout my Ph.D. The past few months have been daunting, but you were constantly there to remind me that life will work itself out and that the right fit for my next step will come along. Although I did not want to believe you then, I will begrudgingly admit you were right. Thank you for fostering my curiosity and creativity while training me to show restraint and keep a critical mind. You allowed me to explore my ideas, which gave me the confidence to pursue more complex problems. I will forever remember the lessons you taught me and am extraordinarily thankful I had the privilege to be a member of your group. I would also like to thank Dr. Bollivar, my undergraduate mentor. You were the one who gave me the confidence to pursue a Ph.D., and many of the things you taught me, both in and out of the lab, are things I still rely on today. I cannot thank you enough for your support. In addition to Dr. Bollivar, I want to thank my IWU Spartan teammates: Rachel, Emily, Hanna, Cassie, Shannon, Rachel, and Alyssa. You all are the best lifelong friends I could have ever asked for!

Next, I would like to thank my committee: Dr. Borhan, Dr. Draths, Dr. Wulff, and Dr. Fink. You all have impacted my time here at MSU in a beneficial way. Whether it was through guiding me during my second-year seminar, writing recommendation letters, allowing me to use equipment, or calming me down as I had a meltdown during the IPSPT *in vivo* boot camp, I would not have been able to finish this journey without you. I would also like to thank Dr. Dorrance and Dr. Neubig, as well as the other members of the pharmacology

department. I was nervous about joining another department farther into my Ph.D. career. However, you all welcomed me immediately and became a place of comfort for me.

Much of my time in the pharmacology department was spent with Dr. Erika Lisabeth. I can't truly express my immense gratitude for Erika. You became a second mentor, a friend, and a role model all in one! I would not have survived the AlphaLISA project without you. You taught me to be kind to everyone but remain firm in my ideas and values. You taught me to trust my gut but to not be afraid to ask for help. Finally, you taught me to speak up; my ideas will never be heard if I never share them.

To my mom, dad, and Anna, I am fortunate to have you all as my family. Each of you constantly support me and remind me to work hard and persevere. In a similar vein, I want to thank you, Jake, for putting up with my anxiety and my moodiness. I am also so proud of everything you have accomplished! Speaking of putting up with me, I want to express my eternal gratitude to Allison, Maggie, and Natalie. Allison, you are my terror twin, and I am so happy that we lived up to that name. Through your support and advice, you have been instrumental in any success I have had in my PhD. I can only fathom getting through this with you. I am so lucky to have you in my life and for a life filled with adventure and laughter. Maggie, you are one of the most incredible people I know. You have been there for some of the most challenging points of my life, and your baked goods have brought light to many dark periods. Natalie, I know that no matter what happened, I could always call or text you. You have supported me in everything I have done and reminded me to keep pushing forward.

To Grace and Katarina, I am privileged to call you two friends. Both of you have taught me so much and have become an inspiration to me. Taylor, thank you for all the existential

and pep talks and always being down to do something fun! Even if it means driving to Kalamazoo for an Oktoberfest! I also want to extend a special thanks to Charles. You have quickly become a good friend; I am incredibly grateful. A heartfelt thank you to the current Tepe group: Shannon, Sydney, Dare, Miracle, Konika, Evan, Kyra, Bahar, and Daniel. You have all helped me in so many ways. Thank you for always listening to another presentation or indulging in some of Allison I's wilder ideas, like group Halloween costumes. In addition, I thank Sydney for all your help with editing my papers and this dissertation. You have taught me so much! Finally, this should not come as a shock to anyone who knows me. I want to thank my cats; they have been the best companions I could ask for. Special shout out to Osmium.

TABLE OF CONTENTS

LIST OF ABBREVIATIONS.....	ix
CHAPTER ONE The Responsibility of the Proteasome in Maintaining the Proteostasis Network and Opportunity for a novel Neurodegenerative Disease Therapeutic Pathway.....	1
1.1 Proteostasis.....	2
1.2 Ubiquitin-Proteasome System.....	9
1.3 Proteasome Dysfunction in Human Pathology.....	18
1.4 Exogenous 20S Proteasome Enhancers.....	23
REFERENCES.....	30
CHAPTER TWO Design, Development, and Biological Evaluation of Novel Chlorpromazine Analogs as 20S Proteasome Enhancers.....	51
2.1 Introduction.....	52
2.2 Series I Chlorpromazine Analogs.....	55
2.3 Series II Chlorpromazine Analogs.....	61
2.4 Series III Chlorpromazine analogs.....	74
2.5 Conclusion.....	91
REFERENCES.....	93
APPENDIX.....	99
CHAPTER THREE Development of Cellular Models Recapitulating Proteasomal Impairment Seen in Synucleinopathies.....	206
3.1 Introduction.....	207
3.2 Proteasomal Impairment Induced by p25 α / α -synuclein Aggregates.....	209
3.3 Proteasomal Impairment Model Through Interruption of 20S Assembly ..	223
3.4 Conclusion.....	235
REFERENCES.....	236
APPENDIX.....	245
CHAPTER FOUR Development and Utilization of the First Cell-Based High-Throughput Screen for 20S Proteasome Enhancers.....	262
4.1 Introduction.....	263
4.2 Development and Utilization of AlphaLISA Based High-Throughput Screen.....	265
4.3 Screening of 25,000 Compounds.....	282
4.4 Conclusion.....	287
REFERENCES.....	289
APPENDIX.....	292
CHAPTER FIVE Materials and Miscellaneous.....	300
5.1 Materials.....	301
5.2 Miscellaneous.....	307

LIST OF ABBREVIATIONS

3D	3 Dimensional
4 Å MS	Molecular Sieves
AcOH	Acetic Acid
AD	Alzheimer' Disease
ALP	Autophagy Lysosome Pathway
AlphaLISA	Amplified Luminescent Proximity Homogeneous Assay Linked Immunosorbent Assay
ALS	Amyotrophic Lateral Sclerosis
AMC	Amino Methyl Coumarin
APCI	Atmospheric-Pressure Chemical Ionization
ATF6	Activating Transcription Factor 6
ATP	Adenosine Triphosphate
BCA	Bicinchoninic Acid Assay
Boc-LRR-AMC	Tert-Butoxyl-Leucyl-Arginyl-Arginyl-7-Amino-4- Methylcoumarin
BTZ	Bortezomib
Calc'd	Calculated
CHX	Cycloheximide
C-L	Caspase-Like
CNS	Central Nervous System
CPZ	Chlorpromazine
CT-L	Chymotrypsin-Like
D2R	Dopamine 2 Receptor
DCM	Dichloromethane
DLB	Dementia with Lewy Bodies
DMEM	Dulbecco's Modified Eagle Medium

DMF	Dimethylformamide
DMSO	Dimethyl Sulfoxide
DPR	Dipeptide Repeat
DTE	Dithioerythritol
DTT	Dithiothreitol
DUB	Deubiquitinating Enzyme
EC200	200% Effective Concentration
ECL	Enhanced Chemiluminescence
EDTA	Ethylenediaminetetraacetic Acid
EGFR	Epidermal Growth Factor
Equiv.	Equivalent
ER	Endoplasmic Reticulum
ERAD	Endoplasmic Reticulum Associated Protein Degradation
EtOH	Ethanol
FBS	Fetal Bovine Serum
FDA	Food and Drug Administration
FRET	Fluorescence Resonance Energy Transfer
GCI	Glial Cytoplasmic Inclusions
GFP	Green Fluorescent Protein
h	Hour
HbYX	Hydrophobic- Tyrosine- Any Amino Acid
HEK	Human Embryonic Kidney
HEPES	4-(2-Hydroxyethyl)-1-Piperazineethanesulfonic Acid
HRMS	High Resolution Mass Spectrometry
HSR	Heat-Shock Response
IC50	Concentration with 50% Inhibition

IDPs	Intrinsically Disordered Protein
eIF2 α	Initiator Factor 2 α
IRE1	Inositol-Requiring Enzyme 1
Min.	Minute
MSA	Multiple System Atrophy
NAC	Non- β -amyloid Component
NIH	National Institutes of Health
NQO1/NQO2	NAD(P)H Quinone Dehydrogenase 1/2
ODC	Ornithine Decarboxylase
PAGE	Poly Acrylamide Gel Electrophoresis
PBS	Phosphate-Buffered Saline
PC12	Pheochromocytoma Cells of the Rat Adrenal Medulla
PD	Parkinson's Disease
PERK	Unfolded Protein Response
PEST	Proline (P)-Gluatamic Acid (E)-Serine (S)-Threonine (T)
PFFs	Prefomed Fibrils
PROTACs	PROteolysis-Targeting Chimeras
PVDF	Polyvinylidene Difluoride
RIDD	Regulated by IRE1 Dependent Decay
RIPA	Radioimmunoprecipitation Assay
ROS	Reactive Oxygen Species
Rpn	Non-ATPase Regulatory Particle
Rpt	ATPase Regulatory Particle
rt	Room Temperature
SAR	Structure Activity Relationship
SD	Standard Deviation

SDS	Sodium Dodecyl Sulfate
Suc-LLVY-AMC	Succinyl-Leucyl-Leucyl-Valyl-Tyrosyl-7-Amido-4-Methylcoumarin
TEA	Triethylamine
THF	Tetrahydrofuran
T-L	Trypsin-Like
TPPP	Tubulin Polymerization Promoting Protein
UPR	Unfolded Protein Response
UPS	Ubiquitin Proteasome System
WT	Wild Type
Z-LLE-AMC	Carboxylbenzyl-Leucyl-Leucyl-Glutamyl-7-Amido-4-Methylcoumarin

CHAPTER ONE

The Responsibility of the Proteasome in Maintaining the Proteostasis Network and Opportunity for a Novel Neurodegenerative Disease Therapeutic Pathway

1.1 Proteostasis

1.1.1 Proteostasis Network

Proteins are the most adaptable type of macromolecules and allow for the occurrence of a cell's incredibly complex inner workings. The intricacy of the protein composition, termed the proteome, in a cell is dependent on the cell's overall function and location.¹

The integrity of a cell's proteome is maintained through proteostasis, which is a highly orchestrated balance between protein synthesis, folding, and degradation.^{2, 3}

Proteostasis is achieved through the cross-coordination of various cellular pathways, collectively called the proteostasis network.⁴ The proteostasis network includes translational protein complexes,² molecular chaperones,⁵ the ubiquitin-proteasome system (UPS),³ and the autophagy pathways (**Figure 1.1**).⁶ Furthermore, several peripheral signaling pathways modulate the proteostasis network's activity, including the unfolded protein response (UPR),⁷ the heat-shock response (HSR),⁸ and inflammatory pathways.⁹ The overarching responsibility of the proteostasis network is two-fold.^{2, 4} The proteostasis network ensures that properly folded proteins are generated, maintained, and trafficked to the correct cellular location to carry out the protein's intended function. Secondly, the proteostasis network prevents the accumulation of misfolded or superfluous proteins through the appropriate degradation pathways.^{2, 4} However, the efficiency of the proteostasis network is perturbed through aging,² exposure to environmental stress,¹⁰ or diminished capacity of one or more of the involved cellular pathways, i.e., proteasomal dysfunction.^{3, 11} The critical role of the proteostasis network in both cell health and, inversely, pathogenesis has led to the development of therapeutics that target the various pathways involved in the proteostasis network.

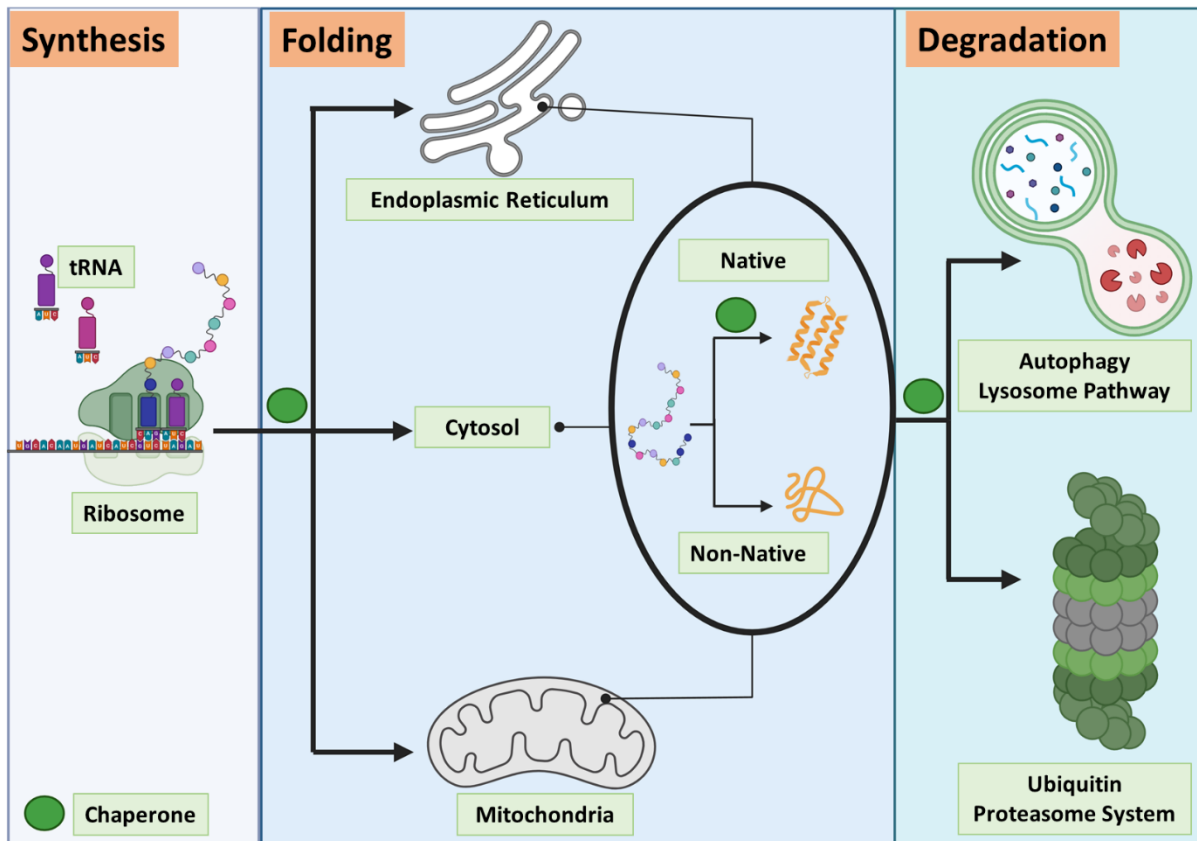


Figure 1.1: The components and flow of the proteostasis network. *Created with BioRender

1.1.2 Protein Synthesis and Folding

The proteome of eukaryotic cells is highly complex and varies drastically between cell and tissue types, emphasizing the need for a tightly regulated process to control the expression and folding of new proteins. The process of synthesizing new proteins is a multi-step journey that begins in the nucleus of a cell, where mRNA is produced.¹² The mRNA, or messenger RNA, contains the genetic instructions for the creation of a specific protein.¹² The mature mRNA will leave the nucleus and interact with a complex known as the ribosome. Once the mRNA interacts with the ribosome, a process called translation will occur,¹³ creating a *de novo* polypeptide. Ribosomes are mainly located in the cytosol,

the mitochondria, and bound to the membrane of the ER.¹³ Ribosomes, called mitoribosomes, exist in the mitochondria, which are required for the expression of the genes encoded in the mitochondria's reduced genome.^{14, 15, 16, 17} In contrast, the rationale for ribosomes tethered to the membrane of the ER is not as straightforward. The ER is responsible for the protein synthesis and folding of secreted and integral membrane proteins, as well as a subpopulation of cytosolic proteins.^{18, 19} A short gene sequence on specific mRNA acts as an address tag for the delivery of the mRNA to ribosomes that are bound to the ER membrane.^{20, 21} Once the mRNA is delivered to the ER bound ribosome, a complex recognizes the tag and slows the elongation of the *de novo* polypeptide until a new proteinaceous channel is formed in the ER membrane.^{22, 23} The newly constructed channel allows the freshly synthesized polypeptide to enter into the ER to be folded directly.²¹

Typically, newly synthesized proteins adopt a defined 3D conformation tuned to the intended biological functions.^{24, 25, 26, 27} However, a class of proteins called intrinsically disordered proteins (IDPs) are an exception to this observation. IDPs lack a stable 3D conformation and only acquire a tertiary structure when interacting with partner molecules, allowing for a range of diverse biological activities.^{28, 29, 30, 31} The ultimate conformation that proteins reside in is typically the most thermodynamically favored one, termed the native state.^{2, 5, 32} Due to the breadth of possible conformations a polypeptide can adopt, the mechanism of protein folding reactions is exceedingly complex and heterogeneous. These reactions rely on the cooperation of several weak and noncovalent interactions.^{25, 33, 34} For example, hydrophobic forces are necessary to drive the

polypeptide chain's collapse to hide nonpolar amino acid residues within the folds.^{25, 33, 34, 35}

To facilitate the formation of the native state of the freshly synthesized polypeptides, a network of molecular chaperones promotes folding through ATP-dependent^{36, 37} and independent protein binding (**Figure 1.2**).^{38, 39} Molecular chaperones are defined as any protein that interacts with, stabilizes, or aids *de novo* polypeptides in acquiring a functionally active conformation while absent in the new proteins final structure (**Figure 1.2**).^{40, 41} Due to the scope of responsibilities of molecular chaperones, this class of proteins consists of structurally unrelated proteins that form cooperative networks.^{42, 43, 44} A large subset of molecular chaperones are called heat-shock proteins (HSP) due to the upregulated expression of these proteins under stress conditions.^{5, 45} In addition to aiding in the cytosolic folding of *de novo* polypeptides, molecular chaperones assist in their transportation to appropriate subcellular compartments before folding.^{46, 47, 48} However, if the *de novo* polypeptides are not intercepted by molecular chaperones, polypeptide chains can rapidly misfold, forming non-native structures.

Furthermore, the misfolded polypeptide chains can form aggregates through intramolecular interactions. To combat misfolded protein aggregates, molecular chaperones also participate in disaggregating and reactivating the non-natively folded polypeptide chains (**Figure 1.2**). However, if the molecular chaperones cannot successfully disaggregate the misfolded proteins, protein degradation pathways are recruited.

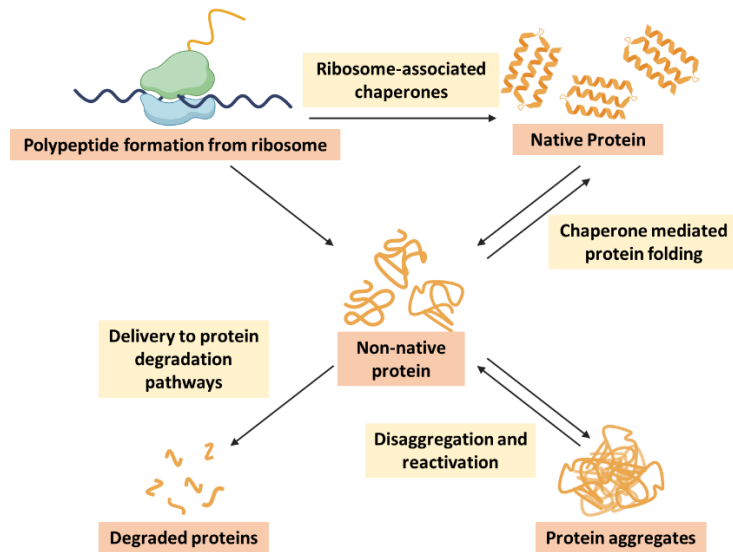


Figure 1.2: Molecular chaperones are responsible for binding and aiding in the formation of native structure of *de novo* poly peptide chains.

De novo polypeptide chains emerge from the ribosome, where they can interact with molecular chaperones to aid in the formation of their native protein structure. These polypeptide chains can also form a non-native conformation, leading to intra-molecular interactions and the formation of protein aggregates. Molecular chaperones can work to disaggregate and reactivate the aggregates, ultimately forming the native conformation of the protein. However, if the level of non-native proteins exhausts the concentration of molecular chaperones, the degradation of the non-native proteins is signaled. *Created with BioRender

1.1.3 Protein Degradation

In parallel to controlled protein synthesis, regulated degradation of redundant, damaged, and aggregated proteins is vital.^{49, 50} The degradation of proteins is not only necessary

for their destruction but also acts as a recycling process, with the resulting peptide fragments reutilized in the synthesis of new proteins or to carry on as additional signaling components.^{51, 52, 53} The synthesis and degradation of various proteins depend on different stimuli and cellular conditions with the flexibility to quickly alter the proteome landscape.^{54, 55} Like the protein synthesis pathways, proteolytic systems depend on molecular chaperones. Damaged or redundant proteins are recognized by molecular chaperones, resulting in either the refolding of damaged proteins or the facilitation of their delivery to protein degradation machinery.^{56, 57, 58} Eukaryotic cells depend on two main degradation pathways: the ubiquitin-proteasome system (UPS) and the autophagy lysosomal pathway (ALP). Initially, the UPS and ALP were thought to degrade proteins through unspecific bulk recycling.⁵⁹ However, it is now understood that the degradation of proteins through the UPS and ALP is highly regulated, and both systems are responsible for removing different categories of proteins.^{60, 61} For example, the size of the substrate significantly influences which pathway is responsible for its degradation.^{59, 62} The UPS is the primary degradation route for short-lived, misfolded, and damaged proteins.^{60, 50} The activity of the UPS is essential for regulating numerous cellular functions, such as cell signaling, cell cycle progression, and proliferation.⁶³ The central degradation machinery in the UPS is the 26S proteasome.⁶⁰ The mechanism of protein degradation and the structure of the proteasome is detailed in **section 1.2**. In contrast, the ALP removes large cellular components, such as protein aggregates and damaged organelles.⁶⁴ The degradation ability of the ALP is dependent on the formation of the autolysosome.^{64, 65} The formation of the autolysosome and subsequent protein degradation can be summarized in several steps: initiation of the pre-autophagosomal

membrane, nucleation of the membrane, elongation of the phagophore, maturation of the autophagosome, fusion of the autophagolysosome, and degradation of the protein through the autolysosome (**Figure 1.3**).⁶⁴ The formation of the autophagosome will encapsulate the protein targeted for degradation. The autophagosome fusion to the lysosome will introduce the targeted proteins to proteolytic enzymes called cathepsins, which are responsible for the majority of protein degradation within the autolysosomes.⁶⁶ The UPS and ALP are vital for cell health and act as the final line of defense against cytotoxicity caused by proteostasis imbalance, called proteotoxicity. While both degradation pathways are linked to the pathogenesis of human disease and are central to developing novel therapeutic pathways, the connection between human pathogenesis and UPS will be the focus hereafter. Furthermore, the modulation of the UPS as a novel therapeutic pathway will be detailed.

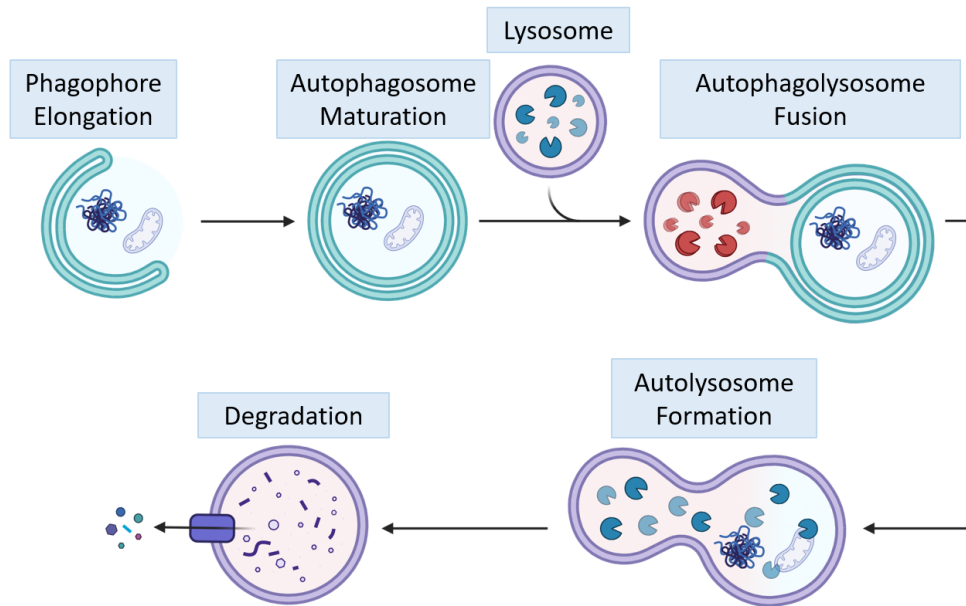


Figure 1.3: The steps of protein degradation through the ALP. *Created with BioRender

1.2 Ubiquitin-Proteasome System

1.2.1 Proteasome Structure and Assembly

In 1980, a 700-kDa multi-catalytic proteinase complex was isolated that proteolytically cleaved proteins after their hydrophobic, basic, and acidic residues. The multi-catalytic activity of the proteinase complex suggested that the protein might contain multiple catalytic sites with distinct activities.^{67, 68, 69, 70} In the late 1980s, electron micrographs illuminated the stacked ring conformation of the 700 kDa complex⁷¹ and termed the 20S proteasome shortly after.⁷² Eukaryotic 20S proteasomes contain four heptameric rings stacked together, with two α -rings sandwiching two β -rings.^{19-20, 23-24} The α -rings control a 13Å gated pore, with an amino termini tail from each subunit interlacing to form the

“gate.”⁷³ The gated pore regulates the access of protein substrates to the proteolytic sites housed in the β -rings.^{73, 74}

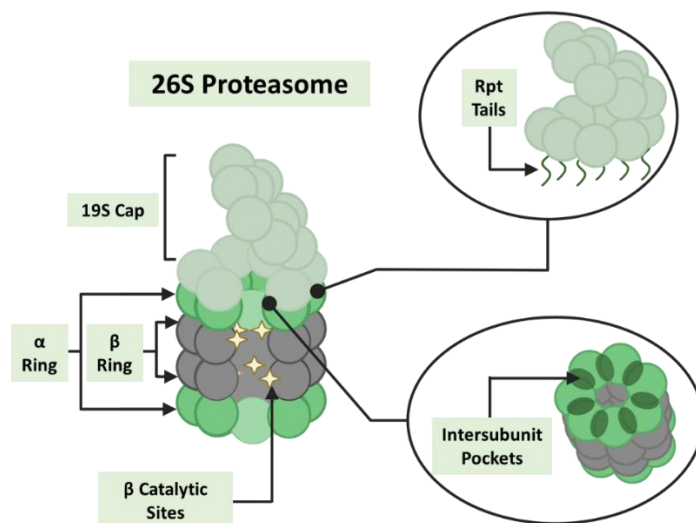


Figure 1.4: A schematic of the 26S proteasome and its components. *Created with BioRender

In total, there are six proteolytically active β -subunits (three in each β -ring) that contain a catalytic threonine residue: the $\beta 1$, $\beta 2$, and $\beta 5$. The three catalytic sites exhibit different protease activity: the $\beta 1$ exhibits caspase-like activity, cleaving after acidic residues, the $\beta 2$ cleaves after basic residues in a trypsin-like manner, and the $\beta 5$ preferentially cleaves after hydrophobic residues through chymotrypsin-like activity (**Figure 1.4**).

The assembly of the catalytic core that comprises the 20S proteasome begins with the formation of the α -ring.^{75, 76, 77, 78, 79} Two heterodimeric molecular chaperones, PAC1-PAC2 and PAC3-PAC4, mediate the formation of the α -ring.^{78, 77} The exact order of the addition of the α -subunits is under debate. However, evidence suggests that an $\alpha 4$ - $\alpha 5$ - $\alpha 6$ - $\alpha 7$ intermediates first form.^{77, 78, 80, 81, 82} Furthermore, it is hypothesized that $\alpha 4$ and $\alpha 7$ initially interact with one another through the N-termini tails that will later act as the

gate to the pore.⁸³ The mechanism of the addition of $\alpha 5$ and $\alpha 6$ is unknown. However, the two heterodimers, PAC1-PAC2 and PAC3-PAC4, will bind between the $\alpha 4$ and $\alpha 5$ subunits on the top and bottom faces of the α -ring intermediate, respectively (**Figure 1.5**).^{77, 78, 84} The PAC1-PAC2 heterodimer combats the formation of non-productive, or dead-end, complexes.^{78, 85} In contrast, the PAC3-PAC4 heterodimer is necessary for the prevention of aberrant dimerization of the α -ring intermediates.^{79, 85} The order of addition of the remaining α -subunits is elusive. However, the addition of the $\alpha 2$ and $\alpha 3$ subunits depends on the addition of the $\alpha 1$ subunit.⁷⁷ Interestingly, the silencing of the expression of $\alpha 3$ does not prevent the formation of the α -ring but leads to the construction of larger intermediates.^{79, 86} The $\alpha 4$ subunit, in the absence of $\alpha 3$, can insert twice into the α -ring, forming $\alpha 1$ - $\alpha 2$ - $\alpha 4$ - $\alpha 4$ - $\alpha 5$ - $\alpha 6$ - $\alpha 7$ ring, accounting for the larger intermediates identified (**Figure 1.5**).^{79, 86}

The α -ring serves as a scaffold for the formation of the β -rings. The catalytic β -subunits ($\beta 1$, $\beta 2$, and $\beta 5$) and two non-catalytic β -subunits ($\beta 6$ and $\beta 7$) are expressed with a pro-peptide on the N-terminal.^{87, 88, 89} The pro-peptide hides the catalytic threonine residue and will be cleaved during the final assembly step.^{87, 88} To ensure the β -subunits are correctly oriented, the N-termini of the β -subunits will be maintained in the inner portion of the newly forming ring, and the C-termini will remain on the outside.^{90, 91} Analogous to the formation of the α -rings, the establishment of the β -ring depends on a molecular chaperone called POMP, also known as hUMP1 or proteasemblin.^{90, 91} The $\beta 2$ subunit initiates the formation of the β -ring and adds to the α -ring with POMP, causing PAC3-PAC4 to leave the freshly assembled α -ring.^{92, 93} After POMP and $\beta 2$ are added to the α -ring intermediate, $\beta 3$ and $\beta 4$ are added, creating an intermediate called the 13S.^{91, 92, 94}

The addition of the β 1, β 5, and β 6 occurs to form the 15S intermediate.^{91, 92, 94} The insertion of the final β -subunit, β 7, triggers the dimerization of two 15S intermediates, yielding the 20S proteasome.^{91, 90} After the formation of the naïve 20S proteasome, the pro-peptides are autocatalytically cleaved, causing the degradation of POMP and the PAC1-PAC2 heterodimer, ultimately creating the mature 20S proteasome.^{90, 95, 96}

The mature 20S proteasome is the active isoform capable of proteolytically degrading unstructured proteins, accounting for 20% of the proteasome's total cellular targets.⁹⁷ However, the 20S proteasome is ineffective in the degradation of folded proteins due to the defined size of the pore opening, sterically occluding proteins from entering the catalytic barrel.⁷³ Upon activation of the 20S proteasome with native proteins or chemical agents,^{98, 99, 100, 101} the conformation of the N-terminal tails changes, inducing an open gated conformation.^{74, 102} However, structured proteins must be unfolded to be processed by the 20S proteasome β -catalytic sites.^{102, 103, 104} Both the activation of the 20S proteasome and the linearization of target proteins is achieved through the complexation with regulatory particles, such as the PA700/19S cap.^{104, 105} The 19S cap is comprised of nineteen proteins, with ten proteins serving as the "base" and nine proteins serving as the "lid."^{106, 107} The base of the 19S cap is responsible for interacting with pockets that are formed between the α -subunits on the top of the 20S proteasome. Six of the ten base proteins of the 19S cap are AAA-ATPases, called the Rpt tails (Rpt1-6), which directly bind to the α -rings intersubunit pockets.^{73, 108, 109} The Rpt tails possess a HbYX amino acid motif on the C-terminal.^{110, 111} The Hb represents hydrophobic, Y is the tyrosine residue, and X is any amino acid.^{110, 111} More insight into the HbYX motif has been gained recently.¹¹² The Gestwicki group identified that the amino acid residue before the Hb

amino acid was also crucial for inducing an open-gated conformation of the 20S proteasome, terming it the YFY motif.¹¹² Furthermore, the variable amino acid (X) was more specific than initially predicted, and an alanine or threonine residue in this location preferentially leads to the formation of the open-gated conformation.¹¹² The Rpt tails induce an open gated conformation of 20S proteasome and the AAA-ATPase activity of the Rpt tails disrupt the higher order structure of the folded protein substrate prior to their subsequent degradation through ATP hydrolysis.^{50, 113, 114} The remaining four proteins on the base of the 19S cap are termed “regulatory particle non-ATPases” (Rpn).^{113, 115, 116} The Rpn components of the 19S caps interact with numerous other proteins, including the 20S proteasome itself.^{116, 117} The final key role of the 19S cap is the recognition of proteins that are tagged with ubiquitin, which signal for their rapid degradation. The relationship between ubiquitin and proteasomal degradation is covered in the next subsection (1.2.3).

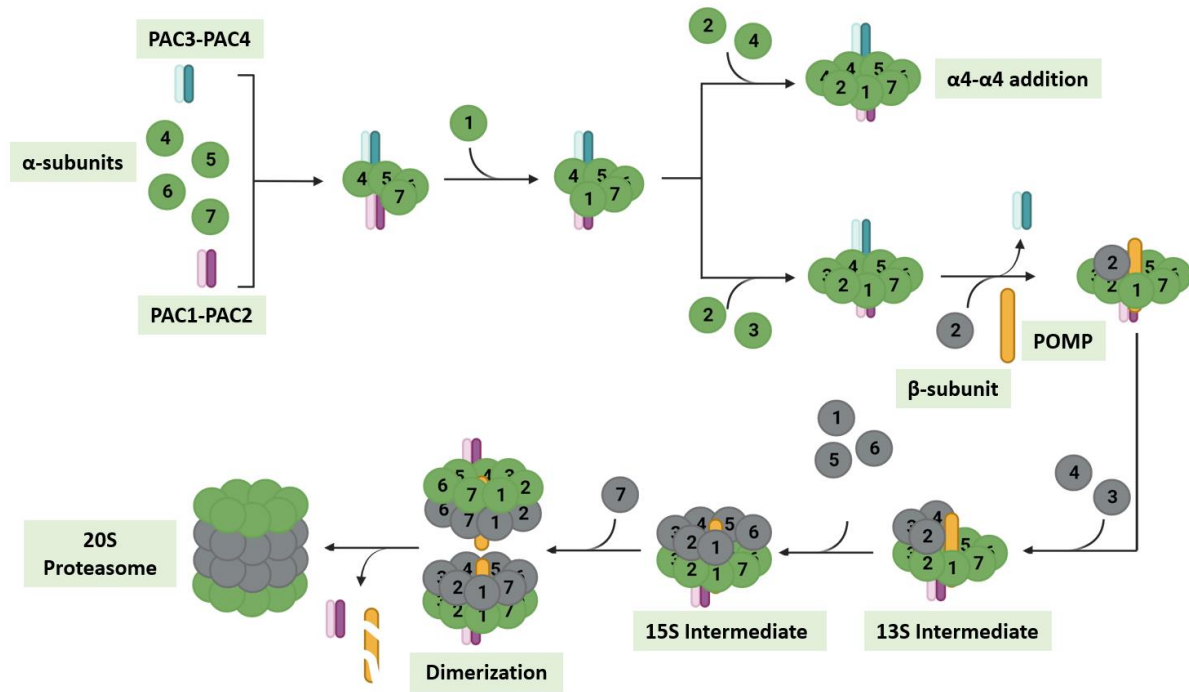


Figure 1.5: The assembly of the 20S proteasome. *Created with BioRender

1.2.2 Ubiquitin-Dependent Degradation

The UPS processes a spectrum of protein types in the cell; however, protein substrates degraded by the 26S proteasome must be tagged for degradation and contain an unstructured initiation region.^{103, 118} Ubiquitin is a small protein, 76 amino acids in length, and forms polyubiquitin chains which the Rpn subunits of 19S cap recognizes to initiate the degradation of protein substrates.^{119, 120, 121} Ubiquitin covalently attaches to a lysine on the protein substrate by forming an isopeptide bond.^{119, 120, 121} The polyubiquitin chain formation relies on ubiquitin's seven internal lysine residues (K6, K11, K27, K29, K33, K48, and K63). The fate of the protein substrate depends on the location of the lysine (K) attached to the polyubiquitin chain. The formation of a polyubiquitin chain on K48 is a canonical signal for proteasome-mediated degradation.^{122, 123} Thus, the buildup of

ubiquitin in the cell is a good indicator of the cell's proteostasis network's health, indicating the efficiency of the degradation pathways.

The attachment process of ubiquitin to the targeted protein involves three critical enzymes: the ubiquitin activating enzyme (E1), the ubiquitin conjugating enzyme (E2), and the ubiquitin ligase (E3). The E1 enzyme activates the ubiquitin protein through a two-step process: the initial formation of a ubiquitin-adenylate intermediate and the subsequent reaction with a E1 cysteine residue, forming a E1-ubiquitin thioester (**Figure 1.6**).^{124, 125, 126} Following the ubiquitin activation reaction, the ubiquitin conjugating enzyme (E2) is recruited. The activated ubiquitin protein is then transferred from E1 to a catalytic cysteine on E2 through transesterification (**Figure 1.6**).^{126, 127, 128} The final step is the addition of the ubiquitin to the specific protein substrate, mediated by E3 ligases. There is a plethora of E3 ligases (~600)¹²⁹ that are specific for certain protein substrates.^{130, 131} Depending on the E3 ligase, the ubiquitin is transferred to the substrate protein either directly from the E2 or following a thioester formation between the E3 ligase and ubiquitin (**Figure 1.6**).^{132, 133}

The ubiquitin addition to the protein substrate is repeated, forming a chain of 4 or more ubiquitin proteins. Rpn subunits of 19S cap first bind to proteins with the polyubiquitin chain through an ATP-dependent and reversible reaction.^{134, 135, 136} The protein substrate is then deubiquitinated by 26S proteasome associated enzymes, called deubiquitinating enzymes (DUBs).⁶³ Lastly, the 19S cap unfolds structured proteins through ATP-hydrolysis, before ultimately translocating the protein in the catalytic barrel of the 20S proteasome and subsequent proteolytic degradation.^{110, 114}

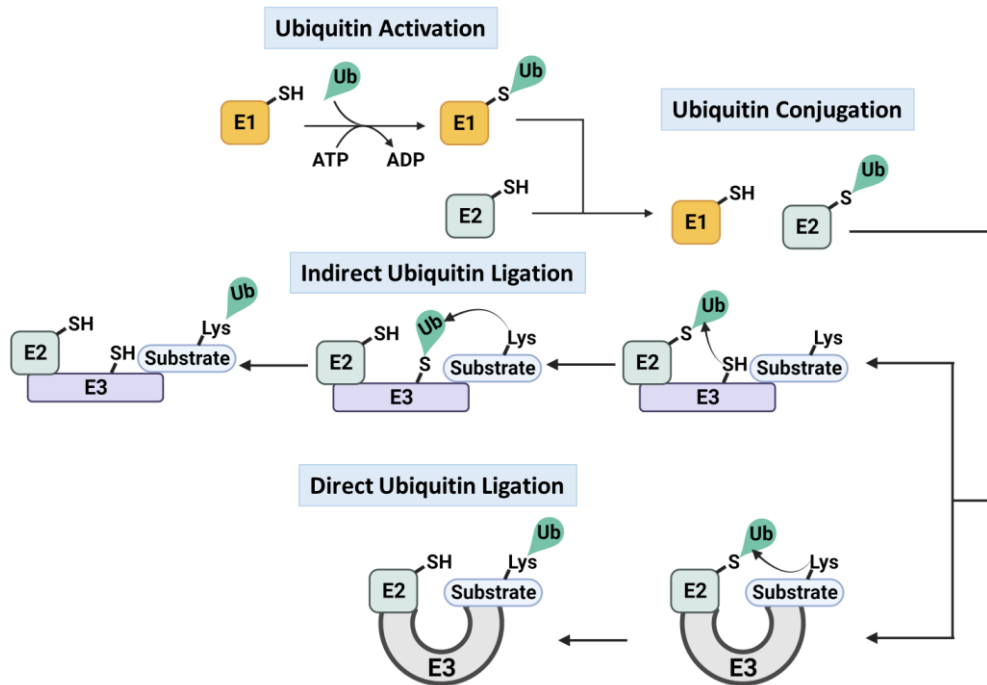


Figure 1.6: The ubiquitin processing cascade between E1, E2, and E3 enzymes.

*Created with BioRender

1.2.3 Ubiquitin-Independent Degradation

As discussed, the 20S proteasome is a vital component of the 26S proteasome complex and mediates the degradation of structured proteins that have been ubiquitinated and linearized before degradation. However, the stand-alone 20S proteasome can degrade proteins that lack a stable 3D conformation in a ubiquitin-independent manner.^{97, 137, 138, 139} Moreover, the 20S proteasome has been identified to degrade IDPs more efficiently than the 26S proteasome.^{97, 137, 138, 139} In addition, the analysis of nine human cell lines revealed that more than 50% of the identified proteasome exists as the 20S proteasome isoform and mediates the cleavage of more than 20% of all cellular proteins.^{97, 140} As mentioned in **section 1.1.1**, IDPs lack a stable 3D conformation, only retaining a folded structure through the interaction with binding partners.^{28, 29, 30, 31} The interaction between

IDPs and a binding partner has the potential to alter the route as to which the IDP is degraded.^{141, 142} A well-characterized example of differing degradation mechanism of the same protein is the degradation of the IDP, ornithine decarboxylase (ODC).¹⁴¹ ODC is a highly regulated enzyme in the biosynthesis pathway of polyamines, playing a critical role in cellular proliferation.^{143, 144} ODC has a high turnover rate in cells and can exist as an inactive monomer or as an active and structured homodimer.^{145, 146} Unlike other structured proteins, the homodimeric form of ODC is not degraded through a ubiquitin-dependent manner, rather an additional protein, termed an antizyme, interacts with one of the ODC dimers, creating a new heterodimer. The 26S proteasome then degrades the antizyme/ODC heterodimer in a ubiquitin-independent manner.^{146, 147, 148} However, it has been demonstrated that the intrinsically disordered monomeric form of ODC is degraded by the stand-alone 20S proteasome.^{99, 100, 149, 150}

The regulation of the 20S proteasome-mediated degradation heavily depends on confirmation of the gated pore opening. The 20S proteasome exists mainly in the closed-gated conformation, occluding protein substrates from entering the catalytic chamber.^{151, 152} However, the activity of the 20S proteasome can be enhanced or inhibited with the association of non-regulatory particle proteins.^{149, 153, 154, 155} For example, NAD(P)H quinone oxidoreductase 1 and 2 (NQO1 and NQO2) physically interact with the 20S proteasome, inducing an active conformation and modulating the degradation of IDPs, such as ODC.¹⁴⁹ Furthermore, the direct binding of the IDP, α -synuclein, to the α 7 subunit of the 20S proteasome has been demonstrated to induce its degradation.¹⁵⁶ Thus, the development of small molecules that directly interact with the intersubunit pockets of the

20S proteasome has the potential for creating a novel paradigm in the modulation of the proteostasis network.

1.3 Proteasome Dysfunction in Human Pathology

1.3.1 Aging and Oxidative Damage

As discussed, the maintenance of proteostasis relies on the synchronous activity of several cellular pathways and is contingent on the balance between protein synthesis and degradation. Protein damage is a natural and frequent occurrence in cellular organisms and occurs through various mechanisms.¹⁵⁷ One common mechanism of protein damage is by reactive oxygen species (ROS) generated during innate cellular processes, such as mitochondrial production of ATP,^{158, 159} and in response to xenobiotics,¹⁶⁰ cytokines,¹⁶¹ and infection.¹⁶² A buildup of ROS causes oxidative damage to proteins, often resulting in conformational alterations to the protein structures, rendering them inactive or functionally abnormal.^{163, 164, 165} Cellular degradation pathways are vital for efficiently clearing oxidatively damaged and misfolded proteins. The UPS represents the major proteolytic machinery for the removal of oxidatively damaged proteins.^{166, 167, 168, 169} In particular, the 20S proteasome is the critical proteasome isoform for removing oxidatively damaged and misfolded proteins due to its own resistance to oxidative damage.^{170, 171, 172} In response to oxidative stress, the 26S proteasome dissociates to increase the levels of the stand-alone 20S proteasome to combat the formation of oxidatively damaged proteins.^{173, 174} Furthermore, the 20S proteasome interacts with abnormally exposed hydrophobic patches of the misfolded proteins, inducing an active conformation of the 20S proteasome, enhancing the degradation rate of the misfolded proteins.¹⁶⁷ However,

there is a marked decline in the efficiency of the cellular machinery that aids in maintaining proteostasis as an organism ages, including the ubiquitin-proteasome system.

The diminished proteasome activity observed in aging organisms can occur through several mechanisms: decreased expression of proteasome subunits,^{175, 176} alteration or replacement of proteasome subunits,¹⁷⁷ disassembly of the proteasome,¹⁷⁸ and protein aggregates inducing proteasomal impairment.^{101, 179, 180} While any form of diminished proteasomal activity is detrimental, the protein aggregate-induced proteasomal impairment causes catastrophic feedback loops. The inhibition of the proteasome will allow for the further accumulation of misfolded and disordered proteins. The increasing concentration of the misfolded and damaged proteins can form new aggregates, further impairing the activity of the proteasome, propagating a noxious cycle.¹⁸¹ The impact of diminished proteasomal activity is especially pronounced in long-lived cells that divide slowly or not at all, such as neuronal cells. In addition, neuronal cells are exceptionally metabolically active, creating high ROS levels through ATP production in the mitochondria.^{182, 183, 184} The high ROS production and lowered proteasome activity result in catastrophic events, such as neuronal cell death. Thus, age-related neurodegenerative diseases are a prime example of proteostasis collapse, and the targeting of the UPS provides a promising therapeutic pathway.

1.3.2 Synucleinopathies

As alluded, as a person ages, the risk of developing a neurodegenerative disease steadily increases. Synucleinopathies are a pathologically heterogeneous class of neurodegenerative diseases unified by α -synuclein aggregates in neurons or glial cells.¹⁸⁵ α -synuclein aggregates observed in neuronal cells are termed Lewy bodies,

which are characteristic of either Parkinson's disease (PD) or dementia with Lewy bodies (DLB).^{186, 187} The existence of α -synuclein aggregates in the glial cells called oligodendrocytes are classified as glial cytoplasmic inclusions and are a key feature of multiple system atrophy (MSA).¹⁸⁸ As mentioned, α -synuclein is an IDP^{189, 190} (91% disordered via PONDR) and is a substrate of the 20S proteasome.¹⁹¹ The expression of α -synuclein, encoded by the SNCA gene,¹⁹² is highly localized in the presynaptic terminals of dopaminergic neurons.^{193, 194} The exact physiological role of α -synuclein remains undefined. Nevertheless, it is hypothesized to play a role in synaptic maintenance and release of neurotransmitters.^{195, 196}

Typically, α -synuclein exists as a monomer comprised of three distinct domains: the N-terminal lipid binding α -helix, non- β -amyloid component (NAC) central domain, and the C-terminal acidic tail (**Figure 1.7A**). The amphipathic N-terminal (residues 1-87) is a positively charged region that contains seven imperfect repeats, each containing a KTKEGV hexameric motif.^{197, 198} The core region of α -synuclein (residues 61-95) is heavily involved in the formation of α -synuclein aggregates and fibrils due to its propensity to form β -pleated sheets.^{199, 200} Lastly, the C-terminal of α -synuclein (residues 96-140) is an acidic tail, owing to the ten glutamine and five aspartic acid residues in this region.²⁰¹ Furthermore, the truncation of the C-terminal increases the potential for the aggregation of α -synuclein.²⁰²

Like the physiological function of α -synuclein, the exact role of α -synuclein in Parkinson's disease and other synucleinopathies is elusive. While most cases of PD are sporadic, mutations in the SNCA gene lead to the development of familial PD.²⁰³ In addition to whole gene multiplications,^{204, 205, 206} the A53T,²⁰⁷ A30P,²⁰⁸ and E46K²⁰⁹ missense

mutations are linked to familial cases of PD (**Figure 1.7A**). Under pathological conditions, α -synuclein accumulates throughout the cell and forms aggregates.^{210, 211, 212} During the aggregation process, α -synuclein forms toxic oligomeric species that disrupt several cellular pathways, including the UPS.^{179, 213, 214} It is hypothesized that the toxic oligomeric species of α -synuclein inhibit the activity of the 20S proteasome through directly binding to the proteasome itself.^{101, 179, 215}

Emerging evidence suggest that α -synuclein aggregates can spread from neuron to neuron in a prion-like fashion.^{215, 216, 217, 218} In response to the excess α -synuclein in the cytosol, an increased activation of microglia, the cytosol α -synuclein scavenger, has been reported.^{219, 220} In addition, production of proinflammatory cytokines are also increased, indicating that inflammation could be an important driving force for the progression of PD and MSA.^{221, 222} In several mouse models, increased inflammation and oxidative stress has been shown to propagate α -synuclein aggregation.²²¹⁻²²³ Despite the prevalence and deleterious nature of synucleinopathies, there are no approved disease-controlling therapeutics and current treatments are limited to symptom management.^{224, 225} Targeting α -synuclein directly with small molecules has proven to be difficult, due to the flexible and dynamic nature of α -synuclein.^{226, 227} Thus, a new paradigm for targeting α -synuclein must be identified in order to prevent the aggregation of α -synuclein seen in neurodegenerative diseases.

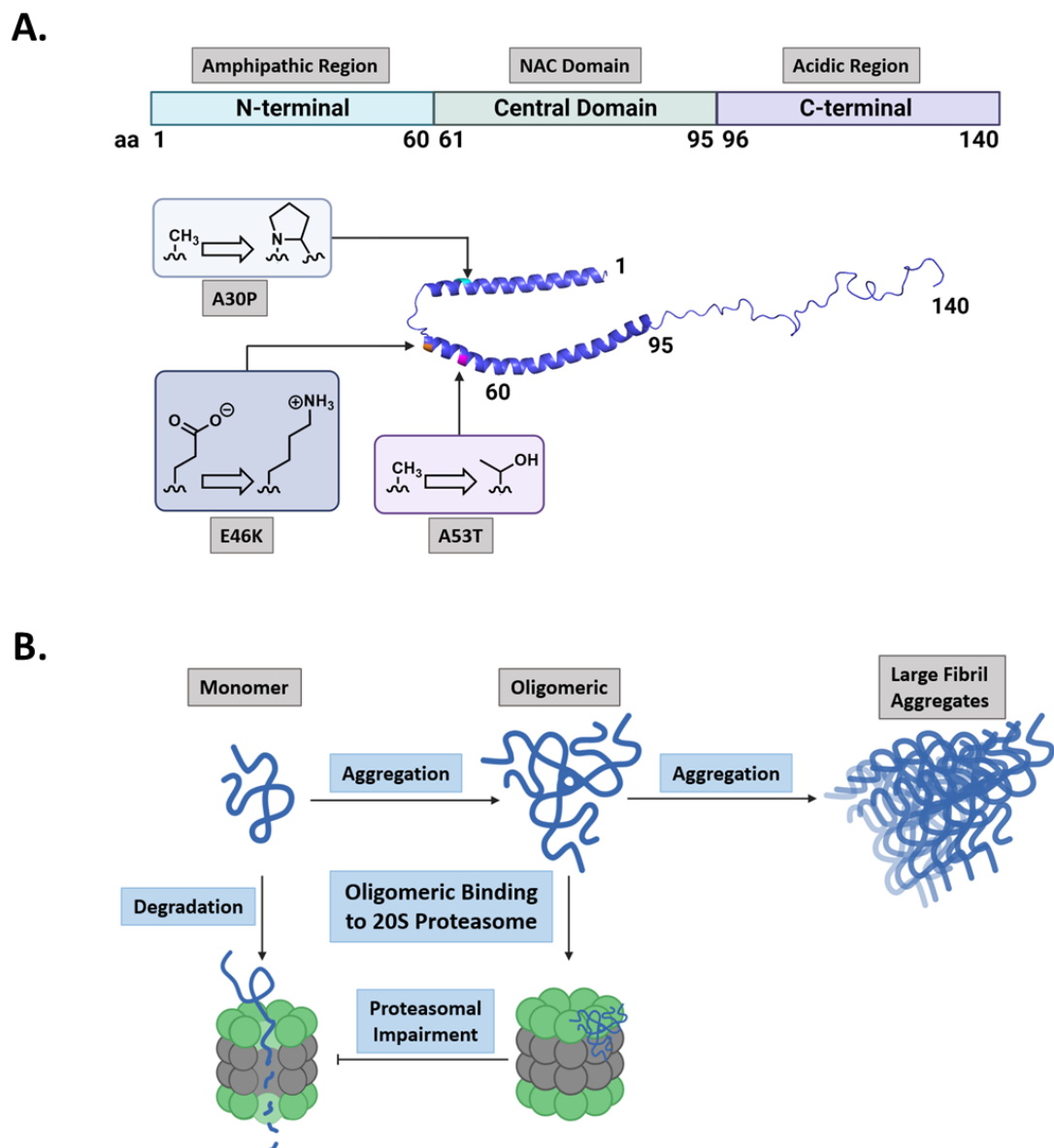


Figure 1.7: Structure of monomeric α -synuclein and aggregation process.

(A) The structure of α -synuclein with the amphipathic N-terminal, the NAC central domain, and the acidic tail of the C-terminal. The mutations of the SNCA gene and the structural alteration of the amino acids that are linked to familial PD.

(B) The aggregation process and impact on proteasomal activity.

*Created with BioRender and α -synuclein PDB 1XQ8

1.4 Exogenous 20S Proteasome Enhancers

The enhancement of endogenous degradation machinery to “drug the undruggable” has gained significant attention. The modulation of the UPS has become a central focus in developing therapeutics that target IDPs associated with human pathology, including neurodegenerative disease. Considerable attention is focused on manipulating ubiquitin-dependent degradation of proteins by creating bimodule molecules called PROteolysis-Targeting Chimeras (PROTACs).²²⁸ PROTACs increase the ubiquitination of a protein through selectively tethering the target substrate to the appropriate E3 ligase. One end of a PROTAC interacts with the target substrate, while the other end interacts with an E3 ligase, with a linker connecting the two molecules.²²⁸ Due to the double-target nature of PROTACs, they tend to be large molecules that do not possess many drug-like properties and have poor cell permeability.²²⁹ However, there are examples of well-designed PROTACs that have overcome the innate limitations and have entered into phase-II clinical trials.²³⁰ Furthermore, proteins that lack explicit 3D binding sites, such as IDPs, create significant hurdles in identifying small molecules that can directly bind to these proteins.^{226, 227} The targeted degradation of IDPs and misfolded proteins through the ubiquitin-independent pathway presents solutions to the pitfalls seen in the development of PROTACs.

As discussed, the stand-alone 20S proteasome is responsible for the efficient degradation of unfolded substrates, including IDPs and oxidatively damaged proteins.^{97, 137, 138} The use of small molecules to induce an open gated conformation presents a novel way to enhance the degradation of “undruggable” proteins. Choi and co-workers created an open-gated mutant 20S proteasome and observed a marked delay in the aggregation of

the Alzheimer's disease-associated IDP, tau.²³¹ Thus, supporting that through the induction an open-gated conformation of the 20S proteasome, degradation rate of pathogenic IDPs, such as tau and α -synuclein, will be enhanced.

Recently, there has been significant progress in the development of small molecules and peptides that can enhance the proteolytic activity of the 20S proteasome.^{98, 99, 100, 101, 150, 232, 233, 234, 235, 236, 237} The design of exogenous 20S proteasome enhancers initially centered around recapitulating the interactions between the Rpt tails HbYX motif^{84, 110, 238} and the intersubunit pockets on the α -rings of the 20S proteasome. Several synthetic peptides have been modeled after the HbYX sequence and show increased degradation of oxidized proteins.^{237, 239, 240, 241} The HbYX motif modeled synthetic peptides are valuable research probes but are not viable therapeutic options due to the metabolic instability and low cell permeability of peptide-based therapeutics.²⁴²

More recently, small molecules that stimulate the 20S proteasome have been reported.^{98, 99, 100, 101, 150, 232, 234, 235, 236} Small molecule 20S proteasome enhancers are hypothesized to function in two ways: inducing an open gated conformation or by selectively increasing the turnover rate of the catalytic sites in the β -rings. In 2007, Betulinic acid, a triterpene natural product, was identified as a 20S proteasome enhancer that selectively activates the chymotryptic-like site (**Figure 1.8**).^{243, 244} Structure-activity relationship (SAR) studies were conducted to identify betulinic acid analogs with improved 20S proteasome enhancement capabilities.²⁴³ However, the synthetic alterations of betulinic acid yielded molecules that exhibited proteasome inhibition.²³⁵ Furthermore, the activation of the 20S proteasome with betulinic acid did not translate to the enhanced degradation of full-length IDPs and was later identified to enhance the activity of the 20S proteasome through the

denaturation of the N-termini tails of the α -subunit in a similar manner as a detergent.²³⁵

243

The Kodadek group proposed that small molecules could induce or maintain the open-gated conformation of the 20S proteasome.²³⁵ In a high-throughput screen of the National Institute of Health (NIH) Clinical Collection, twelve potential 20S proteasome stimulators were identified. Of the twelve hit molecules, AM-404 and MK-866 were the most promising lead compounds (**Figure 1.8**).²³⁵ Using a cell line that expressed α -synuclein conjugated to a green fluorescent protein (GFP), the ability of AM-404 and MK-866 to enhance the proteasome mediated degradation of α -synuclein was investigated.²³⁵ Subsequently, Trader and co-workers reported that AM-404 had a 4-fold increase in the proteasome-mediated degradation of α -synuclein compared to untreated cells, while MK-866 had around a 3-fold increase.²³⁵ However, even though MK-866 and AM-404 were established to be excellent chemical probes they are not practical candidates for further evaluation as a potential therapeutic due to their poor cellular potency ($EC_{50} \sim 30 \mu\text{M}$).²³⁵

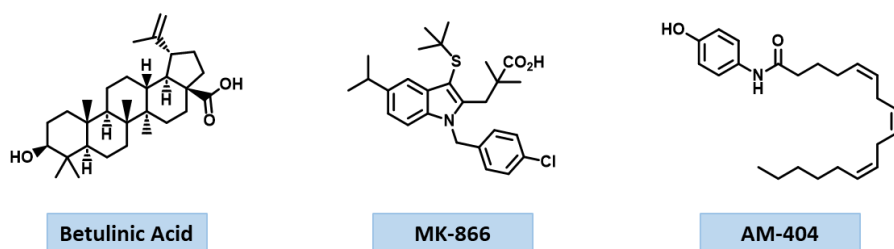


Figure 1.8: Structure of Betulinic acid, MK-866, and AM-404.

The Tepe lab has been very successful in the identification and development of novel 20S proteasome enhancers. The first 20S proteasome enhancer identified in the Tepe lab was an imidazoline, TCH-165.⁹⁹ Prof. Gaczynska, in collaboration with the Tepe lab,

utilized atomic force microscopy to visualize the biophysical effects of TCH-165 treatment on purified 20S proteasome. When the 20S proteasome was treated with TCH-165, the ratio between open to closed-gated conformation favored that of the open-gated conformation, providing the first biophysical evidence of a gate-modulating 20S proteasome enhancer (**Figure 1.9A**).⁹⁹ The Tepe lab next sought to identify a potential mechanism for the induction of the open-gated conformation by TCH-165. Using molecular docking studies, TCH-165 is predicted to bind to the intersubunit pocket formed between the $\alpha 1$ and $\alpha 2$ subunits, hereafter termed the $\alpha 1/2$ pocket (**Figure 1.9B**).⁹⁹ A competition experiment using the Rpt tail of the 19S cap that docks into the $\alpha 1/2$ pocket, Rpt 3,¹¹⁰ was then conducted. The samples of purified 20S proteasome treated with Rpt3 did not exhibit any enhanced proteolytic activity, which aligns with previous studies.²⁴⁵ In contrast, 20S proteasome treated with 1 μM of TCH-165 had a 200% increase in proteolytic activity as compared to a DMSO treated control sample. When Rpt3 and TCH-165 were added to the 20S proteasome together, a 150% increase in proteolytic activity was observed, indicating that both TCH-165 and Rpt3 were competitively binding to the $\alpha 1/2$ pocket (**Figure 1.9C**).⁹⁹ In addition, TCH-165 enhances the degradation of IDPs, such dipeptide repeats (DPR),²⁴⁶ as seen in the neurodegenerative disease amyotrophic lateral sclerosis (ALS). Furthermore, the enhanced 20S proteasome mediated degradation of the DPRs protected rat neurons from DPR-associated toxicity.²⁴⁶ However, it is essential to know that the physical properties that an active central nervous system (CNS) drug must exhibit are stricter than pharmaceuticals developed for other systems. The cLogP metric, which identifies the lipophilicity of a small molecule, must be calculated to be between 1.5 and 2.5 for viable CNS agents.^{247, 248, 249} Moreover, the

molecular weight of a small molecule is suggested to remain under 450 and under 377 for an orally available drug.^{250, 251, 252} Lastly, CNS active agents are typically limited to two functionalities that can participate in hydrogen bonding.^{253, 254} Due to TCH-165's high molecular weight (595 g/mol) and predicted low lipophilicity (cLogP 8.9), it is a poor candidate for CNS therapeutics (**Figure 1.9D**).

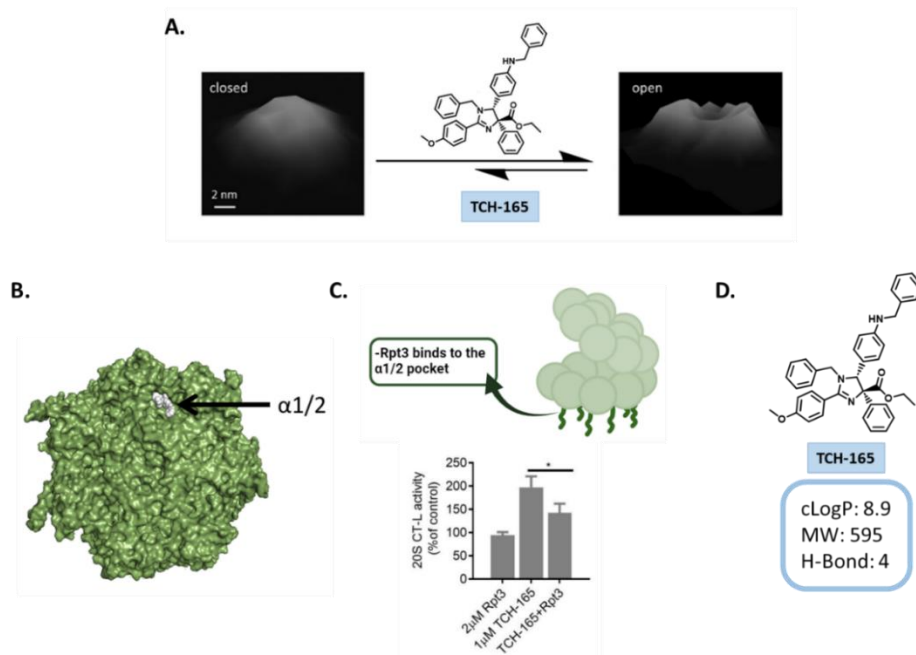


Figure 1.9: Evaluation of TCH-165 as a 20S proteasome enhancer.

(A) The addition of TCH-165 shifts the ratio between closed and open gated conformation of the 20S proteasome to the open gated conformation, as seen through AFM imaging.⁹⁶

(B) Molecular docking studies predict TCH-165 to interact with the $\alpha 1/2$ pocket on the 20S proteasome, using the 4R3O PDB file.

(C) The competition experiment with Rpt3 and TCH-165 supports that TCH-165 and Rpt3 competitively bind to the $\alpha 1/2$ pocket.

(D) The structure and physical properties of TCH-165.

To identify 20S proteasome enhancers that had potential as CNS-available therapeutic, the Tepe lab conducted a high-throughput screen of the NIH Clinical Collection and the Prestwick Libraries.^{100, 101} From the high-throughput screen, two FDA-approved neuroleptic agents, chlorpromazine and fluspirilene, were deemed the most promising lead compounds (**Figure 1.10**). The development of chlorpromazine analogs as novel 20S proteasome enhancers is described in **Chapter 2**. Fluspirilene was identified to enhance the activity of all three catalytic sites within the β -rings of the 20S proteasome. Furthermore, 2.2 μM of fluspirilene enhanced the activity of the 20S proteasome 200%, or 2-fold, over the DMSO vehicle control, hereafter termed EC_{200} .¹⁰¹ Dr. Martinez-Fiolek and Dr. Keel developed fluspirilene analogs and identified acylfluspirilene as a more potent 20S proteasome enhancer, with an EC_{200} of 1.9 μM (**Figure 1.10**).¹⁰¹ Moreover, fluspirilene and acylfluspirilene restored proteasomal activity in the presence of α -synuclein aggregates.¹⁰¹ However, fluspirilene and acylfluspirilene show poor potency in cells, with 30 μM being the effective concentration displaying enhanced 20S proteasome-mediated degradation of α -synuclein.¹⁰¹ Moreover, the Mosey Lab synthesized a class of 3,4-dihydroquinazoline based small molecules that Dr. Martinez-Fiolek identified to enhance the activity of the 20S proteasome.²¹⁸ The 3,4-dihydroquinazolines are found in several natural products. The most potent 3,4-dihydroquinazoline (dihydroquinazolines **18**) based molecule identified in this study displayed an EC_{200} of 1.3 μM (**Figure 1.10**).²¹⁸ While there has been success in developing small molecules that exhibit relatively potent enhancement of the 20S proteasome, efficient cellular 20S proteasome enhancers have yet to be identified. Expanding the chemical space of 20S proteasome enhancers is vital in identifying potent and efficient cellular proteasome enhancers. To develop the chemical

space of 20S proteasome enhancers, screening methods centered around cell-based assays must be established to ensure newly identified compounds enhance cellular proteasome degradation of full-length IDPs. In addition, disease-relevant cellular models must be created to evaluate 20S proteasome enhancers thoroughly as potential neurodegenerative disease therapeutics.

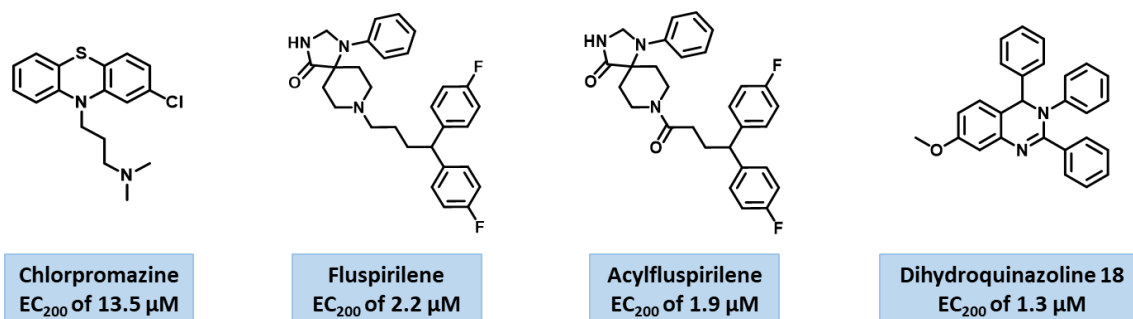


Figure 1.10: Structure and EC₂₀₀ of chlorpromazine,^{95, 97} fluspirilene,⁹⁸ acylfluspirilene,⁹⁸ and dihydroquinazoline 18.²¹⁸

REFERENCES

- (1) Harper, J. W.; Bennett, E. J. Proteome complexity and the forces that drive proteome imbalance. *Nature* **2016**, 537 (7620), 328-338.
- (2) Hipp, M. S.; Kasturi, P.; Hartl, F. U. The proteostasis network and its decline in ageing. *Nat. Rev Mol. Cell Biol.* **2019**, 20, 421-435.
- (3) Hegde, A. N.; Upadhyaya, S. C. The ubiquitin-proteasome pathway in health and disease of the nervous system. *Trends Neurosci.* **2007**, 30 (11), 587-595.
- (4) Jayaraj, G. G.; Hipp, M. S.; Hartl, F. U. Functional modules of the proteostasis network. *Cold Spring Harb. Perspect. Biol.* **2020**, 12 (1).
- (5) Kim, Y. E.; Hipp, M. S.; Bracher, A.; Hayer-Hartl, M.; Hartl, F. U. Molecular chaperone functions in protein folding and proteostasis. *Annu. Rev. Biochem.* **2013**, 82, 323-325.
- (6) Bourdenx, M.; Gavathiotis, E.; Cuervo, A. M. Chaperone-mediated autophagy: a gatekeeper of neuronal proteostasis. *Autophagy* **2021**, 17 (8), 2040-2042.
- (7) Hetz, C.; Chevet, E.; Oakes, S. A. Proteostasis control by the unfolded protein response. *Nat. Cell Biol.* **2015**, 17 (7), 829-838.
- (8) Hu, C.; Yang, J.; Qi, Z.; Wu, H.; Wang, B.; Zou, F.; Mei, H.; Liu, J.; Wang, W.; Liu, Q. Heat shock proteins: Biological functions, pathological roles, and therapeutic opportunities. *Med. Comm.* **2022**, 3 (3), 161-200.
- (9) Pintado, C.; Macias, S.; Dominguez-Martin, H.; Castano, A.; Ruano, D. Neuroinflammation alters cellular proteostasis by producing endoplasmic reticulum stress, autophagy activation and disrupting ERAD activation. *Sci. Rep.* **2017**, 7 (1), 8100-8112.
- (10) Bouchecareilh, M.; Balch, W. E. Proteostasis: a new therapeutic paradigm for pulmonary disease. *Proc. Am. Thorac. Soc.* **2011**, 8 (2), 189-195.
- (11) Tsakiri, E. N.; Gumeni, S.; Vougas, K.; Pendin, D.; Papassideri, I.; Daga, A.; Gorgoulis, V.; Juhasz, G.; Scorrano, L.; Trougakos, I. P. Proteasome dysfunction induces excessive proteome instability and loss of mitostasis that can be mitigated by enhancing mitochondrial fusion or autophagy. *Autophagy* **2019**, 15 (10), 1757-1773.
- (12) Merrick, W. C. Mechanism and regulation of eukaryotic protein synthesis. *Microbiol. Rev.* **1992**, 56 (2).
- (13) Opron, K.; Burton, Z. F. Ribosome structure, function, and early evolution. *Int. J. Mol. Sci.* **2018**, 20 (1), 40-65.

- (14) Smits, P.; Smeitink, J. A.; van den Heuvel, L. P.; Huynen, M. A.; Ettema, T. J. Reconstructing the evolution of the mitochondrial ribosomal proteome. *Nucleic Acids Res.* **2007**, *35* (14), 4686-4703.
- (15) Greber, B. J.; Ban, N. Structure and function of the mitochondrial ribosome. *Annu. Rev. Biochem.* **2016**, *85*, 103-132.
- (16) Andersson, S. G.; Zomorodipour, A.; Andersson, J. O.; Sicheritz-Ponten, W.; Alsmark, C. M.; Podowski, R. M.; Naslund, A. K.; Eriksson, A.; Winkler, H. H.; Kurland, C. G. The genome sequence of *Rickettsia prowazekii* and the origin of mitochondria. *Nature* **1998**, *396*, 133-140.
- (17) Kummer, E.; Ban, N. Mechanisms and regulation of protein synthesis in mitochondria. *Nat. Rev. Mol. Cell Biol.* **2021**, *22* (5), 307-325.
- (18) Schwarz, D. S.; Blower, M. D. The endoplasmic reticulum: structure, function and response to cellular signaling. *Cell Mol. Life Sci.* **2016**, *73* (1), 79-94.
- (19) Jan, C. H.; Williams, C. C.; Weissman, J. S. Principles of ER cotranslational translocation revealed by proximity-specific ribosome profiling. *Science* **2014**, *346* (6210), 1257521.
- (20) Blobel, G.; Dobberstein, B. Transfer of proteins across membranes. I. Presence of proteolytically processed and unprocessed nascent immunoglobulin light chains on membrane-bound ribosomes of murine myeloma. *J. Cell Biol.* **1975**, *67*, 835-851.
- (21) Hebert, D. N.; Molinari, M. In and out of the ER: protein folding, quality control, degradation, and related human diseases. *Physiol. Rev.* **2007**, *87* (4), 1377-1408.
- (22) Walter, P.; Blobel, G. Purification of a membrane-associated protein complex required for protein translocation across the endoplasmic reticulum. *Proc. Natl. Acad. Sci. U.S.A* **1980**, *77*, 7112-7116.
- (23) Walter, P.; Blobel, G. Signal recognition particle contains a 7S RNA essential for protein translocation across the endoplasmic reticulum. *Nature* **1982**, *299*, 691-698.
- (24) Bartlett, A. I.; Radford, S. E. An expanding arsenal of experimental methods yields an explosion of insights into protein folding mechanisms. *Nat. Struct. Mol. Biol.* **2009**, *16* (6), 582-588.
- (25) Dobson, C. M.; Sali, A.; Karplus, M. Protein Folding: A perspective from theory and experiment. *Angew. Chem. Int. Ed. Engl.* **1998**, *37*, 868-893.
- (26) Orengo, C. A.; Todd, A. E.; Thornton, J. M. From protein structure to function. *COSB* **1999**, *9* (3), 374-382.

- (27) Anfinsen, C. B.; Haber, E.; Sela, M.; White, F. H. The kinetics of formation of native ribonuclease during oxidation of the reduced polypeptide chain. *Proc. Natl. Acad. Sci. U. S. A.* **1961**, *47*, 1309-1314.
- (28) Dunker, A. K., Babu, M. M., Barbar, E., Blackledge, M., Bondos, S. E. *et al* What's in a name? Why these proteins are intrinsically disordered. *Intrinsically Disordered Proteins* **2013**, *1* (1).
- (29) Dunker, A. K.; Lawson, J. D.; Brown, C. J.; Williams, R. M.; Romero, P.; Oh, J. S.; Oldfield, C. J.; Campen, A. M.; Ratliff, C. M.; Hipps, K. W.; *et al*. Intrinsically disordered protein. *J. Mol. Graph. Model* **2001**, *19* (1), 26-59.
- (30) Dunker, A. K.; Silman, I.; Uversky, V. N.; Sussman, J. L. Function and structure of inherently disordered proteins. *Curr. Opin. Struct. Biol.* **2008**, *18* (6), 756-764.
- (31) van der Lee, R., Buljan, M., Weatheritt, R. J., Daughdrill, G. W.; Dunker, K. A.; Fuxreiter, M, Gough, J., *et al*. Classification of Intrinsically Disordered Regions and Proteins *Chem. Rev.* **2014**, *114*, 6589-6631.
- (32) Schellman, J. A. The thermodynamic stability of proteins. *Ann. Rev. Biophys. Chem.* **1987**, *16*, 115-137.
- (33) Lazaridas, T.; Karplus, M. Effective energy function for proteins in solution. *Proteins* **1999**, *35*, 133-152.
- (34) Makhatadze, G. I.; Privalov, P. L. Energetics of protein structure. *Adv. Protein Chem.* **1995**, *47*, 1-119.
- (35) Eichner, T.; Kalverda, A. P.; Thompson, G. S.; Homans, S. W.; Radford, S. E. Conformational conversion during amyloid formation at atomic resolution. *Mol. Cell* **2011**, *41* (2), 161-172.
- (36) Qi, R.; Sarbeng, E. B.; Liu, Q.; Le, K. Q.; Xu, X.; Xu, H.; Yang, J.; Wong, J. L.; Vorvis, C.; Hendrickson, W. A.; *et al*. Allosteric opening of the polypeptide-binding site when an Hsp70 binds ATP. *Nat. Struct. Mol. Biol.* **2013**, *20* (7), 900-907.
- (37) Kityk, R.; Kopp, J.; Sinning, I.; Mayer, M. P. Structure and dynamics of the ATP-bound open conformation of Hsp70 chaperones. *Mol. Cell* **2012**, *48* (6), 863-874.
- (38) Saio, T.; Kawagoe, S.; Ishimori, K.; Kalodimos, C. G. Oligomerization of a molecular chaperone modulates its activity. *Elife* **2018**, *7*.
- (39) Quan, S.; Koldewey, P.; Tapley, T.; Kirsch, N.; Ruane, K. M.; Pfizenmaier, J.; Shi, R.; Hofmann, S.; Foit, L.; Ren, G.; *et al*. Genetic selection designed to stabilize proteins uncovers a chaperone called Spy. *Nat. Struct. Mol. Biol.* **2011**, *18* (3), 262-269.

- (40) Hartl, F. U.; Hayer-Hartl, M. Converging concepts of protein folding in vitro and in vivo. *Nat. Struct. Mol. Biol.* **2009**, *16* (6), 574-581.
- (41) Hartl, F. U. Molecular chaperones in cellular protein folding. *Nature* **1996**, *381*, 571-579.
- (42) Albanese, V.; Yam, A. Y.; Baughman, J.; Parnot, C.; Frydman, J. Systems analyses reveal two chaperone networks with distinct functions in eukaryotic cells. *Cell* **2006**, *124* (1), 75-88.
- (43) del Alamo, M.; Hogan, D. J.; Pechmann, S.; Albanese, V.; Brown, P. O.; Frydman, J. Defining the specificity of cotranslationally acting chaperones by systematic analysis of mRNAs associated with ribosome-nascent chain complexes. *PLoS Biol.* **2011**, *9* (7).
- (44) Dekker, C.; Stirling, P. C.; McCormack, E. A.; Filmore, H.; Paul, A.; Brost, R. L.; Costanzo, M.; Boone, C.; Leroux, M. R.; Willison, K. R. The interaction network of the chaperonin CCT. *EMBO J.* **2008**, *27* (13), 1827-1839.
- (45) Hartl, F. U.; Bracher, A.; Hayer-Hartl, M. Molecular chaperones in protein folding and proteostasis. *Nature* **2011**, *475* (7356), 324-332.
- (46) Dierks, T.; Klappa, P.; Wiech, H.; Zimmermann, R. The role of molecular chaperones in protein transport into the endoplasmic reticulum. *Philos. Trans. R. Soc. Lond. B. Biol. Sci.* **1993**, *339* (1289), 335-341.
- (47) Mayer, M. P. Hsp70 chaperone dynamics and molecular mechanism. *Trends Biochem. Sci.* **2013**, *38* (10), 507-514.
- (48) Craig, E. A. Hsp70 at the membrane: driving protein translocation. *BMC Biol.* **2018**, *16* (1), 11-22.
- (49) Labbadia, J.; Morimoto, R. I. The biology of proteostasis in aging and disease. *Annu. Rev. Biochem.* **2015**, *84*, 435-464.
- (50) Bard, J. A. M.; Goodall, E. A.; Greene, E. R.; Jonsson, E.; Dong, K. C.; Martin, A. Structure and function of the 26S proteasome. *Annu. Rev. Biochem.* **2018**, *87*, 697-724.
- (51) Liu, H.; Urbe, S.; Clague, M. J. Selective protein degradation in cell signalling. *Semin. Cell Dev. Biol.* **2012**, *23* (5), 509-514.
- (52) Davies, D.; Humphery, T. J. Amino acid recycling in relation to protein turnover. *Plant Physiol.* **1977**, *61*, 54-58.
- (53) Mortimore, G.; Lardeux, B. R.; Adams, C. E. Regulation of microautophagy and basal protein turnover in rat liver. Effects of short-termstarvation. *J. Biol. Chem.* **1988**, *263*, 2506-2512.

- (54) Segref, A.; Vakkayil, K. L.; Padvitski, T.; Li, Q.; Kroef, V.; Lormann, J.; Korner, L.; Finger, F.; Hoppe, T. Thermosensation in *Caenorhabditis elegans* is linked to ubiquitin-dependent protein turnover via insulin and calcineurin signaling. *Nat. Commun.* **2022**, *13* (1), 5874-5891.
- (55) Kristensen, A. R.; Gsponer, J.; Foster, L. J. Protein synthesis rate is the predominant regulator of protein expression during differentiation. *Mol. Syst. Biol.* **2013**, *9*, 689-701.
- (56) Gardner, R. G.; Nelson, Z. W.; Gottschling, D. E. Degradation-mediated protein quality control in the nucleus. *Cell* **2005**, *120* (6), 803-815.
- (57) Martinez-Vicente, M.; Sovak, G.; Cuervo, A. M. Protein degradation and aging. *Exp. Gerontol.* **2005**, *40*, 622-633.
- (58) Heck, J. W.; Cheung, S. K.; Hampton, R. Y. Cytoplasmic protein quality control degradation mediated by parallel actions of the E3 ubiquitin ligases Ubr1 and San1. *Proc. Natl. Acad. Sci. U.S.A.* **2010**, *107* (3), 1106-1111.
- (59) Pojl, C.; Dikic, I. Cellular quality control by the ubiquitin-proteasome system and autophagy. *Science* **2019**, *366*, 818-822.
- (60) Thibaudeau, T. A.; Smith, D. M. A practical review of proteasome pharmacology. *Pharmacol. Rev.* **2019**, *71*, 170-197.
- (61) Khandia, R.; Dadar, M.; Munjal, A.; Dhama, K.; Karthik, K.; Tiwari, R.; Yattoo, M. I.; Iqbal, H. M. N.; Singh, K. P.; Joshi, S. K.; et al. A comprehensive review of autophagy and its various roles in infectious, non-infectious, and lifestyle diseases: Current knowledge and prospects for disease prevention, novel drug design, and therapy. *Cells* **2019**, *8* (7), 674-738.
- (62) Lu, Y.; Lee, B. H.; King, R. W.; Finley, D.; Kirschner, M. W. Substrate degradation by the proteasome: a single-molecule kinetic analysis. *Science* **2015**, *348* (6231), 1250834-1250854.
- (63) Finley, D. Recognition and processing of ubiquitin-protein conjugates by the proteasome. *Annu. Rev. Biochem.* **2009**, *78*, 477-513.
- (64) Li, P.; Ma, Y.; Yu, C.; Wu, S.; Wang, K.; Yi, H.; Liang, W. Autophagy and aging: Roles in skeletal muscle, eye, brain and hepatic tissue. *Front. Cell Dev. Biol.* **2021**, *9*, 752962-752974.
- (65) Yin, Z.; Pascual, C.; Klionsky, D. J. Autophagy: Machinery and regulation. *Microb. Cell* **2016**, *3* (12), 588-596.

- (66) Schulze, H.; Kolter, T.; Sandhoff, K. Principles of lysosomal membrane degradation: Cellular topology and biochemistry of lysosomal lipid degradation. *Biochim. Biophys. Acta.* **2009**, *1793* (4), 674-683.
- (67) Voges, D.; Zwickl, P.; Baumeister, W. The 26S proteasome: A molecular machine designed for controlled proteolysis. *Annu. Rev. Biochem.* **1999**, *68*, 1015-1068.
- (68) Arendt, C. S.; Hochstrasser, M. Identification of the yeast 20S proteasome catalytic centers and subunit interactions required for active-site formation. *Proc. Natl. Acad. Sci USA* **1997**, *94*, 7156-7161.
- (69) Wilk, S.; Orlowski, M. Cation-sensitive neutral endopeptidase: Isolation and specificity of the bovine pituitary enzyme. *J. Neurochem.* **1980**, *35*, 1172-1182.
- (70) Wilk, S.; Orlowski, M. Evidence that pituitary cation-sensitive neutral endopeptidase is a multicatalytic protease complex. *J. Neurochem.* **1983**, *40*, 842-849.
- (71) Tanaka, K.; Yoshimura, T.; Ichihara, A.; Ikai, A.; Nishigai, M.; Kameyama, K.; Takagi, T. Proteasomes (multi-protease complexes) as 20 S ring-shaped particles in a variety of eukaryotic cells. *J. Biol. Chem.* **1988**, *263*, 16209-16217.
- (72) Arrigo, A. P.; Tanaka, K.; Goldberg, A. L.; Welch, W. J. Identity of the 19S 'prosome' particle with the large multifunctional protease complex of mammalian cells (the proteasome). *Nature* **1988**, *331*, 192-194.
- (73) Groll, M.; Bajorek, M.; Kohler, A.; Moroder, L.; Rubin, D. M.; Glickman, M. H.; Finley, D. A gated channel into the proteasome core particle. *Nat. Struct. Biol* **2000**, *7*, 1062-1067.
- (74) Kohler, A.; Cascia, P.; Leggett, D. S.; Woo, K. M.; Goldberg, A. L.; Finley, D. The axial channel of the proteasome core particle is gated by the Rpt2 ATPase and controls both substrate entry and product release. *Mol. Cell.* **2001**, *7*, 1143-1152.
- (75) Schnell, H. M.; Walsh, R. M., Jr.; Rawson, S.; Kaur, M.; Bhanu, M. K.; Tian, G.; Prado, M. A.; Guerra-Moreno, A.; Paulo, J. A.; Gygi, S. P.; et al. Structures of chaperone-associated assembly intermediates reveal coordinated mechanisms of proteasome biogenesis. *Nat. Struct. Mol. Biol.* **2021**, *28* (5), 418-425.
- (76) Rousseau, A.; Bertolotti, A. Regulation of proteasome assembly and activity in health and disease. *Nat. Rev. Mol. Cell Biol.* **2018**, *19* (11), 697-712.
- (77) Wu, W.; Sahara, K.; Hirayama, S.; Zhao, X.; Watanabe, A.; Hamazaki, J.; Yashiroda, H.; Murata, S. PAC1-PAC2 proteasome assembly chaperone retains the core alpha4-alpha7 assembly intermediates in the cytoplasm. *Genes Cells* **2018**, *23* (10), 839-848.

- (78) Hirano, Y.; Hendil, K. B.; Yashiroda, H.; Iemura, S.; Nagane, R.; Hioki, Y.; Natsume, T.; Tanaka, K.; Murata, S. A heterodimeric complex that promotes the assembly of mammalian 20S proteasomes. *Nature* **2005**, *437* (7063), 1381-1385.
- (79) Le Tallec, B.; Barrault, M. B.; Courbeyrette, R.; Guerois, R.; Marsolier-Kergoat, M. C.; Peyroche, A. 20S proteasome assembly is orchestrated by two distinct pairs of chaperones in yeast and in mammals. *Mol. Cell* **2007**, *27* (4), 660-674.
- (80) Satoh, T.; Yagi-Utsumi, M.; Okamoto, K.; Kurimoto, E.; Tanaka, K.; Kato, K. Molecular and structural basis of the proteasome alpha subunit assembly mechanism mediated by the proteasome-assembling chaperone PAC3-PAC4 heterodimer. *Int. J. Mol. Sci.* **2019**, *20* (9), 2231-2240.
- (81) Sekiguchi, T.; Satoh, T.; Kurimoto, E.; Song, C.; Kozai, T.; Watanabe, H.; Ishii, K.; Yagi, H.; Yanaka, S.; Uchiyama, S.; et al. Mutational and combinatorial control of self-assembling and disassembling of human proteasome alpha subunits. *Int. J. Mol. Sci.* **2019**, *20* (9), 2308-2321.
- (82) Li, D.; Dong, Q.; Tao, Q.; Gu, J.; Cui, Y.; Jiang, X.; Yuan, J.; Li, W.; Xu, R.; Jin, Y.; et al. c-Abl regulates proteasome abundance by controlling the ubiquitin-proteasomal degradation of PSMA7 subunit. *Cell* **2015**, *10* (4), 484-496.
- (83) Apcher, G. S.; Maitland, J.; Dawson, S.; Sheppard, P.; Mayer, R. J. The alpha4 and alpha7 subunits and assembly of the 20S proteasome. *FEBS Lett.* **2004**, *569* (1), 211-216.
- (84) Kusmierczyk, A. R.; Kunjappu, M. J.; Kim, R. Y.; Hochstrasser, M. A conserved 20S proteasome assembly factor requires a C-terminal HbYX motif for proteasomal precursor binding. *Nat. Struct. Mol. Biol.* **2011**, *18* (5), 622-629.
- (85) Kusmierczyk, A. R.; Hochstrasser, M. Some assembly required: dedicated chaperones in eukaryotic proteasome biogenesis. *Biol. Chem.* **2008**, *389* (9), 1143-1451.
- (86) Padmanabhan, A.; Vuong, S. A.; Hochstrasser, M. Assembly of an evolutionarily conserved alternative proteasome isoform in human cells. *Cell Rep.* **2016**, *14* (12), 2962-2974.
- (87) Chen, P.; Hochstrasser, M. Autocatalytic subunit processing couples active site formation in the 20S proteasome to completion of assembly. *Cell* **1996**, *86*, 961-972.
- (88) Witt, S.; Kwon, Y. D.; Sharon, M.; Felderer, K.; Beuttler, M.; Robinson, C. V.; Baumeister, W.; Jap, B. K. Proteasome assembly triggers a switch required for active-site maturation. *Structure* **2006**, *14* (7), 1179-1188.
- (89) Abi Habib, J.; Lesenfans, J.; Vigneron, N.; Van den Eynde, B. J. Functional Differences between Proteasome Subtypes. *Cells* **2022**, *11* (3), 421-446.

- (90) Ramos, P. C.; Hockendorff, J.; Johnson, E. S.; Varshavsky, A.; Dohmen, R. J. Ump1p is required for proper maturation of the 20S proteasome and becomes its substrate upon completion of the assembly. *Cell* **1999**, *92*, 489-499.
- (91) Li, X.; Kusmierczyk, A. R.; Wong, P.; Emili, A.; Hochstrasser, M. beta-Subunit appendages promote 20S proteasome assembly by overcoming an Ump1-dependent checkpoint. *EMBO J.* **2007**, *26* (9), 2339-2349.
- (92) Hirano, Y.; Kaneko, T.; Okamoto, K.; Bai, M.; Yashiroda, H.; Furuyama, K.; Kato, K.; Tanaka, K.; Murata, S. Dissecting beta-ring assembly pathway of the mammalian 20S proteasome. *EMBO J.* **2008**, *27* (16), 2204-2213.
- (93) Fricke, B.; Heink, S.; Steffen, J.; Kloetzel, P. M.; Kruger, E. The proteasome maturation protein POMP facilitates major steps of 20S proteasome formation at the endoplasmic reticulum. *EMBO Rep.* **2007**, *8* (12), 1170-1175.
- (94) Frentzel, S.; Pesold-Hurt, B.; Seelig, A.; Kloetzel, P. M. 20S proteasomes are assembled via distinct precursor complexes *J. Mol. Biol.* **1994**, *236*, 975-981.
- (95) Kock, M.; Nunes, M. M.; Hemann, M.; Kube, S.; Dohmen, R. J.; Herzog, F.; Ramos, P. C.; Wendler, P. Proteasome assembly from 15S precursors involves major conformational changes and recycling of the Pba1-Pba2 chaperone. *Nat. Commun.* **2015**, *6*, 6123-6132.
- (96) Hirano, Y.; Hayashi, H.; Iemura, S.; Hendil, K. B.; Niwa, S.; Kishimoto, T.; Kasahara, M.; Natsume, T.; Tanaka, K.; Murata, S. Cooperation of multiple chaperones required for the assembly of mammalian 20S proteasomes. *Mol. Cell* **2006**, *24* (6), 977-984.
- (97) Baugh, J. M.; Viktorova, E. G.; Pilipenko, E. V. Proteasomes can degrade a significant proportion of cellular proteins independent of ubiquitination. *J. Mol. Biol.* **2009**, *386* (3), 814-827.
- (98) Staerz, S. D.; Jones, C. L.; Tepe, J. J. Design, synthesis, and biological evaluation of potent 20S proteasome activators for the potential treatment of alpha-synucleinopathies. *J. Med. Chem.* **2022**, *65*, 6631-6642.
- (99) Njomen, E.; Osmulski, P. A.; Jones, C. L.; Gaczynska, M.; Tepe, J. J. Small molecule modulation of proteasome assembly. *Biochemistry* **2018**, *57* (28), 4214-4224.
- (100) Jones, C. L.; Njomen, E.; Sjogren, B.; Dexheimer, T. S.; Tepe, J. J. Small molecule enhancement of 20S proteasome activity targets intrinsically disordered proteins. *ACS Chem. Biol.* **2017**, *12*, 2240-2247.
- (101) Fiolek, T. J.; Keel, K. L.; Tepe, J. J. Fluspirilene analogs activate the 20S proteasome and overcome proteasome impairment by intrinsically disordered protein oligomers. *ACS Chem. Neurosci.* **2021**, *12*, 1438-1448.

(102) Kohler, A.; Bajorek, M.; Moroder, L.; Rubin, D. M.; Huber, R.; Glickam, M. H.; Finley, D. The substrate translocation channel of the proteasome. *Biochimie*. **2001**, *83*, 325-332.

(103) Prakash, S.; Tian, L.; Ratliff, K. S.; Lehotzky, R. E.; Matouschek, A. An unstructured initiation site is required for efficient proteasome-mediated degradation. *Nat. Struct. Mol. Biol.* **2004**, *11* (9), 830-837.

(104) Tomita, T.; Matouschek, A. Substrate selection by the proteasome through initiation regions. *Protein Sci.* **2019**, *28* (7), 1222-1232.

(105) Peters, J. M.; Franke, W. W.; Kleinschmidt, J. A. Distinct 19S and 20S subcomplexes of the 26S proteasome and their distribution in the nucleus and the cytoplasm. *J. Bio. Chem.* **1994**, *269*, 7709-7718.

(106) DeMartino, G. N.; Moomaw, C. R.; Zagnitko, O. P.; Proske, R. J.; Chu-Ping, M.; Afednis, S. J.; Swaffield, J. C.; Slaughter, C. A. PA700, an ATP-dependent activator of the 20S proteasome, is an ATPase containing multiple members of a nucleotide-binding protein family. *J. Bio. Chem.* **1994**, *269*, 20878-20884.

(107) Glickman, M. H.; Rubin, D. M.; Coux, O.; Wefes, I.; Pfeifer, G.; Cjeka, Z.; Baumeister, W.; Fried, V. A.; Finley, D. A subcomplex of the proteasome regulatory particle required for ubiquitin-conjugate degradation and related to the COP9-signalosome and eIF3. *Cell* **1998**, *94*, 615-623.

(108) Braun, B. C.; Glickman, M.; Kraft, R.; Dahlmann, B.; Kloetzel, P. M.; Finley, D.; Schmidt, M. The base of the proteasome regulatory particle exhibits chaperone-like activity. *Nature* **1999**, *1*, 221-226.

(109) Liu, C. W.; Millen, L.; Roman, T. B.; Xiong, H.; Gilbert, H. F.; Noiva, R.; DeMartino, G. N.; Thomas, P. J. Conformational remodeling of proteasomal substrates by PA700, the 19S regulatory complex of the 26S proteasome. *J. Biol. Chem.* **2002**, *277* (30), 26815-26820.

(110) Smith, D. M.; Chang, S. C.; Park, S.; Finley, D.; Cheng, Y.; Goldberg, A. L. Docking of the proteasomal ATPases' carboxyl termini in the 20S proteasome's alpha ring opens the gate for substrate entry. *Mol. Cell* **2007**, *27* (5), 731-744.

(111) Forster, A.; Masters, E. I.; Whitby, F. G.; Robinson, H.; Hill, C. P. The 1.9 Å structure of a proteasome-11S activator complex and implications for proteasome-PAN/PA700 interactions. *Mol. Cell* **2005**, *18* (5), 589-599.

(112) Opoku-Nsiah, K. A.; de la Pena, A. H.; Williams, S. K.; Chopra, N.; Sali, A.; Lander, G. C.; Gestwicki, J. E. The YPhi motif defines the structure-activity relationships of human 20S proteasome activators. *Nat. Commun.* **2022**, *13* (1), 1226-1237.

- (113) Bar-Nun, S.; Glickman, M. H. Proteasomal AAA-ATPases: structure and function. *Biochim. Biophys. Acta* **2012**, *1823* (1), 67-82.
- (114) Peth, A.; Besche, H. C.; Goldberg, A. L. Ubiquitinated proteins activate the proteasome by binding to Usp14/Ubp6, which causes 20S gate opening. *Mol. Cell* **2009**, *36* (5), 794-804.
- (115) Martinez-Fonts, K.; Davis, C.; Tomita, T.; Elsasser, S.; Nager, A. R.; Shi, Y.; Finley, D.; Matouschek, A. The proteasome 19S cap and its ubiquitin receptors provide a versatile recognition platform for substrates. *Nat. Commun.* **2020**, *11* (1), 477-492.
- (116) Rosenzweig, R.; Osmulski, P. A.; Gaczynska, M.; Glickman, M. H. The central unit within the 19S regulatory particle of the proteasome. *Nat. Struct. Mol. Biol.* **2008**, *15* (6), 573-580.
- (117) Elsasser, S.; Gali, R. R.; Schwickart, M.; Larsen, C. N.; Leggett, D. S.; Muller, B.; Feng, M. T.; Tubing, F.; Dittmar, G. A.; Finley, D. Proteasome subunit Rpn1 binds ubiquitin-like protein domains. *Nat. Cell Biol.* **2002**, *4* (9), 725-730.
- (118) Takeuchi, J.; Chen, H.; Coffino, P. Proteasome substrate degradation requires association plus extended peptide. *EMBO J.* **2007**, *26* (1), 123-131.
- (119) Ciechanover, A.; Heller, H.; Elias, S.; Haas, A. L.; Hershko, A. ATP-dependent conjugation of reticulocyte proteins with the polypeptide required for protein degradation. *Proc. Natl. Acad. Sci. U.S.A.* **1980**, *77*, 1365-1368.
- (120) Hershko, A.; Ciechanover, A.; Heller, H.; Haas, A. L.; Rose, I. A. Proposed role of ATP in protein breakdown: conjugation of proteins with multiple chains of the polypeptide of ATP-dependent proteolysis. *Proc. Natl. Acad. Sci. U.S.A.* **1980**, *77*, 1783-1786.
- (121) Wilkinson, K. D.; Urban, M. K.; Haas, A. L. Ubiquitin is the ATPdependent proteolysis factor I of rabbit reticulocytes. *J. Biol. Mol.* **1980**, *225*, 7529-7532.
- (122) Komander, D. The emerging complexity of protein ubiquitination. *Biochem. Soc. Trans.* **2009**, *37*, 937-953.
- (123) Xu, P.; Duong, D. M.; Seyfried, N. T.; Cheng, D.; Xie, Y.; Robert, J.; Rush, J.; Hochstrasser, M.; Finley, D.; Peng, J. Quantitative proteomics reveals the function of unconventional ubiquitin chains in proteasomal degradation. *Cell* **2009**, *137* (1), 133-145.
- (124) Haas, A. L.; Warms, J. V.; Hershko, A.; Rose, I. A. Ubiquitin-activating enzyme. *Mech. role protein-ubiquitin Conjug. J. Biol. Chem.* **1982**, *257*, 2543-2548.
- (125) Lv, Z.; Yuan, L.; Atkison, J. H.; Aldana-Masangkay, G.; Chen, Y.; Olsen, S. K. Domain alternation and active site remodeling are conserved structural features of ubiquitin E1. *J. Biol. Chem.* **2017**, *292* (29), 12089-12099.

- (126) Yuan, L.; Lv, Z.; Adams, M. J.; Olsen, S. K. Crystal structures of an E1-E2-ubiquitin thioester mimetic reveal molecular mechanisms of transthioesterification. *Nat. Commun.* **2021**, *12* (1), 2370-2383.
- (127) Hershko, A.; Heller, H.; Elias, S.; Ciechanover, A. Components of ubiquitin-protein ligase system. Resolution, affinity purification, and role in protein breakdown. *J. Biol. Chem.* **1983**, *258*, 8206-8214.
- (128) Pickart, C. M.; Rose, I. A. F. Functional heterogeneity of ubiquitin carrier proteins. *J. Biol. Chem.* **1985**, *260*, 1573-1581.
- (129) George, A. J.; Hoffiz, Y. C.; Charles, A. J.; Zhu, Y.; Mabb, A. M. A Comprehensive atlas of E3 ubiquitin ligase mutations in neurological disorders. *Front. Genet.* **2018**, *9*, 29.
- (130) Li, W.; Bengtson, M. H.; Ulbrich, A.; Matsuda, A.; Reddy, V. A.; Orth, A.; Chanda, S. K.; Batalov, S.; Joazeiro, C. A. Genome-wide and functional annotation of human E3 ubiquitin ligases identifies MULAN, a mitochondrial E3 that regulates the organelle's dynamics and signaling. *PLoS One* **2008**, *3* (1).
- (131) Metzger, M. B.; Hristova, V. A.; Weissman, A. M. HECT and RING finger families of E3 ubiquitin ligases at a glance. *J. Cell Sci.* **2012**, *125*, 531-537.
- (132) Huibregtse, J. M.; Scheffner, M.; Beaudenon, S.; Howley, P. M. A family of proteins structurally and functionally related to the E6-AP ubiquitin-protein ligase. *Proc. Natl. Acad. Sci. U. S. A.* **1995**, *92*, 2563-2567.
- (133) Budhidarmo, R.; Nakatani, Y.; Day, C. L. RINGs hold the key to ubiquitin transfer. *Trends Biochem. Sci.* **2012**, *37* (2), 58-65.
- (134) Schreiner, P.; Chen, X.; Husnjak, K.; Randles, L.; Zhang, N.; Elsasser, S.; Finley, D.; Dikic, I.; Walters, K. J.; Groll, M. Ubiquitin docking at the proteasome through a novel pleckstrin-homology domain interaction. *Nature* **2008**, *453* (7194), 548-552.
- (135) Husnjak, K.; Elsasser, S.; Zhang, N.; Chen, X.; Randles, L.; Shi, Y.; Hofmann, K.; Walters, K. J.; Finley, D.; Dikic, I. Proteasome subunit Rpn13 is a novel ubiquitin receptor. *Nature* **2008**, *453* (7194), 481-488.
- (136) Peth, A.; Uchiki, T.; Goldberg, A. L. ATP-dependent steps in the binding of ubiquitin conjugates to the 26S proteasome that commit to degradation. *Mol. Cell* **2010**, *40* (4), 671-681.
- (137) Ben-Nissan, G.; Sharon, M. Regulating the 20S proteasome ubiquitin-independent degradation pathway. *Biomolecules* **2014**, *4*, 862-884.
- (138) Deshmukh, F. K.; Yaffe, D.; Olshina, M. A.; Ben-Nissan, G.; Sharon, M. The contribution of the 20S proteasome to proteostasis. *Biomolecules* **2019**, *9* (5), 190-205.

- (139) Liu, C. W.; Corboy, M. J.; DeMartino, G. N.; Thomas, P. J. Endoproteolytic activity of the proteasome. *Science* **2003**, *299* (5605), 408-411.
- (140) Fabre, B.; Lambour, T.; Garrigues, L.; Ducoux-Petit, M.; Amalric, F.; Monsarrat, B.; Burlet-Schiltz, O.; Bousquet-Dubouch, M. P. Label-free quantitative proteomics reveals the dynamics of proteasome complexes composition and stoichiometry in a wide range of human cell lines. *J. Proteome Res.* **2014**, *13* (6), 3027-3237.
- (141) Asher, G.; Tsvetkov, P.; Kahana, C.; Shaul, Y. A mechanism of ubiquitin-independent proteasomal degradation of the tumor suppressors p53 and p73. *Genes Dev.* **2005**, *19* (3), 316-321.
- (142) Coffino, P. Regulation of cellular polyamines by antizyme. *Nat. Rev. Mol. Cell Biol.* **2001**, *2*, 188-194.
- (143) Kern, A. D.; Oliveira, M. A.; Coffino, P.; Hackert, M. L. Structure of mammalian ornithine decarboxylase at 1.6 Å resolution: stereochemical implications of PLP-dependent amino acid decarboxylases. *Structure* **1999**, *7*, 567-581.
- (144) Tobias, K. E.; Mamroud-Kidron, E.; Kahana, C. Gly387 of murine ornithine decarboxylase is essential for the formation of stable homo dimers. *Eur. J. Biochem.* **1993**, *218*, 245-250.
- (145) Kahana, C.; Asher, G.; Shaul, Y. Mechanisms of protein degradation: an odyssey with ODC. *Cell Cycle* **2005**, *4* (11), 1461-1464.
- (146) Mamroud-Kidron, E.; Omer-Itsicovich, M.; Bercovich, Z.; Tobias, K. E.; Rom, E.; Kahana, C. A unified pathway for the degradation of ornithine decarboxylase in reticulocyte lysate requires interaction with the polyamine induced protein, ornithine decarboxylase antizyme. *Eur. J. Biochem.* **1994**, *226*, 547-554.
- (147) Glass, J. R.; Gerner, E. W. Spermidine mediates degradation of ornithine decarboxylase by a non-lysosomal, ubiquitin-independent mechanism. *J. Cell. Physiol.* **1987**, *130*, 133-141.
- (148) Murakami, Y.; Matsufuji, S.; Kameji, T.; Hayashi, S.; Igarashi, K.; Tamura, T.; Tanaka, K.; Ichihara, A. Ornithine decarboxylase is degraded by the 26S proteasome without ubiquitination. *Nature* **1992**, *360*, 597-599.
- (149) Asher, G.; Bercovich, Z.; Tsvetkov, P.; Shaul, Y.; Kahana, C. 20S proteasomal degradation of ornithine decarboxylase is regulated by NQO1. *Mol. Cell* **2005**, *17* (5), 645-655.
- (150) Staerz, S. D.; Lisabeth, E. M.; Njomen, E.; Dexheimer, T. S.; Neubig, R. R.; Tepe, J. J. Development of a cell-based AlphaLISA assay for high-throughput screening for small molecule proteasome modulators. *ACS Omega* **2023**, *8*, 15650-15659.

- (151) Tanaka, K.; Yoshimura, T.; Ichihara, A. Role of substrate in reversible activation of proteasomes (multi-protease complexes) by sodium dodecyl sulfate. *Journal of Biochemistry* **1989**, *106*, 495-500.
- (152) Osmulski, P. A.; Gaczynska, M. Atomic force microscopy reveals two conformations of the 20S proteasome from fission yeast. *J. Biol. Chem.* **2000**, *275*, 11317-113174.
- (153) Moscovitz, O.; Ben-Nissan, G.; Fainer, I.; Pollack, D.; Mizrachi, L.; Sharon, M. The Parkinson's-associated protein DJ-1 regulates the 20S proteasome. *Nat. Commun.* **2015**, *6*, 6609-6621.
- (154) Moscovitz, O.; Tsvetkov, P.; Hazan, N.; Michaelievski, I.; Keisar, H.; Ben-Nissan, G.; Shaul, Y.; Sharon, M. A mutually inhibitory feedback loop between the 20S proteasome and its regulator, NQO1. *Mol. Cell* **2012**, *47* (1), 76-86.
- (155) Deshmukh, F. K.; Ben-Nissan, G.; Olshina, M. A.; Fuzesi-Levi, M. G.; Polkinghorn, C.; Arkind, G.; Leushkin, Y.; Fainer, I.; Fleishman, S. J.; Tawfik, D.; et al. Allosteric regulation of the 20S proteasome by the Catalytic Core Regulators (CCRs) family. *Nat. Commun.* **2023**, *14* (1), 3126-3149.
- (156) Alvarez-Castelao, B.; Goethals, M.; Vandekerckhove, J.; Castano, J. G. Mechanism of cleavage of alpha-synuclein by the 20S proteasome and modulation of its degradation by the RedOx state of the N-terminal methionines. *Biochim. Biophys. Acta* **2014**, *1843* (2), 352-365.
- (157) Pickering, A. M.; Davies, K. J. Degradation of damaged proteins: the main function of the 20S proteasome. *Prog. Mol. Biol. Transl. Sci.* **2012**, *109*, 227-248.
- (158) Boveris, A. Determination of the production of superoxide radicals and hydrogen peroxide in mitochondria. *Methods Enzymol.* **1984**, *105*, 429-435.
- (159) Turrens, J. F.; Boveris, A. Generation of super oxide anion by the NADH dehydrogenase of bovine heart mitochondria. *Biochem. J.* **1980**, *191*, 421-427.
- (160) Pagano, G. Redox-modulated xenobiotic action and ROS formation: a mirror or a window? *Hum. Exp. Toxicol.* **2002**, *21* (2), 77-81.
- (161) Kim, J. Y.; Ro, J. Y. Signal pathway of cytokines produced by reactive oxygen species generated from phorbol myristate acetate-stimulated HMC-1 cells. *Scand. J. Immunol.* **2005**, *62* (1), 25-35.
- (162) Spooner, R.; Yilmaz, O. The role of reactive-oxygen-species in microbial persistence and inflammation. *Int. J. Mol. Sci.* **2011**, *12* (1), 334-352.
- (163) Davies, M. J. The oxidative environment and protein damage. *Biochim. Biophys. Acta* **2005**, *1703* (2), 93-109.

- (164) Davies, M. J. Protein oxidation and peroxidation. *Biochem. J.* **2016**, *473* (7), 805-825.
- (165) Hawkins, C. L.; Davies, M. J. Detection, identification, and quantification of oxidative protein modifications. *J. Biol. Chem.* **2019**, *294* (51), 19683-19708.
- (166) Kiffin, R.; Christian, C.; Knecht, E.; Cuervo, A. M. Activation of chaperone-mediated autophagy during oxidative stress. *Mol. Biol. Cell* **2004**, *15* (11), 4829-4840.
- (167) Davies, K. J. Degradation of oxidized proteins by the 20S proteasome. *Biochemie* **2001**, *83*, 301-310.
- (168) Goldberg, A. L. Protein degradation and protection against misfolded or damaged proteins. *Nature* **2003**, *426*, 895-899.
- (169) Farout, L.; Mary, J.; Vinh, J.; Szweda, L. I.; Friguet, B. Inactivation of the proteasome by 4-hydroxy-2-nonenal is site specific and dependant on 20S proteasome subtypes. *Arch. Biochem. Biophys.* **2006**, *453* (1), 135-142.
- (170) Pickering, A. M.; Koop, A. L.; Teoh, C. Y.; Ermak, G.; Grune, T.; Davies, K. J. The immunoproteasome, the 20S proteasome and the PA28alpha beta proteasome regulator are oxidative-stress-adaptive proteolytic complexes. *Biochem. J.* **2010**, *432* (3), 585-594.
- (171) Reinheckel, T.; Sitte, N.; Ullrich, O.; Kuckelkorn, U.; Davies, K. J. Comparative resistance of the 20S and 26S proteasome to oxidative stress. *Biochem. J.* **1998**, *335*, 637-642.
- (172) Reinheckel, T.; Ullrich, O.; Sitte, N.; Grune, T. Differential impairment of 20S and 26S proteasome activities in human hematopoietic K562 cells during oxidative stress. *Arch. Biochem. Biophys.* **2000**, *377*, 65-68.
- (173) Parajuli, N. A cycle of altered proteasome and reactive oxygen species production in renal proximal tubular cells. *Toxicol. Forensic. Med.* **2019**, *4* (1), 13-17.
- (174) Bonea, D.; Noureddine, J.; Gazzarrini, S.; Zhao, R. Oxidative and salt stresses alter the 26S proteasome holoenzyme and associated protein profiles in *Arabidopsis thaliana*. *BMC Plant Biol.* **2021**, *21* (1), 486-505.
- (175) Lee, C.; Klopp, R. G.; Weindruch, R.; Prolla, T. Gene expression profile of aging and its retardation by caloric restriction. *Science* **1999**, *285*, 1390-1393.
- (176) Ly, D. H.; Lockhart, D. J.; Lerner, R. A.; Schultz, P. G. Mitotic misregulation and human aging. *Science* **2000**, *287*, 2486-2492.
- (177) Ferrington, D. A.; Husom, A. D.; Thompson, L. V. Altered proteasome structure, function, and oxidation in aged muscle *FASEB J.* **2005**, *19*, 1-24.

- (178) Vernace, V. A.; Arnaud, L.; Schmidt-Glenewinkel, T.; Figueiredo-Pereira, M. E. Aging perturbs 26S proteasome assembly in *Drosophila melanogaster*. *FASEB J.* **2007**, *21* (11), 2672-2682.
- (179) Thibaudeau, T. A.; Anderson, R. T.; Smith, D. M. A common mechanism of proteasome impairment by neurodegenerative disease-associated oligomers. *Nat. Commun.* **2018**, *9*, 1097-1111.
- (180) Grune, T.; Jung, T.; Merker, K.; Davies, K. J. Decreased proteolysis caused by protein aggregates, inclusion bodies, plaques, lipofuscin, ceroid, and 'aggresomes' during oxidative stress, aging, and disease. *Int. J. Biochem. Cell Biol.* **2004**, *36* (12), 2519-2530.
- (181) Cuanalo-Contreras, K.; Schulz, J.; Mukherjee, A.; Park, K. W.; Armijo, E.; Soto, C. Extensive accumulation of misfolded protein aggregates during natural aging and senescence. *Front Aging Neurosci.* **2022**, *14*, 1090109-1090123.
- (182) Halliwell, B. Reactive oxygen species and the central nervous system. *J. Neurochem.* **1991**, *59*, 1609-1623.
- (183) Sala, A. J.; Bott, L. C.; Morimoto, R. I. Shaping proteostasis at the cellular, tissue, and organismal level. *J. Cell Biol.* **2017**, *216* (5), 1231-1241.
- (184) Massaad, C. A.; Klann, E. Reactive oxygen species in the regulation of synaptic plasticity and memory. *Antioxid. Redox. Signal* **2014**, *14*, 2013-2054.
- (185) Koga, S.; Sekiya, H.; Kondru, N.; Ross, O. A.; Dickson, D. W. Neuropathology and molecular diagnosis of Synucleinopathies. *Mol. Neurodegener.* **2021**, *16*, 83-107.
- (186) Spillantini, M. G.; Schmidt, M. L.; Lee, V. M. Y.; Trojanowski, J. Q.; Jakes, R.; Goedert, M. α -Synuclein in Lewy bodies. *Nature* **1997**, *388*, 839-840.
- (187) Fares, M. B.; Jagannath, S.; Lashuel, H. A. Reverse engineering Lewy bodies: how far have we come and how far can we go? *Nat. Rev. Neurosci.* **2021**, *22*, 111-131.
- (188) Heras-Garvin, A.; Stefanova, N. MSA: From basic mechanisms to experimental therapeutics. *Parkinsonism Relat. Disord.* **2020**, *73*, 94-104.
- (189) Alderson, T. R.; Markley, J. L. Biophysical characterization of alpha-synuclein and its controversial structure. *Intrinsically Disord. Proteins* **2013**, *1* (1), 18-39.
- (190) Bisi, N.; Feni, L.; Peqini, K.; Perez-Pena, H.; Ongerì, S.; Pieraccini, S.; Pellegrino, S. α -Synuclein: An all inclusive trip around its structure, influencing factors and applied techniques. *Front. Chem.* **2021**, *9*, 666585-666612.

- (191) Xue, B.; Dunbrack, R. L.; Williams, R. W.; Dunker, A. K.; Uversky, V. N. PONDR-FIT: a meta-predictor of intrinsically disordered amino acids. *Biochim. Biophys. Acta* **2010**, *1804* (4), 996-1010.
- (192) Jakes, R.; Spillantini, M. G.; Goedert, M. Identification of two distinct synucleins from human brain. *FEBS Lett.* **1994**, *345*, 27-32.
- (193) Iwai, A. M., E.; Yoshimoto, M.; Ge, N.; Flanagan, L.; de Silva, H. A.; Kittel, A.; Saitoh, T. The precursor protein of non-A beta component of Alzheimer's disease amyloid is a presynaptic protein of the central nervous system. *Neuron* **1995**, 467-475.
- (194) Bendor, J. T.; Logan, T. P.; Edwards, R. H. The function of alpha-synuclein. *Neuron* **2013**, *79* (6), 1044-1087.
- (195) Bras, I. C.; Outeiro, T. F. Alpha-synuclein: Mechanisms of release and pathology progression in synucleinopathies. *Cells* **2021**, *10*, 375-394.
- (196) Lehtonen, S.; Sonninen, T. M.; Wojciechowski, S.; Goldsteins, G.; Koistinaho, J. Dysfunction of cellular proteostasis in Parkinson's Disease. *Front. Neurosci.* **2019**, *13*, 457-476.
- (197) Sode, K.; Ochiai, S.; Kobayashi, N.; Usuzaka, E. Effect of reparation of repeat sequences in the human α -synuclein on fibrillation ability. *Int. J. Biol. Sci.* **2007**, *3*, 1-7.
- (198) Davidson, W. S.; Jonas, A.; Clayton, D. F.; George, J. M. Stabilization of α -synuclein secondary structure upon binding to synthetic membranes. *J. Biol. Chem.* **1998**, *273*, 9443-9449.
- (199) Rodriguez, J. A.; Ivanova, M. I.; Sawaya, M. R.; Cascio, D.; Reyes, F. E.; Shi, D.; Sangwan, S.; Guenther, E. L.; Johnson, L. M.; Zhang, M.; et al. Structure of the toxic core of alpha-synuclein from invisible crystals. *Nature* **2015**, *525* (7570), 486-490.
- (200) Ueda, K.; Fukushima, H.; Masliah, E.; Xia, Y.; Iwai, A.; Yoshimoto, M.; Otero, D. A.; Kondo, J.; Ihara, Y.; Saitoh, T. Molecular cloning of cDNA encoding an unrecognized component of amyloid in Alzheimer disease. *Proc. Natl. Acad. Sci. U.S.A.* **1993**, *90*, 11282-11286.
- (201) Crowther, R. A.; Jakes, R.; Spillantini, M. G.; Goedert, M. Synthetic filaments assembled from C-terminally truncated α -synuclein. *FEBS Lett.* **1998**, *436*, 309-312.
- (202) Li, W.; West, N.; Colla, E.; Pletnikova, O.; Troncoso, J. C.; Marsh, L.; Dawson, T. M.; Jakala, P.; Hartmann, T.; Price, D. L.; et al. Aggregation promoting C-terminal truncation of α -synuclein is a normal cellular process and is enhanced by the familial Parkinson's disease-linked mutations. *PNAS* **2005**, *102*, 2162-2167.

- (203) Gasser, T.; Hardy, J.; Mizuno, Y. Milestones in PD genetics. *Mov. Disord.* **2011**, *26* (6), 1042-1048.
- (204) Chartier-Harlin, M. C.; Kachergus, J.; Roumier, C.; Mouroux, V.; Douay, X.; Lincoln, S.; Levecque, C.; Larvor, L.; Andrieux, J.; Hulihan, M.; et al. Alpha-synuclein locus duplication as a cause of familial Parkinson's disease. *Lancet* **2004**, *364* (9440), 1167-1169.
- (205) Fuchs, J.; Nilsson, C.; Kachergus, J.; Munz, M.; Larsson, E. M.; Schule, B.; Langston, J. W.; Middleton, F. A.; Ross, O. A.; Hulihan, M.; et al. Phenotypic variation in a large Swedish pedigree due to SNCA duplication and triplication. *Neurology* **2007**, *68* (12), 916-922.
- (206) Singleton, A. B.; Farrer, M.; Johnson, J.; Singleton, A.; Hague, S.; Kachergus, J.; Hulihan, M.; Peuralinna, T.; Dutra, A.; Nussbaum, R.; et al. Alpha-synuclein locus triplication causes Parkinson's disease. *Science* **2003**, *302*, 841-841.
- (207) Polymeropoulos, M. H.; Lavedan, C.; Leroy, E.; Ide, S. E.; Dehejia, A.; Dutra, A.; Pike, B.; Root, H.; Rubenstein, J.; Boyer, R.; et al. Mutation in the alpha-synuclein gene identified in families with Parkinson's disease. *Science* **1997**, *276* (5321), 2045-2047.
- (208) Kruger, R.; Kuhn, W.; Muller, T.; Woitalla, D.; Graeber, M.; Kosel, S.; Przuntek, H.; Eppelen, J. T.; Schols, L.; Riess, O. Ala30Pro mutation in the gene encoding alpha-synuclein in Parkinson's disease. *Nature* **1998**, *18*, 106-108.
- (209) Boyer, D. R.; Li, B.; Sun, C.; Fan, W.; Zhou, K.; Hughes, M. P.; Sawaya, M. R.; Jiang, L.; Eisenberg, D. S. The alpha-synuclein hereditary mutation E46K unlocks a more stable, pathogenic fibril structure. *Proc. Natl. Acad. Sci. U.S.A.* **2020**, *117* (7), 3592-3602.
- (210) Conway, K. A.; Harper, J. D.; Lansbury, P. T. Accelerated in vitro fibril formation by a mutant alpha-synuclein linked to early-onset Parkinson disease. *Nat. Med.* **1998**, *11*, 1318-1320.
- (211) Kaye, R.; Dettmer, U.; Lesne, S. E. Soluble endogenous oligomeric alpha-synuclein species in neurodegenerative diseases: Expression, spreading, and cross-talk. *J. Parkinsons Dis.* **2020**, *10*, 791-818.
- (212) Guerrero-Ferreira, R.; Taylor, N. M.; Mona, D.; Ringler, P.; Lauer, M. E.; Riek, R.; Britschgi, M.; Stahlberg, H. Cryo-EM structure of alpha-synuclein fibrils. *Elife* **2018**, *7*.
- (213) Deger, J. M.; Gerson, J. E.; Kaye, R. The interrelationship of proteasome impairment and oligomeric intermediates in neurodegeneration. *Aging Cell* **2015**, *14*, 715-724.
- (214) Hipp, M. S.; Park, S. H.; Hartl, F. U. Proteostasis impairment in protein-misfolding and -aggregation diseases. *Trends Cell Biol.* **2014**, *24*, 506-514.

- (215) Ma, J.; Gao, J.; Wang, J.; Xie, A. Prion-like mechanisms in Parkinson's disease. *Front. Neurosci.* **2019**, *13*, 552-565.
- (216) Jan, A.; Goncalves, N. P.; Vaegter, C. B.; Jensen, P. H.; Ferreira, N. The prion-like spreading of alpha-synuclein in Parkinson's disease: Update on models and hypotheses. *Int. J. Mol. Sci.* **2021**, *22* (15), 8338-8360.
- (217) Rey, N. L.; Steiner, J. A.; Maroof, N.; Luk, K. C.; Madaj, Z.; Trojanowski, J. Q.; Lee, V. M.; Brundin, P. Widespread transneuronal propagation of alpha-synucleinopathy triggered in olfactory bulb mimics prodromal Parkinson's disease. *J. Exp. Med.* **2016**, *213* (9), 1759-1778.
- (218) Dehay, B.; Vila, M.; Bezard, E.; Brundin, P.; Kordower, J. H. Alpha-synuclein propagation: New insights from animal models. *Mov. Disord.* **2016**, *31* (2), 161-168.
- (219) Ferreira, S. A.; Romero-Ramos, M. Microglia response during Parkinson's disease: alpha-synuclein intervention. *Front. Cell Neurosci.* **2018**, *12*, 247-263.
- (220) Hoenen, C., Gustin, A., Birck, C., Kirchmeyer, M., Beaume, N., Felten, P., Grandbarbe, L., Heuschling, P., Heurtaux, T. Alpha-synuclein proteins promote proinflammatory cascades in microglia: Stronger effects of the A53T mutant. *PLOS One* **2016**, *11* (9).
- (221) Gao, G. M.; Kotzbauer, P. T.; Uryu, K.; Leight, S.; Trojanowski, J. Q.; Lee, V. M. Neuroinflammation and oxidation/nitration of alpha-synuclein linked to dopaminergic neurodegeneration. *J. Neurosci.* **2008**, *30*, 7687-7698.
- (222) Stojkowska, I.; Wagner, B. M.; Morrison, B. E. Parkinson's disease and enhanced inflammatory response. *Exp. Biol. Med.* **2015**, *240* (11), 1387-1395.
- (223) He, Q.; Yu, W.; Wu, J.; Chen, C.; Lou, Z.; Zhang, Q.; Zhao, J.; Wang, J.; Xiao, B. Intranasal LPS-mediated Parkinson's model challenges the pathogenesis of nasal cavity and environmental toxins. *PLoS One* **2013**, *8* (11), e78418.
- (224) Fouka, M.; Mavroeydi, P.; Tsaka, G.; Xilouri, M. In search of effective treatments targeting alpha-synuclein toxicity in synucleinopathies: Pros and cons. *Front. Cell Dev. Biol.* **2020**, *8*, 559791-559823.
- (225) Song, J.; Kim, J.; Lee, M. J.; Ahn, J. H.; Lee, D. Y.; Youn, J.; Chung, M. J.; Kim, Z.; Cho, J. W. Differential diagnosis between Parkinson's disease and atypical parkinsonism based on gait and postural instability: Artificial intelligence using an enhanced weight voting ensemble model. *Parkinsonism Relat. Disord.* **2022**, *98*, 32-37.
- (226) Zhang, Y.; Cao, H.; Liu, Z. Binding cavities and druggability of intrinsically disordered proteins. *Protein Sci.* **2015**, *24*, 688-705.

(227) Deshmukh, F. K.; Sharma, N.; Giri, R. Therapeutic interventions of cancers using intrinsically disordered proteins as drug targets: c-Myc as model system. *Cancer Inform.* **2017**, *16*, 1176935117699408-1176935117699415.

(228) Bekes, M.; Langley, D. R.; Crews, C. M. PROTAC targeted protein degraders: the past is prologue. *Nat. Rev. Drug. Discov.* **2022**, *21* (3), 181-200.

(229) Gao, H.; Sun, X.; Rao, Y. PROTAC Technology: Opportunities and Challenges. *ACS Med. Chem. Lett.* **2020**, *11* (3), 237-240.

(230) Xie, H.; Liu, J.; Alem Glison, D. M.; Fleming, J. B. The clinical advances of proteolysis targeting chimeras in oncology. *Explor. Target Antitumor Ther.* **2021**, *2* (6), 511-521.

(231) Choi, W. H.; de Poot, S. A. H.; Lee, J. H.; Kim, J. H.; Han, D. H.; Kim, Y. K.; Finley, D.; Lee, M. J. Open-gate mutants of the mammalian proteasome show enhanced ubiquitin-conjugate degradation. *Nat. Commun.* **2016**, *7*, 10963-10974.

(232) Fiolek, T. J.; Magyar, C. L.; Wall, T. J.; Davies, S. B.; Campbell, M. V.; Savich, C. J.; Tepe, J. J.; Mosey, R. A. Dihydroquinazolines enhance 20S proteasome activity and induce degradation of alpha-synuclein, an intrinsically disordered protein associated with neurodegeneration. *Bioorg. Med. Chem. Lett.* **2021**, *36*, 127821-127826.

(233) Osmulski, P. A.; Karpowicz, P.; Jankowska, E.; Bohmann, J.; Pickering, A. M.; Gaczynska, M. New peptide-based pharmacophore activates 20S proteasome. *Molecules* **2020**, *25* (6), 1439-1456.

(234) Coleman, R. A.; Muli, C. S.; Zhao, Y.; Bhardwaj, A.; Newhouse, T. R.; Trader, D. J. Analysis of chain length, substitution patterns, and unsaturation of AM-404 derivatives as 20S proteasome stimulators. *Bioorg. Med. Chem. Lett.* **2019**, *29* (3), 420-423.

(235) Trader, D. J.; Simanski, S.; Dickson, P.; Kodadek, T. Establishment of a suite of assays that support the discovery of proteasome stimulators. *Biochim. Biophys. Acta. Gen. Subj.* **2017**, *1861* (4), 892-899.

(236) Zhou, H.; Shao, M.; Guo, B.; Li, C.; Lu, Y.; Yang, X.; ShengnanLi; Li, H.; Zhu, Q.; Zhong, H.; et al. Tetramethylpyrazine analogue T-006 promotes the clearance of alpha-synuclein by enhancing proteasome activity in Parkinson's disease models. *Neurotherapeutics* **2019**, *16* (4), 1225-1236.

(237) Thomas, T. A.; Smith, D. M. Proteasome activator 28gamma (PA28gamma) allosterically activates trypsin-like proteolysis by binding to the alpha-ring of the 20S proteasome. *J. Biol. Chem.* **2022**, *298* (8), 102140-102153.

- (238) Rabl, J.; Smith, D. M.; Yu, Y.; Chang, S. C.; Goldberg, A. L.; Cheng, Y. Mechanism of gate opening in the 20S proteasome by the proteasomal ATPases. *Mol. Cell* **2008**, *30* (3), 360-368.
- (239) Gillette, T. G.; Kumar, B.; Thompson, D.; Slaughter, C. A.; DeMartino, G. N. Differential roles of the COOH termini of AAA subunits of PA700 (19 S regulator) in asymmetric assembly and activation of the 26 S proteasome. *J. Biol. Chem.* **2008**, *283* (46), 31813-31822.
- (240) Gizynska, M.; Witkowska, J.; Karpowicz, P.; Rostankowski, R.; Chocron, E. S.; Pickering, A. M.; Osmulski, P.; Gaczynska, M.; Jankowska, E. Proline- and Arginine-rich peptides as flexible allosteric modulators of human proteasome activity. *J. Med. Chem.* **2019**, *62* (1), 359-370.
- (241) Dal Vechio, F. H.; Cerqueira, F.; Augusto, O.; Lopes, R.; Demasi, M. Peptides that activate the 20S proteasome by gate opening increased oxidized protein removal and reduced protein aggregation. *Free Radic. Biol. Med.* **2014**, *67*, 304-313.
- (242) Lau, J. L.; Dunn, M. K. Therapeutic peptides: Historical perspectives, current development trends, and future directions. *Bioorg. Med. Chem.* **2018**, *26* (10), 2700-2707.
- (243) Huang, L.; Ho, P.; Chen, C. H. Activation and inhibition of the proteasome by betulinic acid and its derivatives. *FEBS Lett.* **2007**, *581* (25), 4955-4959.
- (244) Huang, L.; Chen, C. H. Proteasome regulators: Activators and inhibitors. *Curr. Med. Chem.* **2009**, *10*, 931-939.
- (245) Kumar, B.; Kim, Y. C.; DeMartino, G. N. The C terminus of Rpt3, an ATPase subunit of PA700 (19 S) regulatory complex, is essential for 26 S proteasome assembly but not for activation. *J. Biol. Chem.* **2010**, *285* (50), 39523-39535.
- (246) Vanecek, A. S.; Mojsilovic-Petrovic, J.; Kalb, R. G.; Tepe, J. J. Enhanced degradation of mutant C9ORF72-derived toxic dipeptide repeat proteins by 20S proteasome activation results in restoration of proteostasis and neuroprotection. *ACS Chem. Neurosci.* **2023**, *14* (8), 1493-1448.
- (247) Hansch, C.; Leo, A. J. Substituent constant for correlation analysis in chemistry and biology. *J. Med. Chem.* **1979**, *20*, 304-306.
- (248) van de Waterbeemd, H.; Cameish, G.; Folkers, G.; Chretien, J. R.; Raevsky, O. A. Estimation of blood-brain barrier crossing of drugs using molecular size and shape, and H-bonding characteristics. *J. Drug Target* **1998**, *6*, 151-165.
- (249) Fichert, T.; Yazdanian, M.; Proudfoot, J. R. A structure-permeability study of small drug-like molecules. *Bioorg. Med. Chem. Lett.* **2003**, *13*, 719-722.

(250) Levin, V. A. Relationship of octanol/water partition coefficient and molecular weight to rat brain capillary permeability. *J. Med. Chem.* **1980**, 23, 682-684.

(251) van de Waterbeemed, H.; Atkinson, F.; Cole, S.; Green, C. Lipophilicity and other parameters affecting brain penetration. *Cent. Nerv. Syst. Agents Med. Chem.* **2002**, 2, 229-240.

(252) Hansch, C.; Bjorkroth, J.; Leo, A. J. Hydrophobicity and centralnervous system agents: on the principle of minimal hydrophobicity in drug design. *Pharm. Sci.* **1987**, 76, 663.

(253) Osterberg, T.; Norinder, U. Prediction of polarsurface area and drug transport processes using simple parameters and PLS statistics. *J. Chem. Inf. Comput. Sci.* **2000**, 40, 1408-1411.

(254) Leeson, P. D.; Davis, A. M. Time-related differences in the physical property profiles of oral drugs. *J. Med. Chem.* **2004**, 47, 6338-6348.

CHAPTER TWO

Design, Development, and Biological Evaluation of Novel Chlorpromazine Analogues as 20S Proteasome Enhancers

2.1 Introduction

An estimated 6 million Americans aged 65 and up suffer from Alzheimer's disease (AD) and 1 million from Parkinson's disease (PD).¹ Despite the prevalence of these neurodegenerative diseases, therapeutics that can halt or slow down their progression remain scarce. Currently, there is only one FDA-approved therapeutic for AD, donanemab, and none for the treatment of PD or other neurodegenerative diseases. Donanemab is a humanized IgG1 antibody that recognizes an N-terminal pyroglutamate A β epitope, which may show efficacy in early-onset AD patients.³ Furthermore, as the population ages, the occurrence of these neurodegenerative diseases is predicted to increase due to the rise of mitochondrial dysfunction incidence, leading to amassed production of free radicals and oxidative stress.⁴ In addition, an age-related decline in the activity of crucial degradation pathways, such as the ubiquitin-proteasome system, gives rise to abnormal deposits of neuronal-based proteins.^{5, 6, 7}

The major component of the neuronal deposits seen in AD and PD are proteins that lack a stable 3D conformation classified as IDPs, such as α -synuclein and amyloid- β .^{8, 9, 10} Specifically in PD, neuronal deposits termed Lewy Bodies result from the accumulation of an IDP predominantly found in dopaminergic neurons, called α -synuclein.¹¹ While most PD cases are sporadic, genetic mutations are linked to the familial forms of PD,¹² including a missense mutation with an alanine exchanged for a threonine, A53T. The A53T mutated α -synuclein is expressed and aggregates at a higher rate than wild-type α -synuclein.^{13, 14, 15} Although there has been little success in directly targeting IDPs themselves, activation of the proteasome-mediated degradation pathway is a promising new approach to prevent IDP accumulation.^{16, 17, 18, 19}

The proteasome is responsible for the degradation of most intracellular proteins, including redundant, oxidatively damaged, and IDPs, as detailed in **Chapter 1**.²⁰ However, exogenous proteasome activators, such as small molecules or peptides, remain scarce.^{21,22, 23} In addition to the imidazolines,²¹ the Tepe group identified additional classes of 20S proteasome activators, the dihydroquinazolines²⁴ and analogs of the FDA-approved therapeutic, fluspirilene.²⁵ Furthermore, as mentioned, the Trader and Kodadek groups identified two promising 20S proteasome activators, AM-404 and MK-866.^{26, 27} Considering the relatively high μM activity that many of these agents display, more potent 20S proteasome enhancers are needed to investigate the clinical potential of this new therapeutic paradigm.

To meet the need for more potent 20S proteasome enhancers, the Tepe lab conducted a high throughput screen of the NIH Health Clinical Collection and the Prestwick Libraries, identifying an FDA-approved neuroleptic D2R agonist, chlorpromazine (CPZ) as a 20S proteasome activator.²³ CPZ is a first generation antipsychotic for the treatment of schizophrenia.²⁸ CPZ treats the positive symptoms (hallucinations, delusions, disordered speech, etc.) of schizophrenia by blocking the dopamine 2-receptors (D2R) activity.^{29, 30} Through extensive SAR studies and space-filling computational models, the critical structural components needed for the interaction between CPZ and the D2Rs were identified.^{31, 32} The protonation of the alkylamine side chain is essential for CPZ's interaction with the D2R receptors, which is required for neuroleptic activity.^{33, 34, 35} While CPZ's primary interaction is with D2R, it is a highly promiscuous drug,³⁰ interacting with muscarinic, histamine, and adrenergic receptors, accounting for side effects such as dry

mouth, drowsiness, and hypotension.^{29, 36} Therefore, developing CPZ analogs as a viable neurodegenerative therapeutic requires abolishing the interaction with the D2R.

Previously, Dr. Corey Jones focused on developing CPZ analogs that have diminished D2R activity but maintain or improve 20S proteasome stimulation. He focused on the substitution of the dimethylamine side chain, producing a phenothiazine with an aryl ester tail (CJ-7-42) (**Figure 2.1A**).²³ The development of CJ-7-42 represented the most drug-like analog in this study and exhibited the highest 20S proteasome activation with no detectable D2R activity.²³ However, a more potent and efficient small molecule activator remained desirable to investigate the therapeutic effects of 20S proteasome activation. I returned to the structure of the parent compound, CPZ, to design and synthesize additional analogs to evaluate the various structural components of CPZ, such as the core, pendant group, and methylene chain linker that are depicted in **Figure 2.1B**. In **section 2.2**, the apparent planarity of the phenothiazine core was first evaluated. **Section 2.3** described the alteration of the dimethyl amine tail and its impact on 20S proteasome activity. Finally, **section 2.4** explored the substitution of alternative heterocycles as the core group to identify alternatives to the problematic phenothiazine motif. From the studies I conducted, potent and efficient small molecules were identified that displayed significantly improved potency. The potency shown by the CPZ analogs also translated to cellular models by substantially preventing the accumulation of pathological A53T α -synuclein at $< 1 \mu\text{M}$ concentrations.^{2, *Second paper has been submitted to iScience.}

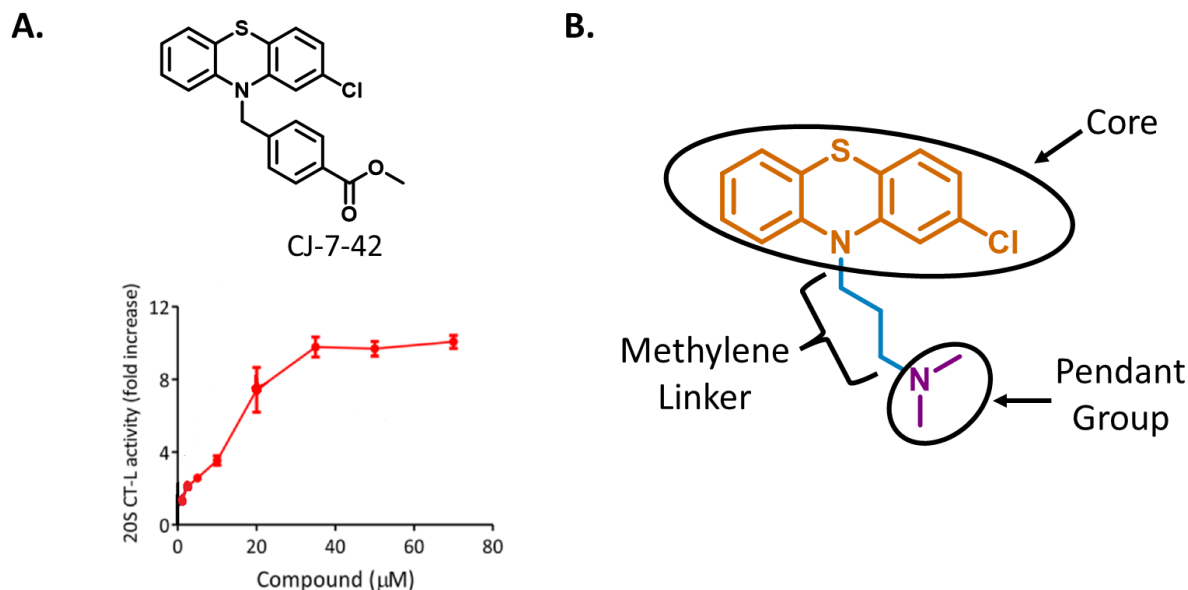


Figure 2.1: Chlorpromazine modification and functional group classification.

(A) The structure of CJ-7-42 and the enhancement of CT-L site of the 20S proteasome treated with CJ-7-42.²³ (B) The structure of chlorpromazine and the classification of the core, methylene linker, and pendant group.

2.2 Series I Chlorpromazine Analogs

2.2.1 Rational

The first question I wanted to answer while designing new Chlorpromazine analogs was: what structural features were needed to stimulate the 20S proteasome? To answer this, I first looked at the apparent planarity of phenothiazines and its effect on 20S proteasome stimulation (**Figure 2.2A-C**). I set out to synthesize Chlorpromazine analogs that maintained two aryl rings connected by nitrogen but lacked planarity. A series of diphenylamine analogs that maintained the dimethylamine tail were first synthesized. Then, I wanted to compare the diphenylamine analogs' activity with analogs containing a

planar core structure, such as a carbazole. Using a carbazole core may also shed light on the impact of the sulfur on 20S proteasome stimulation.

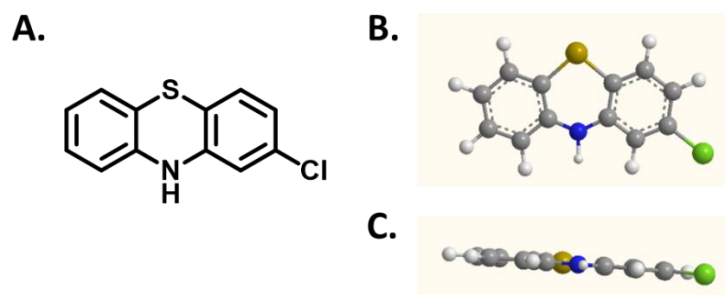


Figure 2.2: Planarity of the phenothiazine core.

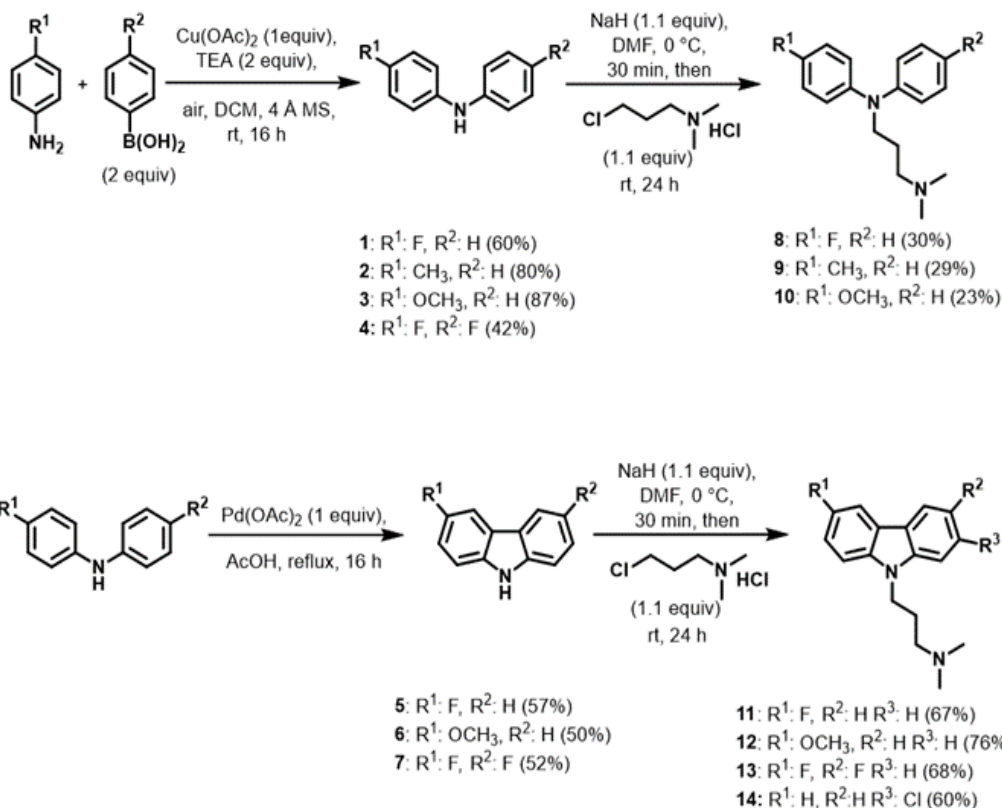
(A) The structure of the phenothiazine core. (B) Face-on and (C) bottom view of a 3D rendering of 2-chlorophenothiazine.

2.2.2 Synthesis of Series I Chlorpromazine Analogs

I coupled a substituted aniline with either phenylboronic acid or a para-substituted phenylboronic acid to synthesize the diphenylamine core. I treated the mixture with CuOAc_2 , a weak base, and an oxidant, typically atmospheric air. Initially, K_2CO_3 was used as the base,³⁷ and the reaction vessel was exposed to atmospheric air, giving low and highly variable yields. I exchanged the K_2CO_3 for TEA, which has been reported to provide higher yields to a larger scope of substrates.³⁸ The atmospheric air was maintained as the oxidant through an unattached needle added into a septum on the round bottom flask. These conditions produced yields of 20-30% for the same substrate. However, excess water can inhibit the reaction from proceeding.³⁸ In the middle of a Michigan summer, the humidity of the atmospheric air varied drastically from week to week, potentially accounting for the inconsistent yields. To address this variability, I replaced the unattached needle with a balloon filled with oxygen, and 4 Å molecular sieves were

added, producing moderate and more consistent yields ranging from 42% to 88% depending on the starting material. Using the optimized conditions, phenylboronic acid was added to a mixture of substituted aniline, CuOAc₂, TEA, and 4 Å molecular sieves in DCM (**Scheme 2.1**).³⁸ Four diphenylamine cores were synthesized (compounds **1** to **4**) with 42% to 88% yields.

The freshly synthesized diphenylamine cores were carried forward in two reactions: the formation of carbazoles and the coupling with the dimethylamine tail seen in chlorpromazine. Three carbazoles were synthesized via oxidative PdOAc₂ catalyzed cross-coupling.³⁹ Compounds **1**, **3**, and **4** were added to a solution of PdOAc₂ in AcOH and refluxed for 16 hours (**Scheme 2.1**).⁴⁰ The fluoro, methoxy, and bis-fluoro substituted carbazoles, compounds **5-7**, were synthesized in 50% to 57% yield (**Scheme 2.1**).



Scheme 2.1: The synthetic pathway to produce compounds 1-14.

For the synthesis of the final analogs, compounds **1-3**, **5-7**, and a purchased 3-chloro-carbazole were treated with 3-chloro-dimethylaminopropane HCl salt in the presence of NaH in DMF, producing compounds **8-13** (Scheme 2.1) in yields ranging from 23% to 78%. However, the addition of the 3-chloro-dimethylaminopropane to the bis(4-fluorophenyl) amine was unsuccessful. In addition, the coupling with the diphenylamine cores produced significantly lower yields, likely due to the generally reduced nucleophilicity compared to the carbazole counterparts. Diphenylamines have rotatable bonds that could produce conformations that block the lone pair of electrons on the

nitrogen from interacting with the alkyl halide. It has been reported that the alkylation of bis(4-fluorophenyl)amine can occur at higher temperatures in moderate yields.^{41, 42} When I attempted to heat the reaction mixture, no product formation was seen, attributed to extensive side reactions occurring with the 3-chloro-dimethylaminopropane as it has been reported to polymerize, in addition to the formation of four-membered rings in the presence of heat.⁴³

2.2.3 Initial Evaluation of Series I Analogs Activity Towards the 20S Proteasome

The activity of compounds **8-14** towards the 20S proteasome was assessed by utilizing the standard fluorogenic 7-amino-methylcoumarin (AMC) conjugated small peptide substrates that correspond to each of the catalytic sites in the 20S proteasome: chymotrypsin-like site (Suc-LLVY-AMC), caspase-like site (Z-LLE-AMC), and trypsin-like site (Boc-LRR-AMC).^{21, 23, 27} When the 20S proteasome degrades the small peptide substrate, the AMC fluorophore is released, resulting in a fluorescent emission. The fluorescence is then quantified to measure the rate of proteolytic cleavage. Treating the 20S proteasome with varying concentrations of the drug of interest allowed for the determination of the EC₂₀₀. Compounds were added to wells that contained 0.5 nM of purified human proteasome in a 6-point titration with final concentrations from 1.25 μM to 80 μM.

The overall enhancement of the rate of proteolysis of the 20S proteasome by a small molecule was first evaluated by adding a combination of all three peptide substrates to the treated sample. The combination of all three substrates represents a more accurate measurement of proteolytic activity of the proteasome because the catalytic sites housed

in the β ring of the 20S proteasome communicate through allosteric interactions.⁴⁴ For example, when a protein substrate encounters the chymotrypsin-like site, a conformational change will occur activating the caspase-like site.⁴⁴ The fluorescent output, due to release of the AMC fluorophore, was then converted to the fold increase compared to a vehicle control sample. However, there was no fold increase identified, the small peptide assay revealed that none of the series one compounds were active (**Figure 2.3**).

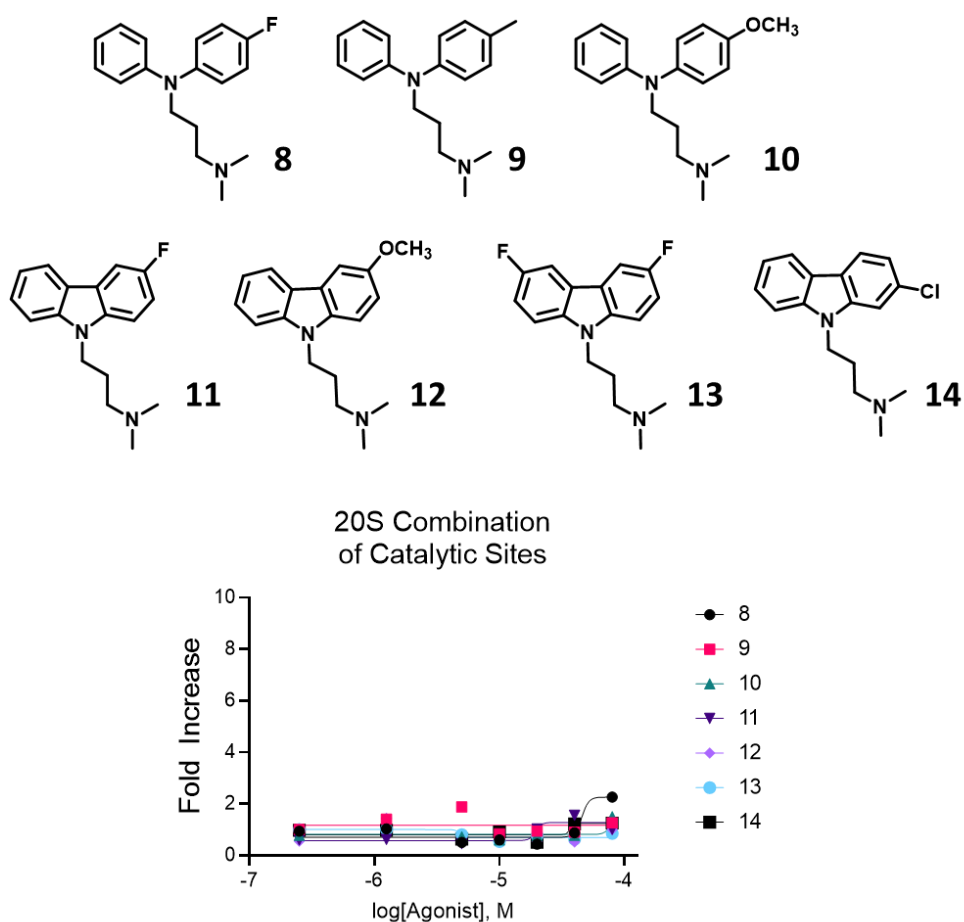


Figure 2.3: Structure and Inactivity of compounds 8-14 towards the 20S.

2.3 Series II Chlorpromazine Analogs

2.3.1 Rational

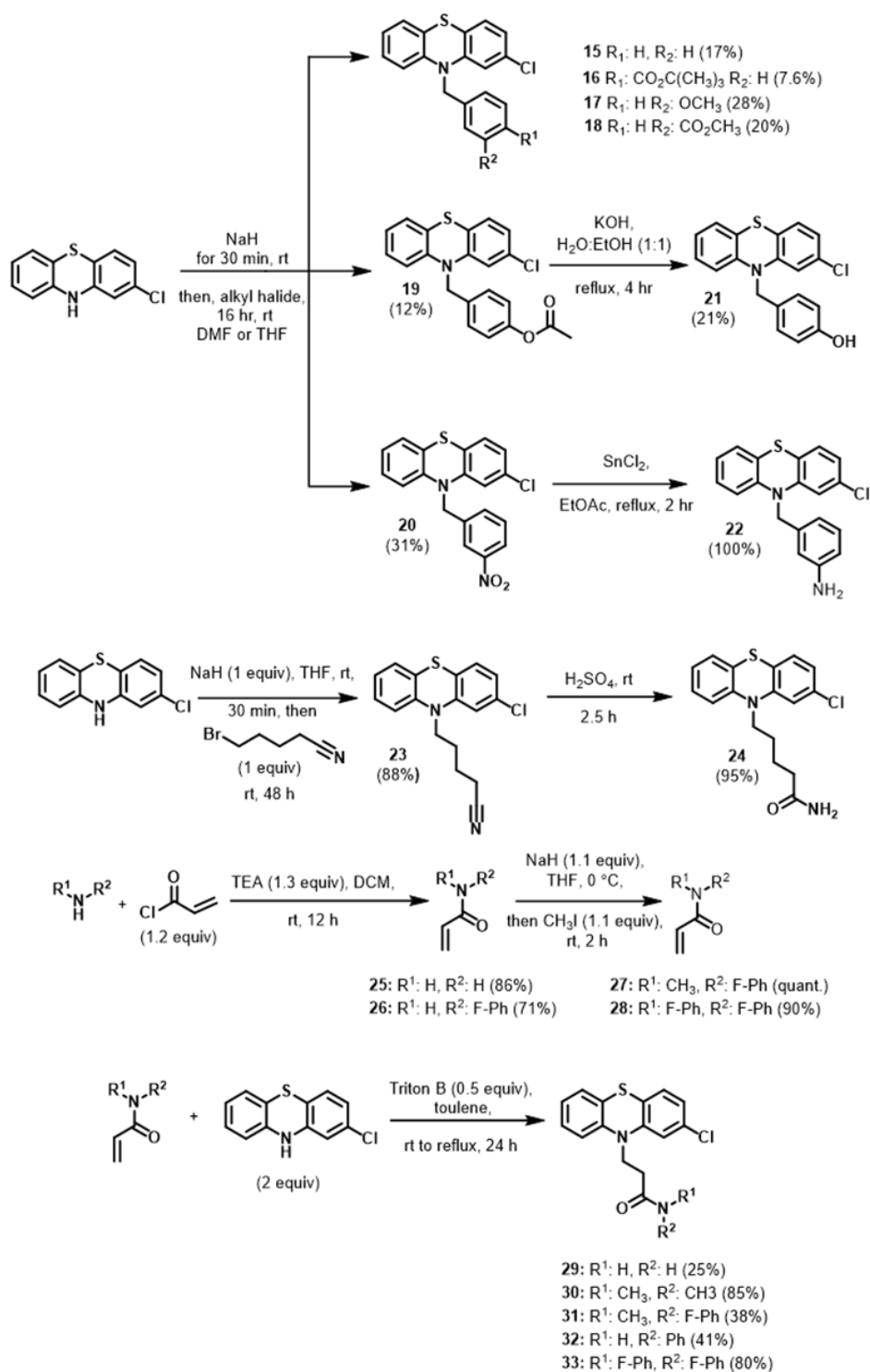
As described, none of the diphenylamine or the carbazole analogs showed any promising 20S proteasome stimulation. Thus, I turned my attention towards altering the dimethylamine tail of CPZ. However, Dr. Jones explored the alteration of the 2-chlorophenothiazine core coupled to the benzyl ester pendant group seen in CJ-7-42, producing molecules that displayed no activity towards the 20S proteasome. Building off the work that Dr. Jones had done, I continued in the development of CPZ analogs that had alternative pendant groups.

2.3.2 Synthesis of Series II Chlorpromazine Analogs

In our quest to identify a more robust pendant group, Dr. Jones and I investigated different benzyl- and amide-based pendant groups. Dr. Jones began by synthesizing compounds **15-24**. As a control, Dr. Jones synthesized a non-substituted benzyl group (**15**) by treating 2-chlorophenothiazine with NaH followed by the addition of (bromomethyl)-benzene (**Scheme 2.2**).² Similarly, a general procedure of deprotonating 2-chlorophenothiazine with NaH and then adding a halogenated benzyl group was used to prepare compounds **16-20** (**Scheme 2.2**).² The role of the aryl ester moiety in activating the 20S proteasome was explored by substituting the ester with carboxylate or an alcohol. The carboxylate derivative (**19**) was prepared by treating 2-chloro-phenothiazine with NaH and 4-(bromomethyl)phenyl acetate. Compound **19** was then treated with KOH to produce the alcohol derivative (**21**). Next, the impact of the size of the substituent was investigated by exchanging the methyl ester with a tert-butyl ester to provide compound **16**. To examine

the effect of different substituents on the meta position, benzyl derivatives that were substituted in the meta position with an ether (**17**), ester (**18**), and amine (**22**) were synthesized. The original parent compound, CPZ, contains a dimethylamine group attached to the phenothiazine core by a 3-carbon linker. Compound **22** was designed to mimic the amine pendant group (albeit a less basic one) while maintaining the benzyl moiety by converting a nitro group to an amine. The nitro-benzyl (**20**) group was added to the 2-chlorophenothiazine group using the abovementioned general procedure. The nitro moiety was then reduced using SnCl₂ to generate compound **22** in quantitative yields (**Scheme 2.2**).²

Next, we investigated the scope of the pendant motifs on the phenothiazine core. New pendant moieties were designed to mimic the dimethyl amine group of CPZ. The clinical neuroleptic activity of CPZ is largely attributed to its interaction with the D2R, which requires protonation of the dimethylamine group of CPZ.^{45,46} Therefore, the interaction with the D2R can be abrogated using less basic nitrogen, such as amides or anilines in the pendant position.^{33, 34} In addition to altering the basicity, the length of the methylene linker was modified to investigate the effect of flexibility and distance on 20S proteasome activation. An amide containing compound, **24**, was prepared via the nitrile intermediate (**23**) obtained by treating 2-chlorophenothiazine with 5-bromovaleronitrile. The nitrile group was then converted to the amide in a 95% yield using an H₂SO₄ catalyzed hydrolysis (**Scheme 2.2**).²



Scheme 2.2: The synthetic pathways to produce compounds 23-33.

A second amide containing compound, **29**, was synthesized to compare the two-methylene chain seen in CPZ to the four-methylene linker (**24**). The amide was further modified to include additional substituents. Compound **30** was designed to have a similar pendant to the parent compound CPZ, in the form of a dimethylamide.² Based on the activity displayed by CJ-7-42, I explored other pendant groups containing aromatic moieties. An *N*-methyl-*N*-(4-fluorophenyl)acrylamide was coupled with 2-chlorophenothiazine in the presence of Triton B, producing compound **31** (38%). Then, an unsubstituted anilide was installed and the secondary amide derivative (**32**) was synthesized (**Scheme 2.2**).

Finally, I designed compound **33** to mimic the disubstituted amine group of CPZ, but with an electron depleted nitrogen to prevent *N*-protonation. The bis(fluorophenyl) amine starting material was synthesized using a Chan-Lam-Evans like coupling that was previously reported.³⁸ The bis(fluorophenyl) amine was transformed to acrylamide (**28**) by treating the amine with acryloyl chloride and TEA in DCM and refluxed overnight. The acryl amide was coupled to the 2-chlorophenothiazine core using Triton B in toluene and then refluxed for 24 hours, resulting in compound **33** (50%) (**Scheme 2.2**).

2.3.3 Initial Evaluation of Series II Analogs Activity Towards the 20S Proteasome

The activity of compounds **15-24** and **29-33** towards the 20S proteasome was then assessed using the standard fluorogenic 7-amino-methylcoumarin (AMC) conjugated small peptide assay, described in **section 2.2.3**. The desired compounds were added to wells that contained 0.5 nM of purified human proteasome in a 6-point titration with final concentrations from 1.25 μ M to 80 μ M. The overall enhancement of the rate of 20S

proteasome proteolysis by a small molecule was first evaluated by adding an equimolar mixture of all three peptide substrates to the treated sample. The combination of all three substrates represents a more accurate measurement of the proteolytic activity of the proteasome because the catalytic sites housed in the β ring of the 20S proteasome communicate through allosteric interactions. For example, when a protein substrate encounters the chymotrypsin-like site, a conformational change activates the caspase-like site.⁴⁴ The individual contribution of each of the three catalytic sites was subsequently evaluated by adding only the corresponding peptide probes to gain insight into the contribution of each site on the overall enhanced proteolytic activity. Due to the release of the AMC fluorophore, the fluorescent output was converted to the fold increase compared to a vehicle control sample, and the EC_{200} was calculated. To rigorously eliminate false positives due to minor changes in background activity (0-20%), compounds that exhibited a maximum fold enhancement of <2 fold (i.e., <200%) at a concentration >20 μ M were considered inactive (**Table 2.1**).

Several derivatives of CPZ significantly enhanced 20S-mediated proteolysis. The unsubstituted benzyl derivative (**15**) enhanced 20S proteasome-mediated proteolysis 2-fold (i.e., 200% increase over vehicle control) at a relatively low EC_{200} of 1.5 μ M. Compound **15**'s overall rate of proteolysis appeared to be due to the enhanced activity at the chymotrypsin-like and trypsin-like sites. The *tert*-butyl ester (**16**), the acetate (**19**), and hydroxyl (**21**) derivatives were all deemed inactive as they did not reach a 200% increase in proteasome activity. Analog **17** has an EC_{200} of 1.5 μ M, like compound CJ-7-42 (1.4 μ M). Compound **17** is less than half as efficient as CJ-7-42 (maximum fold of 4),

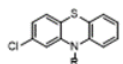
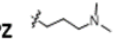
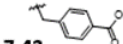
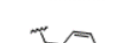
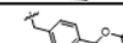
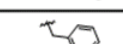
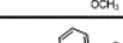
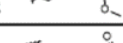
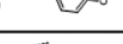

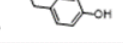
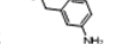
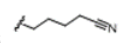
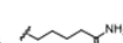
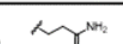
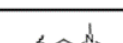
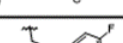
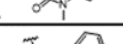
 CPZ	CT-L/Casp-L/ T-L		Casp-L site		T-L site		CT-L site	
	EC ₂₀₀	Max Fold	EC ₂₀₀	Max Fold	EC ₂₀₀	Max Fold	EC ₂₀₀	Max Fold
	13.5 μM	4	>80 μM	--	>80 μM	--	7 μM	8
	1.4 μM	9	2.7 μM	7	2.6 μM	15	1.9 μM	12
	1.5 μM	2	>80 μM	--	3.1 μM	2	2.8 μM	3
	>80 μM	--	>80 μM	--	>80 μM	--	>80 μM	--
	1.5 μM	4	1.3 μM	4	5.4 μM	2	>80 μM	--
	2.4 μM	6	9.7 μM	4	1.9 μM	8	2.4 μM	6
	>80 μM	--	>80 μM	--	>80 μM	--	>80 μM	--
	1.1 μM	8	1.2 μM	12	1.6 μM	8	1.1 μM	9
	>80 μM	--	>80 μM	--	>80 μM	--	>80 μM	--
	3.6 μM	8	3.8 μM	10	9.2 μM	10	6.5 μM	9
	>80 μM	--	>80 μM	--	>80 μM	--	>80 μM	--
	>80 μM	--	>80 μM	--	>80 μM	--	>80 μM	--
	>80 μM	--	>80 μM	--	>80 μM	--	>80 μM	--
	>80 μM	--	>80 μM	--	>80 μM	--	>80 μM	--
	>80 μM	--	>80 μM	--	>80 μM	--	>80 μM	--
	40 μM	2.5	>80 μM	--	80 μM	2	>80 μM	--
	0.4 μM	11	1.8 μM	9.4	0.3 μM	6	0.7 μM	9.4

Table 2.1 (on previous page): Enhancement of the combination and individual catalytic sites of the 20S proteasome with compounds 15-24 and 29-33.²

The rate increases in proteolytic degradation of the combination of the Suc-LLVY-AMC, the chymotrypsin-like probe (CT-L), Z-LLE-AMC, the caspase-like probe (Casp-L), and Boc-LRR-AMC, the trypsin-like probe (T-L), and of the rate of degradation of

Table 2.1 (cont'd)

each individual probe, by purified human 20S proteasome treated with compounds **15-24** and **29-33** is displayed. The activity is categorized as max fold and EC₂₀₀. The EC₂₀₀ represents the concentration needed to double (i.e. 200%) the rate of substrate degradation compared to vehicle control. Max fold is the maximum fold rate increase compared to vehicle control.

suggesting that either the carbonyl group aids activation and/or it may impact the interactions of the benzyl ring. Interestingly, the meta derivative of CJ-7-42 (**18**) had a higher EC₂₀₀ (2.4 μM) but a lower maximum fold increase of 6 (i.e., a 600% increase over vehicle control). In contrast, compound **20** had a similar maximum fold increase of 8 (i.e., 800% increase over vehicle control) and had a relatively low EC₂₀₀ (1.1 μM). The transformation of the nitro group into the primary amine did not affect the overall 20S proteasome activation but did raise the EC₂₀₀ (3.6 μM). Overall, the alterations of the benzyl group did not result in a drastic change in potency or efficiency.

The alterations of the original aliphatic amine group of CPZ yielded less straightforward results. Compounds **23**, **24**, **29**, **30**, and **31** were inactive, and compound **32** showed low activation (maximum 2.5-fold increase over vehicle control). Remarkably, adding two aryl groups to the nitrogen enhances 20S proteasome activation significantly. Compound **33** was by far the most potent 20S proteasome activator, with an overall EC₂₀₀ of 0.4 μM. The potency of compound **33** is significant as it is the first reported sub-μM 20S proteasome activator. Compound **33** displayed a maximum 11-fold (i.e., 1100% increase over vehicle control) enhancement of the proteolytic activity of the 20S proteasome, with

potent EC_{200} values and fold enhancements of each of the three catalytic sites. Compound **33** activated the trypsin-like, chymotrypsin-like, and caspase-like sites with an EC_{200} of 0.3 μ M (6-fold maximum enhancement), an EC_{200} of 0.7 μ M (9.4-fold maximum enhancement), and an EC_{200} of 1.8 μ M, (9.4-fold maximum enhancement), respectively. The enhancement of the 20S proteasome by compound **33** was then compared to CJ-7-42 and CPZ (**Figure 2.4**).

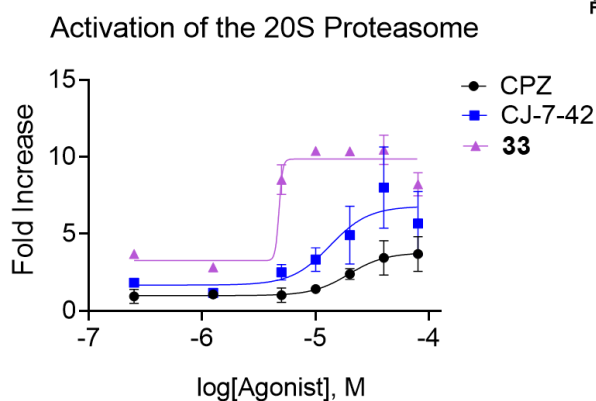
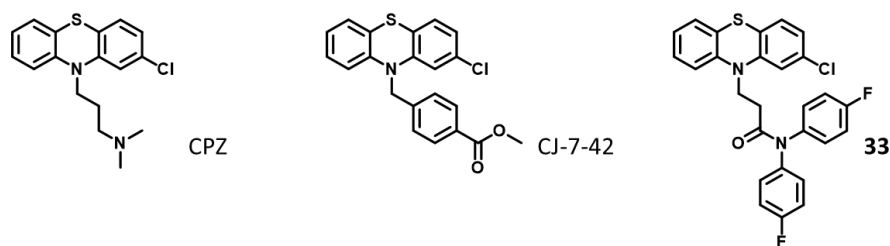


Figure 2.4: The comparison of the enhancement of the 20S proteasome by CPZ, CJ-7-42, and compound **33.**

Fold increase in proteolytic degradation of an equimolar mixture of three fluorogenic peptide probes (Suc-LLVY-AMC, Z-LLE-AMC and Boc-LRR-AMC) treated 20S proteasome in the presence of a concentration range (0-80 μ M) of either CPZ, CJ-7-42, or compound **33**, compared to vehicle control. Data was collected in triplicate (n=3).

2.3.4 Predicted Interactions of Series II Analogs with the 20S Proteasome, Utilizing Molecular Docking

We have previously reported that molecular docking studies clarify the interaction of our compounds with the 20S proteasome.^{23, 25} Herein, I extended the unbiased molecular docking to propose key interactions between the reported compounds and the amino acid residues within the α 1/2 pocket.² Prior docking studies indicate that the CPZ analogue, CJ-7-42, primarily binds in the α 1/2 pocket and possibly interacts with several amino acid residues.²³ We hypothesized that a single amino acid is an anchor point for these small molecules. With the addition of the compounds in series II, a more extensive molecular docking analysis is possible, allowing for the comparison of common amino acid interactions. To perform these studies, I followed the same procedure we utilized previously and further used Discovery Visualizer to investigate further individual interactions with the amino acids in the α 1/2 pocket. ²³ An analysis of the interactions between the amino acids and the active compounds revealed the dominance of CYS161 and TYR159 (**Figure 2.5**). Each of the active compounds had some interaction with these amino acids. However, not all the interactions were of the same type. TYR159 interacts with the active compounds through both parallel π - π stacking and T-shaped π - π stacking, while the inactive compound **19** only interacts through T-shaped π - π stacking, indicating that parallel π - π stacking may be a required interaction. Furthermore, considering the potency difference between compounds **20** and **22**, this interaction may have some “aromatic donor-acceptor” characteristics. The electron-rich benzyl derivative, **22**, is 3x less potent than its electron-poor counterpart, **20**. It has been reported that “face-centered” stacking is often favored during this aromatic donor-acceptor interaction and

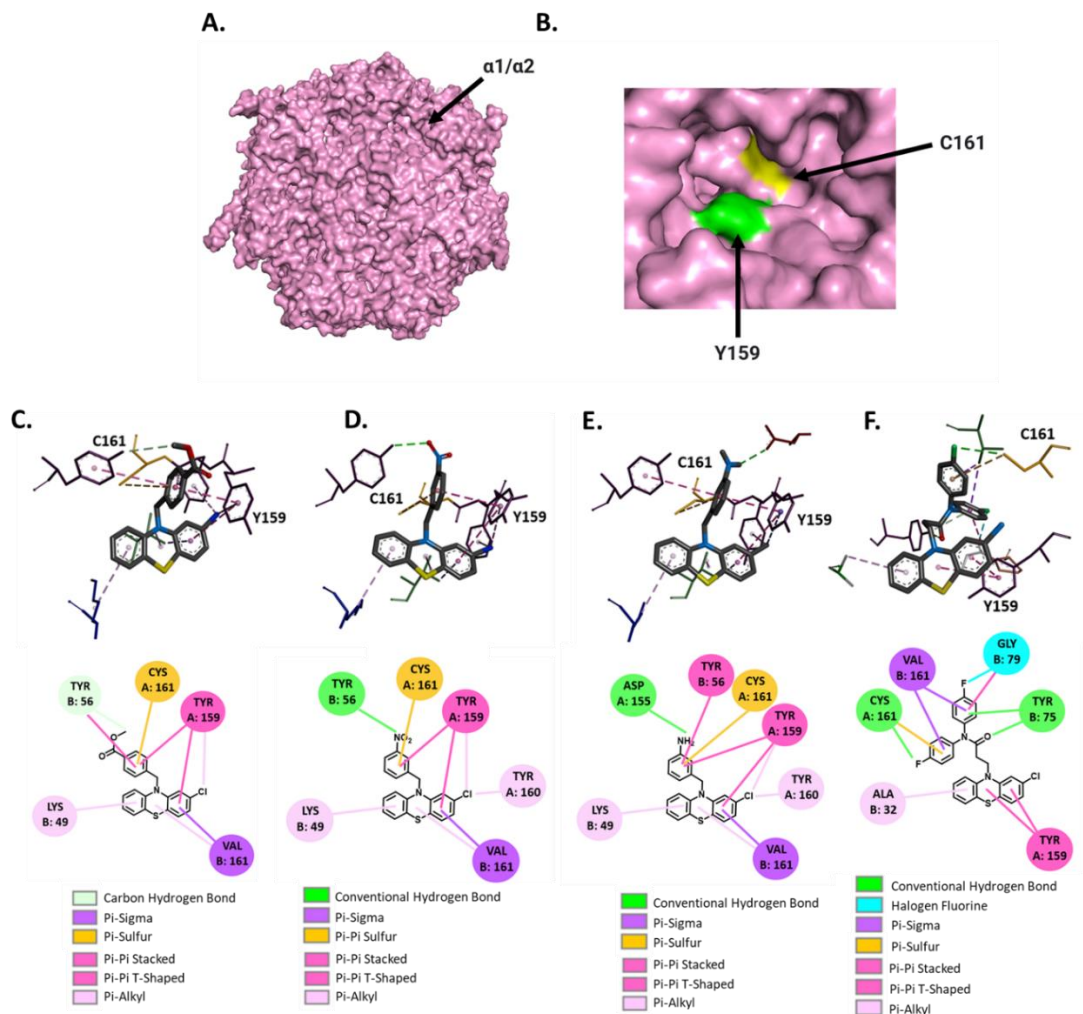


Figure 2.5: The unbiased molecule docking predicted interactions with the compounds 20, 22, 33, and CJ-7-42 with the 20S proteasome. ²

(A) Preferred docking site of CPZ analogs, utilizing Autodock Vina and PyMol, in the $\alpha 1$ -2 intersubunit pocket of the 20S proteasome. (B) Location of two amino acid residues of interest, TYR159 and CYS161. (C) Predicted binding interaction of CJ-7-42, (D) compound **20**, (E) compound **22**, (F) and compound **33**, viewed using BIOVIA Discovery Studio 2020. *20S Proteasome: PDB 4R30

the electron depletion impacts the strength of stacking, as the more electron-deficient arenes stack effectively to the electron-rich donor.⁴⁷ The common interaction types between the active compounds the TYR159 strongly suggest that π - π stacking is a critical interaction between the small molecules and the α 1/2 pocket and requires further exploration. CYS161 interacts with the molecules through either sulfur- π or sulfur-alkyl interactions. Compounds **15**, **17**, **18**, and **32** interact with CYS161 through an edge-on π -sulfur interaction. The weak sulfur-alkyl interaction could explain the diminished activity of the molecules. CJ-7-42 and compounds **20**, **22**, and **33**, are the most potent and efficient small molecules reported and are predicted to interact with CYS161 through an edge-on π -sulfur interactions (**Figure 2.5**). In literature, *ab initio* calculations have been used to determine the ideal geometry for cysteine-pi interactions, identifying an abundance of strong edge-on cysteine- π interactions,^{48, 49} leading us to believe that CYS161 may be paramount for 20S proteasome activation.²

2.3.5 Impact of Series II Analog Enhancement of 20S Proteasome Activity on the Rate of Degradation of Pathogenic Intrinsically Disordered Proteins

Based on the fluorogenic small peptide assay results, I evaluated my compounds' ability to enhance the 20S proteasome-mediated degradation of pathologically relevant IDPs *in vitro* and in cells. In addition to compound **33**, CJ-7-42, CPZ, and TCH-165, a previously reported 20S proteasome enhancer,²¹ were added to directly compare the enhancement of the 20S proteasome mediated-degradation of purified α -synuclein. Purified 20S proteasome was incubated at 37° C with compound **33** (concentrations 2.5 μ M to 15 μ M) or CJ-7-42, CPZ, and TCH-165 (15 μ M) for 45 minutes. Then purified α -synuclein was

added, and the digestion was incubated at 37° C for 3 hours. An SDS loading buffer was added, and the samples were boiled to halt the degradation of α -synuclein. The percentage of remaining α -synuclein was visualized and quantified via immunoblotting (**Figure 2.6A**).²

In agreement with our previous findings, CJ-7-42 increased the degradation rate of full-length α -synuclein,²³ with only 33% α -synuclein remaining. Similarly, CPZ enhanced the degradation of α -synuclein, with only 34% remaining. Compound **33**, however, matched the activity of both CJ-7-42 and CPZ at 10 μ M, with 27% of α -synuclein remaining. When the sample was treated with 15 μ M of compound **33**, over 80% of α -synuclein was degraded, which is similar to the enhanced degradation of α -synuclein in the sample treated with 15 μ M of TCH-165, an efficient, validated 20S proteasome activator.

Encouraged by the *in vitro* results, I evaluated compound **33**'s ability to prevent the accumulation of the A53T mutant α -synuclein in cells. HEK-293T cells were transiently transfected with an A53T mutant α -synuclein plasmid. After 24 hours, the cells were treated with compound **33** (5 μ M, 10 μ M, and 15 μ M), the control compounds TCH-165 (10 μ M), CJ-7-42 (15 μ M), proteasome inhibitor bortezomib (BTZ, 1 μ M), and one sample was treated with 1 μ M BTZ and 10 μ M of compound **33**. The cells were then lysed and the remaining A53T α -synuclein was visualized and quantified via immunoblotting (**Figure 2.6B**). BTZ acted as a negative control, and TCH-165 was once again used as a positive control. Consistent with my *in vitro* results, CJ-7-42 reduced the A53T mutant by around 58%. While at compound **33**'s lowest concentration, 5 μ M, there was a 25% reduction of the A53T mutant, and a dose dependent-enhancement of α -synuclein was observed. At the highest concentration of compound **33** (15 μ M), A53T α -synuclein was decreased by

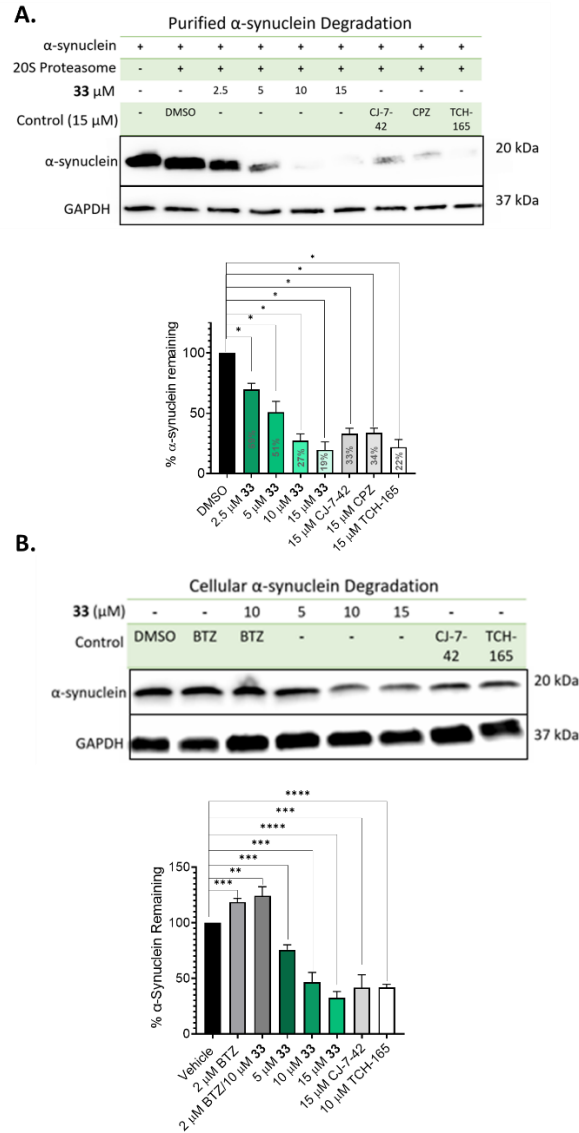


Figure 2.6: Compound 33 enhances 20S proteasome mediated degradation of purified and cellular α -synuclein.²

(A) Degradation of α -synuclein by purified 20S proteasome treated with 2.5 μ M, 5 μ M, 10 μ M, and 15 μ M **33** with 15 μ M of CJ-7-42, 15 μ M CPZ, and 15 μ M the previously reported TCH-165 as a positive control. B) Representative western blot of A53T α -synuclein in HEK-293T cells treated with vehicle (DMSO), BTZ, TCH-165, compound **33**, and CJ-7-42.

Figure 2.6 (cont'd)

Quantification of A53T α -syn remaining for treatments normalized to vehicle control (100%). Quantification of α -synuclein degradation by each compound was done in triplicate. One-way ANOVA statistical analysis was used to determine statistical significance (ns = not significant, * $p < 0.05$)

67% (cell viability >80% in HEK-293T cells at 16h, using Cell Titer Glow). The potency and efficiency displayed by compound **33** towards the 20S proteasome in previous experiments did not translate to the degradation of A53T mutant α -synuclein in HEK-293T cells.

2.4 Series III Chlorpromazine analogs

2.4.1 Rational

The phenothiazine class of therapeutics has diverse biological functions, ranging from neuroleptic drugs to chemotherapeutic agents.^{28, 29, 30} The phenothiazine-based class of compounds not only have the core in common but also share the alkyl connector and the terminal amine tail (**Figure 2.7**).³⁵ In addition, the phenothiazine core and substituents on the tricyclic ring dictate its potency and anticancer activity.^{28, 29, 30} Along with phenothiazine's diverse interaction capabilities, the phenothiazine ring can be metabolized, producing metabolites such as the 7-hydroxylated phenothiazine and the conversion to a sulfoxide (**Figure 2.7**)^{50, 51} To avoid these unwanted interactions and heavy metabolism, small molecules were synthesized that contained the pendant

group seen in compound **33** coupled to alternative heterocyclic cores and their ability to enhance the activity of the 20S proteasome was investigated.

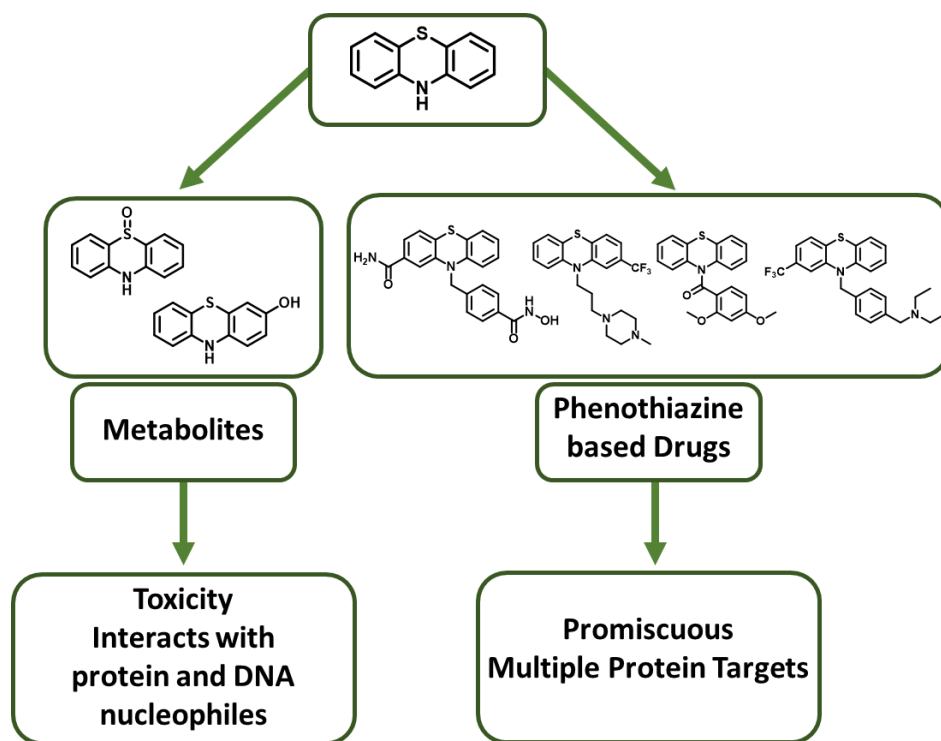


Figure 2.7: Promiscuity of phenthiazine-based drugs and form toxic metabolites.

2.4.2 Synthesis of Series III Chlorpromazine Analogs

The design of the small molecules reported in this section was conducted with two goals: replacing the phenthiazine ring and examining the effect of the methylene linker length on 20S proteasome activation. To accomplish both objectives, the *N,N*-bis(4-fluorophenyl)amine synthesized in **section 2.2** was coupled to either a one- and two-methylene-linked *N,N*-bis(4-fluorophenyl)amide tail. Then, the *N,N*-bis(4-fluorophenyl)amide pendant groups were added to various heterocyclic cores. Synthesis of the amide was achieved upon treatment of *N,N*-bis(fluorophenyl)amine with TEA and

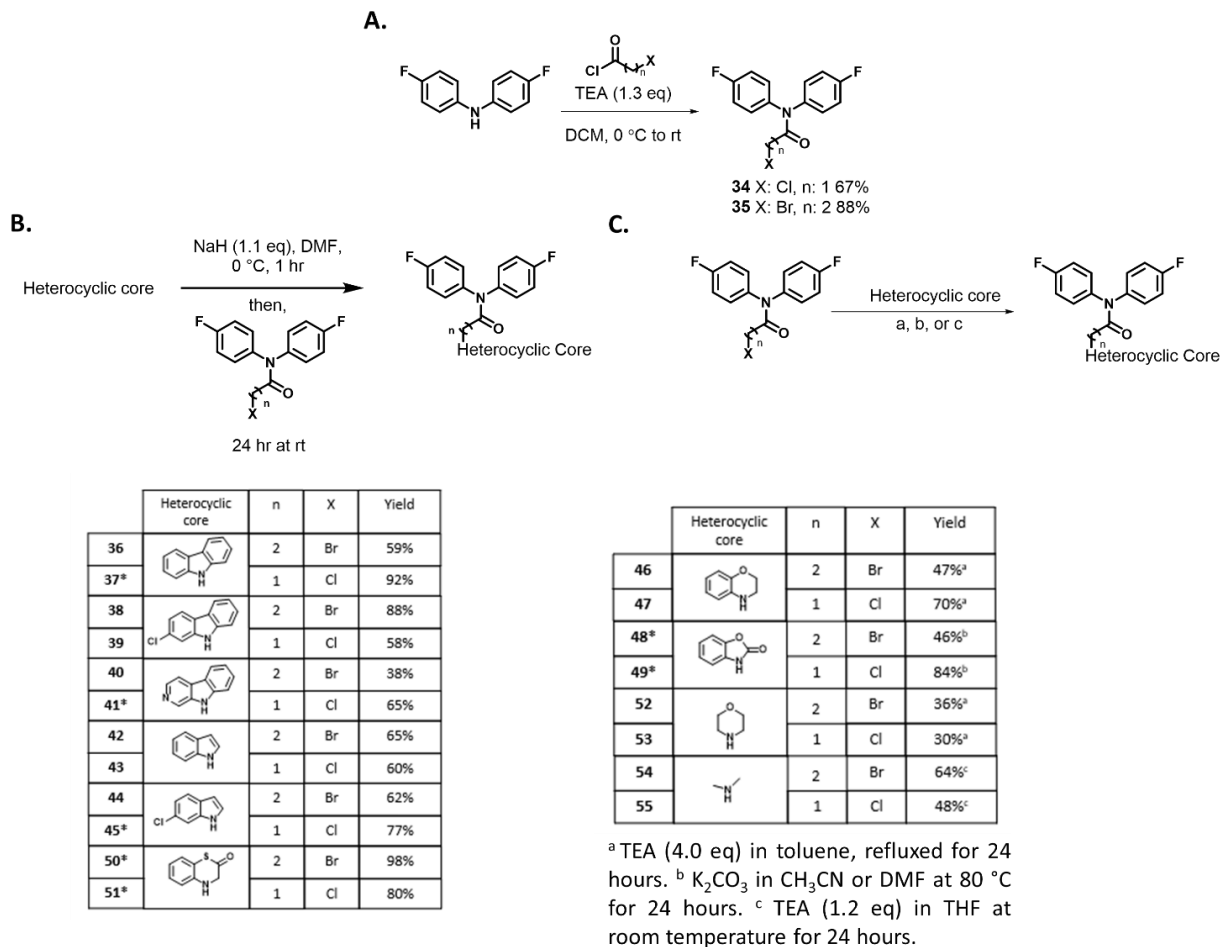
then either 2-chloroacetyl chloride or 3-bromopropanoyl chloride, producing compounds **34** and **35** in 67% and 88% yield, respectively (**Scheme 2.3**).⁵² The two *N,N*-bis(4-fluorophenyl)amide pendant groups were added to a series of nitrogen-containing bi- and tricyclic heterocycles. Each heterocycle was initially treated with a base to deprotonate the nitrogen, and the final analog was achieved upon adding either **34** or **35** (**Scheme 2.3**). This work was done in collaboration with Charles Anamoah, and the compounds with an asterisk next to their number identifier in **Scheme 2.3** were synthesized and characterized by Charles.

A series of carbazole-containing analogs were synthesized to explore the impact of the central ring size in the phenothiazine and the role of the sulfur. An unsubstituted carbazole and a 2-chlorocarbazole were linked to both tails using NaH as the base, producing compounds **36** (59%), **37** (92%), **38** (88%), and **39** (58%) (**Scheme 2.3**). Furthermore, a β -carboline was coupled to **34** and **35** to ascertain whether adding an electron-poor ring would influence 20S proteasome activation. Doing so produced compounds **40** and **41** in 38% and 65% yields, respectively (**Scheme 2.3**).

Thus far, only tricyclic heterocycles have been used to replace the phenothiazine core. To determine if a tricyclic core is necessary for proteasome activation, a series of bicyclic heterocycles coupled with both **34** and **35** were synthesized. Following the syntheses of the carbazole-containing analogs, an unsubstituted indole was first coupled to both **34** and **35** using NaH, producing compounds **42** (65%) and **43** (60%) (**Scheme 2.3**). To compare the activities of compounds **38** and **39**, 2-chloroindole was used as the heterocyclic core. In the presence of NaH, the two-methylene linker provided compound **44** in 62% yield, and the one-methylene linker provided compound **45** (77%) (**Scheme**

2.3). After obtaining the indole counterparts to the carbazoles, we synthesized a bicyclic analog that mimicked the phenothiazine core. Using 3-oxo-3,4-dihydro-2H-1,4-benzothiazine as the replacement for the phenothiazine core, one-methylene, and two-methylene linker versions were synthesized using NaH to provide compounds **50** (98%) and **51** (80%), respectively. Evaluating the impact of hydrogen bond acceptors in the core was also desired; therefore 2-benzoxazinone was coupled to the two-methylene linker using K₂CO₃ in acetonitrile, providing compound **48** in 46% yield, and the one-methylene linker in DMF yielding compound **49** (84%) (**Scheme 2.3**).

The one- and two-methylene-linked *N,N*-bis(4-fluorophenyl)amide tails were then coupled to 1,4-benzoxazine. The 1,4-benzoxazine was treated with TEA and either **34** or **35** (**Scheme 2.3**). The addition of the two-methylene linked *N,N*-bis(4-fluorophenyl)amide tail provided compound **46** in 47% yield, while the one-methylene linked *N,N*-bis(4-fluorophenyl)amide tail yielded compound **47** (70%) (**Scheme 2.3**). To evaluate the necessity of an aromatic group for 20S proteasome activation, two morpholine-containing compounds were synthesized in the same manner as the 1,4-benzoxazine, yielding compounds **52** (36%) and **53** (30%) (**Scheme 2.3**). Finally, the dimethyl amine tail observed in CPZ was coupled to the one- and two-methylene-linked *N,N*-bis(4-fluorophenyl) amide upon treatment with TEA in THF. The dimethyl amine was subsequently added dropwise, yielding the two-methylene linked compound (**54**) in 64% yield and the one-methylene linked compound (**55**) in 48% yield (**Scheme 2.3**).⁵³



Scheme 2.3: The synthetic pathways to produce compounds (A) 34-35, (B) 36-45 and 50-51, and (C) 46-49 and 52-55.

2.4.3 Initial Evaluation of Series II Analogs Activity Towards the 20S Proteasome

Following the synthesis of compounds **36-55**, I evaluated their activity towards the 20S proteasome using a fluorogenic peptide assay described in **section 2.2.3**. I employed an equimolar mixture of the three fluorogenic peptide probes using the same protocol described in the previous sections. In a black 96-well plate, purified human 20S

proteasome was treated with 30 μM , 15 μM , 7.5 μM , and 3.75 μM of each test molecule in DMSO or DMSO only, which functioned as the vehicle control. The EC_{200} was then determined. Compounds with an EC_{200} lower than 3.75 μM were tested in a 9-point concentration range (30 μM to 0.16 μM).

The data collected from these studies are reported in **Figure 2.8**. All molecules containing a tricyclic heterocycle displayed 20S proteasome enhancement, albeit in a range of max fold increases and EC_{200} . For this group of molecules, the impact of the methylene linker length was most evident when comparing the two unsubstituted carbazoles (**Figure 2.8**). The carbazole containing the two-methylene linker, compound **36**, was observed to be a potent and efficient 20S proteasome enhancer with an EC_{200} of 1.6 μM and a max fold increase of 5.8 at 30 μM . In contrast, compound **37**, the one-methylene-linked carbazole, displayed a weaker potency, with an EC_{200} of 3.8 μM . The change in the linker length was better tolerated when a 2-chlorocarbazole was used as the heterocyclic core and displayed an inverse trend compared to compounds **36** and **37**. The one-methylene-linked 2-chlorocarbazole (**39**) showed a higher degree of 20S proteasome activation than its two-methylene counterpart (**38**). Compound **39** had an EC_{200} of 1.2 μM (max fold enhancement of 6.1), compared to compound **38**, which had an EC_{200} of 0.9 μM and a max enhancement of 20S proteasome activity of 4.5-fold (**Figure 2.8**). The two carbolines, **40** and **41**, displayed similar potencies, with an EC_{200} of 3.8 μM and 2.0 μM , respectively. However, the max fold of the two-methylene-linked carboline (**40**) (max-fold of 12) was twice that of the one-methylene counterpart (**41**) (max-fold of 5.5). Comparing

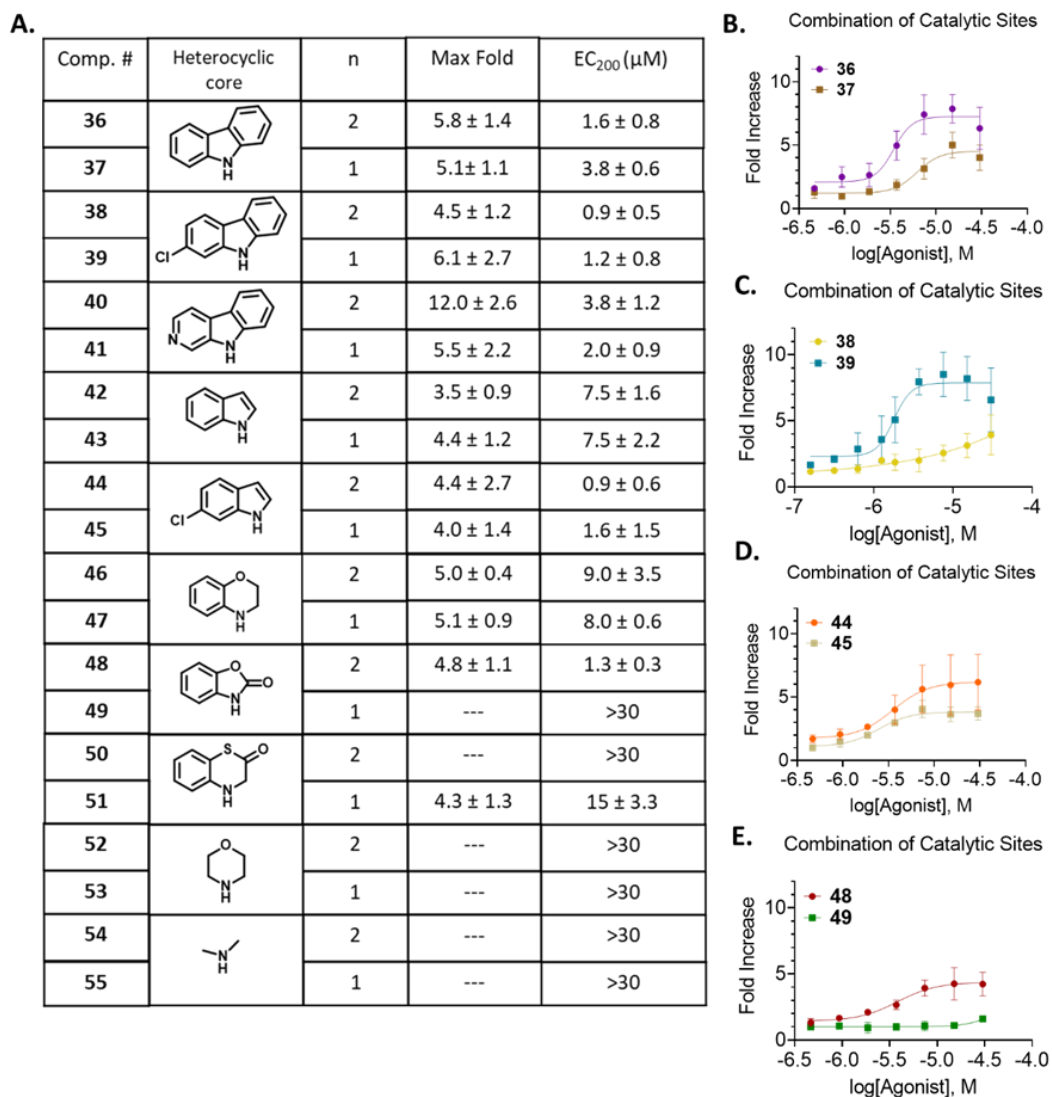


Figure 2.8: Compounds 36-55 ability to enhance the overall activity of the 20S proteasome.

(A) Table depicting the fold increase, denoted as max-fold, in 20S proteasome-mediated proteolysis induced by compounds **36-55**. The EC₂₀₀ depicts the concentration at which the treated 20S proteasome exhibits a 200% enhancement of the rate of degradation of the small peptide substrate as compared to the vehicle control. The activity graphs of (B) **36-37**, (C) **38-39**, (D) **44-45**, and (E) **48-49**.

the activities of these two sets of molecules suggests that the chlorine in the 2-position impacts how the molecules interact with the proteasome.

To understand how the chlorine impacts 20S proteasome activation, an unbiased molecular docking study was performed using Autodock Vina and Discovery Visualizer.

^{54,55} We have previously reported the use of molecular docking as a method to elucidate key interactions between our small molecules and the pockets formed by the α -subunits.²

^{24,23} I found that the 2-chlorophenothiazine linked to the bis(fluorophenyl) amide tail was predicted to favor the α 1/2 pocket of the α -ring of the 20S proteasome, as described in

section 2.3.4.² The preferred interaction with the α 1/2 pocket was observed for the one-methylene linked carbazoles, compounds **37** and **39** (**Figure 2.9A**). This result was quite interesting due to their varying degrees of ability to activate the 20S proteasome. With the only difference between compounds **37** and **39** being the chlorine in the two-position, the preferred conformation and interaction points with the α 1/2 pocket and compounds **37** and **39** were further analyzed.

The molecular docking results of compounds **37** and **39** were overlaid to compare their preferred binding conformation (**Figure 2.9B**). Compound **37** had the carbazole core pointed into the pocket with the bis(fluorophenyl) amide tail closest to CYS161, which I previously identified as a potential key interaction point for 20S proteasome activation, along with TYR159 (**Figure 2.9C**).² In comparison, compound **39** is predicted to have the 2-chlorocarbazole core directly parallel to TYR159 (**Figure 2.9D**). The *N,N*-bis(fluorophenyl) amide tail pointed into the pocket, with one fluorophenyl ring in proximity to CYS161. In contrast, the second fluorophenyl ring sits in the same orientation as the

carbazole core of compound **37**. Consequently, the addition of chlorine flipped the predicted binding conformation, likely explaining the discrepancy in 20S proteasome activity. Next, I wanted to understand how this orientation change impacted compounds **37** and **39**'s interactions with the amino acids in the α 1/2 pocket.

Using BIOVIA Discovery Visualizer, the predicted interactions of compounds **37** and **39** and the α 1/2 pocket were compared (**Figure 2.9C-D**). Unsurprisingly, there were key differences in how compounds **37** and **39** interacted with the α 1/2 pocket. While both compounds interacted with CYS161 through a π -sulfur and π -alkyl interactions, compound **39** has an additional hydrogen bond between the -SH of CYS161 and the fluorine of the bis(fluorophenyl) amide tail. Although this type of hydrogen bonding is considered a weak interaction, it has been observed to increase binding affinity,^{56, 57} potentially explaining the difference in activity of compounds **37** and **39**.

In addition, compound **39** is predicted to interact with TYR159 and TYR75 differently than compound **37**. We had previously identified molecules that interact with TYR159 through one mode of π - π stacking displayed little to no 20S proteasome activation.² Compound **37** interacts with TYR159 through only a π - π T-shaped interaction. In contrast, compound **39** is predicted to have three π - π interactions with TYR159. Lastly, the interactions with TYR75 are of note. Compound **37** interacts with TYR75 through a weak π -donor hydrogen bond as compared to the stronger C=O...H-O for compound **39**.⁵⁸ Compound **39** interacts with CYS161 and TYR159 in a manner that agrees with our previous studies.²

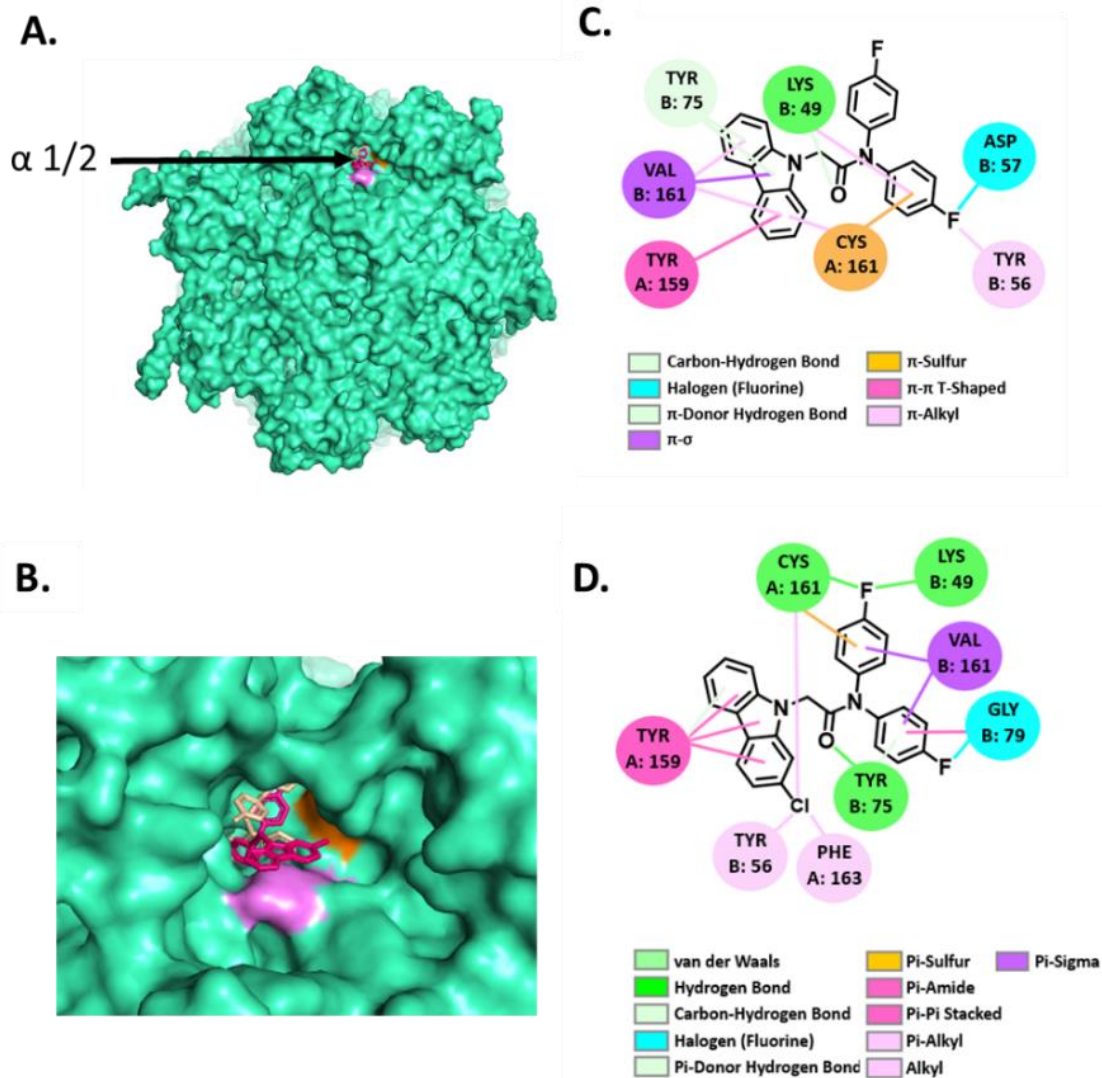


Figure 2.9: The predicted binding interaction of compounds 37 and 39 with the 20S proteasome.

Preferred binding pocket of compounds (A) **37** (wheat) and **39** (pink). (B) Overlay of predicted conformation of compounds **37** (wheat) and **39** (pink) in the α 1/2 pocket with the location of TYR159 highlighted in light pink and CYS161 highlighted in orange. The predicted binding interactions of compounds (C) **37** and (D) **39**. *20S proteasome: PDB 4R3O

The strong hydrogen bonding with TYR75 may explain the potent nature of compound **39**. In contrast to the tricyclic-containing molecules, the bicyclic molecules were generally less efficient and less potent. Only one bicyclic compound, **44**, had an EC₂₀₀ below 1 μM. Compound **44**, a two-methylene-linked 2-chloroindole, was observed to be a potent 20S proteasome activator with an EC₂₀₀ of 0.9 μM and a max fold increase of 4.4. The one-methylene-linked 2-chloroindole (**45**), was as efficient as compound **44** (max-fold of 4.0) but was five times less potent (EC₂₀₀ of 1.6 μM). Compounds **42** and **43** displayed an identical EC₂₀₀ of 7.5 μM and similar 20S proteasome activation efficiencies with max folds of 3.5 and 4.4, respectively. These indoles were also predicted to bind to the α 1/2 pocket and interacted with CYS161 through a π-alkyl interaction. I had previously observed that molecules interacting in this manner displayed weaker EC₂₀₀ and max folds.²

The incorporation of hydrogen bond acceptors was beneficial when connected to the two-methylene linker (**48**, EC₂₀₀ of 1.3 μM) but abrogated all 20S proteasome activity when coupled with the one-methylene linker (**49**). Compound **49** completely lacked any interaction with TYR159, agreeing with my previous assessment that an interaction with TYR159 is important for 20S proteasome activation.² The additional flexibility in some bicyclic ring analogs (**46** and **47**) did not impact the efficiency of 20S proteasome activation but greatly impacted the observed potency, displaying EC₂₀₀ of 9.0 μM (**46**) and 8.0 μM (**48**). However, the complete elimination of the aromatic group in the heterocyclic core abolished all 20S proteasome activity, as seen with compounds **52-55**. With the range of 20S proteasome activity, I carried forward molecules that had an EC₂₀₀ of around 1 μM. The corresponding methylene linker pair was also included to either act as a

negative control or to further evaluate the impact of the linker length on 20S proteasome activation with physiologically relevant proteins.

2.4.4 Impact of Series III Analogs Enhancement of 20S Proteasome Activity on the Rate of Degradation of Pathogenic Intrinsically Disordered Proteins

The ability of the novel 20S proteasome activators to enhance the degradation of a full-length and pathologically relevant protein was evaluated next. Due to the number of molecules exhibiting an EC_{200} around 1 μ M, two concentrations of each compound were assessed (5 μ M and 15 μ M). The validated 20S proteasome activator, TCH-165,²⁰ was used as a positive control, and the 20S proteasome treated with DMSO was used as vehicle control. Purified 20S proteasome was diluted in a 50 mM HEPES and 5 mM DTT buffer (pH 7.2)^{2, 59} to a final concentration of 10 nM. Then, the desired concentration of compounds **36-39**, **44**, **45**, **48**, and **49** or TCH-165 was added to the proteasome solution. The proteasome-drug mixture was incubated for 45 minutes at 37 °C. After the incubation, purified α -synuclein was added to a final concentration of 300 nM. The protein digestion was incubated at 37 °C for an additional 3.5 hours. The remaining full-length α -synuclein was visualized and quantified using immunoblotting (**Figure 2.10**). The positive control, TCH-165, significantly enhanced the 20S proteasome-mediated degradation of α -synuclein at both concentrations, with an average of 60% and 40% α -synuclein remaining at 5 μ M and 15 μ M, respectively. At 15 μ M, several compounds outperformed TCH-165, but only two significantly enhanced the clearance of α -synuclein by the 20S proteasome at 5 μ M. Proteasome treated with 5 μ M and 15 μ M of compound **36** displayed an enhanced degradation of α -synuclein with 45% and 28% α -synuclein remaining,

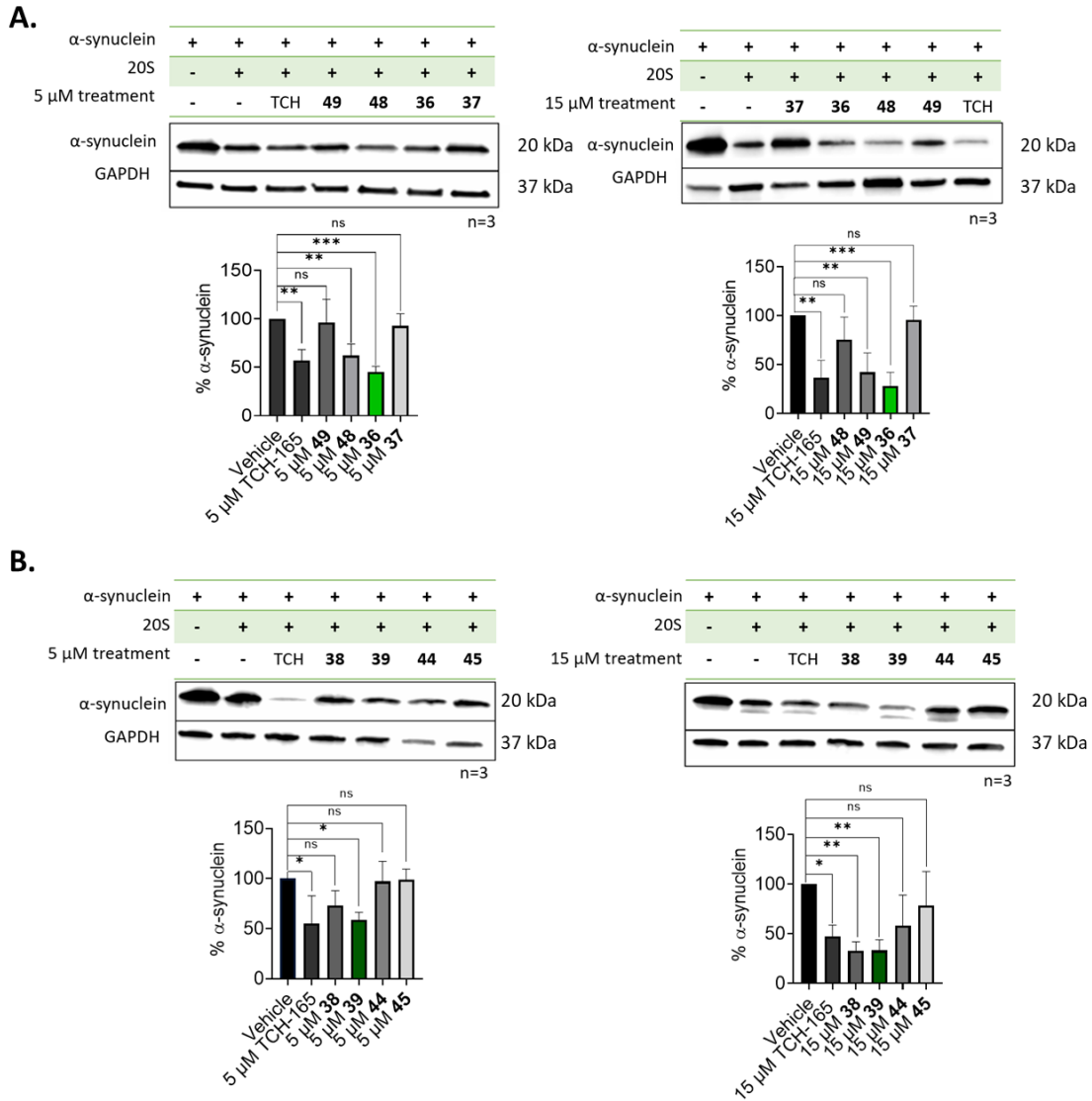


Figure 2.10: Bis(fluoro)diphenyl amide containing analogs enhance the 20S proteasome mediated degradation of purified α-synuclein.

(A and B) The degradation of purified α-synuclein by the 20S proteasome treated with (A) 5 μM and (B) 15 μM of compounds 36-39, 44-45, 48-49, or the positive control, TCH-165. GAPDH was added as a loading control. Each set of assays were done in triplicate. Error bars denote standard deviation. One-way ANOVA statistical analysis was used to determine statistical significance (ns = not significant, *p < 0.05, **p < 0.01, ***p < 0.001, ****p < 0.0001). Error bars based on standard deviation.

respectively (**Figure 2.10**). Consistent with poor activity in the purified proteasome assay, compound **37** did not exhibit significant enhancement of α -synuclein degradation in a secondary assay. Furthermore, the two potent analogs, compounds **38** and **39**, performed very similarly to compound **36** at 15 μ M, with only 33% α -synuclein remaining after 3.5-hour incubation. At 5 μ M, compound **39** outperformed compound **38**. Samples treated with 5 μ M of compound **38** reduced intact α -synuclein by 30%, while samples treated with compound **39** had a 37% reduction of α -synuclein (**Figure 2.10**).

Consistent with the fluorogenic small peptide assay, the bicyclic small molecules did not perform as well as the tricyclic compounds. The potency and efficiency displayed by compound **44** in the fluorogenic peptide assay did not translate to the degradation of a full-length IDP. Samples treated with 5 μ M and 15 μ M of compound **44** displayed no significant change in the rate of α -synuclein degradation compared to the vehicle. Comparable to samples treated with compound **36**, the samples treated with compound **48** displayed an enhanced degradation of α -synuclein at both 5 μ M and 15 μ M, with 65% and 42% α -synuclein remaining, respectively (**Figure 2.10**). Due to the significant enhancement of the 20S proteasome-mediated α -synuclein degradation at both 5 μ M and 15 μ M, the activities of compounds **36** and **39** were next evaluated in HEK-293T cells transiently expressing A53T α -synuclein. The A53T α -synuclein mutant has been utilized in the identification of 20S proteasome activators that could enhance the degradation of α -synuclein in cells at high μ M concentrations.^{2, 25, 27, 60}

With the potency displayed by compounds **36** and **39** in both the fluorogenic peptide assay and the *in vitro* degradation of α -synuclein, I wanted to evaluate if the activity translates to a cellular model. HEK-293T cells were transiently transfected with an A53T

α -synuclein plasmid.² After 48 hours of protein expression, I treated the cells with four concentrations of compounds **36** and **39** (1, 5, 10, and 15 μ M) for 16 hours and then lysed the cells. The levels of A53T α -synuclein were visualized and quantified via immunoblotting (**Figure 2.11**). I also treated samples with 15 μ M of TCH-165 as a positive control, 15 μ M of the structurally related inactive compound **49** as an inactive control, 30 nM of a proteasome inhibitor Bortezomib (BTZ) as a negative control, and DMSO as the vehicle control.

The levels of A53T α -synuclein in cells treated with the four concentrations of compound **36** all had significantly less A53T α -synuclein than the vehicle. With the treatment of 1 μ M, 64% of A53T α -synuclein remained, compared to the untreated control. The other concentrations of compound **36** exhibited an apparent reduction of α -synuclein in a dose-dependent manner, with 5 μ M having 45%, 10 μ M 27%, and 15 μ M with 21% A53T α -synuclein remaining. The TCH-165 control had a larger error range but, on average, had 52% A53T α -synuclein remaining at 15 μ M. While the inactive control (**49**) had no significant effect, BTZ did increase the levels of A53T α -synuclein by 48% via proteasome inhibition (**Figure 2.11A**). In a similar trend, compound **39** performed as well as, if not better, compound **36**. Cells treated with 1 μ M of compound **36** had a 43% decrease of A53T α -synuclein. Compound **39** outperformed compound **36** at 5 μ M, with a reduction of A53T α -synuclein of 70%. The reduction of A53T α -synuclein at 10 μ M and 15 μ M were extremely close, with only 14% and 11% A53T α -synuclein remaining, respectively. The TCH-165 positive control again significantly prevented α -synuclein accumulation with an average of 40% A53T α -synuclein remaining. The inactive structurally related control, **49**,

continued to have no impact on the levels of A53T α -synuclein, and the negative control BTZ increased A53T α -synuclein levels by 35% (**Figure 2.11B**).

The potency displayed by compounds **36** and **39** in the fluorogenic peptide assay was demonstrated in both the degradation of purified α -synuclein *in vitro* and the degradation of A53T α -synuclein in cells. The lowest concentration of both compounds in the previously described studies was 1 μ M. The levels of activity shown by compounds **36** and **39** necessitated the need to explore cellularly activity at lower concentrations. Further studies were done using the HEK-293T cells that were transiently transfected with the A53T α -synuclein. The procedure was identical, but TCH-165 was added at 1 μ M. Due to the slightly better performance of compound **39**, three concentrations were evaluated: 0.5 μ M, 0.75 μ M, and 1 μ M. Cells were also treated with 0.75 μ M and 1 μ M of compound **39**. The addition of 1 μ M of the compounds was used as another positive control due to the lower potency of TCH-165. Compound **39** had no significant decrease of A53T α -synuclein at 0.5 μ M. At 0.75 μ M, compound **36** had 55% A53T α -synuclein remaining, while compound **39** had 72% remaining. The two molecules both performed well at 1 μ M. Cells treated with 1 μ M compound **36** had 42% A53T α -synuclein remaining compared to the samples with the same concentration of compound **39** had 60% left (Figure 2.10C). These studies confirmed that both compounds **36** and **39** prevented A53T α -synuclein accumulation at sub-micromolar concentrations, making them the most potent 20S enhancers reported thus far and suitable tools for further pre-clinical exploration.*Paper

submitted to iScience

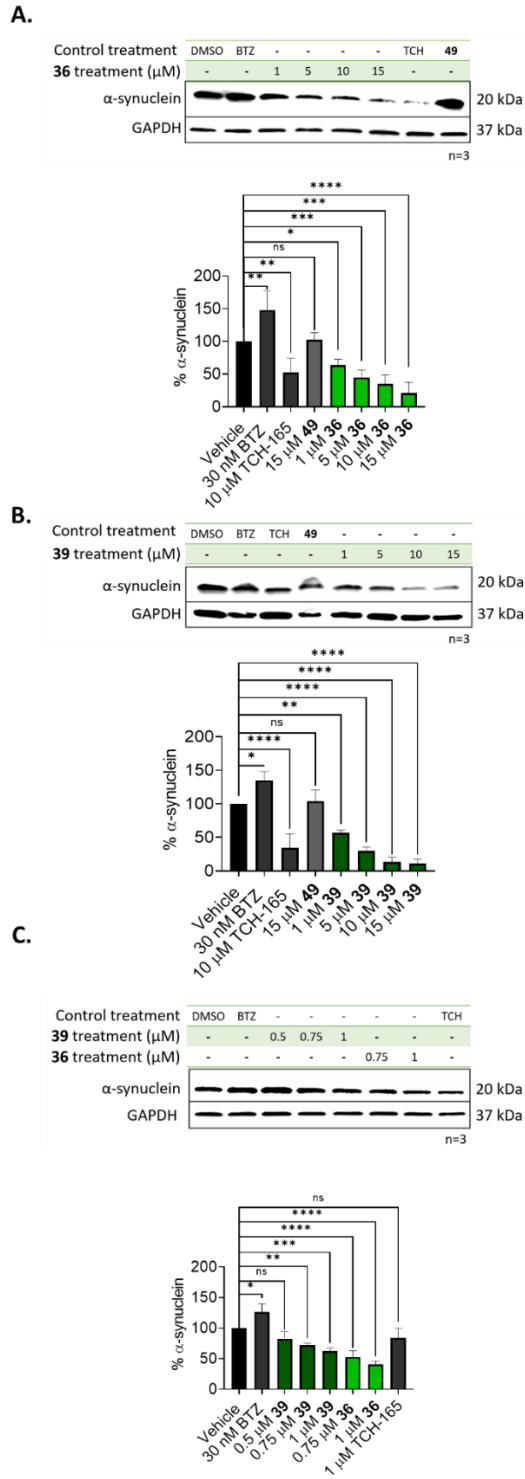


Figure 2.11: Compounds 36 and 39 enhance the 20S proteasome mediated degradation of α -synuclein in cells.

Figure 2.11 (cont'd)

The evaluation of A53T α -synuclein levels in HEK-293T cells once they have been treated with 1, 5, 10, or 15 μ M of compounds (A) 36 and (B) 39, with 15 μ M of an inactive control, 49, 10 μ M of a positive control, TCH-165, and 30 nM of a proteasome inhibitor, BTZ. (C) The experimental set up was repeated, with 0.5, 0.75, and 1 μ M of compound 39, and 0.75 and 1 μ M of compound 36. The quantification of the A53T α -synuclein remaining was normalized using the GAPDH levels. Done in triplicate. With One-way ANOVA statistical analysis was used to determine statistical significance (ns = not significant, *p < 0.05, **p < 0.01, ***p < 0.001, ****p < 0.0001)

2.5 Conclusion

Targeting IDPs to halt or slow down the progression of neurodegenerative diseases is a promising new therapeutic strategy. However, because of the dynamic structure of IDPs, they typically lack binding pockets; thus, targeting IDPs with small molecules directly becomes a daunting and nearly impossible task.⁶¹ The 20S proteasome can directly and selectively degrade IDPs due to their lack of a defined 3D structure. In previous studies, 20S proteasome activation has been observed to enhance the degradation of other physiologically relevant IDPs, such as WT- α -synuclein, tau, and ornithine decarboxylase (ODC).^{21, 24, 25, 2} We have recently reported that small molecule enhancement of the 20S proteasome can be used to overcome proteasome impairment by soluble IDP oligomers.²⁵ While most PD cases are sporadic, genetic mutations have been linked to familial PD.^{13, 14} A missense mutation with an alanine exchanged for a threonine, A53T,

forms a rare type of PD characterized by its early onset and autosomal dominant inheritance.^{13, 14} The A53T mutant α -synuclein is known to express three times as quickly as the wild type and has an increased rate of aggregation.^{13, 14} In the studies described in **Chapter Two**, I evaluated the ability of 20S proteasome activators to prevent the accumulation of a specifically pathogenic α -synuclein containing an A53T mutation. Through the development of CPZ analogs, potent small molecules have been designed and synthesized that can enhance the activity of the 20S proteasome. While compound **33** is the most potent 20S proteasome enhancer in the purified enzymatic assays,² compounds **36** and **39** were identified to enhance the 20S proteasome-mediated degradation of the A53T mutant α -synuclein in cells at sub-micromolar concentrations. The development of these molecules will allow for the thorough investigation of 20S proteasome enhancement as a potential neurodegenerative disease therapeutics. Furthermore, the SAR studies conducted herein have become a road map for the Tepe lab and have laid the foundation for new SAR studies.

REFERENCES

- (1) Marras, C.; Beck, J. C.; Bower, J. H.; Roberts, E.; Ritz, B.; Ross, G. W.; Abbott, R. D.; Savica, R.; Van Den Eeden, S. K.; Willis, A. W.; et al. Prevalence of Parkinson's disease across North America. *NPJ Parkinsons. Dis.* **2018**, *4*, 21-28.
- (2) Staerz, S. D.; Jones, C. L.; Tepe, J. J. Design, synthesis, and biological evaluation of potent 20S proteasome activators for the potential treatment of alpha-synucleinopathies. *J. Med. Chem.* **2022**, *65*, 6631-6642.
- (3) Mintun, M. A.; Lo, A. C.; Duggan Evans, C.; Wessels, A. M.; Ardayfio, P. A.; Andersen, S. W.; Shcherbinin, S.; Sparks, J.; Sims, J. R.; Brys, M.; et al. Donanemab in early Alzheimer's disease. *N. Engl. J. Med.* **2021**, *384* (18), 1691-1704.
- (4) Giorgi, C.; Marchi, S.; Simoes, I. C. M.; Ren, Z.; Morciano, G.; Perrone, M.; Patalas-Krawczyk, P.; Borchard, S.; Jedrak, P.; Pierzynowska, K.; et al. Mitochondria and reactive oxygen species in aging and age-related diseases. *Int. Rev. Cell Mol. Biol.* **2018**, *340*, 209-213.
- (5) Klaips, C. L.; Jayaraj, G. G.; Hartl, F. U. Pathways of cellular proteostasis in aging and disease. *J. Cell Biol.* **2018**, *217* (1), 51-63.
- (6) Labbadia, J.; Morimoto, R. I. The biology of proteostasis in aging and disease. *Annu. Rev. Biochem.* **2015**, *84*, 435-464.
- (7) Bonet-Costa, V.; Pomatto, L. C.; Davies, K. J. The proteasome and oxidative stress in Alzheimer's disease. *Antioxid. Redox. Signal* **2016**, *25* (16), 886-901.
- (8) Nguyen, P. H.; Ramamoorthy, A.; Sahoo, B. R.; Zheng, J.; Faller, P.; Straub, J. E.; Dominguez, L.; Shea, J. E.; Dokholyan, N. V.; De Simone, A.; et al. Amyloid oligomers: a joint experimental/computational perspective on Alzheimer's disease, Parkinson's disease, type II diabetes, and Amyotrophic Lateral Sclerosis. *Chem. Rev.* **2021**, *121* (4), 2545-2647.
- (9) Kaye, R.; Dettmer, U.; Lesne, S. E. Soluble endogenous oligomeric alpha-synuclein species in neurodegenerative diseases: Expression, spreading, and cross-talk. *J. Parkinsons Dis.* **2020**, *10*, 791-818.
- (10) Deger, J. M.; Gerson, J. E.; Kaye, R. The interrelationship of proteasome impairment and oligomeric intermediates in neurodegeneration. *Aging Cell* **2015**, *14*, 715-724.
- (11) Wong, Y. C.; Krainc, D. alpha-synuclein toxicity in neurodegeneration: mechanism and therapeutic strategies. *Nat. Med.* **2017**, *23* (2), 1-13.

- (12) Polymeropoulos, M. H.; Lavedan, C.; Leroy, E.; Ide, S. E.; Dehejia, A.; Dutra, A.; Pike, B.; Root, H.; Rubenstein, J.; Boyer, R.; et al. Mutation in the alpha-synuclein gene identified in families with Parkinson's disease. *Science* **1997**, *276* (5321), 2045-2047.
- (13) Conway, K. A.; Harper, J. D.; Lansbury, P. T. Accelerated in vitro fibril formation by a mutant alpha-synuclein linked to early-onset Parkinson disease. *Nat. Med.* **1998**, *11*, 1318-1320.
- (14) Nahri, L.; Wood, S. J.; Steavenson, S.; Jiang, Y.; Wu, G. M.; Anafi, D.; Kaufman, S. A.; Martin, F.; Sitney, K.; Denis, P.; et al. Both familial Parkinson's disease mutations accelerate alpha-synuclein aggregation. *J. Biol. Chem.* **1999**, *274*, 9843-9846.
- (15) Li, J.; Uversky, V. N.; Fink, A. L. Effect of familial Parkinson's disease point mutations A30P and A53T on the structural properties, aggregation, and fibrillization of human alpha-synuclein. *Biochemistry* **2001**, *40*, 11604-11613.
- (16) Njomen, E.; Tepe, J. J. Proteasome activation as a new therapeutic approach to target proteotoxic disorders. *J. Med. Chem.* **2019**, *62* (14), 6469-6481.
- (17) Jones, C. L.; Tepe, J. J. Proteasome activation to combat proteotoxicity. *Molecules* **2019**, *24* (15), 2841-2869.
- (18) Opoku-Nsiah, K. A.; Gestwicki, J. E. Aim for the core: suitability of the ubiquitin-independent 20S proteasome as a drug target in neurodegeneration. *Transl. Res.* **2018**, *198*, 48-57.
- (19) Coleman, R. A.; Trader, D. J. All about the core: a therapeutic strategy to prevent protein accumulation with proteasome coreparticle stimulators. *ACS Pharmacol. Transl. Sci.* **2018**, *1* (2), 140-142.
- (20) Bard, J. A. M.; Goodall, E. A.; Greene, E. R.; Jonsson, E.; Dong, K. C.; Martin, A. Structure and function of the 26S proteasome. *Annu. Rev. Biochem.* **2018**, *87*, 697-724.
- (21) Njomen, E.; Osmulski, P. A.; Jones, C. L.; Gaczynska, M.; Tepe, J. J. Small molecule modulation of proteasome assembly. *Biochemistry* **2018**, *57* (28), 4214-4224.
- (22) Osmulski, P. A.; Karpowicz, P.; Jankowska, E.; Bohmann, J.; Pickering, A. M.; Gaczynska, M. New peptide-based pharmacophore activates 20S proteasome. *Molecules* **2020**, *25* (6), 1439-1456.
- (23) Jones, C. L.; Njomen, E.; Sjogren, B.; Dexheimer, T. S.; Tepe, J. J. Small molecule enhancement of 20S proteasome activity targets intrinsically disordered proteins. *ACS Chem. Biol.* **2017**, *12*, 2240-2247.
- (24) Fiolek, T. J.; Magyar, C. L.; Wall, T. J.; Davies, S. B.; Campbell, M. V.; Savich, C. J.; Tepe, J. J.; Mosey, R. A. Dihydroquinazolines enhance 20S proteasome activity and

induce degradation of alpha-synuclein, an intrinsically disordered protein associated with neurodegeneration. *Bioorg. Med. Chem. Lett.* **2021**, *36*, 127821-127826.

(25) Fiolek, T. J.; Keel, K. L.; Tepe, J. J. Fluspirilene analogs activate the 20S proteasome and overcome proteasome impairment by intrinsically disordered protein oligomers. *ACS Chem. Neurosci.* **2021**, *12*, 1438-1448.

(26) Coleman, R. A.; Muli, C. S.; Zhao, Y.; Bhardwaj, A.; Newhouse, T. R.; Trader, D. J. Analysis of chain length, substitution patterns, and unsaturation of AM-404 derivatives as 20S proteasome stimulators. *Bioorg. Med. Chem. Lett.* **2019**, *29* (3), 420-423.

(27) Trader, D. J.; Simanski, S.; Dickson, P.; Kodadek, T. Establishment of a suite of assays that support the discovery of proteasome stimulators. *Biochim. Biophys. Acta. Gen. Subj.* **2017**, *1861* (4), 892-899.

(28) Boyd-Kimball, D.; Gonczy, K.; Lewis, B.; Mason, T.; Siliko, N.; Wolfe, J. Classics in chemical neuroscience: chlorpromazine. *ACS Chemical Neuroscience* **2018**, *10* (1), 79-88.

(29) Conely, R. R.; Tamminga, C. A.; Bartko, J. J.; Richardson, C. R.; Peszke, M.; Lingle, J.; Hegerty, J.; Love, R.; Gounaris, C.; Zaremba, S. Olanzapine compared with chlorpromazine in treatment-resistant schizophrenia. *Am. J. Psychiatry* **1998**, *155*, 914-920.

(30) Enna, S. J.; Bennet, J. P.; Burt, D. R.; Creese, I.; Snyder, S. H. Stereospecificity of interaction of neuroleptic drugs with neurotransmitters and correlation with clinical potency. *Nature* **1976**, *263*, 338-341.

(31) Froimowitz, M.; Cody, V. Biologically active conformers of phenothiazines and thioxanthenes. Further evidence for a ligand model of dopamine D2 receptor antagonists. *J. Med. Chem.* **1993**, *36*, 2210-2227.

(32) Feinberg, A. P.; Snyder, S. H. Phenothiazine drugs: structure-activity relationships explained by a conformation that mimics dopamine. *Proc. Natl. Acad. Sci. U.S.A.* **1975**, *72*, 1899-1903.

(33) Pluta, K.; Morak-Mlodawska, B.; Jelen, M. Recent progress in biological activities of synthesized phenothiazines. *Eur. J. Med. Chem.* **2011**, *46* (8), 3179-3189.

(34) Salie, S.; Hsu, N. J.; Semenya, D.; Jardine, A.; Jacobs, M. Novel non-neuroleptic phenothiazines inhibit Mycobacterium tuberculosis replication. *J. Antimicrob. Chemother.* **2014**, *69* (6), 1551-1558.

(35) Jaszczyszyn, A.; Gasiorowski, K.; Swiatek, P.; Malinka, W.; Cieslik-Boczula, K.; Petrus, J.; Czarnik-Matuszewicz, B. Chemical structure of phenothiazines and their biological activity *Pharmacol. Rep.* **2012**, *64*, 16-23.

- (36) Van der Ven, P. F.; Takuma, T.; Baum, B. J. Chlorpromazine inhibition of muscarinic-cholinergic responses in the rat parotid gland. *J. Dent. Res.* **1986**, *65*, 382-386.
- (37) Zhang, Z.; Xie, J.; Shen, B.; Wang, H.; Li, M.; Zhang, J.; Cao, J. Manipulation of electron deficiency of beta-carboline derivatives as bipolar hosts for blue phosphorescent organic light-emitting diodes with high efficiency at 1000 cd m⁻². *J. Mater. Chem. C.* **2016**, *4*, 4226-4235.
- (38) Vantourout, J. C.; Miras, H. N.; Isidro-Llobet, A.; Sproules, S.; Watson, A. J. B. Spectroscopic studies of the Chan-Lam Amination: a mechanism inspired solution to boronic ester reactivity. *J. Am. Chem. Soc.* **2017**, *139*, 4769-4779.
- (39) Watanabe, T.; Oishi, S.; Fujii, N.; Ohno, H. Palladium-catalyzed direct synthesis of carbazoles via one-pot N-arylation and oxidative biaryl coupling: synthesis and mechanistic study. *J. Org. Chem.* **2009**, *74*, 4720-4726.
- (40) Kaliyaperumal, S. A.; Banerjee, S.; Kumar, S. U. K. Palladium mediated intramolecular multiple C-X/C-H cross coupling and C-H activation: synthesis of carbazole alkaloids calothrixin B and murrayaquinone A. *Org. Biomol. Chem.* **2014**, *12* (32), 6105-6113.
- (41) Wise, L. D.; Pattison, I. C.; Butler, D. E.; DeWald, H. A.; Lewis, E. P.; Lobbestael, S. J.; Teclé, H.; Coughenour, L. L.; Downs, D. A.; Poschel, B. P. H. Examination of a series of 8-[3-[Bis(4-fluorophenyl)amino]propyl]-1-aryl-1,3,8-triazaspiro[4.5]decan-4-ones as potential antipsychotic agents. *J. Med. Chem.* **1985**, *28*, 1811-1817.
- (42) Ashraf-Uz-Zaman, M.; Sajib, M. S.; Cucullo, L.; Mikelis, C. M.; German, N. A. Analogs of penfluridol as chemotherapeutic agents with reduced central nervous system activity. *Bioorg. Med. Chem. Lett.* **2018**, *28* (23), 3652-3657.
- (43) Pedersen, M. J.; Skovby, T.; Mealy, M. J.; Dam-Johansen, K.; Kiil, S. A solvent-free base liberation of a tertiary aminoalkyl halide by flow chemistry. *Org. Process Res. Dev.* **2016**, *20* (12), 2043-2049.
- (44) Kisselev, A. F.; Akopian, T. N.; Castillo, V.; Goldberg, A. L. Proteasome active sites allosterically regulate each other, suggesting a cyclical bite-chew mechanism for protein breakdown. *Mol Cell* **1999**, *4*, 395-402.
- (45) Harrold, M. W.; Sriburi, A.; Matsumoto, K.; Miller, D. D.; Farooqui, T.; Uretsky, N. The interaction of ammonium, sulfonium, and sulfide analogs of metoclopramide with the dopamine D2 receptor. *J. Med. Chem.* **1993**, *36* (21), 3166-3170.
- (46) Farooqui, T.; Markovich, K.; Wallace, L.; Miller, D.; Uretsky, N. Interaction of AZA analogs of chlorpromazine with the dopamine D2 receptor. *Gen. Pharmacol.: Vasc. Sys.* **1993**, *24* (1), 147-151.

- (47) Martinez, C. R.; Iverson, B. L. Rethinking the term “pi-stacking”. *Chem. Sci. J.* **2012**, *3* (7).
- (48) Zauhar, R. J.; Colbert, C.L.; Morgan, R.S.; Welsh, W.J. Evidence for a strong sulfur–aromatic interaction derived from crystallographic data. *Biolpolymers* **1999**, *53*, 233-248.
- (49) Duan, G.; Smith Jr.; V. H.; Weaver, D. F. Characterization of aromatic-thiol π -Type hydrogen bonding and phenylalanine-cysteine side chain interactions through ab initio calculations and protein analyses. *Mol. Phys.* **2001**, *99*, 1689-1699.
- (50) Yueng, P. K.; Hubbard, J. W.; Korchinski, E. D.; Midha, K. K. Pharmacokinetics of chlorpromazine and key metabolites. *Eur. J. Clin. Pharmacol.* **1993**, *45*, 563-569.
- (51) Yoshii, K.; Kobayaski, K.; Tsumuji, M.; Tani, M.; Shimada, N.; Chiba, K. Identification of human cytochrome P450 isoforms involved in the 7-hydroxylation of chlorpromazine by human liver microsomes. *Life Sci.* **2000**, *67*, 175-184.
- (52) Cao, J.; Kulkarni, S.; Husbands, S. M.; Bowen, W. D.; Williams, W.; Kopajtic, T.; Katz, J. L.; George, C.; Newmann, A. H. Dual probes for the dopamine transporter and δ 1 receptors: novel piperazinyl alkyl-bis(4'-fluorophenyl)amine analogues as potential cocaine-abuse therapeutic agents. *J. Med. Chem.* **2003**, *46*, 2589-2598.
- (53) Rossi, D.; Pedrali, A.; Urbano, M.; Gaggeri, R.; Serra, M.; Fernandez, L.; Fernandez, M.; Caballero, J.; Ronsisvalle, S.; Prezzavento, O.; et al. Identification of a potent and selective sigma(1) receptor agonist potentiating NGF-induced neurite outgrowth in PC12 cells. *Bioorg. Med. Chem.* **2011**, *19* (21), 6210-6224.
- (54) Eberhardt, J.; Santos-Martins, D.; Tillack, A. F.; Forli, S. AutoDock Vina 1.2.0: New docking methods, expanded force field, and python bindings. *J. Chem. Inf. Model* **2021**, *61* (8), 3891-3898.
- (55) Trott, O.; Olson, A. J. AutoDock Vina: Improving the speed and accuracy of docking with a new scoring function, efficient optimization, and multithreading. *J. Comput. Chem.* **2009**, *31* (2), 455-461.
- (56) Zhou, P. Z., J.; Tian, F.; Shang, Z. Fluorine bonding - How does it work in protein-ligand interactions? *J. Chem. Inf. Model* **2009**, *49*, 2344-2355.
- (57) Bauer, M. R.; Jones, R. N.; Baud, M. G.; Wilcken, R.; Boeckler, F. M.; Fersht, A. R.; Joerger, A. C.; Spencer, J. Harnessing fluorine-sulfur contacts and multipolar interactions for the design of p53 mutant Y220C rescue drugs. *ACS Chem. Biol.* **2016**, *11* (8), 2265-2274.
- (58) Bissantz, C.; Kuhn, B.; Stahl, M. A medicinal chemist's guide to molecular interactions. *J. Med. Chem.* **2010**, *53* (14), 5061-5084.

(59) Mishizen-Eberz, A. J.; Guttman, R. P.; Giasson, B. I.; Day, G. A.; Hodara, R.; Ischiropoulos, H.; Lee, V. M. Y.; Trojanowski, J. Q.; Lynch, D. R. Distinct cleavage patterns of normal and pathologic forms of α -synuclein by calpain I in vitro. *J. Neurochem.* **2003**, *86* (4), 836-847.

(60) Zhou, H.; Shao, M.; Guo, B.; Li, C.; Lu, Y.; Yang, X.; ShengnanLi; Li, H.; Zhu, Q.; Zhong, H.; et al. Tetramethylpyrazine analogue T-006 promotes the clearance of alpha-synuclein by enhancing proteasome activity in Parkinson's disease models. *Neurotherapeutics* **2019**, *16* (4), 1225-1236.

(61) Tsafou, K.; Tiwari, P. B.; Forman-Kay, J. D.; Metallo, S. J.; Toretzky, J. A. Targeting intrinsically disordered transcription factors: Changing the paradigm. *J. Mol. Biol.* **2018**, *430* (16), 2321-2341.

APPENDIX

Chemistry

General Chan-Lam-Evans Coupling: The desired aniline (3 mmol) and corresponding boronic acid (6 mmol) were added into DCM with TEA (6 mmol) and $\text{Cu}(\text{OAc})_2$ (3 mmol) with 4 Å molecular sieves. The solution was stirred at room temperature under air for 16 hours. The resulting mixture was filtered through a silica plug and the solvent was evaporated under reduced pressure. The crude mixture was purified via automated CombiFlash chromatography (silica gel, 20–40 μm , with a gradient mobile phase of 0% - 15% EtOAc in Hexane).

General palladium coupling procedure: The desired diphenylamine (2.1 mmol) and $\text{Pd}(\text{OAc})_2$ (2.1 mmol) were dissolved in room temperature acetic acid and then refluxed for 12 hours. The mixture was then cooled and neutralized with the addition of NaOH dropwise and then washed with DCM (3x5 mL). The organic layer was extracted and dried over anhydrous Na_2SO_4 , filtered, concentrated under reduced pressure. The crude mixture was purified via automated CombiFlash chromatography (silica gel, 20–40 μm , with a gradient mobile phase of 0% - 15% EtOAc in Hexane).

General dimethyl amine pendant addition: A carbazole or a diphenylamine (1 eq) was dissolved in DMF and cooled to 0°C. Then NaH (1.2 eq) was added and stirred for 45 minutes. 3-chloro-N,N-dimethylpropan-1-amine (1 eq) was added, and the solution was brought to room temperature and stirred for 24 hours. The crude mixture was washed with LiBr (3 x 9 mL), and the organic layer was extracted with EtOAc (1 x 10 mL). The organic layer was dried over anhydrous Na_2SO_4 , filtered, concentrated under reduced

pressure, and purified using an automated CombiFlash chromatography (silica gel, 20–40 μm , with a gradient mobile phase of 0% - 30% EtOAc in Hexane, with 1% TEA).

General acylation procedure: The desired amine (1 eq) and TEA (1.33 eq) in DCM were cooled to 0 °C and acryloyl chloride (1.2 eq) was added drop wise. The reaction mixture was warmed to room temperature and left to stir for 12 hours. The crude reaction was washed with 2x 10 mL of Brine and extracted with 2 x 10 mL of DCM. The organic layer was dried over anhydrous Na_2SO_4 , filtered, concentrated under reduced pressure. The crude mixture was purified using an automated CombiFlash chromatograph (silica gel, 20–40 μm , with a gradient mobile phase of 0% - 20% EtOAc in Hexane).

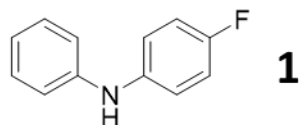
General Michael-Addition procedure: 2-chloro-phenothiazine (2 eq) and the acyl amine (1 eq) were dissolved in toluene, then Triton B (0.5 eq) was added drop wise and the solution was refluxed for 24 hours. The reaction mixture was cooled to room temperature and washed with 2x 10 mL of NaOH (aq) and extracted with 2x 10 mL of EtOAc. The organic layer was dried over anhydrous Na_2SO_4 , filtered, concentrated under reduced pressure. The crude mixture was purified using an automated CombiFlash chromatograph (silica gel, 20–40 μm , with a gradient mobile phase of 0% - 20% EtOAc in Hexane).

General procedure A: The desired heterocycle (1.0 eq) was dissolved in DMF (3.0 mL) and cooled to 0 °C. Then, NaH (1.1 eq) was added, and the mixture stirred at 0 °C for one hour. The corresponding *N,N*-bis(4-fluorophenyl) amide (2 equiv) was added, and the reaction was slowly warmed to room temperature and stirred for 24 hours under inert N_2 gas. The crude mixture was washed with LiBr (3 x 9 mL), and the organic layer was extracted with EtOAc (1 x 10 mL). The organic layer was dried over anhydrous Na_2SO_4 ,

filtered, concentrated under reduced pressure, and purified using an automated CombiFlash chromatography (silica gel, 20–40 μm , with a gradient mobile phase of 0% - 20% EtOAc in Hexane).

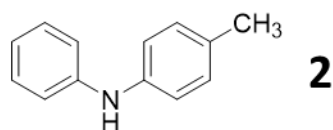
General procedure B: The desired heterocycle (1.0 eq) and the corresponding *N,N*-bis(4-fluorophenyl) amide (1.0 eq) were dissolved in toluene (5.0 mL). Then, TEA (4.0 eq) was added dropwise, and the solution was refluxed for 24 hours under inert N_2 gas. The crude mixture was washed with brine (3 x 5 mL), and the organic layer was extracted with DCM (1 x 10 mL). The organic layer was dried over anhydrous Na_2SO_4 , filtered, concentrated under reduced pressure, and purified using an automated CombiFlash chromatography (silica gel, 20–40 μm , with a gradient mobile phase of 0% - 20% EtOAc in Hexane).

General procedure C: The corresponding *N,N*-bis(4-fluorophenyl) amide (1.0 eq) was dissolved in THF (5 mL), and TEA (1.2 eq) was added dropwise. Then, 2 M dimethyl amine in THF (2.0 eq) was added dropwise, and the solution stirred for 24 hours at room temperature under inert N_2 gas. The crude mixture was washed with brine (3 x 5 mL), and the organic layer was extracted with DCM (10 mL). The crude mixture was dried over Na_2SO_4 , filtered, concentrated under reduced pressure, and purified using an automated CombiFlash chromatography (silica gel, 20–40 μm , with a gradient mobile phase of 0 - 30% EtOAc in Hexane).

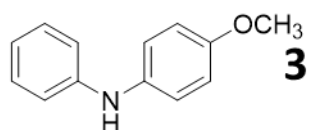


General Chan-Lam-Evans coupling produced an orangey brown oil (58%). ^1H NMR (Chloroform-*d*, 500 MHz) δ 7.30 - 7.25(m, 2H), 7.09 – 7.04 (m, 2H), 7.03 – 6.97 (m, 4H),

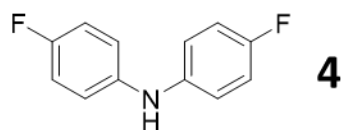
6.93 (tt, $J = 7.3, 1.1$ Hz, 1H), 5.58 (s, 1H). $^{13}\text{C}\{\text{H}\}$ NMR (Chloroform- d , 126 MHz) δ 159.0, 157.1, 143.9, 138.9 (d, $J = 2.4$ Hz), 129.4, 120.6 (d, $J = 8.9$ Hz), 116.8, 116.0 (d, $J = 22.6$ Hz). IR: 3400 cm^{-1} , 2959 cm^{-1} , 1582 cm^{-1} , 1468 cm^{-1} . HRMS (APCI) m/z : $[\text{M}+\text{H}]^+$ calc'd for ($\text{C}_{12}\text{H}_{11}\text{FN}^+$) 188.0876; Could not be found due to poor ionization.



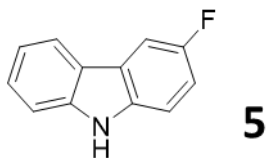
General Chan-Lam-Evans coupling produced a yellow solid (88%). ^1H NMR (Chloroform- d , 500 MHz) δ 7.2 -7.23 (m, 2H), 7.12-7.08 (m, 2H), 7.04-7.00 (m, 4H), 6.91-6.89 (m, $J = 7.4, 1.1$ Hz, 1H), 5.61 (s, 1H), 2.32 (s, 3H). $^{13}\text{C}\{\text{H}\}$ NMR (Chloroform- d , 126 MHz) δ 143.9, 140.3, 130.9, 129.9, 129.3, 120.3, 118.9, 116.8, 20.7. IR: 3380 cm^{-1} , 3006 cm^{-1} . HRMS (APCI) m/z : $[\text{M}+\text{H}]^+$ calc'd for ($\text{C}_{13}\text{H}_{14}\text{N}^+$) 184.1226; Could not be found due to poor ionization.



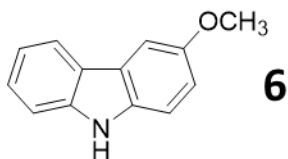
General Chan-Lam-Evans coupling produced a yellow oil (87%) ^1H NMR (DMSO- d_6 , 500 MHz) δ 7.82 (s, 1H), 7.17 - 7.11 (m, 2H), 7.05 - 7.00 (m, 2H), 6.93 - 6.87 (m, 2H), 6.87 - 6.83 (m, 2H), 6.69 (tt, $J = 7.2, 1.1$ Hz, 1H), 3.70 (s, 3H). $^{13}\text{C}\{\text{H}\}$ NMR (DMSO- d_6 , 126 MHz) δ 154.2, 145.6, 136.5, 129.5, 120.8, 118.7, 115.2, 115.0, 55.7. IR: 3383 cm^{-1} , 2908 cm^{-1} . HRMS (APCI) m/z : $[\text{M}+\text{H}]^+$ calc'd for ($\text{C}_{13}\text{H}_{14}\text{NO}^+$) 200.1075; Could not be found due to poor ionization.



General Chan-Lam-Evans coupling produced a yellow oil (0.270 g, 44%). ^1H NMR (DMSO- d_6 , 500 MHz) δ 8.04 (s, 1H), 7.07 – 7.02 (m, 4H), 7.02 – 6.98 (m, 4H). $^{13}\text{C}\{^1\text{H}\}$ NMR (DMSO- d_6 , 126 MHz) δ 157.6, 155.7, 140.7 ($J = 2.2$ Hz), 118.5 (d, $J = 7.7$ Hz), 116.2 (d, $J = 22.1$ Hz). IR: 3400 cm^{-1} , 3097 cm^{-1} . HRMS (APCI) m/z : [(M+H)+] calcd for ($\text{C}_{12}\text{H}_{10}\text{F}_2\text{N}^+$) 206.0781; Found 206.0862.

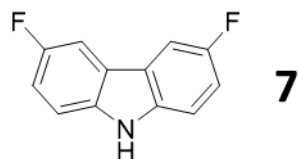


General Chan-Lam-Evans coupling produced a pink solid (57%). MP: 207 °C-209 °C. ^1H NMR (Chloroform- d , 500 MHz) δ 8.05 – 8.00 (m, 2H), 7.73 (ddt, $J = 8.8, 4.3, 0.5$ Hz, 1H), 7.48 – 7.38 (m, 2H), 7.35 (ddd, $J = 8.8, 4.3, 0.5$ Hz, 1H), 7.24 (m, 1H), 7.16 (m, 1H). $^{13}\text{C}\{^1\text{H}\}$ NMR (Chloroform- d , 126 MHz) δ 140.5, 135.7, 126.4, 120.6, 119.5, 113.7, 113.5, 111.1, 111.0, 110.8, 106.1, 105.9. IR: 3600 cm^{-1} , 2922 cm^{-1} . HRMS (APCI) m/z : [M+H] $^+$ calc'd for ($\text{C}_{12}\text{H}_9\text{FN}^+$) 186.0719; Found 186.0724.

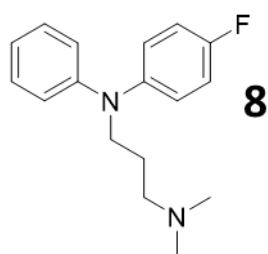


General palladium coupling produced a salmon pink solid (50%) MP: 151 °C-153 °C. ^1H NMR (Chloroform- d , 500 MHz) δ 8.06 – 8.02 (m, 1H), 7.91 (s, 1H), 7.56 (d, $J = 2.5$ Hz, 1H), 7.42 - 7.38 (m, 2H), 7.34 (dd, $J = 8.8, 0.5$ Hz, 1H), 7.24 – 7.19 (m, 1H), 7.07 (dd, $J = 8.7, 2.5$ Hz, 1H), 3.94 (s, 3H). $^{13}\text{C}\{^1\text{H}\}$ NMR (Chloroform- d , 126 MHz) δ 153.89, 140.25, 134.34, 125.79, 123.77, 123.35, 120.24, 119.04, 115.06, 111.29, 110.73, 103.14, 56.07.

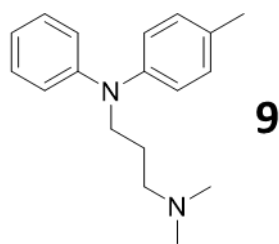
IR: 3385 cm^{-1} , 3061 cm^{-1} . HRMS (APCI) m/z : $[\text{M}+\text{H}]^+$ calc'd for ($\text{C}_{13}\text{H}_{12}\text{NO}^+$) 198.0919; Found 198.1021.



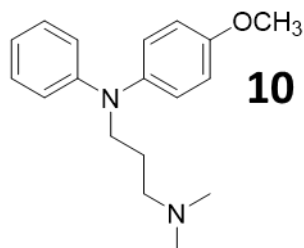
General palladium coupling produced a yellow solid (52%) MP: 199 °C-201°C. ^1H NMR (Chloroform-*d*, 500 MHz) δ 8.00 (s, 1H), 7.67 (ddd, J = 8.8, 2.4, 1.3 Hz, 2H), 7.39 - 7.35 (m, 2H), 7.19 (tdd, J = 8.9, 2.5, 1.3 Hz, 2H). $^{13}\text{C}\{^1\text{H}\}$ NMR (Chloroform-*d*, 126 MHz) δ 158.3, 156.4, 136.8, 114.4 (d, J = 25.7 Hz), 111.5 (d, J = 9.0 Hz), 106.1 (d, J = 23.9 Hz). HRMS (APCI) m/z : $[\text{M}+\text{H}]^+$ calc'd for ($\text{C}_{12}\text{H}_8\text{F}_2\text{N}^+$) 204.0625; Found 204.0661.



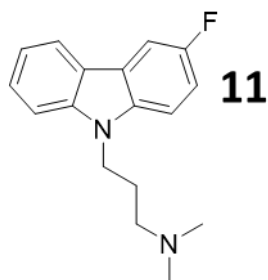
General dimethyl amine pendant addition produced a yellow oil (30%). ^1H NMR (Chloroform-*d*, 500 MHz) δ 7.25-7.18 (m, 2H), 7.10-6.96 (m, 4H), 6.90-6.81 (m, 3H), 3.78-3.64 (m, 2H), 2.42-2.30 (m, 2H), 2.24 (s, 6H), 1.82 (p, J = 7.3 Hz, 2H). $^{13}\text{C}\{^1\text{H}\}$ NMR (Chloroform-*d*, 126 MHz) δ 1148.4, 127.2, 125.3 (d, J = 1.3 Hz), 125.2 (d, J = 1.5 Hz), 119.7, 118.1 (d, J = 2.4 Hz), 116.2, 116.0, 57.0, 50.3, 45.4, 25.4. IR: 3049, 2941 cm^{-1} . HRMS (APCI) m/z : $[\text{M}+\text{H}]^+$ calc'd for ($\text{C}_{17}\text{H}_{22}\text{FN}_2^+$) 273.1722; Found 273.1794.



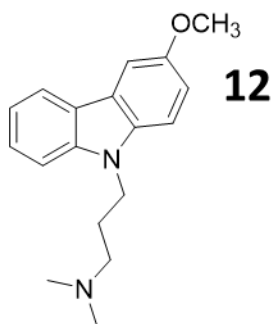
General dimethyl amine pendant addition produced yellow oil (29%). ^1H NMR (Chloroform-*d*, 500 MHz) δ 7.25 - 7.19 (m, 2H), 7.14 - 7.09 (m, 2H), 7.03 - 6.96 (m, 2H), 6.93 - 6.87 (m, 2H), 6.84 (td, 1H), 3.76 - 3.70 (m, 2H), 2.35 - 2.28 (m, 5H), 2.21 (s, 6H), 1.86 - 1.77 (dq, $J = 8.9, 7.3$ Hz, 2H). $^{13}\text{C}\{^1\text{H}\}$ NMR (Chloroform-*d*, 126 MHz) δ 148.53, 145.27, 132.12, 130.02, 129.08, 123.41, 119.43, 118.35, 57.17, 50.25, 45.59, 25.63, 20.78. IR: 3060 cm^{-1} , 2930 cm^{-1} . HRMS (APCI) m/z : $[\text{M}+\text{H}]^+$ calc'd for $(\text{C}_{18}\text{H}_{25}\text{N}_2^+)$ 269.2018; Found 269.2050.



General dimethyl amine pendant addition produced orange oil (23%). ^1H NMR (Chloroform-*d*, 500 MHz) δ 7.21 - 7.15 (m, 2H), 7.13 - 7.08 (m, 2H), 6.93 - 6.89 (m, 2H), 6.79 - 6.73 (m, 3H), 3.83 (s, 3H), 3.73 - 3.66 (m, 2H), 2.33 (t, $J = 7.2$ Hz, 2H), 2.22 (s, 6H), 1.82 (p, $J = 7.3$ Hz, 2H). $^{13}\text{C}\{^1\text{H}\}$ NMR (Chloroform-*d*, 126 MHz) δ 156.5, 149.1, 140.6, 129.0, 127.5, 117.8, 115.5, 114.9, 57.2, 55.5, 50.4, 45.6, 25.6. HRMS (APCI) m/z : $[\text{M}+\text{H}]^+$ calc'd for $(\text{C}_{18}\text{H}_{25}\text{N}_2\text{O}^+)$ 285.1967; Found 285.1313.



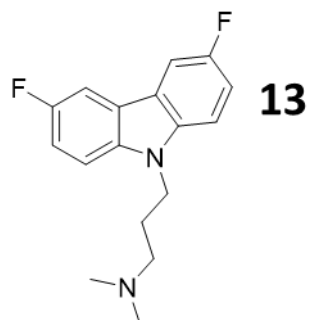
General dimethyl amine pendant addition produced yellow oil (67%). ^1H NMR (Chloroform-*d*, 500 MHz) δ 8.04 (d, $J = 7.8$ Hz, 1H), 7.74 (dd, $J = 8.9, 2.5$ Hz, 1H), 7.50 - 7.44 (m, 2H), 7.39 (dd, $J = 8.9, 4.2$ Hz, 1H), 7.24 - 7.17 (m, 2H), 4.38 (t, $J = 6.9$ Hz, 2H), 2.26 (t, $J = 6.7$ Hz, 2H), 2.22 (s, 6H), 2.00 (q, $J = 6.8$ Hz, 2H). $^{13}\text{C}\{^1\text{H}\}$ NMR (Chloroform-*d*, 126 MHz) δ 158.1, 156.3, 141.3, 136.9, 126.2, 123.1 (d, $J = 9.5$ Hz), 122.4 (d, $J = 4.3$ Hz), 120.5, 118.7, 113.3 (d, $J = 25.6$ Hz), 109.3 (d, $J = 9.0$ Hz), 109.1, 105.9 (d, $J = 23.5$ Hz), 56.5, 45.4, 40.8, 27.0. IR: 3058 cm^{-1} , 2937 cm^{-1} . HRMS (APCI) m/z : $[\text{M}+\text{H}]^+$ calc'd for ($\text{C}_{17}\text{H}_{20}\text{FN}_2^+$) 271.1611; Found 271.1644.



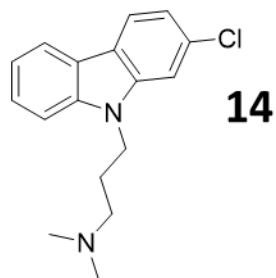
General dimethyl amine pendant addition produced a red oil (76%). ^1H NMR (Chloroform-*d*, 500 MHz) δ 8.07 (dt, $J = 7.8, 1.0$ Hz, 1H), 7.60 (d, $J = 2.5$ Hz, 1H), 7.49 - 7.42 (m, 2H), 7.39 (d, $J = 8.8$ Hz, 1H), 7.23 - 7.18 (m, 1H), 7.12 (dd, $J = 8.8, 2.5$ Hz, 1H), 4.37 (t, $J = 6.9$ Hz, 2H), 3.95 (s, 3H), 2.28 (t, $J = 6.8$ Hz, 2H), 2.23 (s, 6H), 2.02 (p, $J = 6.9$ Hz, 2H). $^{13}\text{C}\{^1\text{H}\}$ NMR (Chloroform-*d*, 126 MHz) δ 153.5, 141.0, 135.6, 125.6, 123.1, 122.6, 120.2,

118.3, 114.8, 109.5, 108.9, 103.2, 56.6, 56.2, 45.5, 40.7, 27.0. IR: 3038 cm^{-1} , 2959 cm^{-1} .

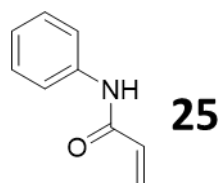
HRMS (APCI) m/z : $[M+H]^+$ calc'd for $(\text{C}_{18}\text{H}_{23}\text{N}_2\text{O}^+)$ 283.1810; Found 283.1724.



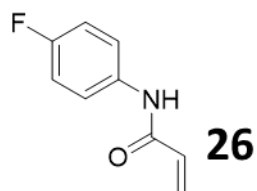
General dimethyl amine pendant addition produced a yellow oil (68%). ^1H NMR (Chloroform- d , 500 MHz) δ 7.69 (dd, $J = 8.8, 2.5$ Hz, 2H), 7.39 (dd, $J = 8.9, 4.2$ Hz, 2H), 7.22 (td, $J = 9.0, 2.5$ Hz, 2H), 4.37 (t, $J = 6.7$ Hz, 2H), 2.27 - 2.20 (m, 8H), 1.99 (p, $J = 6.8$ Hz, 2H). $^{13}\text{C}\{^1\text{H}\}$ NMR (Chloroform- d , 126 MHz) δ 157.9, 156.1, 137.7, 114.1 (d, $J = 25.7$ Hz), 109.7 (d, $J = 8.9$ Hz), 106.1 (d, $J = 23.6$), 56.3, 45.4, 40.9, 26.9. IR: 3073 cm^{-1} , 2968 cm^{-1} . HRMS (APCI) m/z : $[M+H]^+$ calc'd for $(\text{C}_{17}\text{H}_{19}\text{F}_2\text{N}_2^+)$ 289.1516; Found 289.1552.



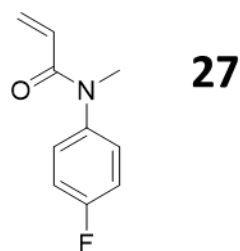
General dimethyl amine pendant addition produced a yellow oil in a (60%). ^1H NMR (Chloroform- d , 500 MHz) δ 8.05 (dt, 1H), 7.98 (d, 1H), 7.51 – 7.43 (m, 3H), 7.30 – 7.22 (m, 1H), 7.19 (dd, 1H), 4.36 (t, $J = 6.8$ Hz, 2H), 2.25 (d, 8H), 2.00 (m, 2H). $^{13}\text{C}\{^1\text{H}\}$ NMR (Chloroform- d , 126 MHz) δ 141.2, 140.8, 131.4, 125.9, 122.3, 121.3, 121.0, 120.3, 119.3, 119.2, 109.1, 109.0, 56.3, 45.4, 40.6, 26.8. IR: 3058 cm^{-1} , 2967 cm^{-1} . HRMS (APCI) m/z : $[M+H]^+$ calc'd for $(\text{C}_{17}\text{H}_{20}\text{ClN}_2^+)$ 288.1315; Found 288.1313.



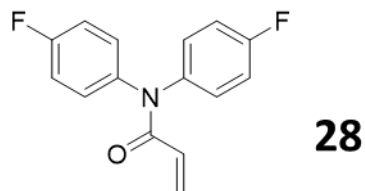
General acylation procedure provided a white solid (86%). ^1H NMR (DMSO- d_6 , 500 MHz) δ 10.12 (br, 1H), 7.68 – 7.61 (m, 2H), 7.31-7.28 (m, 2H), 7.05 (tt, $J = 7.4, 1.2$ Hz, 1H), 6.45-6.40 (m, 1H), 6.24 (dd, $J = 17.0, 2.0$ Hz, 1H), 5.73 (dd, $J = 10.1, 2.0$ Hz, 1H). $^{13}\text{C}\{^1\text{H}\}$ NMR (DMSO- d_6 , 126 MHz) δ 163.6, 139.5, 132.3, 129.2, 127.3, 123.9, 119.8. IR: 3265 cm^{-1} , 3075 cm^{-1} , 1674 cm^{-1} . HRMS (APCI) m/z : [(M+H) $^+$] calcd for (C₉H₁₀NO $^+$) 148.0762; Found 148.0976.



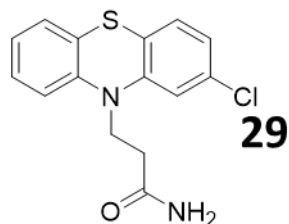
General acylation procedure provided an off-white solid (71%). ^1H NMR (CDCl₃, 500 MHz) δ 7.54 (dd, $J = 8.9, 4.8$ Hz, 2H), 7.33 (br, 1H), 7.07 – 6.99 (m, 2H), 6.44 (dd, $J = 16.9, 1.2$ Hz, 1H), 6.24 (dd, $J = 16.8, 10.2$ Hz, 1H), 5.78 (dd, $J = 10.3, 1.2$ Hz, 1H). $^{13}\text{C}\{^1\text{H}\}$ NMR (DMSO- d_6 , 126 MHz) δ 163.5, 158.6 (d, $J = 240.0$ Hz), 135.9 (d, $J = 2.5$ Hz), 132.2, 127.4, 121.5, 121.5, 115.9, 115.7. IR: 3468 cm^{-1} , 3105 cm^{-1} , 1634 cm^{-1} . HRMS (APCI) m/z : [(M+H) $^+$] calcd for (C₉H₉FNO $^+$) 166.0668; Found 166.0780.



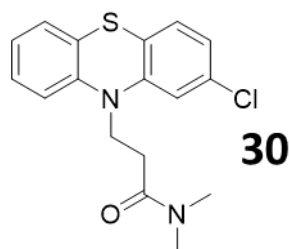
In a round bottom flask with 10 ml of THF, N-(4-fluorophenyl)acrylamide (**26**) (1.2 mmol) was added and the solution was cooled to 0 °C. Then NaH (1.32 mmol) was added and the reaction was warmed to room temperature. After 30 minutes, the reaction was brought back to 0 °C and iodomethane (1.32 mmol) was added drop wise and the reaction was raised to room temperature. After 2 hours, the reaction mixture was washed with (2x 10 ml) water and then extracted with (2x10 ml) ethyl acetate, dried over sodium sulfate, and concentrated in vacuo to produce the title compound in quantitative yields. ¹H NMR (CDCl₃, 500 MHz) δ 7.15 (m, 2H), 7.12 – 7.07 (m, 2H), 6.36 (dd, *J* = 16.8, 2.0 Hz, 1H), 6.03 (dd, *J* = 16.8, 10.3 Hz, 1H), 5.53 (dd, *J* = 10.3, 2.0 Hz, 1H), 3.33 (s, 3H). ¹³C{¹H} NMR (CDCl₃, 126 MHz) δ 165.8, 161.6 (d, *J* = 248.0 Hz), 139.4 (d, *J* = 3.3 Hz), 129.1, 129.0, 128.2, 127.8, 116.6, 116.4, 37.5. IR: 3062 cm⁻¹, 3053 cm⁻¹, 1678 cm⁻¹. HRMS (APCI) *m/z*: [(M+H)+] calcd for (C₁₀H₁₁FNO⁺) 180.0825; Found 180.0842.



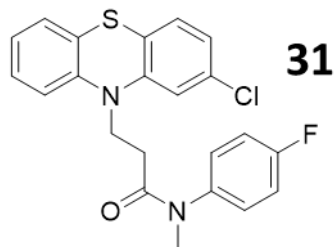
General acylation procedure provided an off-white solid (90%). ¹H NMR (CDCl₃, 500 MHz) δ 7.24 – 7.15 (m, 4H), 7.08 (d, *J* = 8.8 Hz, 4H), 6.48 (dd, *J* = 16.8, 1.8 Hz, 1H), 6.17 (dd, *J* = 16.8, 10.3 Hz, 1H), 5.67 (dd, *J* = 10.3, 1.9 Hz, 1H). ¹³C{¹H} NMR (DMSO-*d*₆, 151 MHz, 338K) δ 165.2, 161.2 (d, *J* = 244.7 Hz), 139.2, 130.2, 129.7 (d, *J* = 168.4), 128.6, 116.6 (d, *J* = 22.8 Hz). IR: 3075 cm⁻¹, 1669 cm⁻¹. HRMS (APCI) *m/z*: [(M+H)+] calcd for (C₁₅H₁₂F₂NO⁺) 260.0887; Found 260.0888.



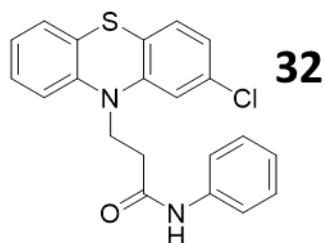
General Michael-addition procedure provided a white solid (25%). ¹H NMR (DMSO-*d*₆, 500 MHz) δ 8.13 (d, *J* = 8.1, 2H), 7.72 (d, *J* = 1.8 Hz, 1H), 7.61 (d, *J* = 8.2 Hz, 1H), 7.47-7.44 (m, 1H), 7.35 (s, 1H), 7.23 – 7.16 (m, 2H), 6.87 (s, 1H), 4.58 (t, *J* = 6.7 Hz, 2H), 2.55 (t, *J* = 6.7 Hz, 2H). ¹³C{¹H} NMR (DMSO-*d*₆, 126 MHz) δ 172.5, 140.9, 140.6, 130.7, 126.6, 122.1, 122.0, 121.5, 120.8, 119.8, 119.4, 110.2, 110.0, 334.8. IR: 3392 cm⁻¹, 3025 cm⁻¹, 2990 cm⁻¹, 1645 cm⁻¹, 1607 cm⁻¹. HRMS (APCI) *m/z*: [(M+H)⁺] calcd for (C₁₅H₁₄ClN₂OS⁺) 305.0515; Found 305.0777.



General Michael-addition procedure provided an off-white solid (85%). ¹H NMR (CDCl₃, 500 MHz) δ 8.05 (d, *J* = 7.8, 1H), 7.99 (d, *J* = 8.2 Hz, 1H), 7.49 – 7.43 (m, 3H), 7.25 (dd, *J* = 6.4, 1.6 Hz, 1H), 7.21 (dd, *J* = 8.2, 1.8 Hz, 1H), 4.69 – 4.64 (m, 2H), 2.91 (s, 3H), 2.84 – 2.78 (m, 2H), 2.71 (s, 3H). ¹³C{¹H} NMR (CDCl₃, 126 MHz) δ 170.5, 140.6, 140.3, 131.6, 126.1, 122.5, 121.6, 121.2, 120.3, 119.6, 119.6, 108.8, 39.4, 37.0, 35.4, 31.9. IR: 3070 cm⁻¹, 2885 cm⁻¹, 1595 cm⁻¹. HRMS (APCI) *m/z*: [(M+H)⁺] calcd for (C₁₇H₁₈ClN₂OS⁺) 333.0828; Found 333.0817.

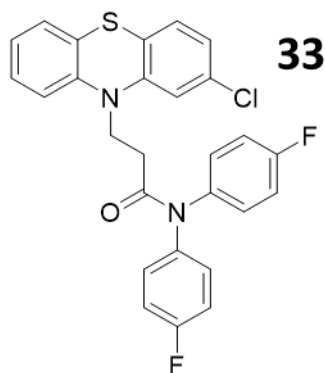


General Michael-addition procedure provided a white solid (38%). ^1H NMR (CDCl_3 , 500 MHz) δ 7.12 (dd, $J = 7.6, 1.5$ Hz, 1H), 7.08 (t, $J = 7.8$ Hz, 1H), 7.01 (d, $J = 8.2$ Hz, 1H), 7.00 – 6.90 (m, 5H), 6.88 (d, $J = 8.1$ Hz, 1H), 6.75 (d, $J = 8.1$ Hz, 1H), 6.71 (d, $J = 2.0$ Hz, 1H), 4.15 (br t, 2H), 3.25 (s, 3H), 2.53 (t, $J = 6.9$ Hz, 2H). $^{13}\text{C}\{^1\text{H}\}$ NMR (CDCl_3 , 126 MHz) δ 170.69, 161.72 (d, $J = 248.4$ Hz), 146.20, 139.43 (d, $J = 3.3$ Hz), 133.36, 128.83, 128.77, 127.92, 127.53, 124.66, 123.38, 123.10, 122.47, 116.77, 116.59, 115.56, 115.45, 43.64, 37.46, 31.28. IR: 3058 cm^{-1} , 2910 cm^{-1} , 1646 cm^{-1} . HRMS (APCI) m/z : [(M+H) $^+$] calcd for ($\text{C}_{22}\text{H}_{19}\text{ClFN}_2\text{OS}^+$) 413.0891; Found 413.9011.

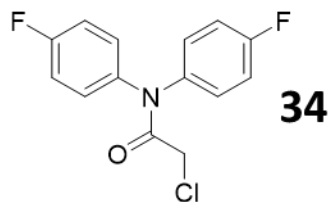


General Michael-addition procedure provided a white oil (41%). ^1H NMR (CDCl_3 , 500 MHz) δ 8.04 (d, $J = 7.8$, 1H), 7.97 (d, $J = 8.2$ Hz, 1H), 7.43 (m, 1H), 7.34 (dt, $J = 8.4, 0.9$ Hz, 1H), 7.26 – 7.23 (m, 1H), 7.20 (dd, $J = 8.2, 1.8$ Hz, 1H), 7.18 – 7.13 (m, 1H), 7.10 (m, 1H), 6.86 – 6.82 (m, 2H), 6.64 – 6.60 (m, 1H), 6.27 – 6.22 (m, 2H), 4.64 (t, $J = 6.6$ Hz, 2H), 2.59 (t, $J = 6.6$ Hz, 2H). $^{13}\text{C}\{^1\text{H}\}$ NMR (CDCl_3 , 126 MHz) δ 170.5, 140.4, 140.2, 136.4, 131.6, 129.8, 129.7, 128.6, 128.3, 127.4, 126.2, 122.3, 121.4, 121.1, 120.2, 119.7, 116.3,

116.1, 109.1, 39.9, 32.7. IR: 3761 cm^{-1} , 3110 cm^{-1} , 2880 cm^{-1} , 1672 cm^{-1} . HRMS (APCI) m/z : [(M+H)+] calcd for ($\text{C}_{21}\text{H}_{18}\text{ClN}_2\text{OS}^+$) 381.0828; Found 381.0941.

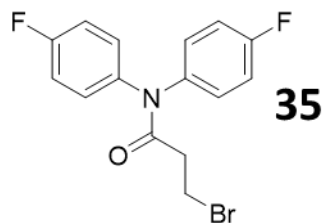


General Michael-addition procedure provided a light pink solid (80%). ^1H NMR (CDCl_3 , 500 MHz) δ 7.24 – 7.16 (m, 3H), 7.13 – 7.06 (m, 2H), 7.02 – 6.88 (m, 8H), 6.79 (dd, J = 8.2, 1.2 Hz, 1H), 6.75 (d, J = 2.0 Hz, 1H), 4.27 (t, J = 6.4 Hz, 2H), 2.71 (t, J = 6.4 Hz, 2H). $^{13}\text{C}\{^1\text{H}\}$ NMR (CDCl_3 , 126 MHz) δ 170.78, 145.28 (d, J = 263.7 Hz), 138.19 (d, J = 3.3 Hz), 133.47, 129.84, 128.16, 128.04, 127.63, 124.98, 123.66, 123.22, 122.61, 116.69 (d, J = 21.7 Hz), 115.92, 115.78, 115.73, 115.64, 43.72, 31.98. IR: 3015 cm^{-1} , 2960 cm^{-1} , 1664 cm^{-1} . HRMS (APCI) m/z : [(M+H)+] calcd for ($\text{C}_{27}\text{H}_{20}\text{ClF}_2\text{N}_2\text{OS}^+$) 493.0953; Found 493.0950.

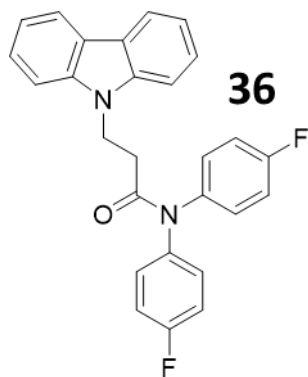


General acylation procedure produced a light-yellow solid (67%). MP: 95-97 $^\circ\text{C}$. ^1H NMR (CD_2Cl_2 , 500 MHz) δ 7.34-7.10 (m, 8H), 4.05 (s, 2H). $^{13}\text{C}\{^1\text{H}\}$ NMR ($\text{DMSO}-d_6$, 126 MHz) δ 166.0, 139.2, 138.2, 131.4, 129.3, 117.2, 116.3, 43.7. IR: 3067 cm^{-1} , 2980 cm^{-1} , 1686 cm^{-1} , 1503 cm^{-1} . HRMS (APCI) m/z : [M+H] $^+$ calc'd for ($\text{C}_{14}\text{H}_{11}\text{ClF}_2\text{NO}^+$) 282.0492; Found

282.0338. ^1H NMR and $^{13}\text{C}\{^1\text{H}\}$ NMR were run in different solvents for better resolution of the observed peaks.

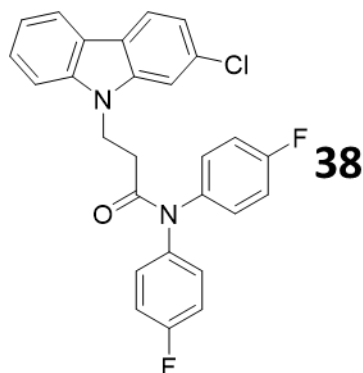


General acylation procedure produced a pale pink solid (88%). MP: 94-96 °C. ^1H NMR (CDCl_3 , 500 MHz) δ 7.22-7.03 (m, 8H), 3.66 (t, J = 6.6 Hz, 2H), 2.82 (t, J = 6.6 Hz, 2H). $^{13}\text{C}\{^1\text{H}\}$ NMR (CDCl_3 , 126 MHz) δ 170.1, 138.1, 138.13, 138.11, 130.3, 127.9, 117.2, 116.0, 37.9, 27.5. IR: 3117 cm^{-1} , 2950 cm^{-1} , 1600 cm^{-1} , 1425 cm^{-1} . HRMS (APCI) m/z : $[\text{M}+\text{H}]^+$ calc'd for ($\text{C}_{15}\text{H}_{13}\text{BrF}_2\text{NO}^+$) 340.0143; Found 340.0063.

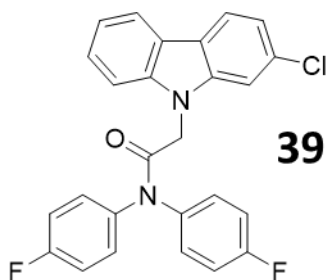


General procedure A produced a white solid (59%). MP: 177-178 °C. ^1H NMR ($\text{DMSO}-d_6$, 500 MHz) δ 8.16 (d, J = 8.0 Hz, 2H), 7.48 (dt, J = 8.0, 0.9 Hz, 2H), 7.42-7.38 (m, 2H), 7.22-7.18 (m, 2H), 7.12 (t, J = 8.4 Hz, 2H), 7.07-7.05 (m, 4H), 6.97 (t, J = 8.1 Hz, 2H), 4.66 (t, J = 6.9 Hz, 2H), 2.65 (t, J = 6.9 Hz, 2H). $^{13}\text{C}\{^1\text{H}\}$ NMR (CDCl_3 , 126 MHz) δ 171.3, 139.9, 137.99, 137.96, 129.6 (d, J = 8.6 Hz), 128.1 (d, J = 8.4 Hz), 125.9, 122.9, 120.3, 119.3, 116.5 (d, J = 22.6 Hz), 115.9 (d, J = 22.9 Hz), 109.0, 40.0, 33.3. IR: 3059 cm^{-1} , 2992 cm^{-1} , 1659 cm^{-1} , 1327 cm^{-1} . HRMS (APCI) m/z : $[\text{M}+\text{H}]^+$ calc'd for ($\text{C}_{27}\text{H}_{21}\text{F}_2\text{N}_2\text{O}^+$)

427.1616; Found 427.1641. ^1H NMR and $^{13}\text{C}\{^1\text{H}\}$ NMR were run in different solvents for better resolution of the observed peaks

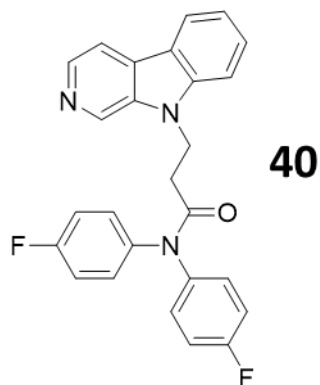


General procedure A produced a white solid in 88% yield. MP: 133-134 °C. ^1H NMR (DMSO- d_6 , 500 MHz) δ 8.17 (dd, J = 8.1, 1.5 Hz, 2H), 7.57 (d, J = 1.8 Hz, 1H), 7.51 (d, J = 8.2 Hz, 1H), 7.45-7.42 (m, 1H), 7.25-7.20 (m, 2H), 7.14-7.00 (m, 8H), 4.64 (t, J = 6.8 Hz, 2H), 2.66 (t, J = 6.8 Hz, 2H). $^{13}\text{C}\{^1\text{H}\}$ NMR (CDCl_3 , 126 MHz) δ 171.0, 140.4, 140.3, 137.92, 137.89, 131.7, 129.6 (d, J = 8.6 Hz), 128.0 (d, J = 8.8 Hz), 126.2, 122.3, 121.5, 121.2, 120.3, 119.9, 119.8, 116.6 (d, J = 22.8 Hz), 116.0 (d, J = 22.5 Hz), 109.2, 109.0, 40.0, 33.3. IR: 3030 cm^{-1} , 2865 cm^{-1} , 1605 cm^{-1} , 1320 cm^{-1} . HRMS (APCI) m/z : $[\text{M}+\text{H}]^+$ calc'd for ($\text{C}_{27}\text{H}_{20}\text{ClF}_2\text{N}_2\text{O}^+$) 462.1227; Found 462.1157. ^1H NMR and $^{13}\text{C}\{^1\text{H}\}$ NMR were run in different solvents for better resolution of the observed peaks.

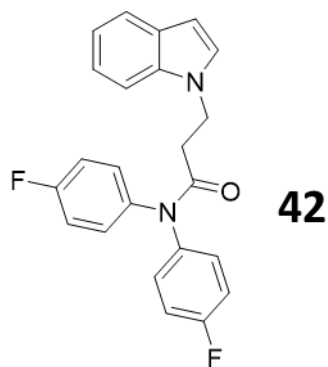


General procedure A produced a light-yellow solid (58%). MP: 129-130 °C ^1H NMR (CDCl_3 , 500 MHz) δ 8.00 (dd, J = 8.1, 1.2 Hz, 1H), 7.91 (d, J = 8.2 Hz, 1H), 7.45-7.42 (m,

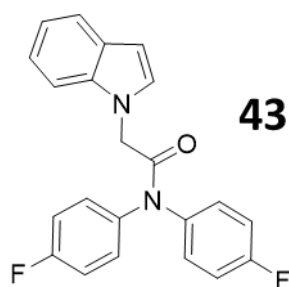
1H), 7.27-7.24 (m, 2H), 7.19 (dd, $J = 8.2, 1.8$ Hz, 1H), 7.16-7.09 (m, 5H), 6.97 (t, $J = 8.3$ Hz, 4H), 4.92 (s, 2H). $^{13}\text{C}\{^1\text{H}\}$ NMR (CDCl_3 , 126 MHz) δ 167.4, 140.8, 140.6, 138.0, 136.8, 131.5, 129.5, 127.4, 126.1, 122.6, 121.7, 121.1, 120.3, 120.2, 120.0, 117.4 (d, $J = 22.5$ Hz), 116.0 (d, $J = 22.8$ Hz), 108.7, 108.6, 46.7. IR: 3057 cm^{-1} , 2960 cm^{-1} , 1670 cm^{-1} , 1280 cm^{-1} . HRMS (APCI) m/z : $[\text{M}+\text{H}]^+$ calc'd for $(\text{C}_{26}\text{H}_{18}\text{ClF}_2\text{N}_2\text{O}^+)$ 447.1070; Found 447.1142.



General procedure A produced a light-yellow solid in 38% yield. MP: 192-193 °C. ^1H NMR (CDCl_3 , 500 MHz) δ 8.82 (s, 1H), 8.51 (s, 1H), 8.19 (dt, $J = 7.9, 1.0$ Hz, 1H), 8.00 (d, $J = 5.0$ Hz, 1H), 7.61-7.58 (m, 1H), 7.50-7.48 (m, 1H), 7.35-7.32 (m, 1H), 6.94-6.74 (m, 6H), 6.62 (dd, $J = 8.7, 4.7$ Hz, 2H), 4.81 (t, $J = 6.5$ Hz, 2H), 2.83 (t, $J = 6.5$ Hz, 2H). $^{13}\text{C}\{^1\text{H}\}$ NMR (CDCl_3 , 126 MHz) δ 170.7, 140.9, 139.2, 137.8, 132.8, 132.1, 129.6 (d, $J = 8.5$ Hz), 128.7, 127.9 (d, $J = 8.7$ Hz), 121.9, 121.2, 121.1, 120.3, 120.1, 116.8 (d, $J = 22.7$ Hz), 116.0 (d, $J = 22.7$ Hz), 111.9, 109.9, 40.1, 33.7. IR: 3078 cm^{-1} , 2895 cm^{-1} , 1620 cm^{-1} , 1355 cm^{-1} . HRMS (APCI) m/z : $[\text{M}+\text{H}]^+$ calc'd for $(\text{C}_{26}\text{H}_{20}\text{F}_2\text{N}_3\text{O}^+)$ 428.1569; Found 428.1480.



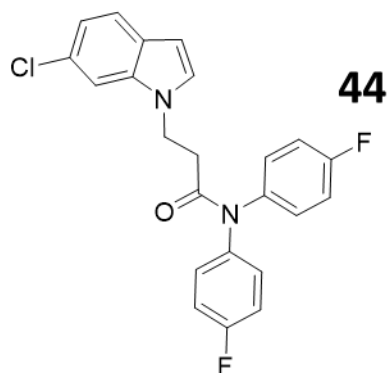
General procedure A produced a white waxy solid in 65% yield. ^1H NMR (CDCl_3 , 500 MHz) δ 7.68-7.66 (m, 1H), 7.18-7.12 (m, 4H), 7.06-6.97 (m, 4H), 6.77 (t, J = 8.2 Hz, 2H), 6.58 (dd, J = 8.6, 4.8 Hz, 2H), 6.53 (d, J = 3.1 Hz, 1H), 4.54 (t, J = 6.2 Hz, 2H), 2.70 (t, J = 6.2 Hz, 2H). $^{13}\text{C}\{^1\text{H}\}$ NMR (CDCl_3 , 126 MHz) δ 171.0, 138.1, 138.0, 135.6, 129.9 (d, J = 8.6 Hz), 128.7, 128.6, 128.1 (d, J = 8.5 Hz), 121.7, 121.1, 119.6, 116.7 (d, J = 22.9 Hz), 116.0 (d, J = 22.6 Hz), 109.3, 101.4, 43.1, 35.0. IR: 3107 cm^{-1} , 2970 cm^{-1} , 1600 cm^{-1} , 1370 cm^{-1} . HRMS (APCI) m/z : $[\text{M}+\text{H}]^+$ calc'd for ($\text{C}_{23}\text{H}_{19}\text{ClFN}_2\text{O}^+$) calc'd for ($\text{C}_{23}\text{H}_{19}\text{F}_2\text{N}_2\text{O}^+$) 377.1460; Found 377.1408.



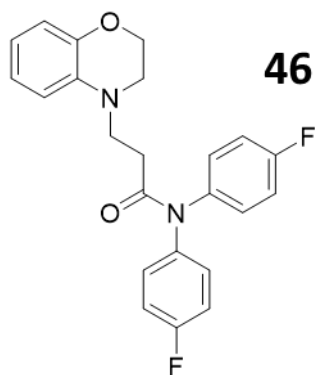
General procedure A produced a white waxy solid (60%). ^1H NMR ($\text{DMSO}-d_6$, 500 MHz) δ 7.74 (s, 2H), 7.51 (dt, J = 7.8, 1.0 Hz, 1H), 7.39-7.29 (m, 5H), 7.22 (d, J = 3.2 Hz, 3H), 7.12-7.09 (m, 1H), 7.01-6.98 (m, 1H), 6.39 (dd, J = 3.2, 0.9 Hz, 1H), 4.88 (s, 2H). $^{13}\text{C}\{^1\text{H}\}$ NMR (CDCl_3 , 126 MHz) δ 167.8, 138.0, 137.2, 136.2, 129.9, 128.6, 128.3, 127.5, 121.9, 121.1, 119.8, 117.3, 115.9, 108.8, 102.4, 49.5. IR: 3047 cm^{-1} , 2960 cm^{-1} , 1630 cm^{-1} , 1395

cm⁻¹. HRMS (APCI) *m/z*: [M+H]⁺ calc'd for (C₂₂H₁₇ClF₂N₂O⁺) 363.1303; Found 363.1177.

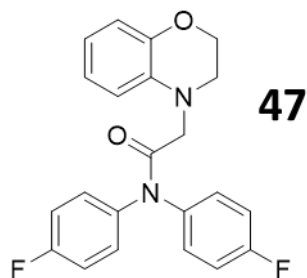
¹H NMR and ¹³C{¹H} NMR were run in different solvents for better resolution of the observed peaks.



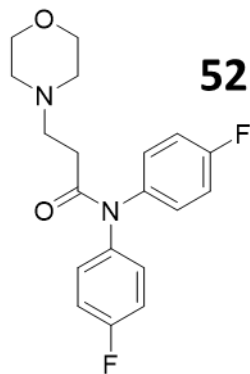
General procedure A produced a waxy light-brown solid (62%). ¹H NMR (DMSO-*d*₆, 500 MHz) δ 7.54 (d, *J* = 8.4 Hz, 1H), 7.42-7.40 (m, 1H), 7.33 (d, *J* = 3.1 Hz, 1H), 7.21-7.11 (m, 8H), 7.02 (dd, *J* = 8.4, 1.9 Hz, 1H), 6.44 (dd, *J* = 3.2, 0.9 Hz, 1H), 4.41 (t, *J* = 6.7 Hz, 2H), 2.62 (t, *J* = 6.7 Hz, 2H). ¹³C{¹H} NMR (CDCl₃, 126 MHz) δ 170.7, 138.0, 137.9, 136.0, 129.9 (d, *J* = 8.3 Hz), 129.5, 128.0 (d, *J* = 8.2 Hz), 127.7, 127.3, 121.9, 120.3, 116.8 (d, *J* = 22.9 Hz), 116.0 (d, *J* = 22.5 Hz), 109.3, 101.6, 43.2, 34.9. IR: 3062 cm⁻¹, 2941 cm⁻¹, 1661 cm⁻¹, 1306cm⁻¹. HRMS (APCI) *m/z*: [M+H]⁺ calc'd for (C₂₃H₁₈ClF₂N₂O⁺) 411.1070; Found 411.1092. ¹H NMR and ¹³C{¹H} NMR were run in different solvents for better resolution of the observed peaks.



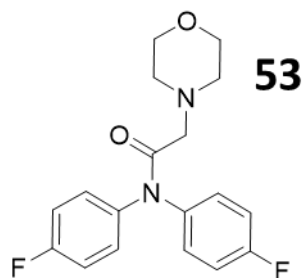
General procedure B produced a brown waxy solid (47%). ^1H NMR (CDCl_3 , 500 MHz) δ 7.20-7.17 (m, 4H), 7.06-7.03 (m, 4H), 6.82-6.77 (m, 2H), 6.71-6.69 (m, 1H), 6.57 (d, J = 8.0 Hz, 1H), 4.25-4.23 (m, 2H), 3.68 (t, J = 6.5 Hz, 2H), 3.38-3.36 (m, 2H), 2.61 (t, J = 6.5 Hz, 2H). $^{13}\text{C}\{^1\text{H}\}$ NMR (CDCl_3 , 126 MHz) δ 171.7, 144.2, 138.4, 134.0, 130.2, 128.0, 121.7, 118.1, 117.1 (d, J = 23.0 Hz), 116.5, 116.0. (d, J = 22.4 Hz), 112.2, 64.4, 47.72, 47.68, 31.8. (*Missing Ar-Carbon around 140 ppm) IR: 3053 cm^{-1} , 2994 cm^{-1} , 1655 cm^{-1} , 1349 cm^{-1} . HRMS (APCI) m/z : $[\text{M}+\text{H}]^+$ calc'd for ($\text{C}_{23}\text{H}_{21}\text{F}_2\text{N}_2\text{O}_2^+$) 395.1566; Found 395.1771.



General procedure B produced a brown waxy solid (70%). ^1H NMR ($\text{DMSO}-d_6$, 500 MHz) δ 7.68 (s, 2H), 7.33-7.18 (m, 6H), 6.75-6.72 (m, 1H), 6.64 (dd, J = 7.8, 1.5 Hz, 1H), 6.52-6.48 (m, 2H), 4.09-4.07 (m, 2H), 3.93 (s, 2H), 3.36-3.33 (m, 2H). $^{13}\text{C}\{^1\text{H}\}$ NMR ($\text{DMSO}-d_6$, 126 MHz) δ 169.1, 143.9, 135.4, 134.1, 131.3, 130.2, 129.0, 121.7, 117.5, 117.2, 116.1, 115.8, 111.8, 64.5, 53.0, 47.8. IR: 3067 cm^{-1} , 2975 cm^{-1} , 1700 cm^{-1} , 1245 cm^{-1} . HRMS (APCI) m/z : $[\text{M}+\text{H}]^+$ calc'd for ($\text{C}_{22}\text{H}_{19}\text{F}_2\text{N}_2\text{O}_2^+$) 381.1409; Found 381.1440.

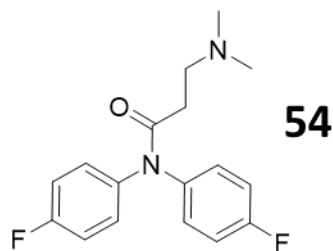


General procedure B produced a white powder (36%) with the following modifications: 1.1 eq of TEA and 1.2 eq of morpholine. MP: 99-101 °C. ^1H NMR (DMSO- d_6 , 500 MHz) δ 7.53-7.19 (m, 8H), 3.50 (t, $J = 4.6$ Hz, 4H), 2.53 (t, $J = 7.3$ Hz, 2H), 2.32 (t, $J = 7.3$ Hz, 2H), 2.22 (t, $J = 4.6$ Hz, 4H). $^{13}\text{C}\{^1\text{H}\}$ NMR (DMSO- d_6 , 126 MHz) 171.5, 139.64, 139.62, 131.3, 129.5, 117.1 (d, $J = 23.9$ Hz), 116.1 (d, $J = 23.7$ Hz), 66.6, 54.6, 53.6, 32.3. IR: 3150 cm^{-1} , 2900 cm^{-1} , 1650 cm^{-1} . HRMS (APCI) m/z : $[\text{M}+\text{H}]^+$ calc'd for ($\text{C}_{19}\text{H}_{21}\text{F}_2\text{N}_2\text{O}_2^+$) 347.1566; Found 347.1722.

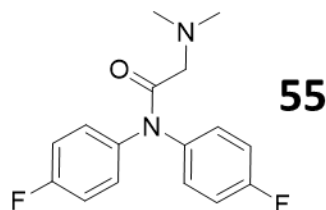


General procedure B produced a white powder (30%) with the following modifications: 3 equiv of TEA and 2 equiv of morpholine. MP: 92-94 °C. ^1H NMR (DMSO- d_6 , 500 MHz) δ 7.53-7.22 (m, 8H), 3.48 (t, $J = 4.6$ Hz, 4H), 3.02 (s, 2H), 2.34 (t, $J = 4.5$ Hz, 4H). $^{13}\text{C}\{^1\text{H}\}$ NMR (CDCl_3 , 126 MHz) δ 169.2, 138.12, 138.08, 130.3, 127.8, 116.7, 115.9, 66.8, 60.8, 53.7. IR: 3100 cm^{-1} , 2890 cm^{-1} , 1630 cm^{-1} . HRMS (APCI) m/z : $[\text{M}+\text{H}]^+$ calc'd for

(C₁₈H₁₉F₂N₂O₂⁺) 333.1409; Found 333.1425. ¹H NMR and ¹³C{¹H} NMR were run in different solvents for better resolution of the observed peaks.

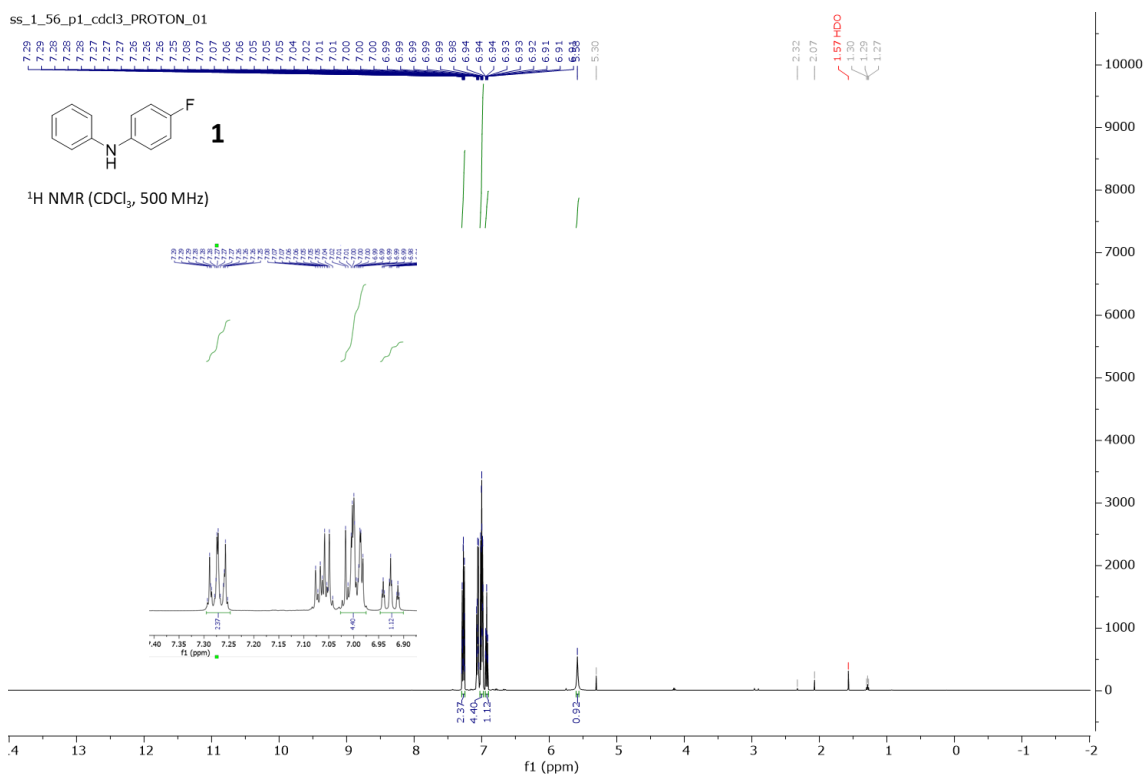


General procedure C produced a white solid (64%). MP: 120-121 °C. ¹H NMR (DMSO-*d*₆, 500 MHz) δ 7.53 (s, 2H), 7.30-7.19 (m, 6H), 2.47 (t, *J* = 7.9, 2H), 2.28 (t, *J* = 7.8, 2H), 2.01 (s, 6H). ¹³C{¹H}NMR (DMSO-*d*₆, 126 MHz) δ 171.6, 139.7, 139.6, 131.3, 129.5, 117.2 (d, *J* = 24.3 Hz), 116.1 (d, *J* = 24.2 Hz), 55.3, 45.4, 32.9. IR: 3060 cm⁻¹, 2939 cm⁻¹, 1663 cm⁻¹, 1495 cm⁻¹, 1236 cm⁻¹. HRMS (APCI) *m/z*: [M+H]⁺ calc'd for (C₁₇H₁₉F₂N₂O⁺) 305.1460; Found 305.1506.

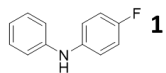


General procedure C produced a white solid (48%). MP: 118-119 °C. ¹H NMR (CDCl₃, 500 MHz) δ 7.28-7.25-7.23 (m, 4H), 7.09-7.01 (m, 4H), 3.06 (s, 2H), 2.34 (s, 6H). ¹³C{¹H} NMR (DMSO-*d*₆, 126 MHz) δ 169.7, 139.5, 139.2, 131.3, 129.5, 116.9, 116.2, 61.0, 45.4. IR: 3062 cm⁻¹, 2942 cm⁻¹, 1665 cm⁻¹, 1232 cm⁻¹. HRMS (APCI) *m/z*: [M+H]⁺ calc'd for (C₁₆H₁₇F₂N₂O⁺) 291.1303; Found 291.1347. ¹H NMR and ¹³C{¹H} NMR were run in different solvents for better resolution of the observed peaks.

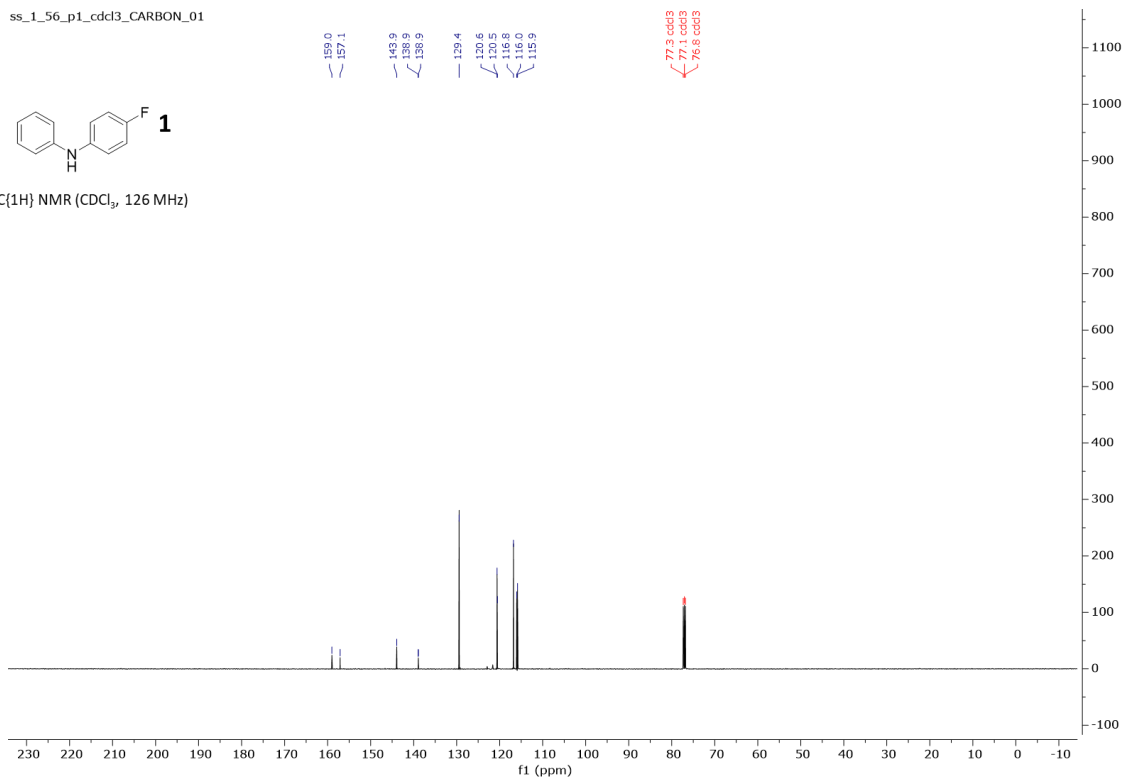
^1H and ^{13}C NMR Spectra



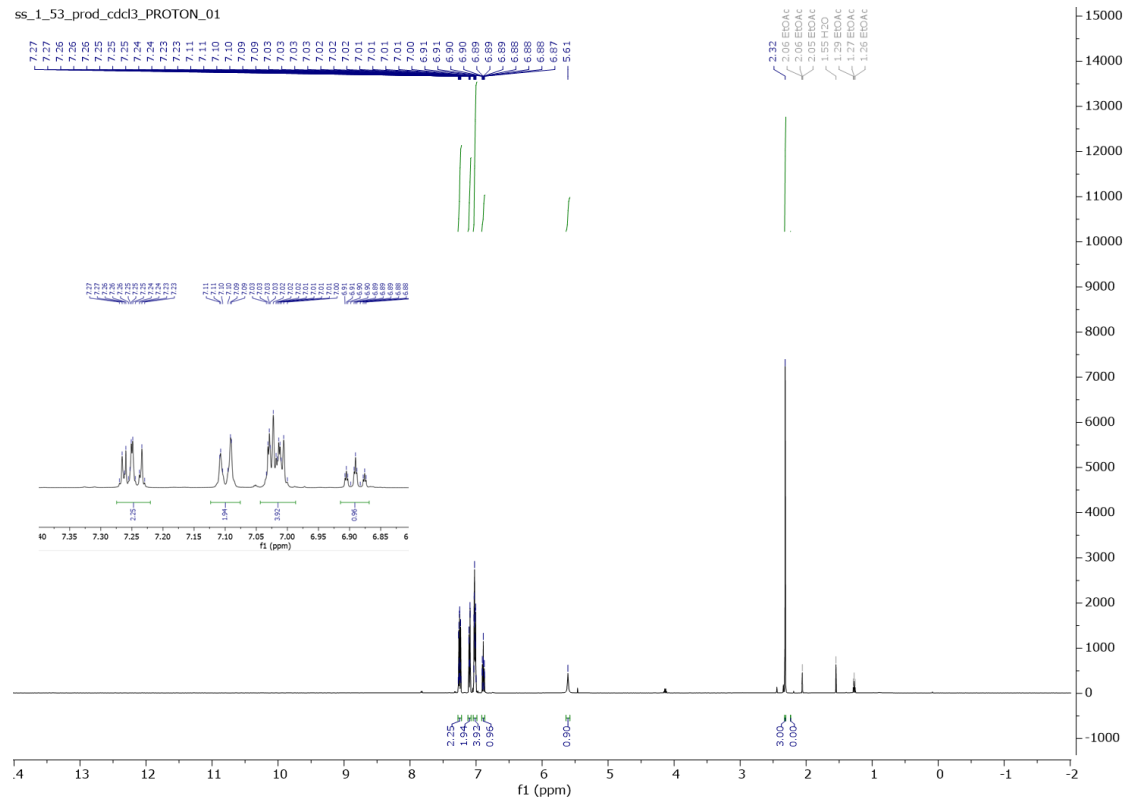
ss_1_56_p1_cdc13_CARBON_01



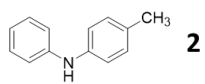
C{1H} NMR (CDCl₃, 126 MHz)



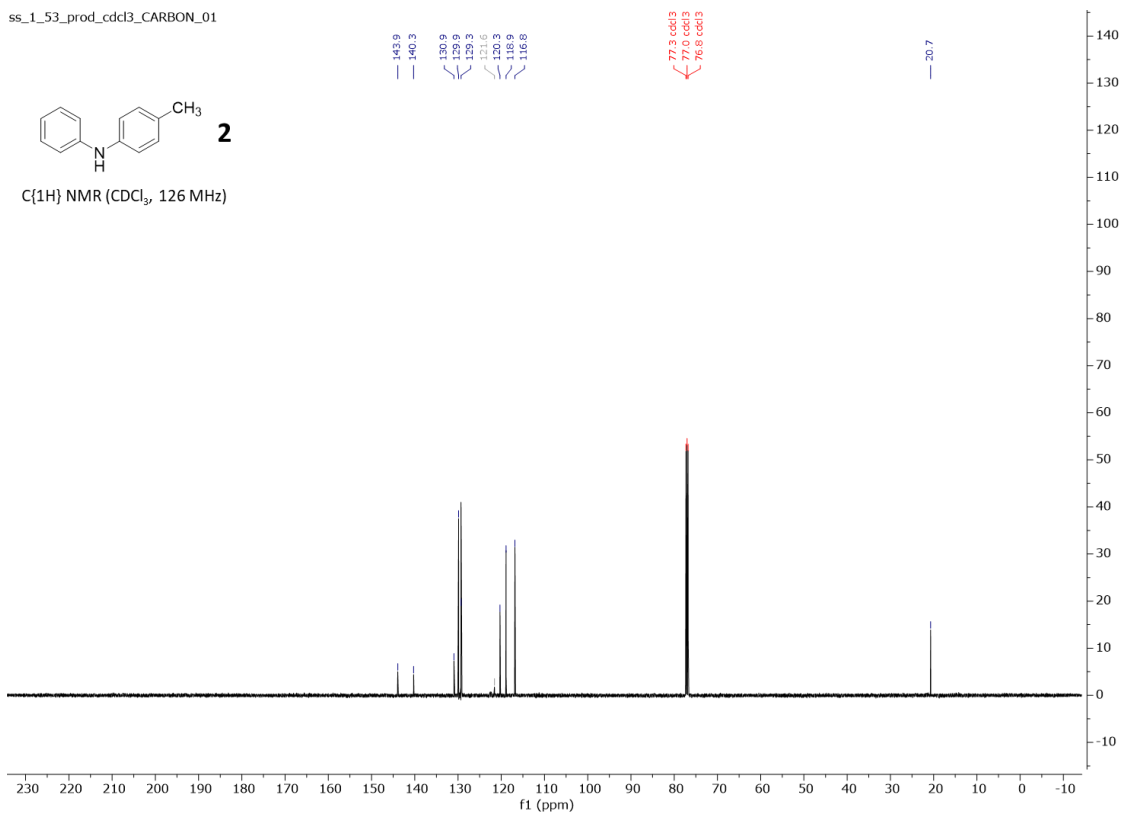
ss_1_53_prod_cdcd3_PROTON_01



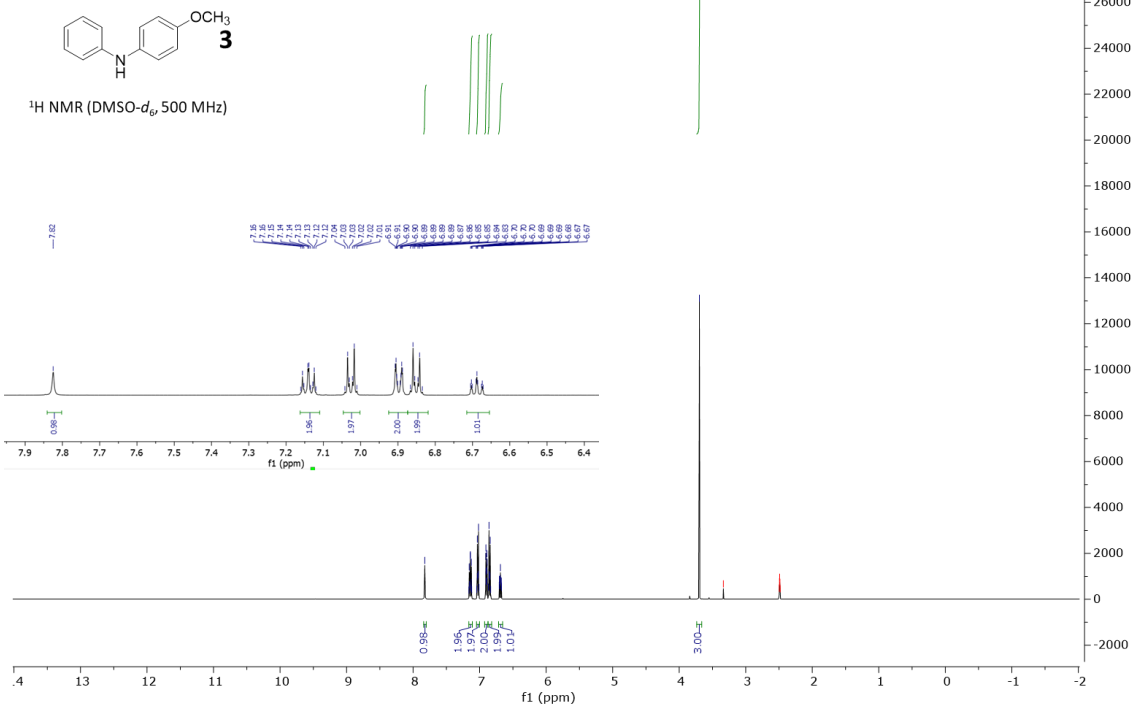
ss_1_53_prod_ccd3_CARBON_01



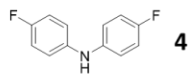
C{1H} NMR (CDCl₃, 126 MHz)



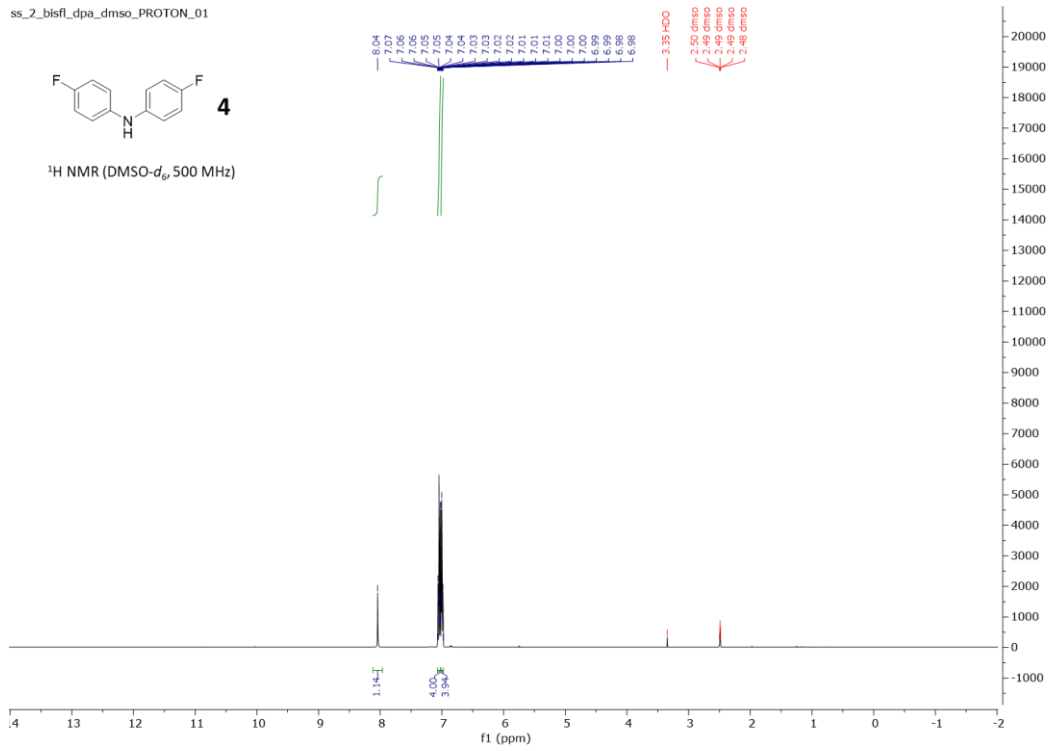
ss_2_methoxy_dpa_dmsO_PROTON_01



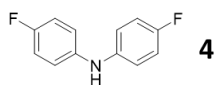
ss_2_bisfl_dpa_dmso_PROTON_01



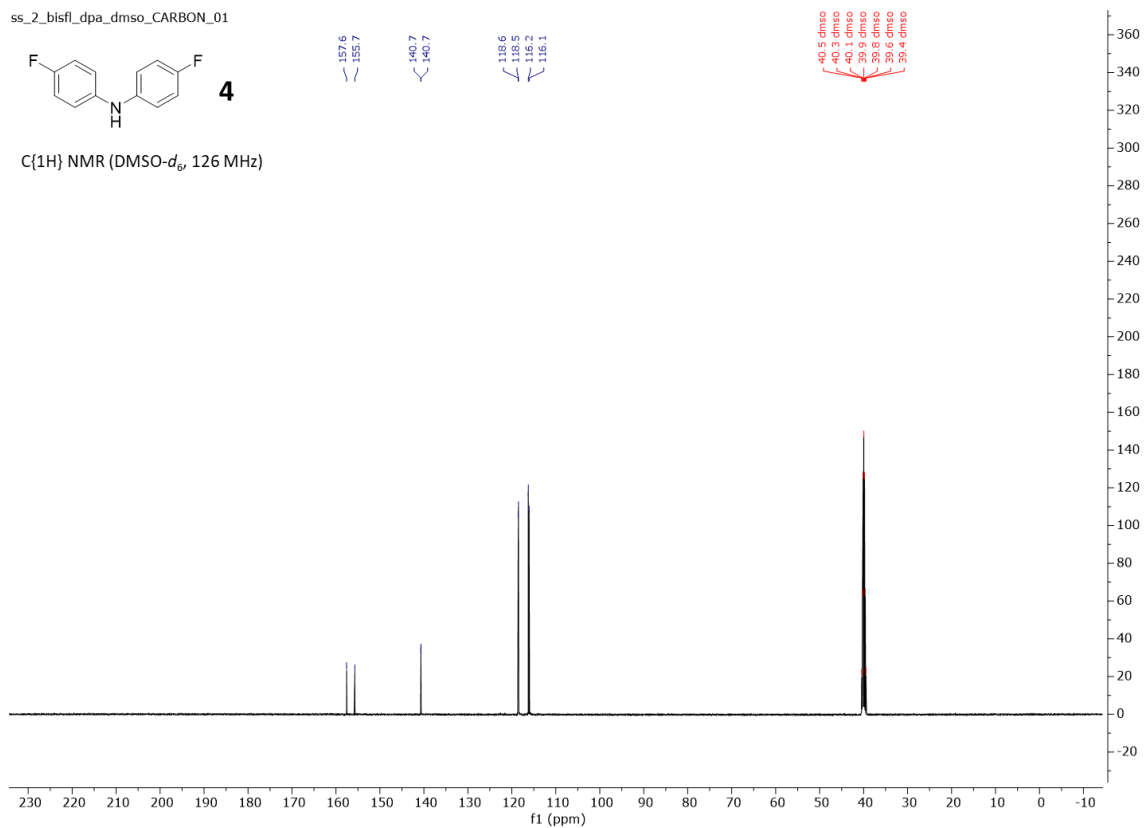
¹H NMR (DMSO-*d*₆, 500 MHz)



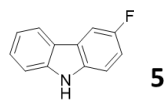
ss_2_bisfl_dpa_dms0_CARBON_01



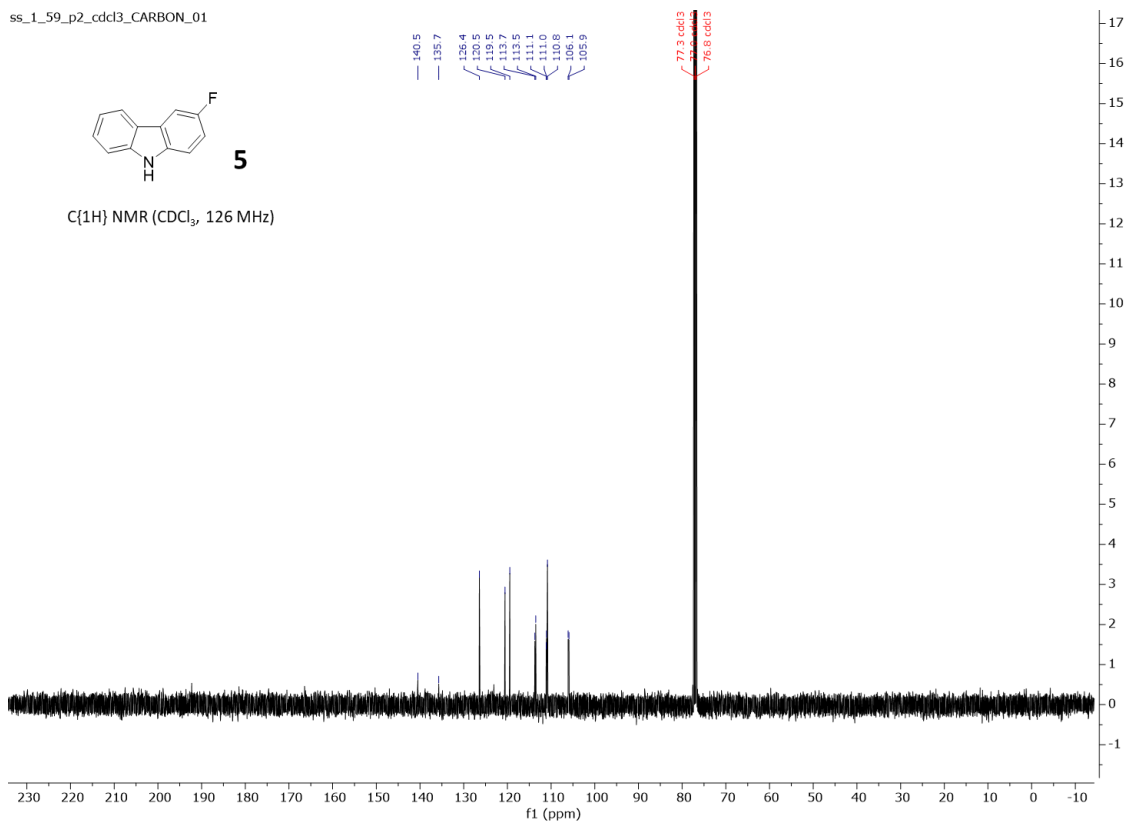
C{1H} NMR (DMSO-*d*₆, 126 MHz)

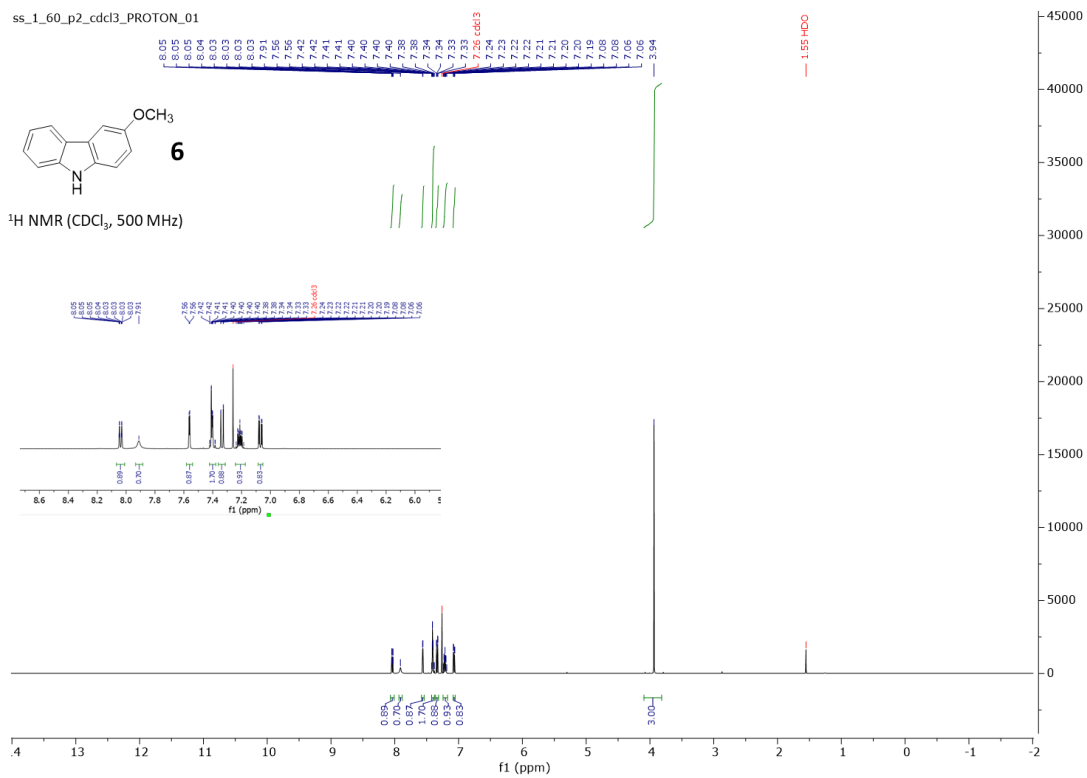


ss_1_59_p2_cdcl3_CARBON_01

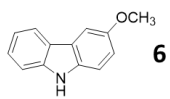


C{1H} NMR (CDCl₃, 126 MHz)

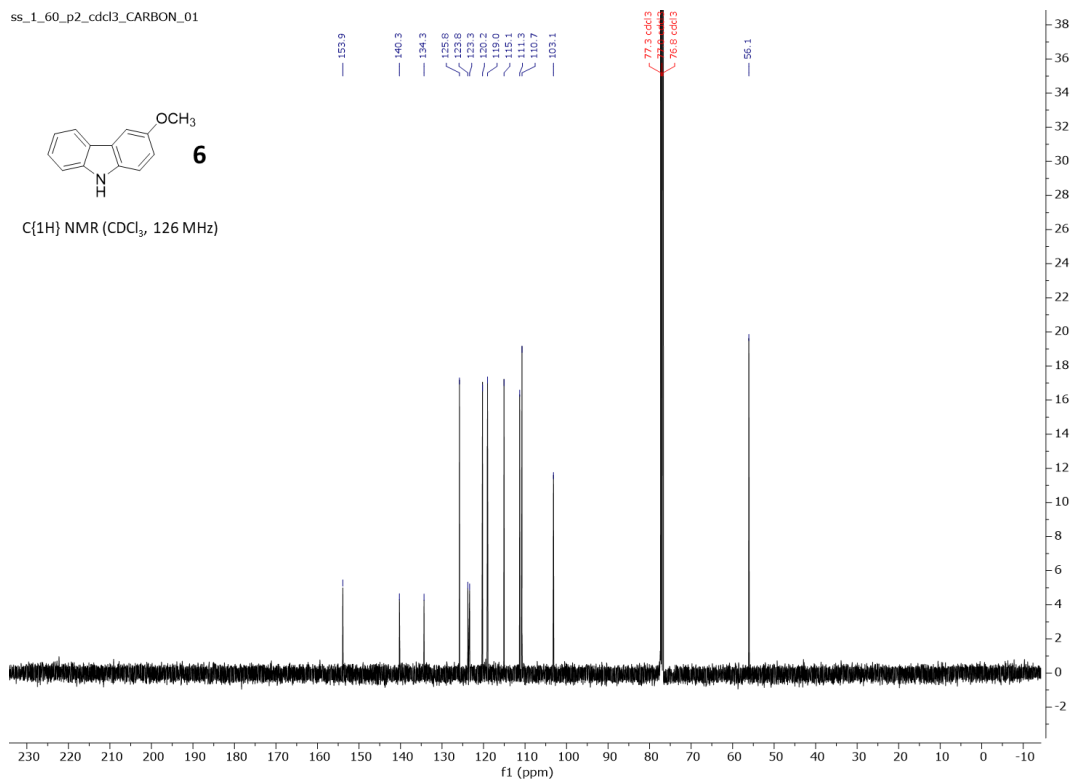




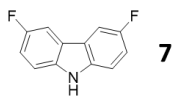
ss_1_60_p2_cdc13_CARBON_01



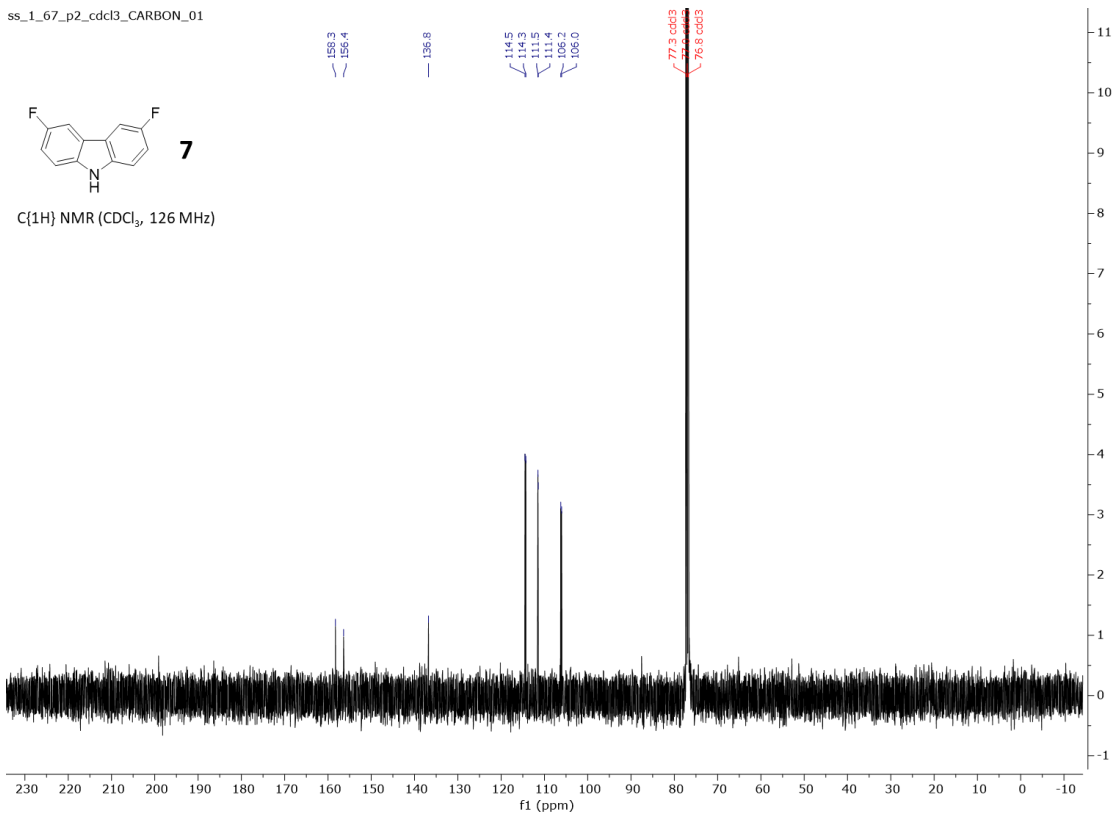
C{1H} NMR (CDCl₃, 126 MHz)



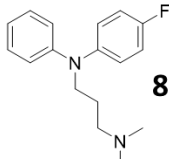
ss_1_67_p2_cdc13_CARBON_01



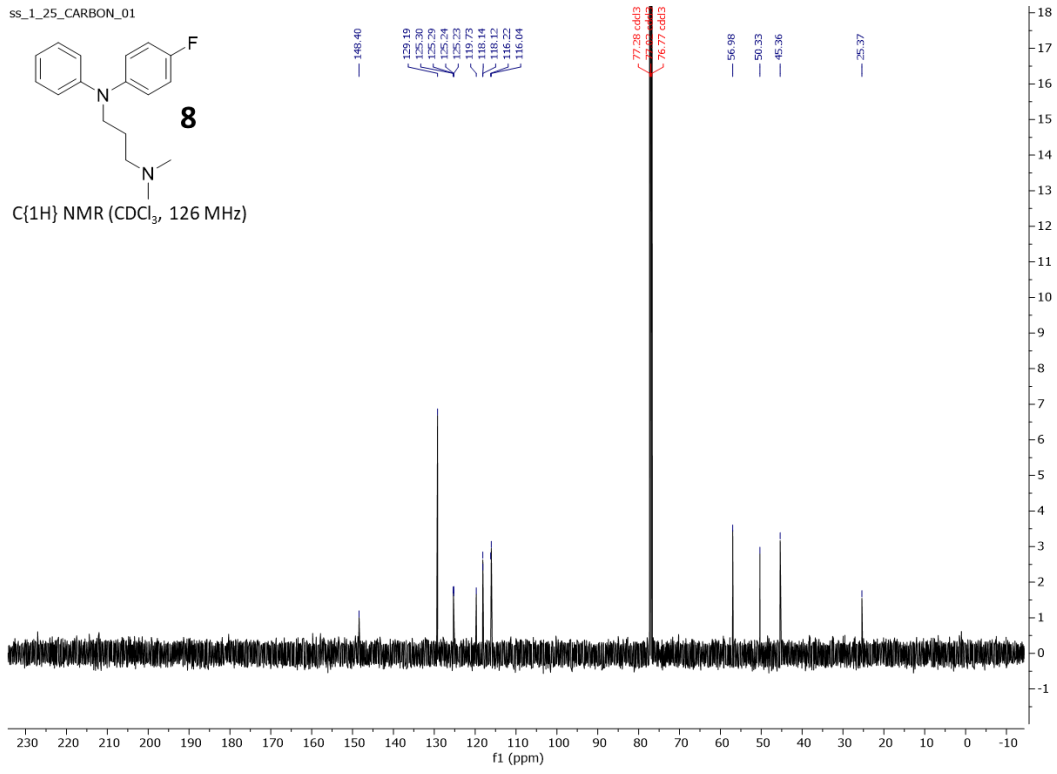
C{1H} NMR (CDCl₃, 126 MHz)

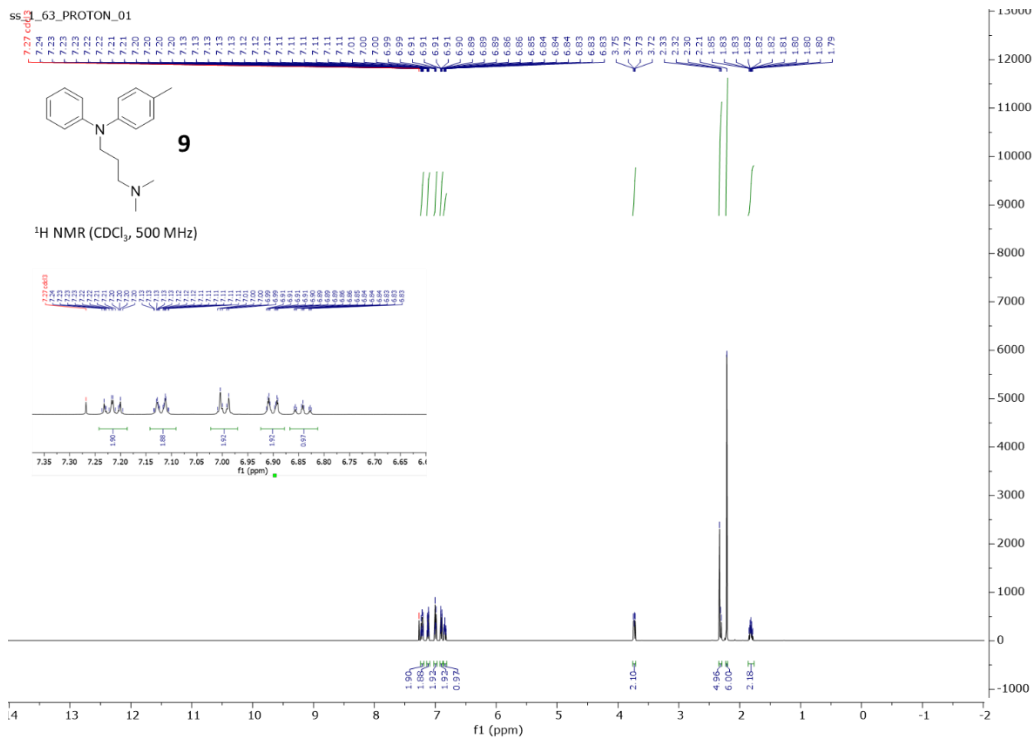


ss_1_25_CARBON_01

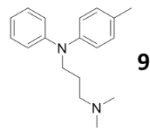


C{1H} NMR (CDCl₃, 126 MHz)

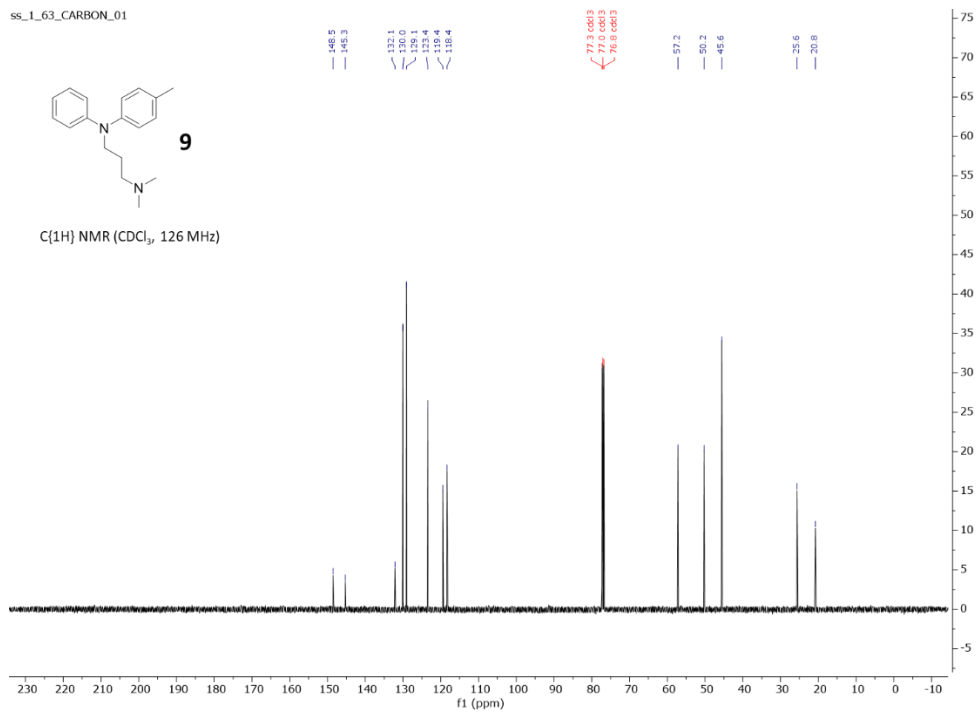




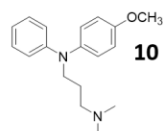
ss_1_63_CARBON_01



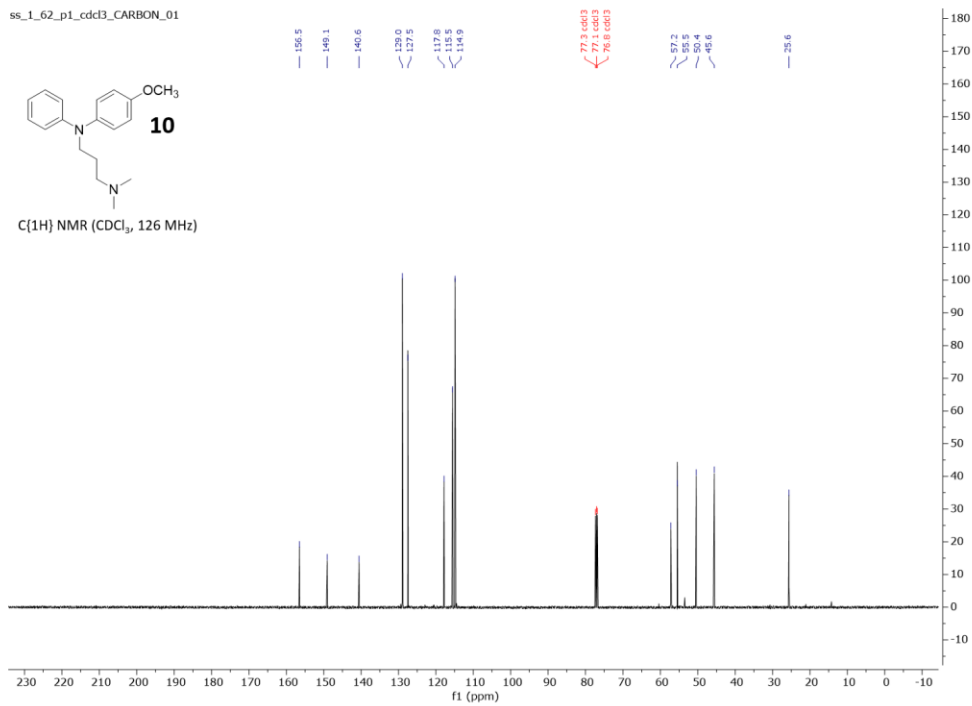
C{1H} NMR (CDCl₃, 126 MHz)



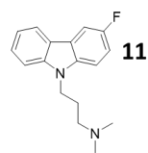
ss_1_62_p1_cdcl3_CARBON_01



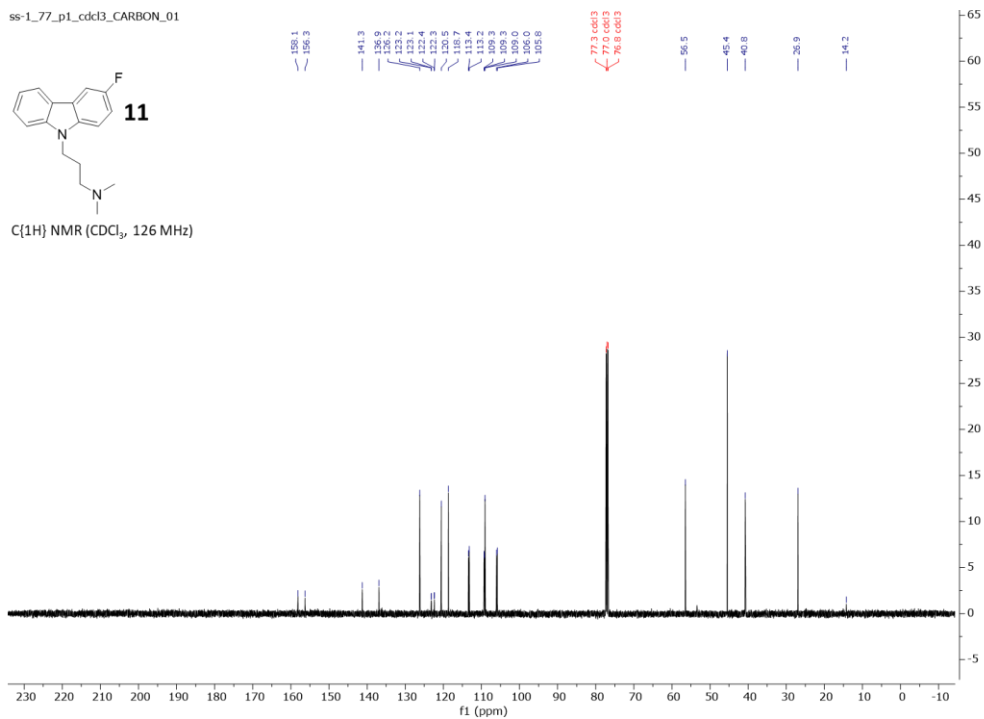
C[1H] NMR (CDCl₃, 126 MHz)



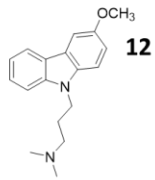
ss-1_77_p1_cdcl3_CARBON_01



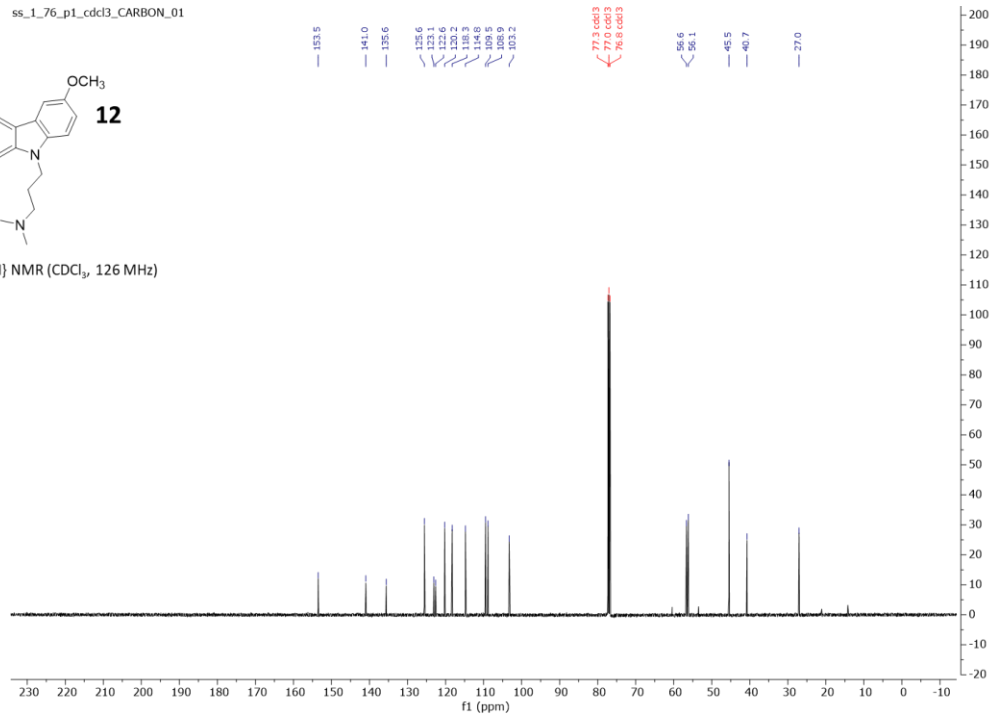
C[1H] NMR (CDCl₃, 126 MHz)



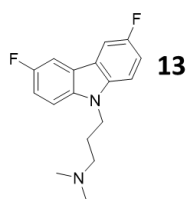
ss_1_76_p1_cdc13_CARBON_01



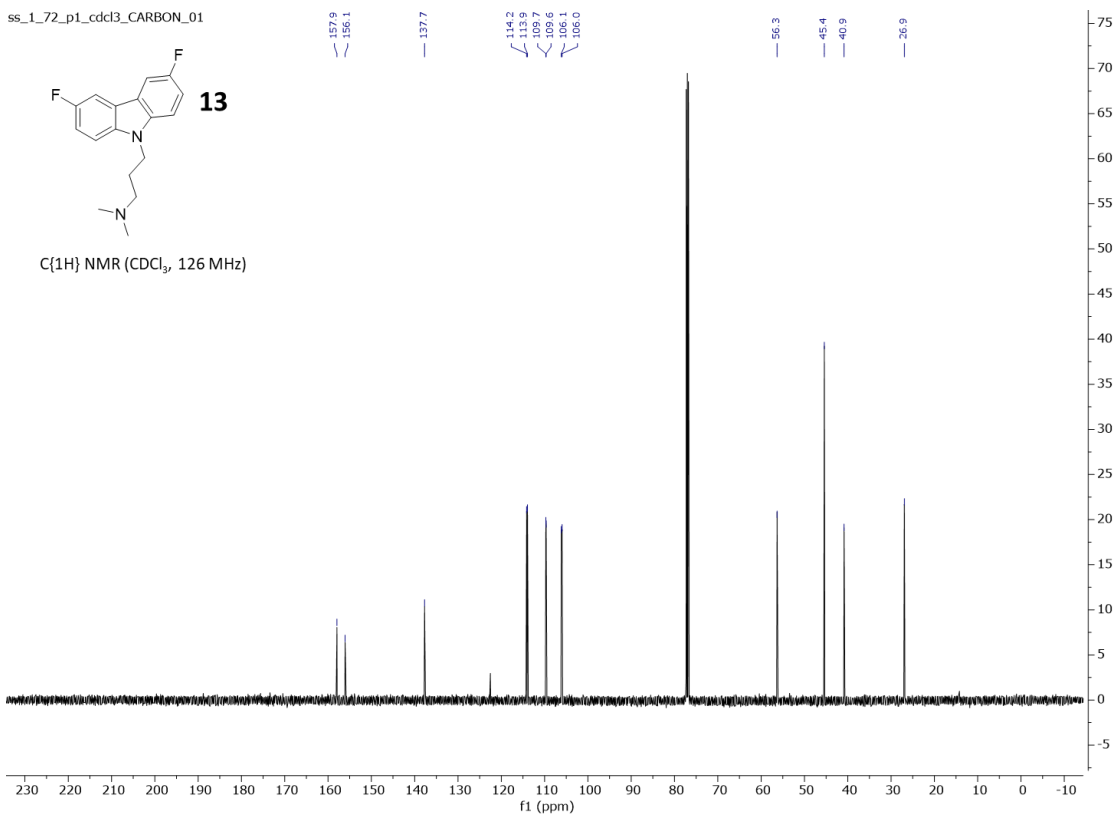
C{1H} NMR (CDCl₃, 126 MHz)

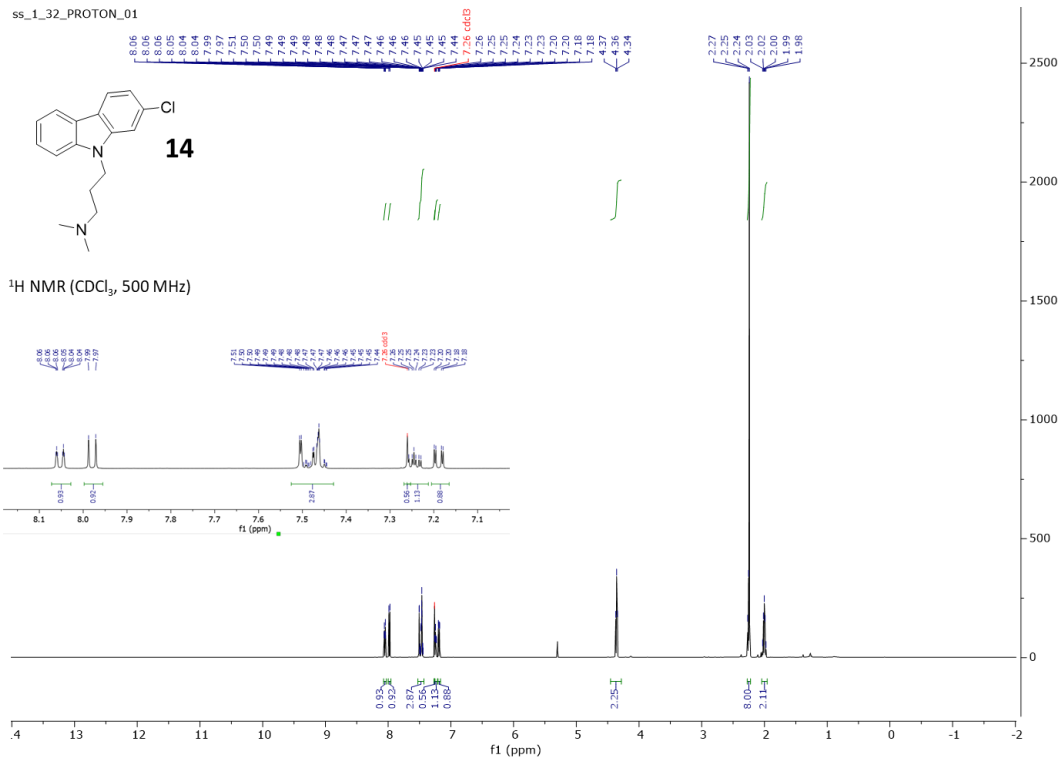


ss_1_72_p1_cdcl3_CARBON_01

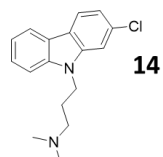


C{1H} NMR (CDCl₃, 126 MHz)

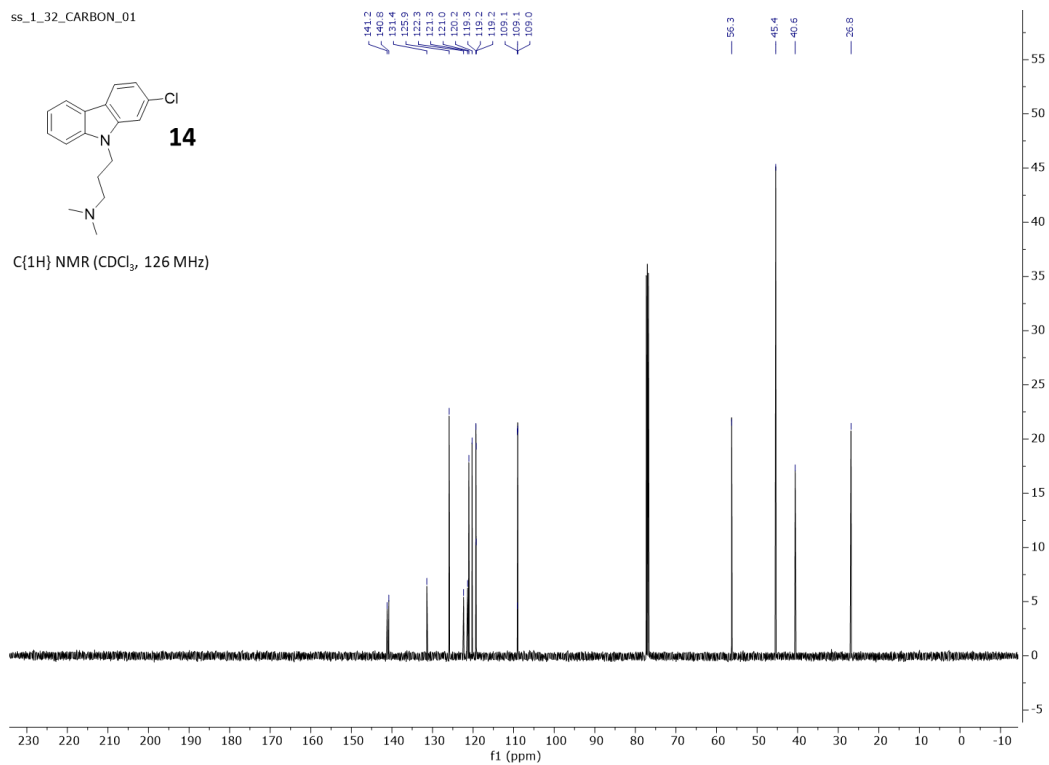


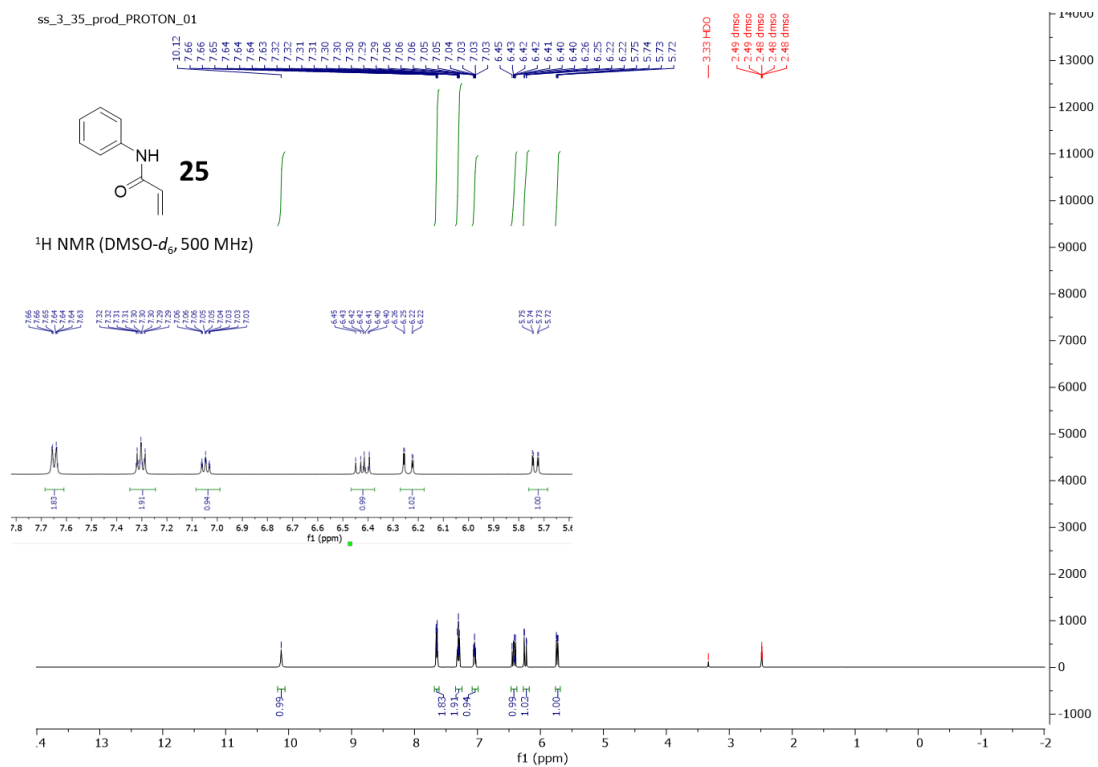


ss_1_32_CARBON_01

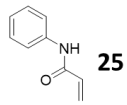


C{1H} NMR (CDCl₃, 126 MHz)

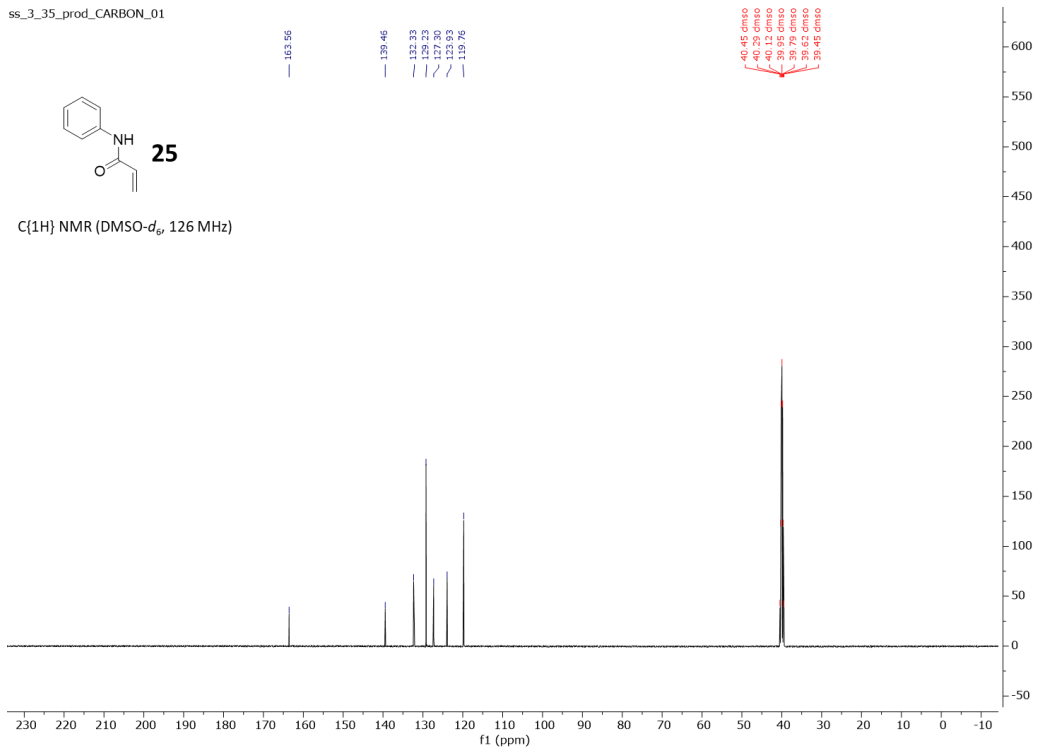




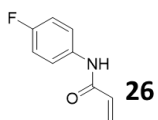
ss_3_35_prod_CARBON_01



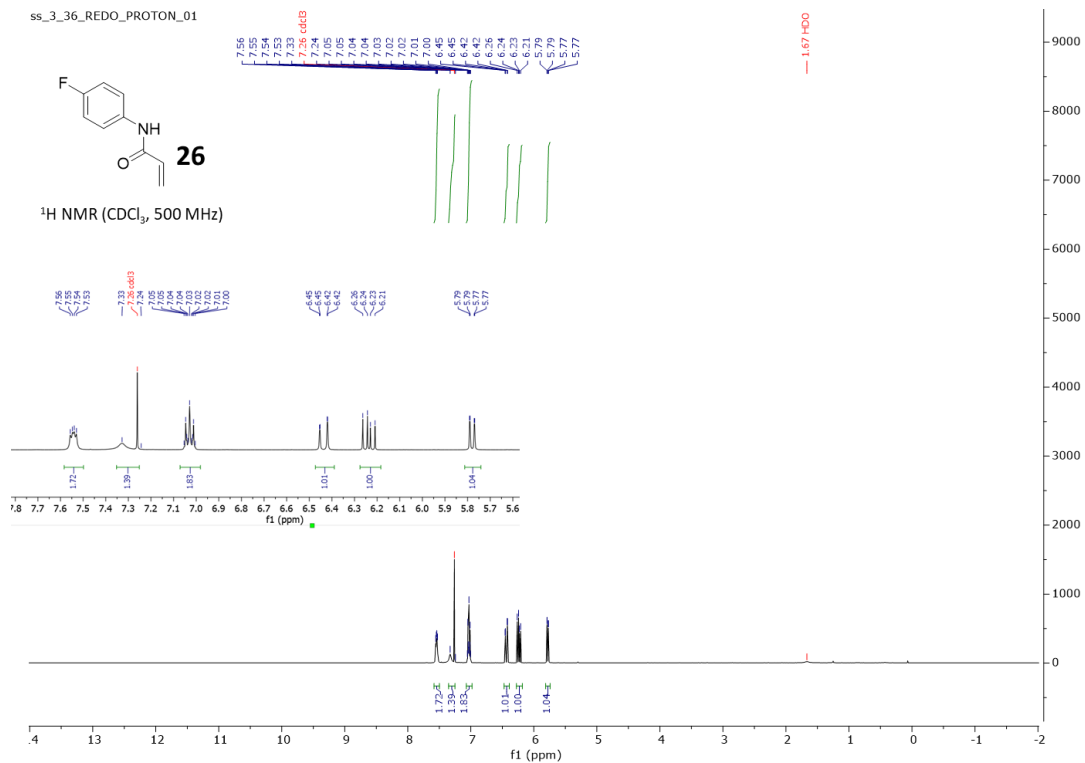
C{1H} NMR (DMSO-*d*₆, 126 MHz)



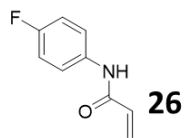
ss_3_36_REDO_PROTON_01



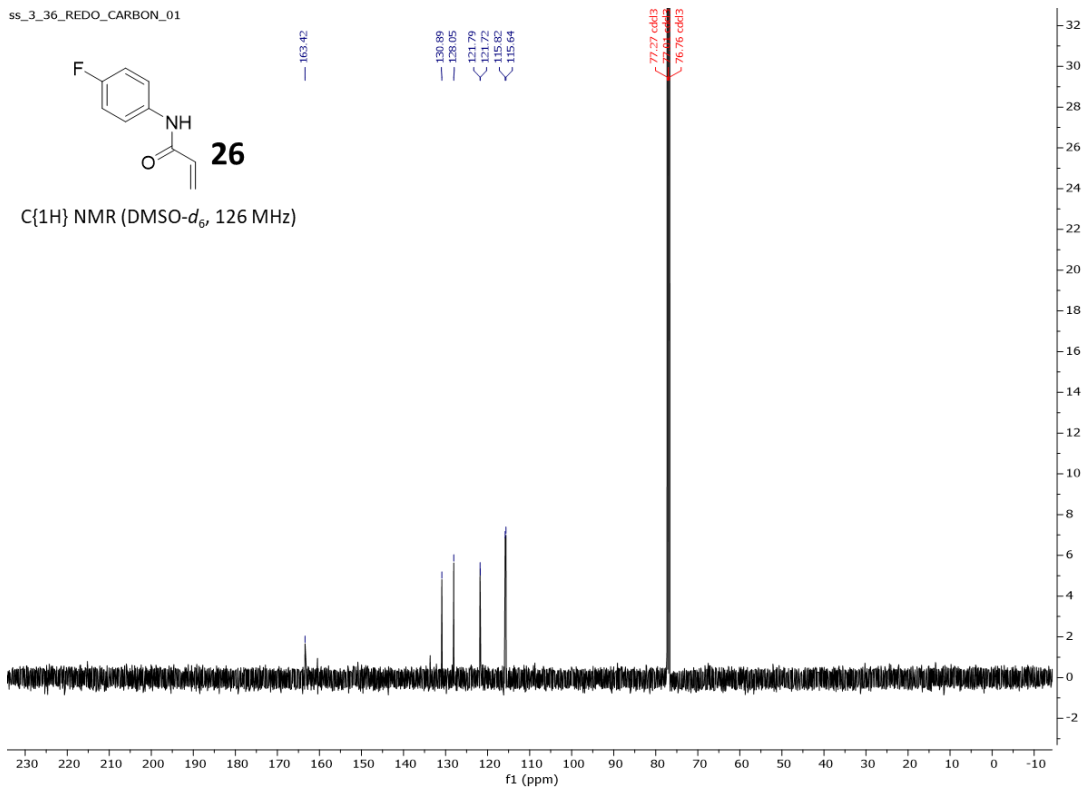
¹H NMR (CDCl₃, 500 MHz)



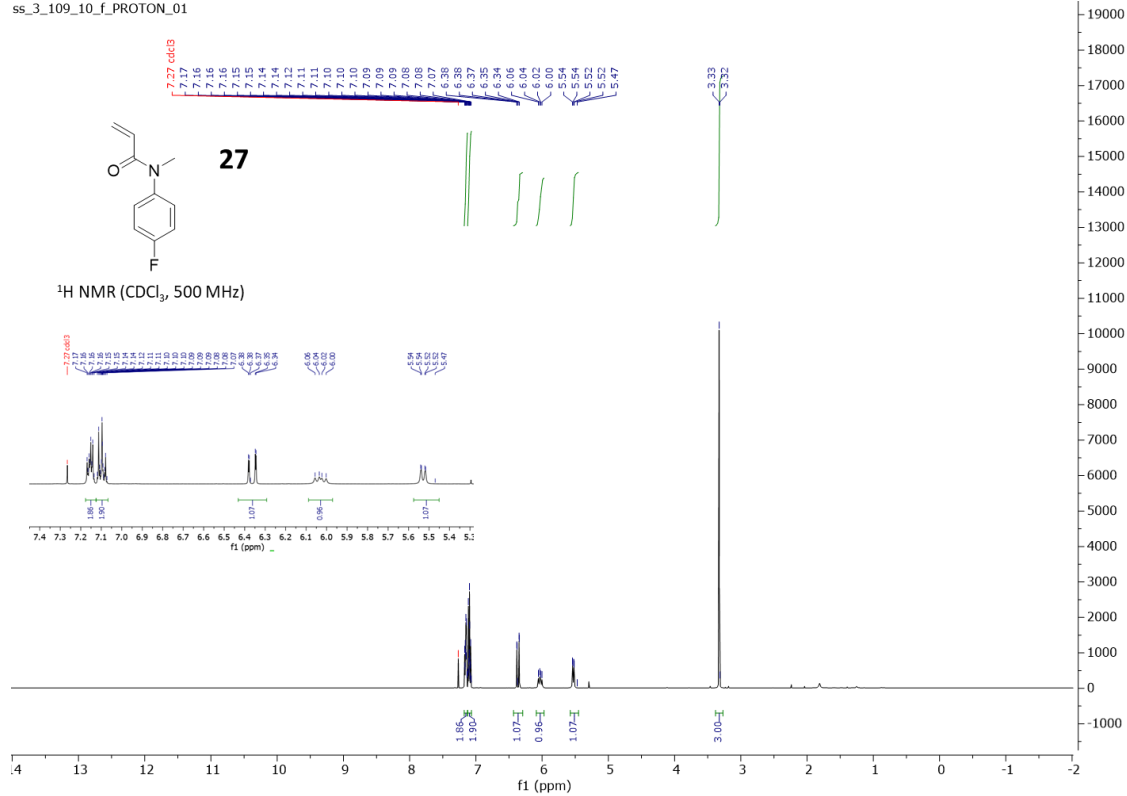
ss_3_36_REDO_CARBON_01



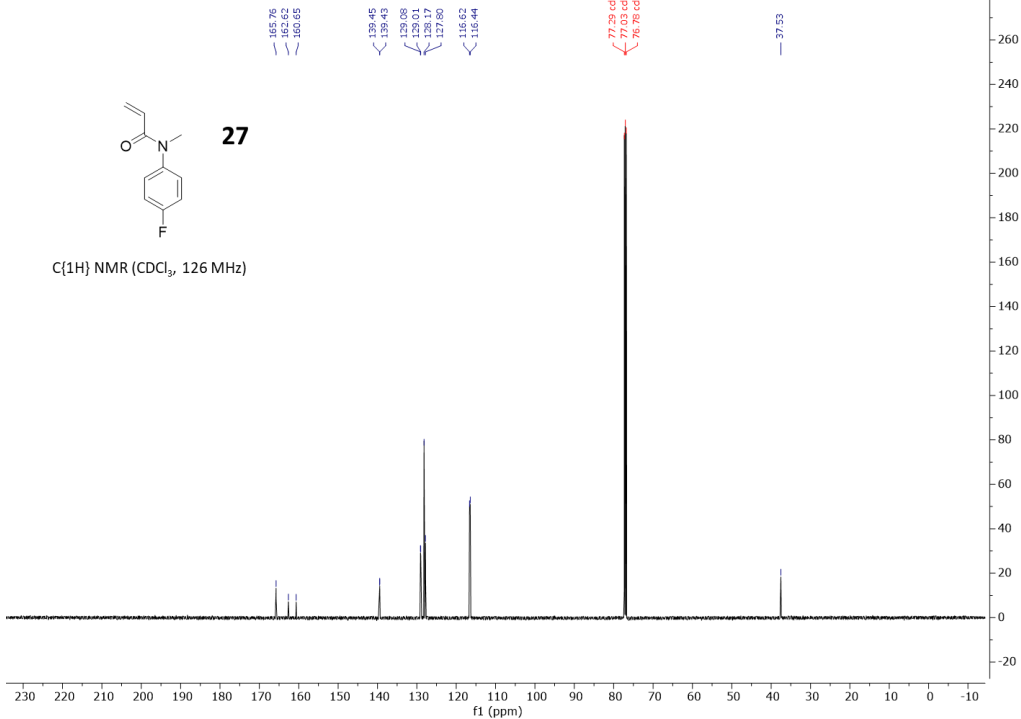
C{1H} NMR (DMSO-*d*₆, 126 MHz)



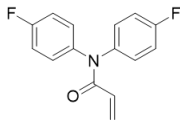
ss_3_109_10_f_PROTON_01



ss_3_109_10_f_CARBON_01

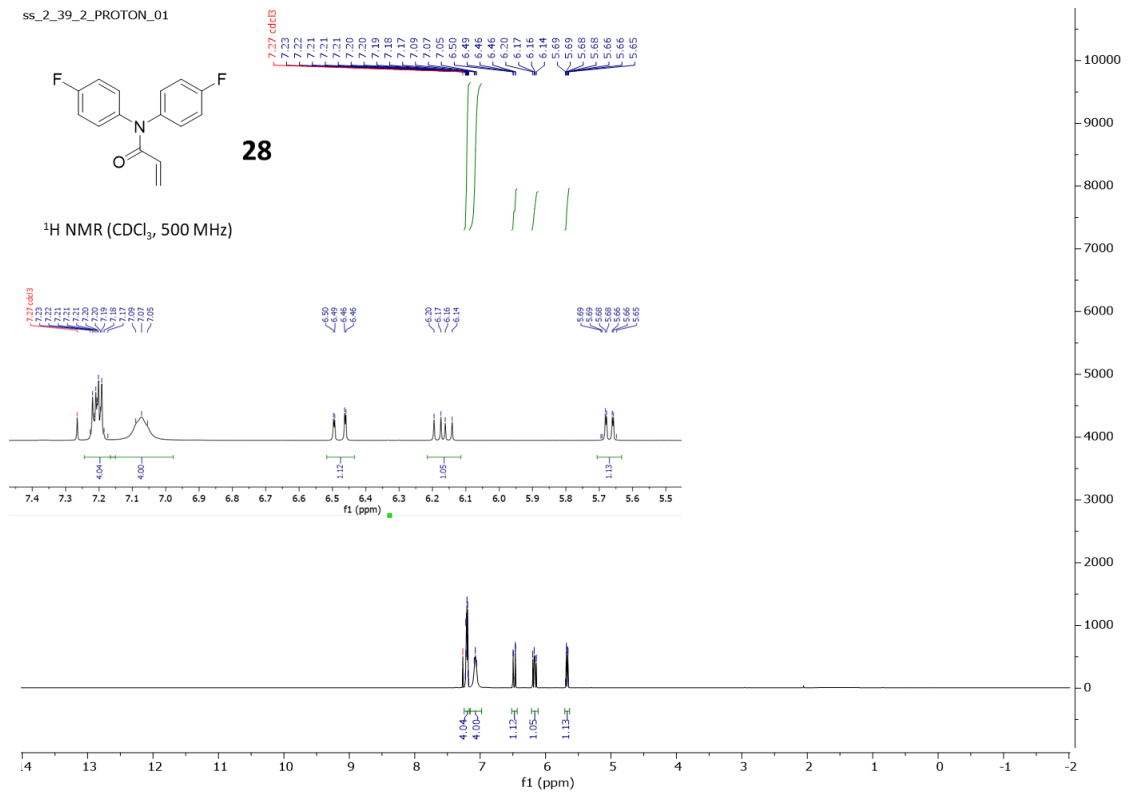


ss_2_39_2_PROTON_01

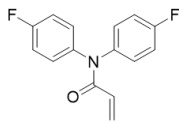


28

¹H NMR (CDCl₃, 500 MHz)

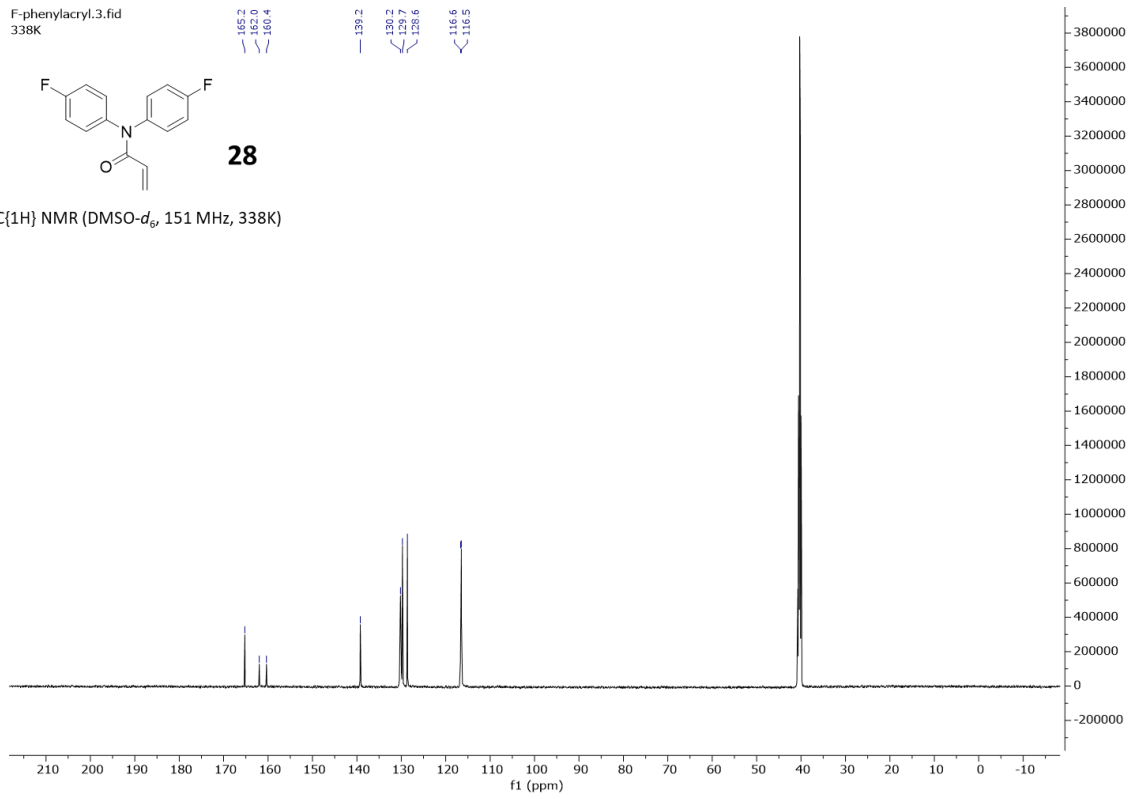


F-phenylacryl.3.fid
338K

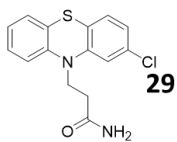


28

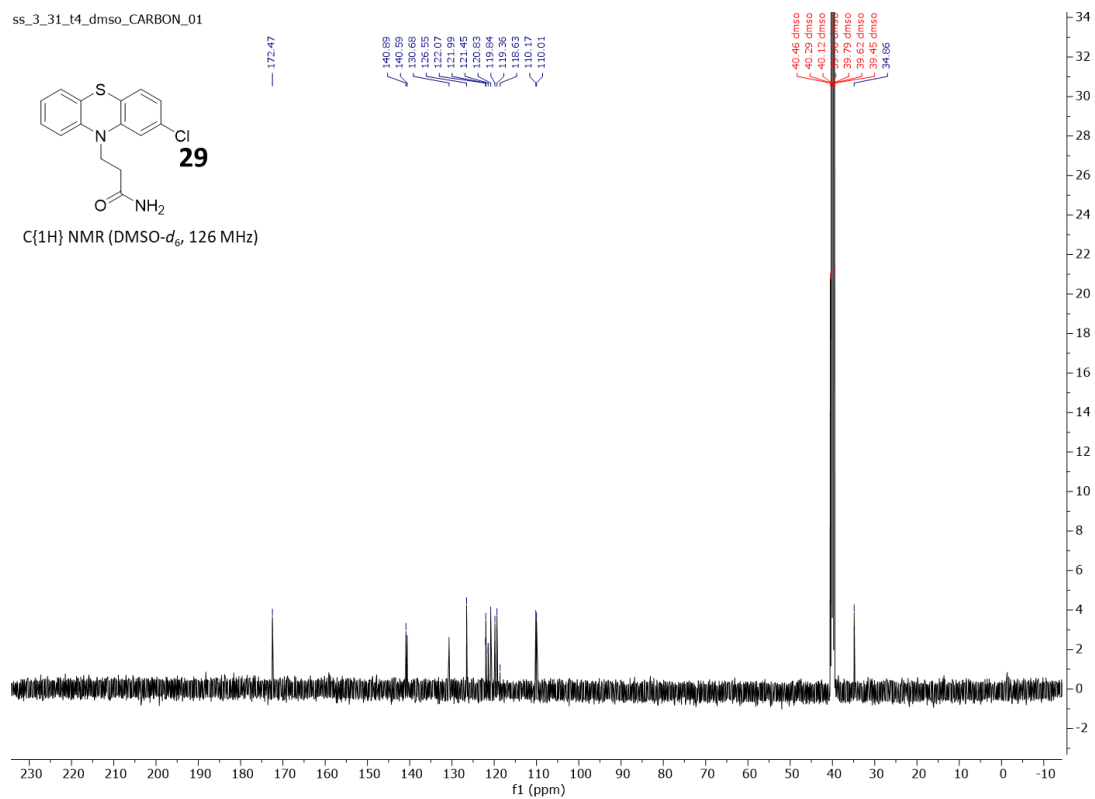
C{1H} NMR (DMSO-*d*₆, 151 MHz, 338K)



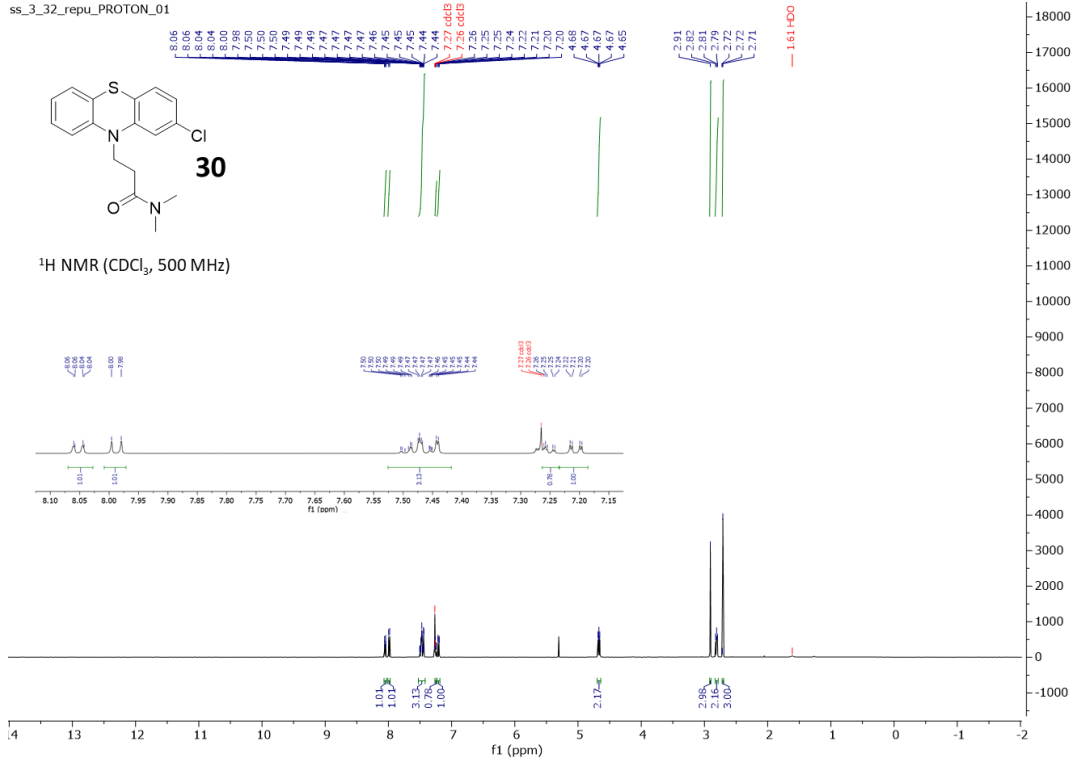
ss_3_31_t4_dmsO_CARBO_N_01



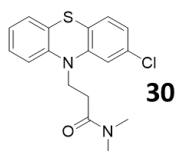
C{1H} NMR (DMSO-d₆, 126 MHz)



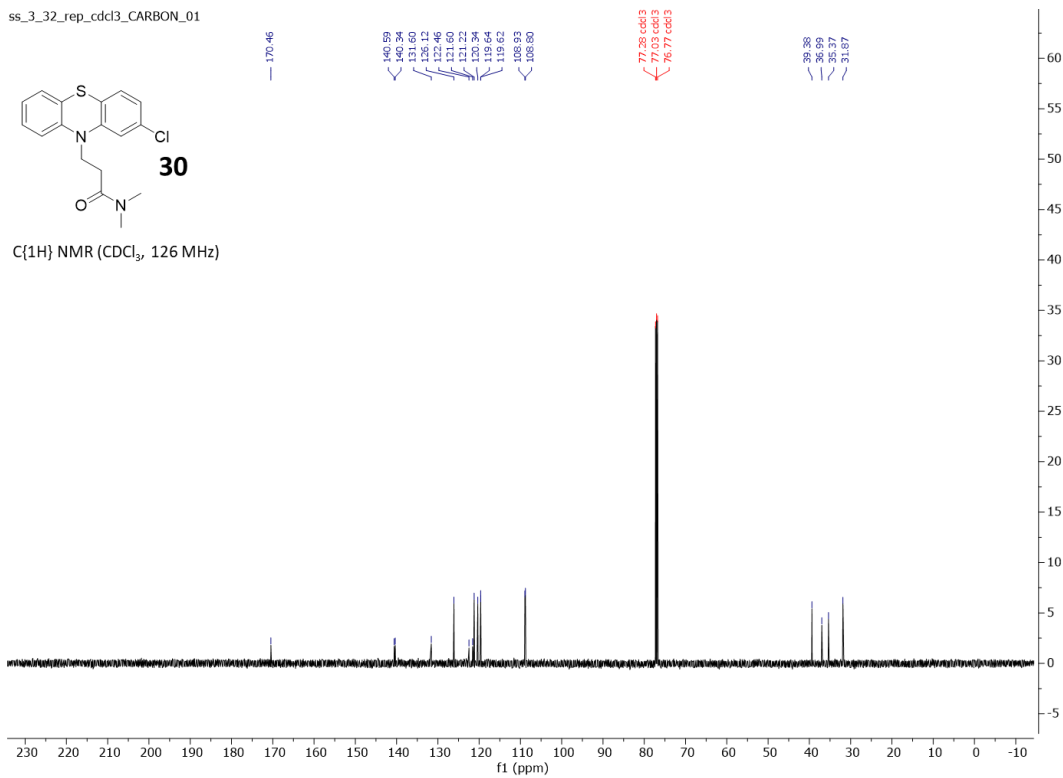
ss_3_32_repu_PROTON_01



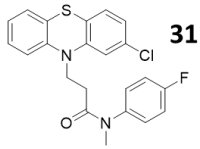
ss_3_32_rep_cdc13_CARBON_01



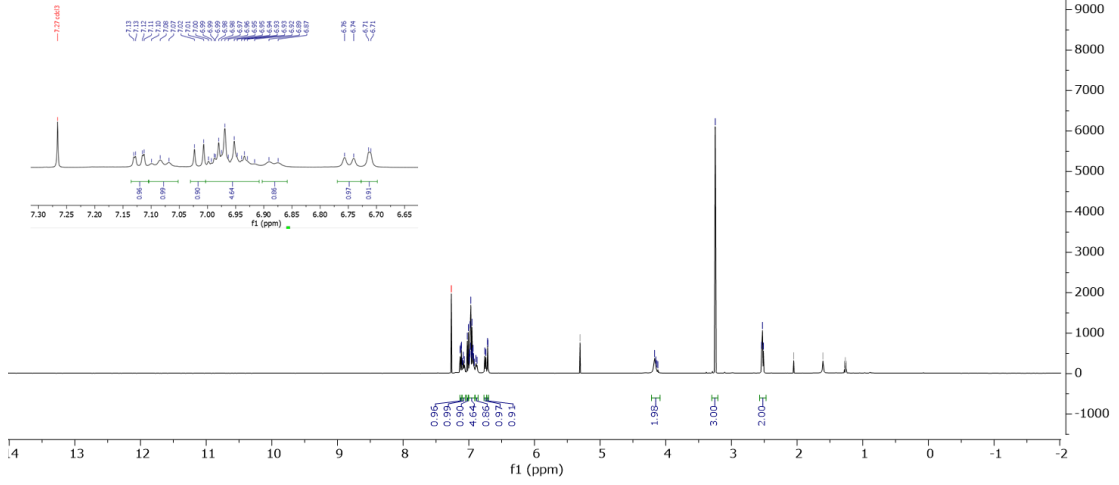
C{1H} NMR (CDCl₃, 126 MHz)



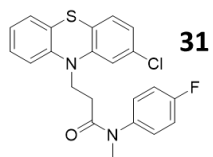
ss_3_109_14_f-PROTON_01



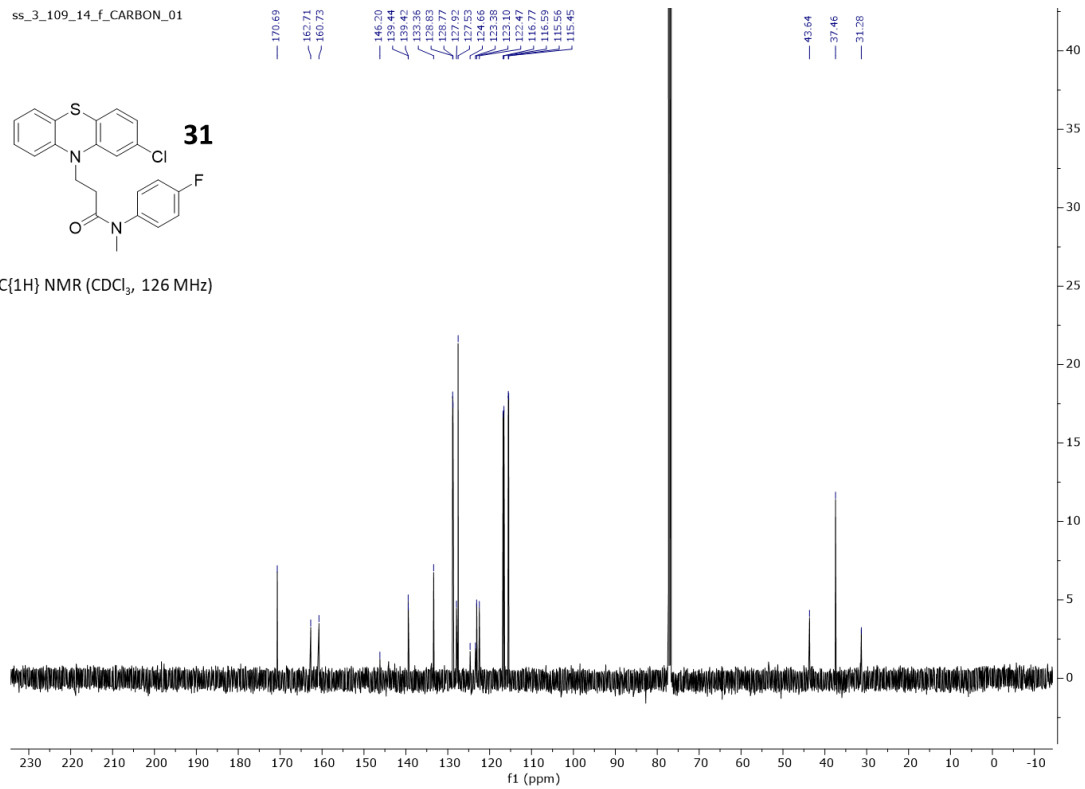
¹H NMR (CDCl₃, 500 MHz)



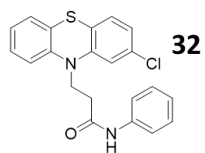
ss_3_109_14_f_CARBON_01



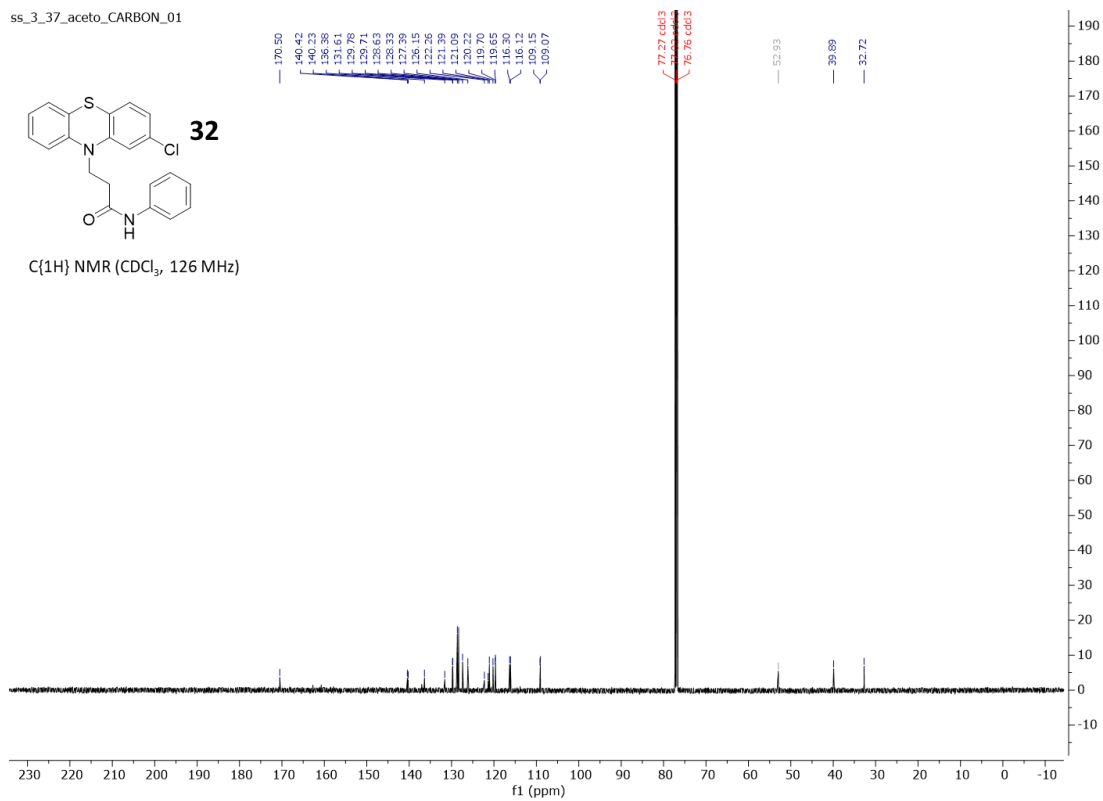
C{1H} NMR (CDCl₃, 126 MHz)



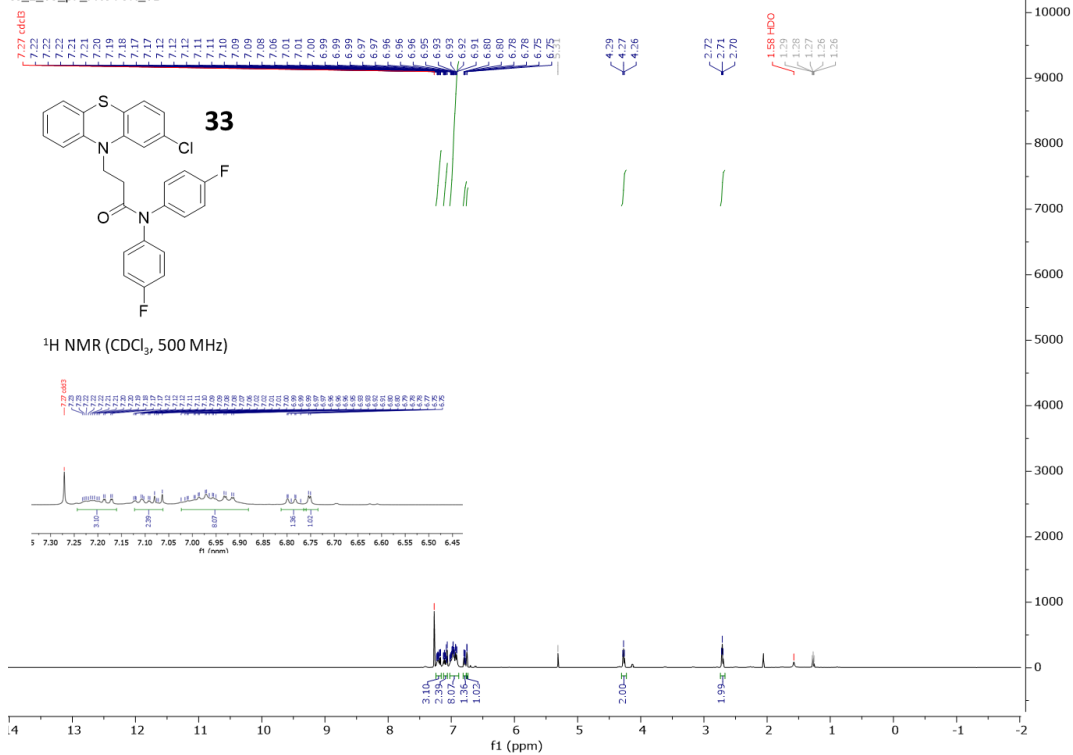
ss_3_37_aceto_CARON_01



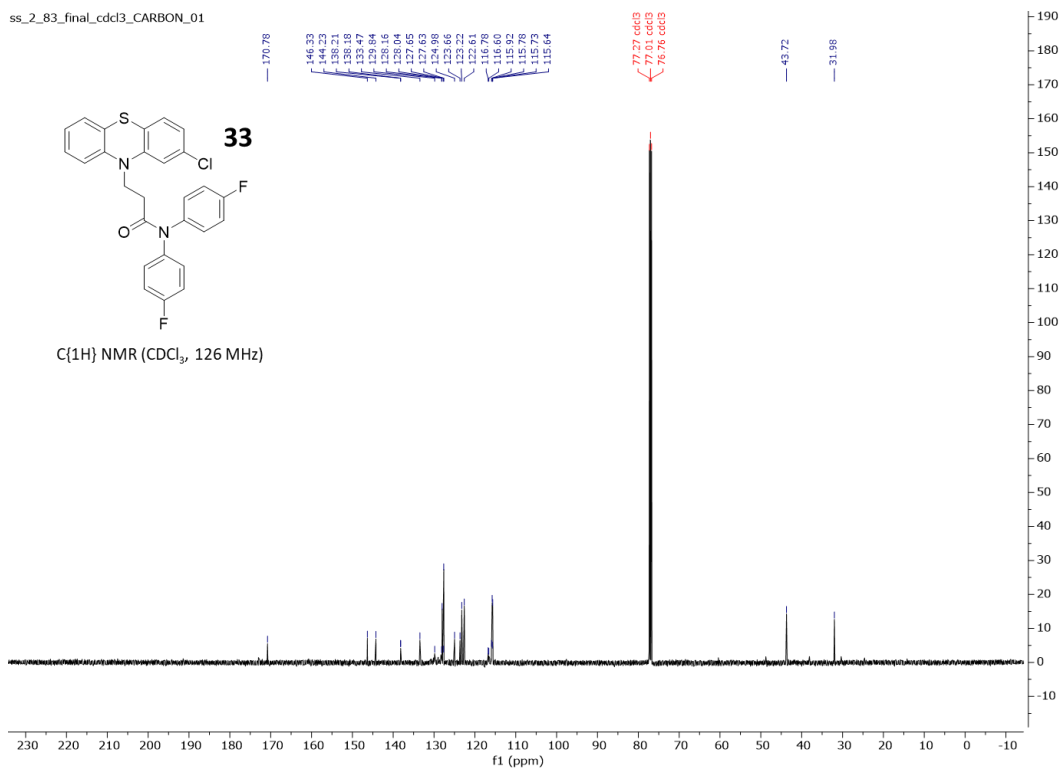
C{1H} NMR (CDCl₃, 126 MHz)



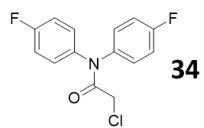
ss_2_83_p7_PROTON_01



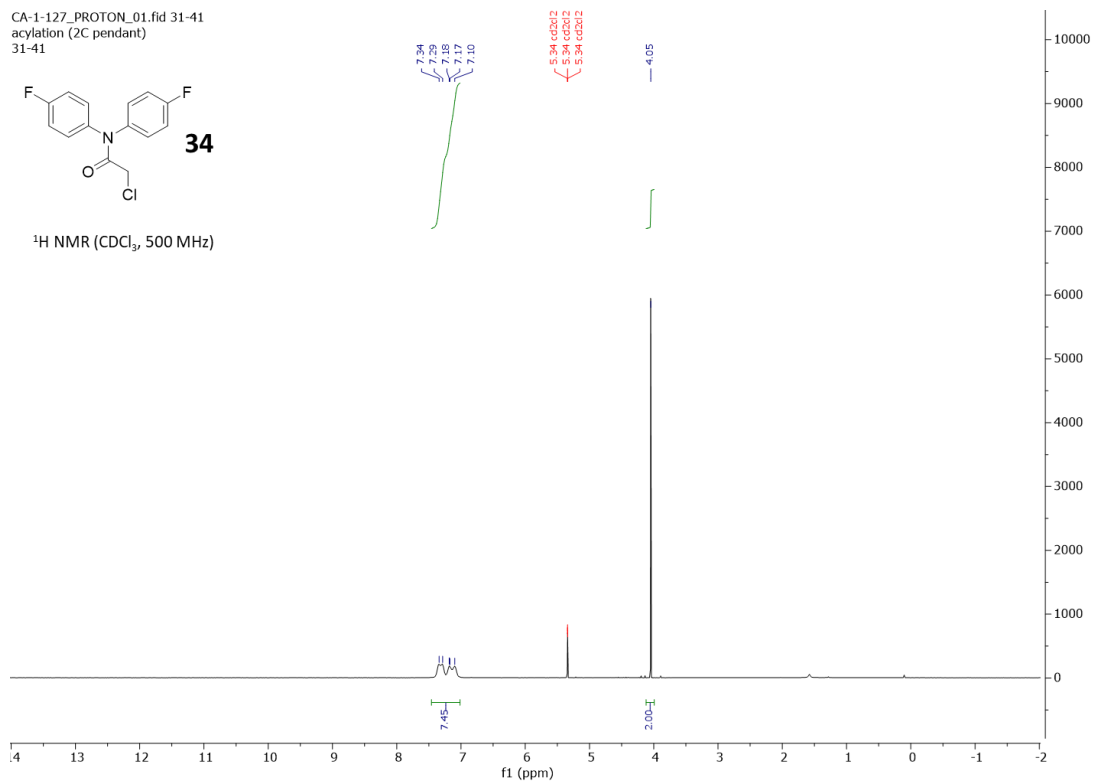
ss_2_83_final_cdcl3_CARBON_01



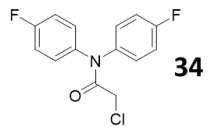
CA-1-127_PROTON_01.fid 31-41
acylation (2C pendant)
31-41



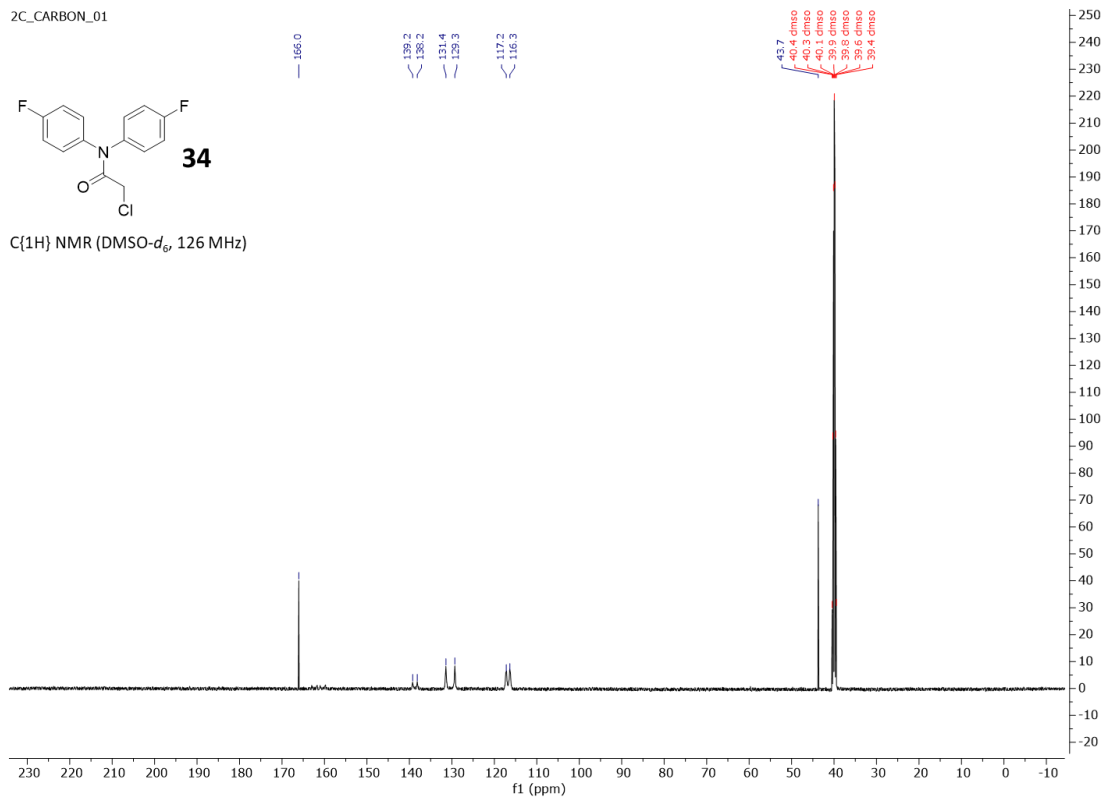
$^1\text{H NMR}$ (CDCl_3 , 500 MHz)



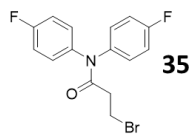
2C_CARBON_01



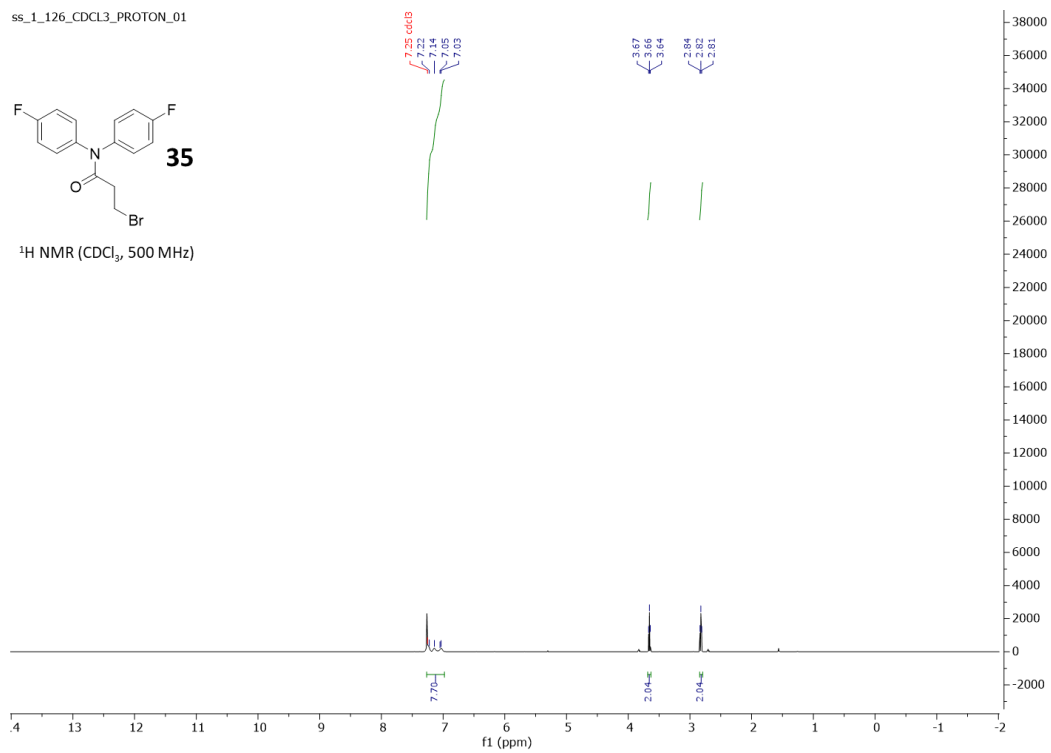
C{1H} NMR (DMSO-*d*₆, 126 MHz)



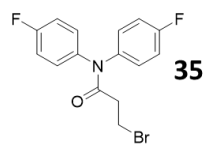
ss_1_126_CDCL3_PROTON_01



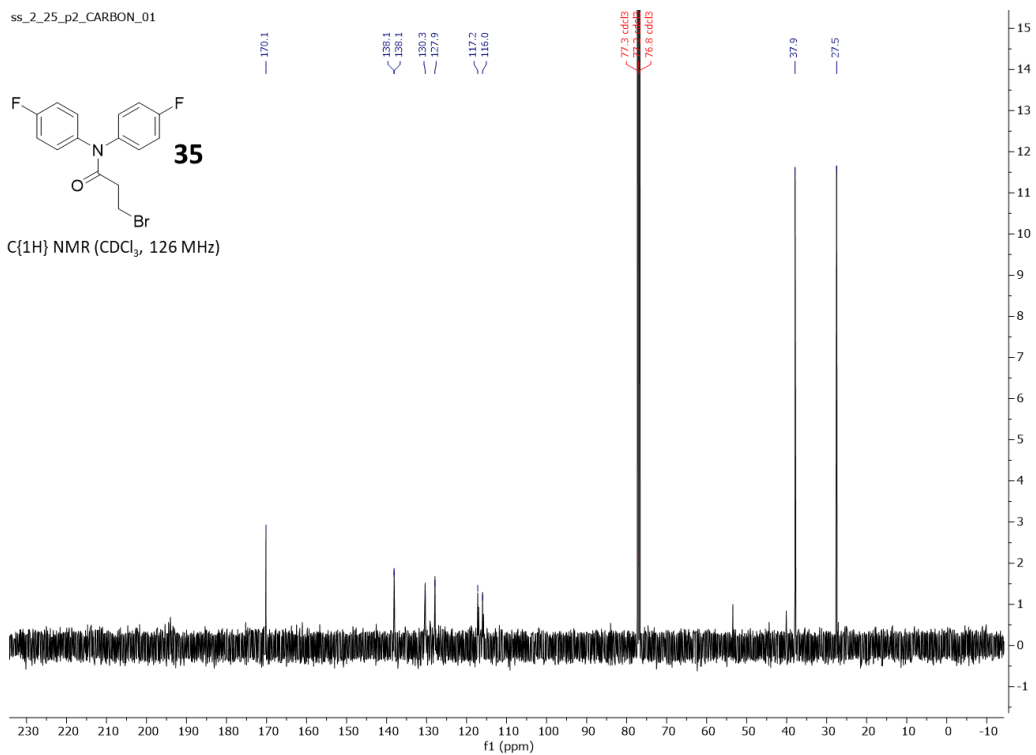
¹H NMR (CDCl₃, 500 MHz)

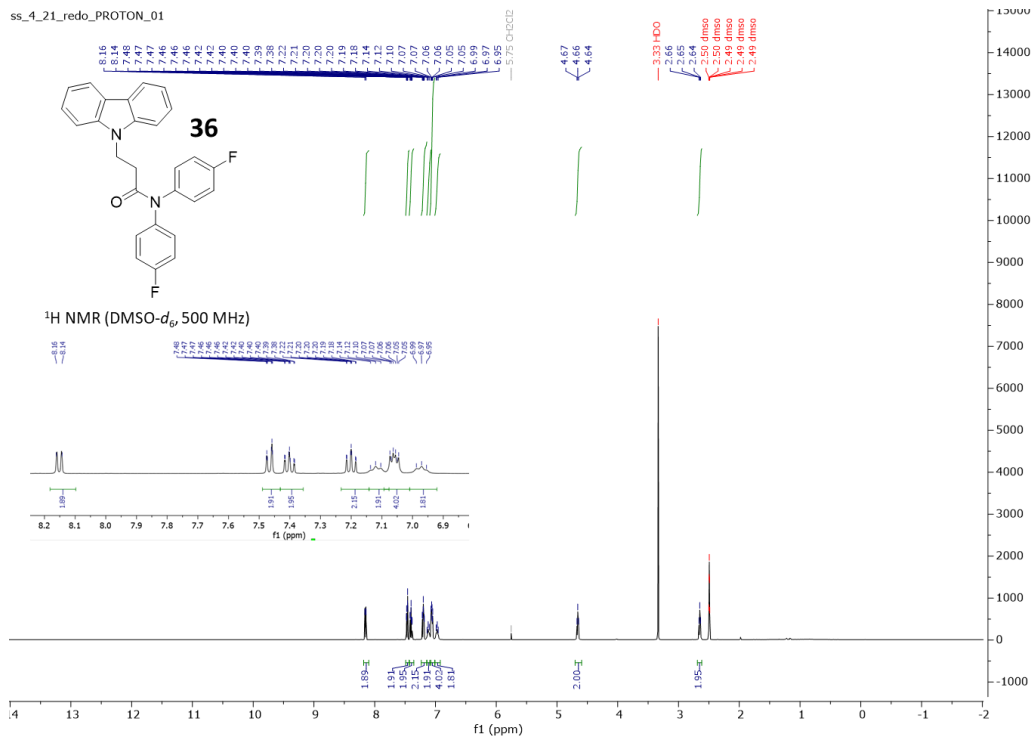


ss_2_25_p2_CARBON_01

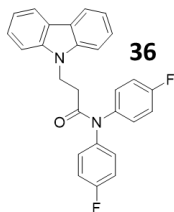


C{1H} NMR (CDCl₃, 126 MHz)

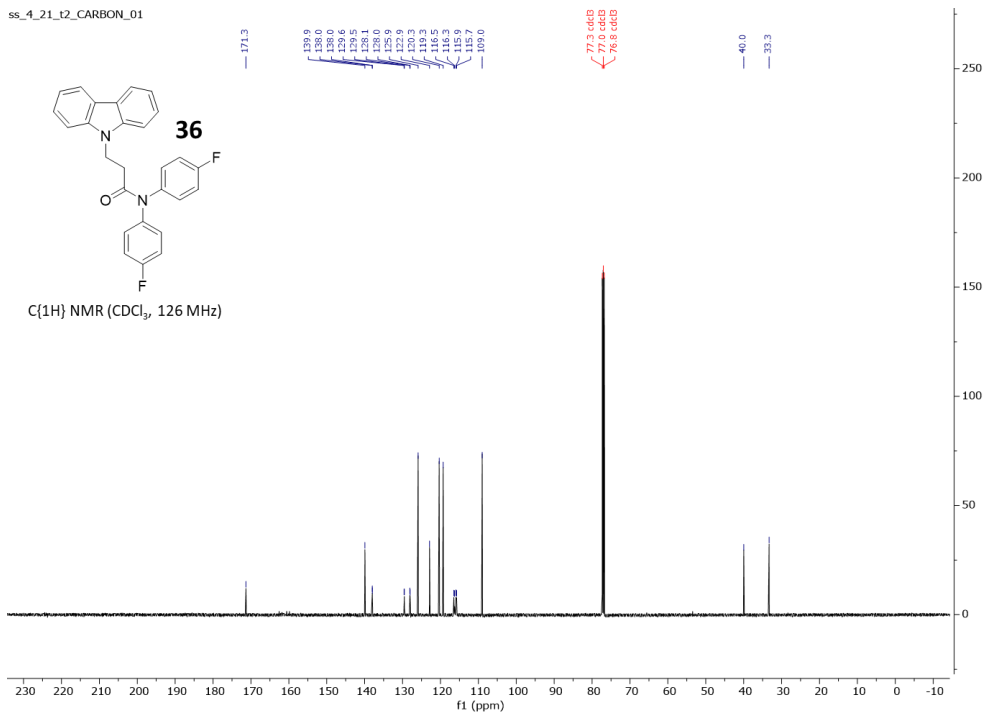


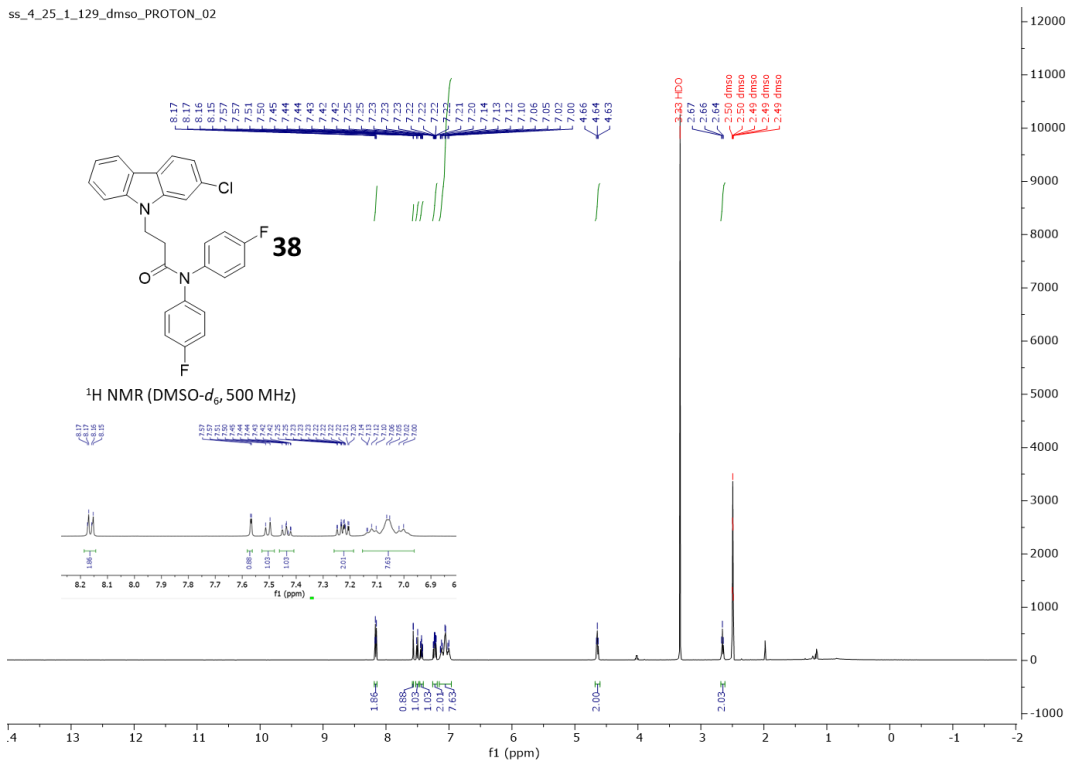


ss_4_21_t2_CARBON_01

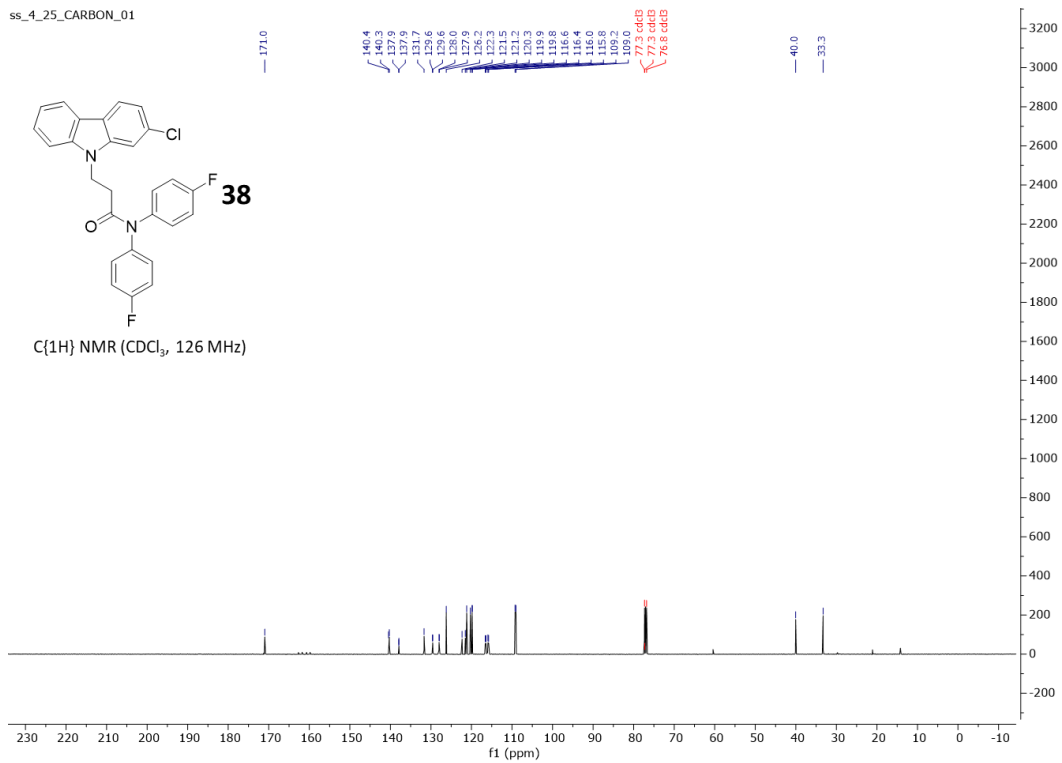
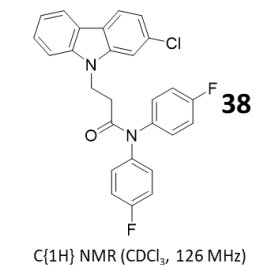


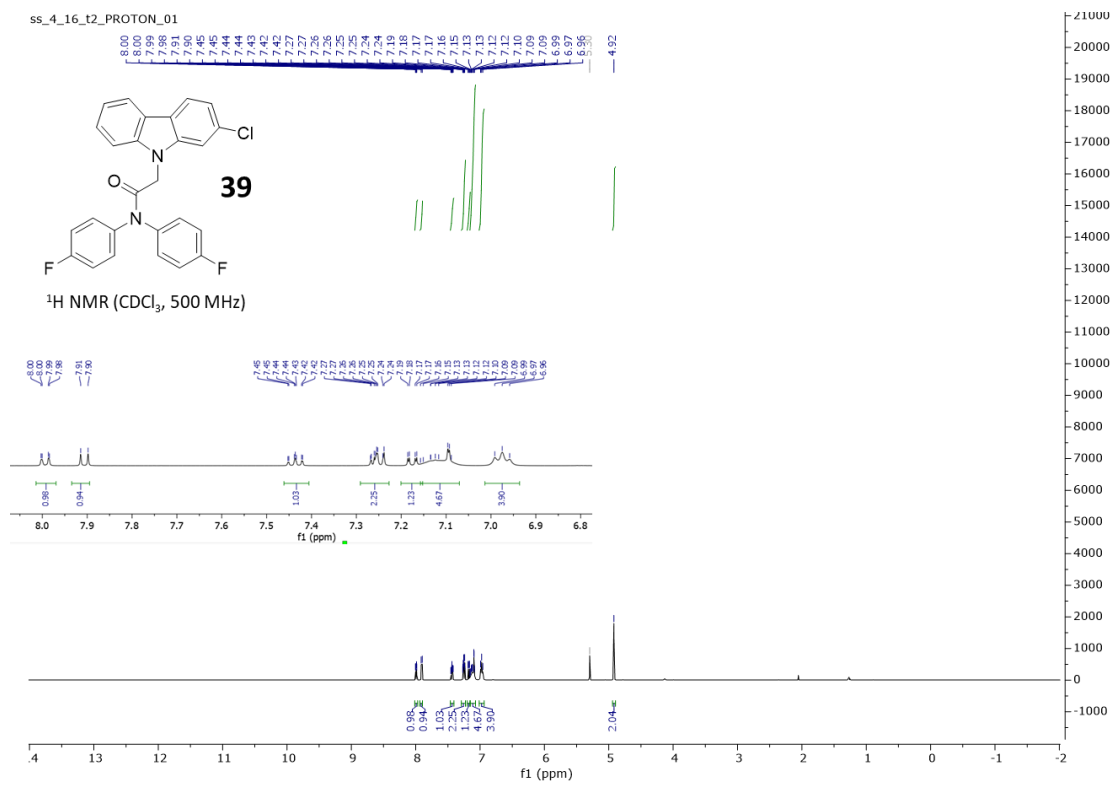
C{1H} NMR (CDCl₃, 126 MHz)



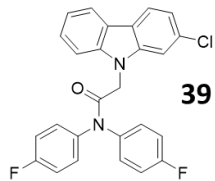


ss_4_25_CARBON_01

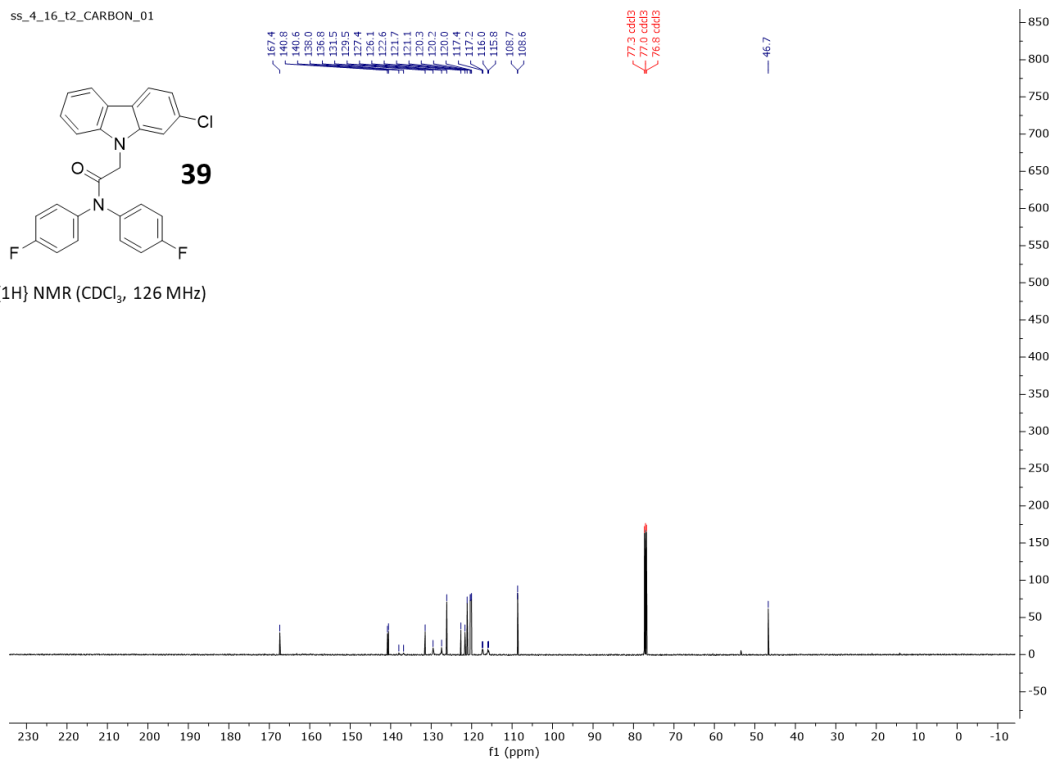




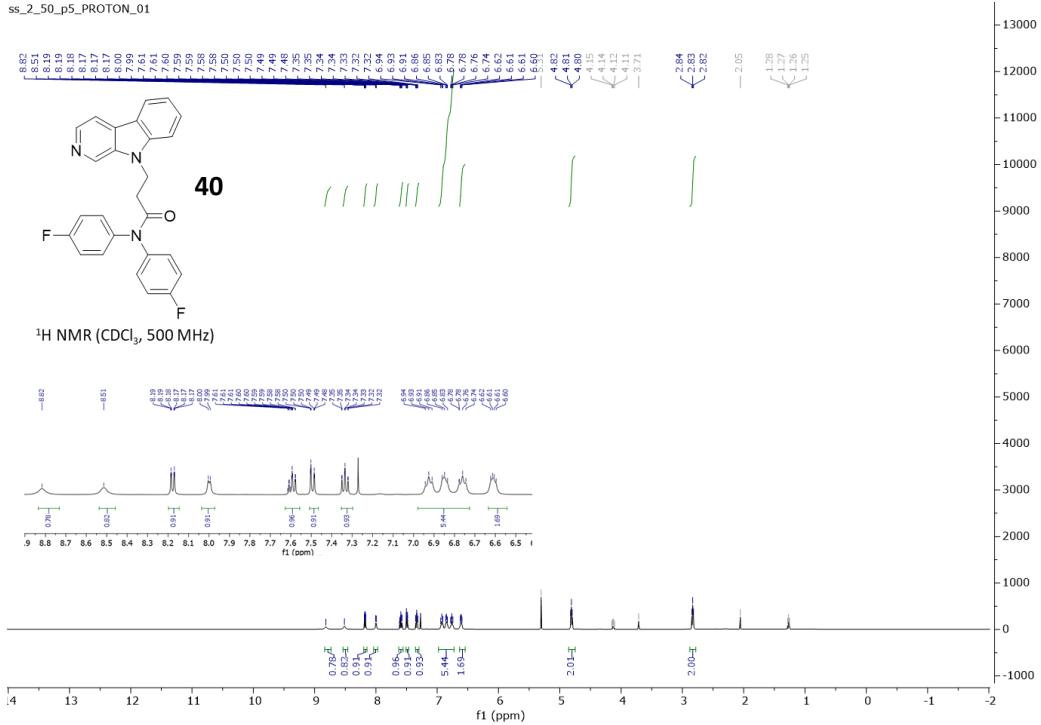
ss_4_16_t2_CARBON_01



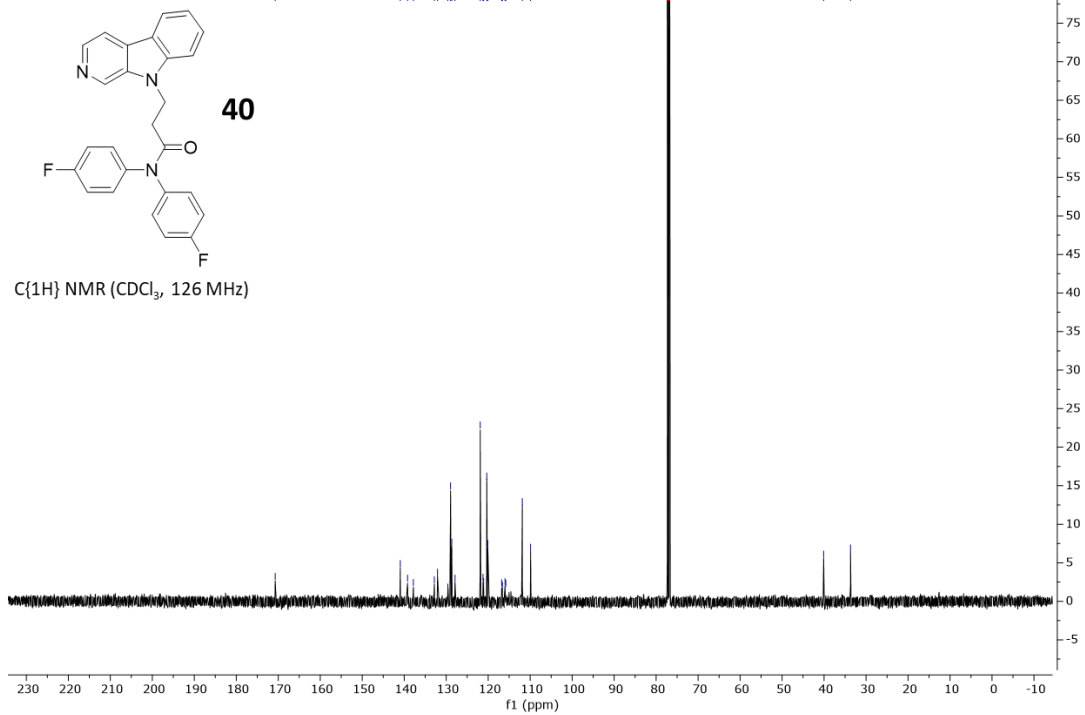
C{1H} NMR (CDCl₃, 126 MHz)



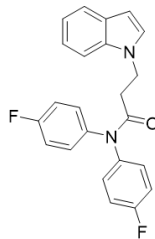
ss_2_50_p5_PROTON_01



SS-4-20_CARBON_01

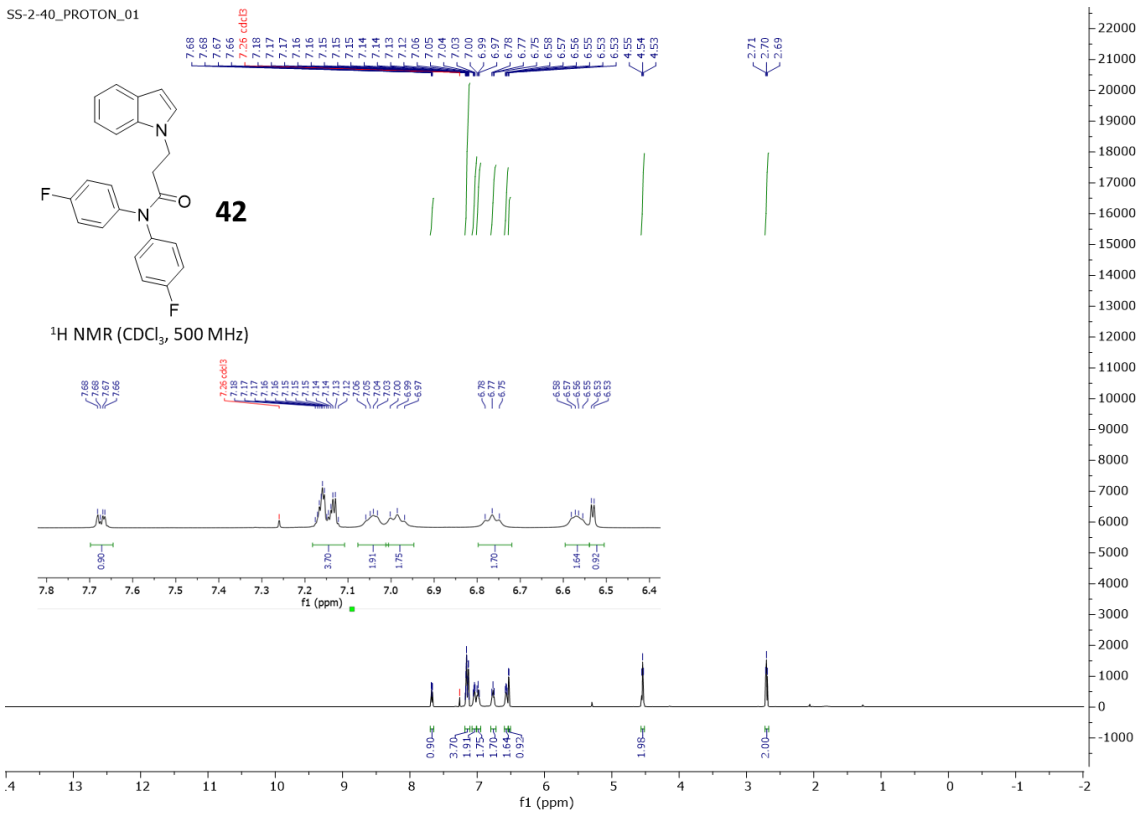


SS-2-40_PROTON_01

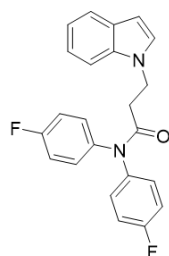


42

$^1\text{H NMR}$ (CDCl_3 , 500 MHz)

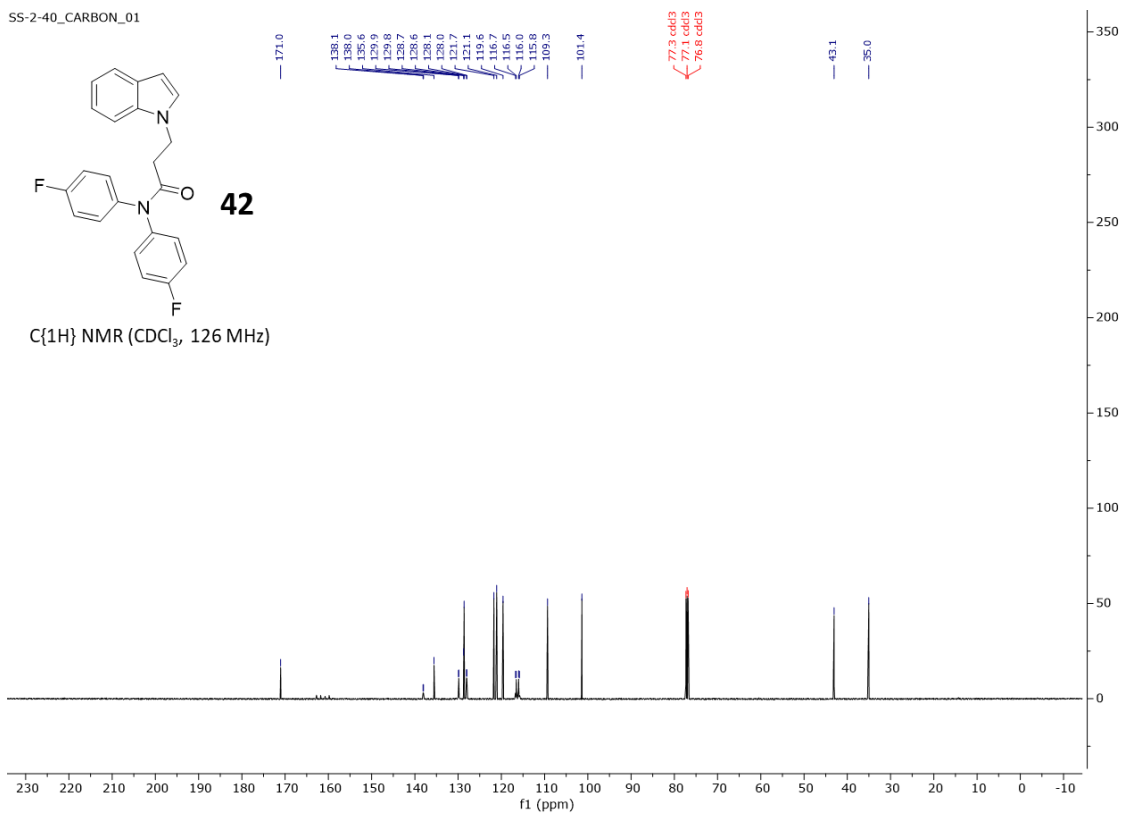


SS-2-40_CARBON_01

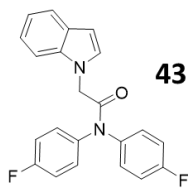


42

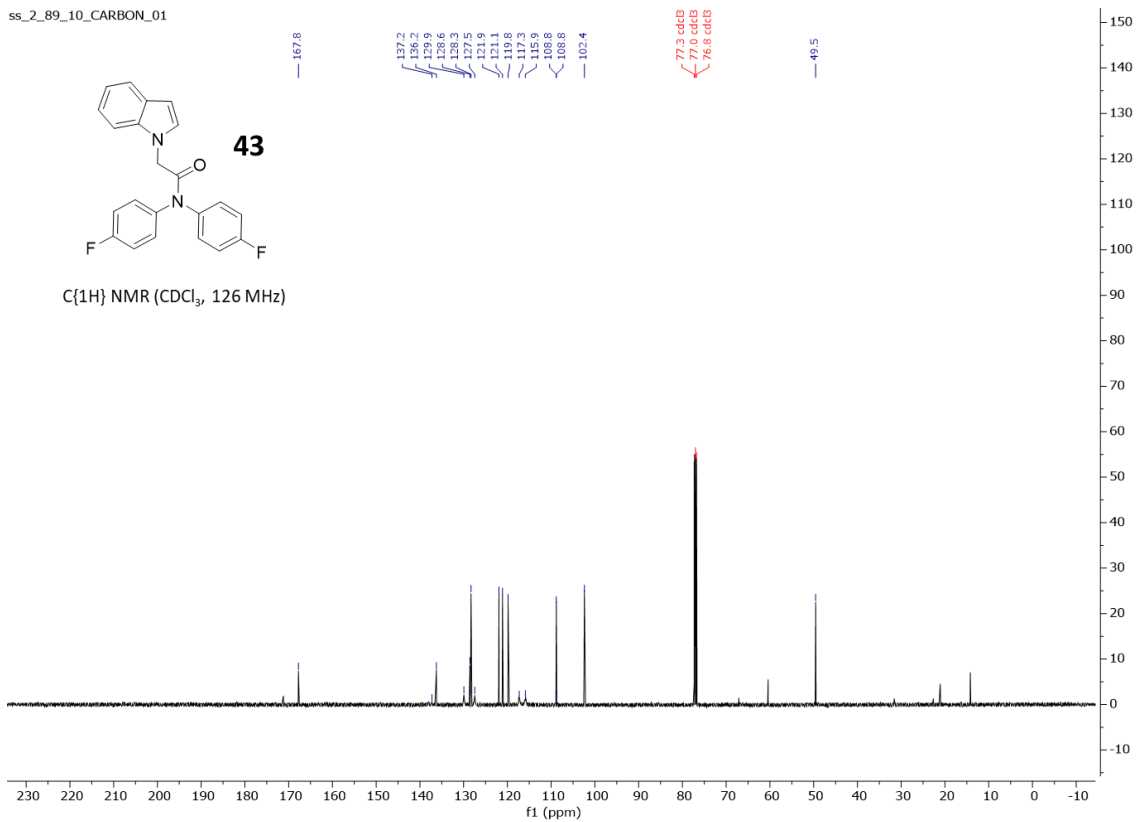
C{1H} NMR (CDCl₃, 126 MHz)



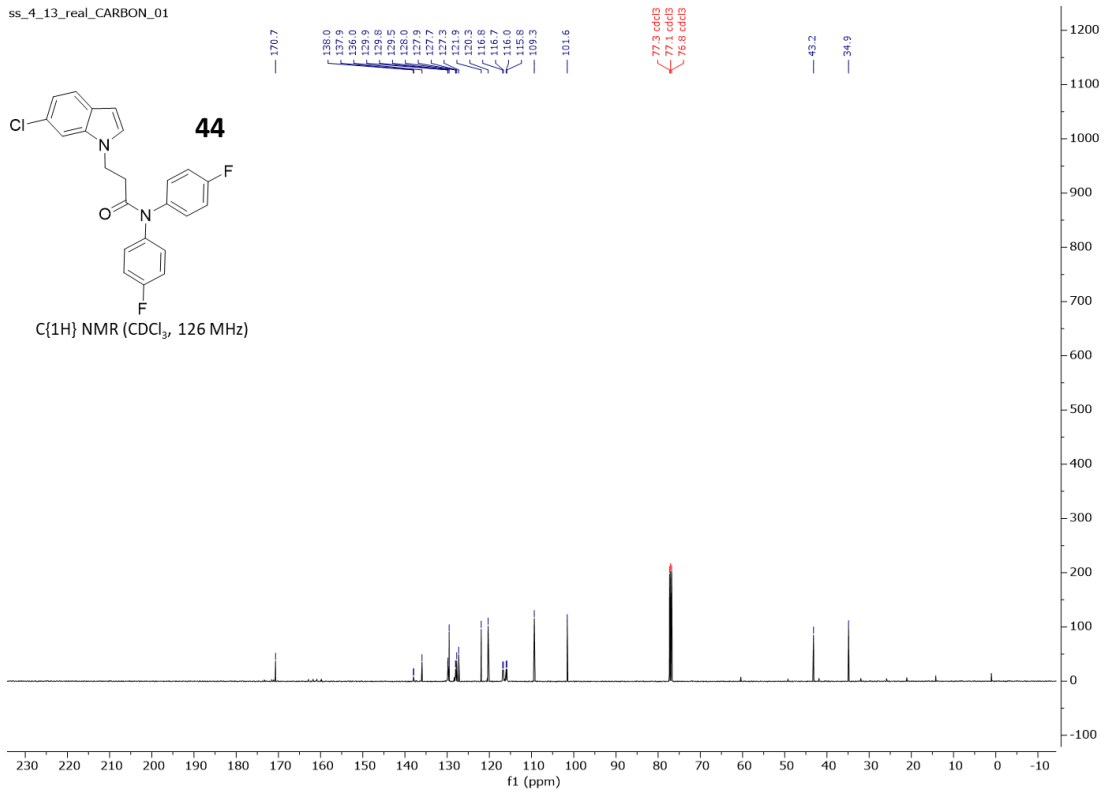
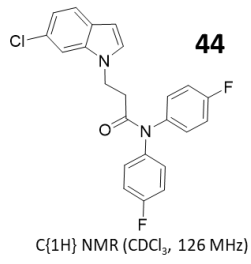
ss_2_89_10_CARBON_01



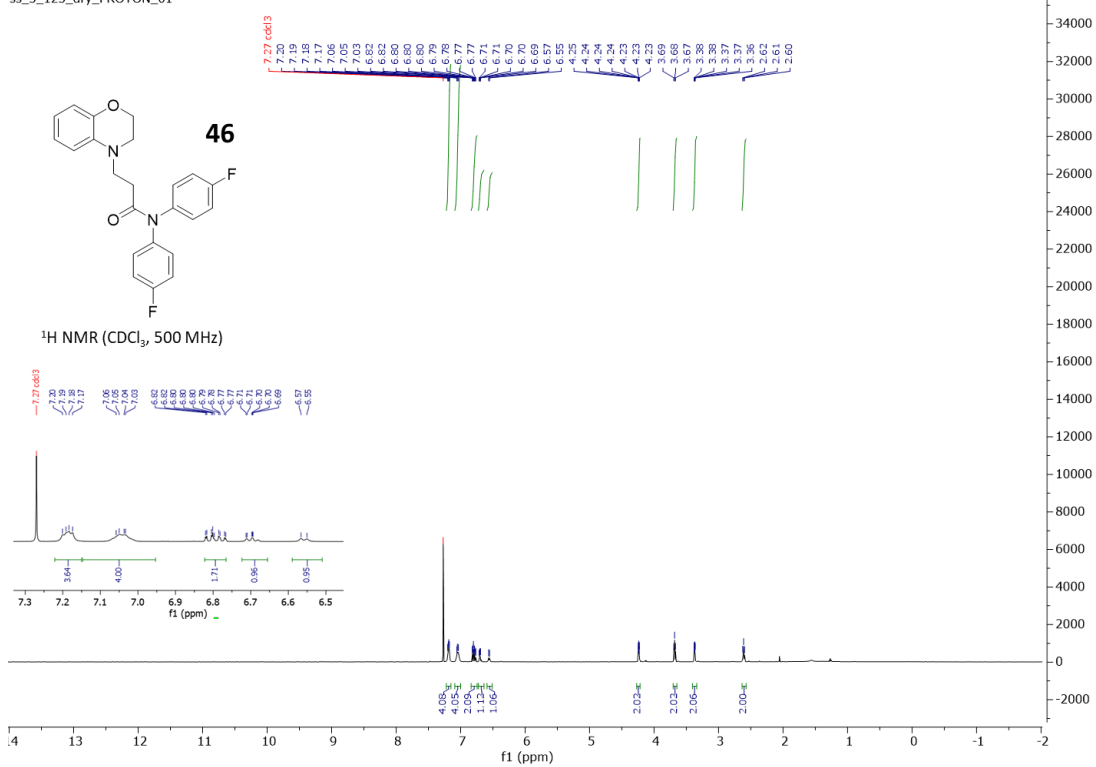
C{1H} NMR (CDCl₃, 126 MHz)



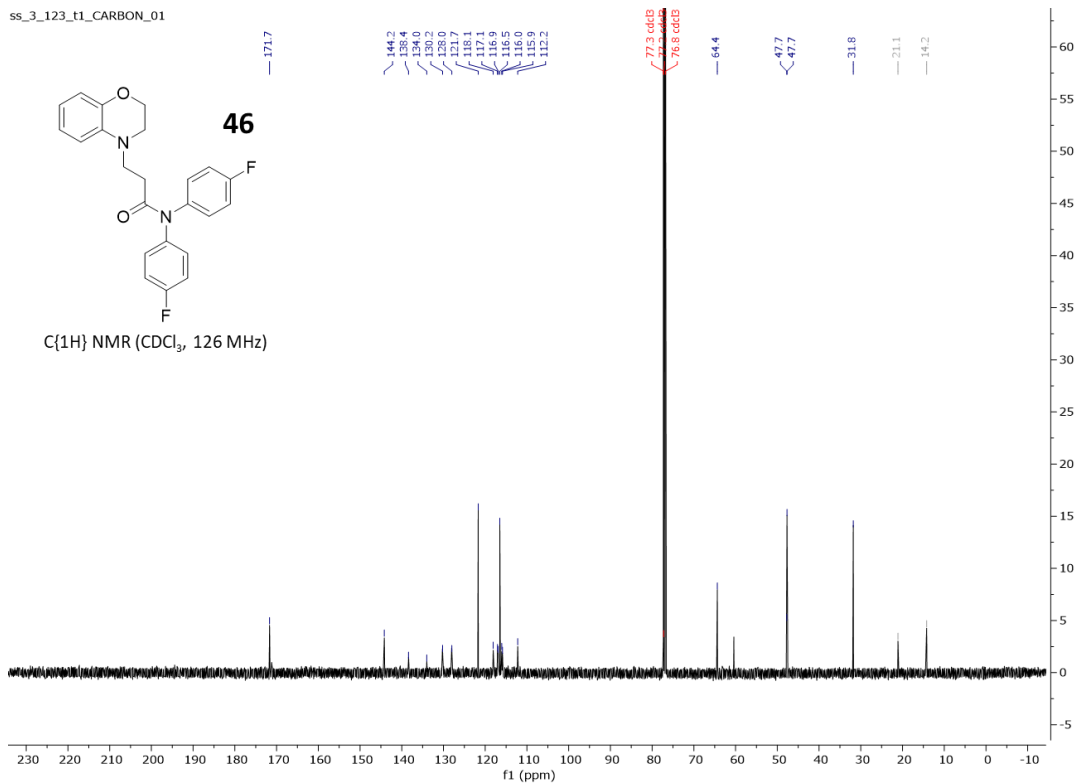
ss_4_13_real_CARBON_01



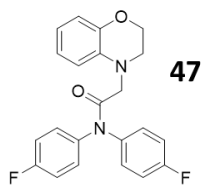
ss_3_123_dry_PROTON_01



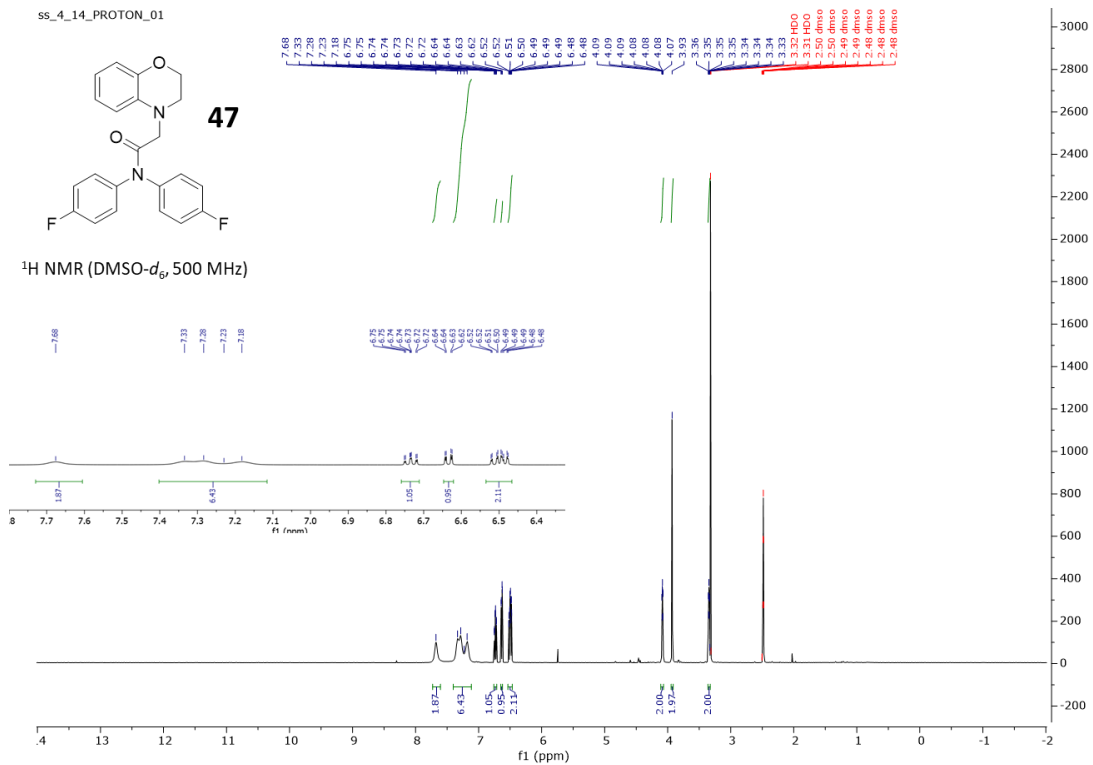
ss_3_123_t1_CARBON_01



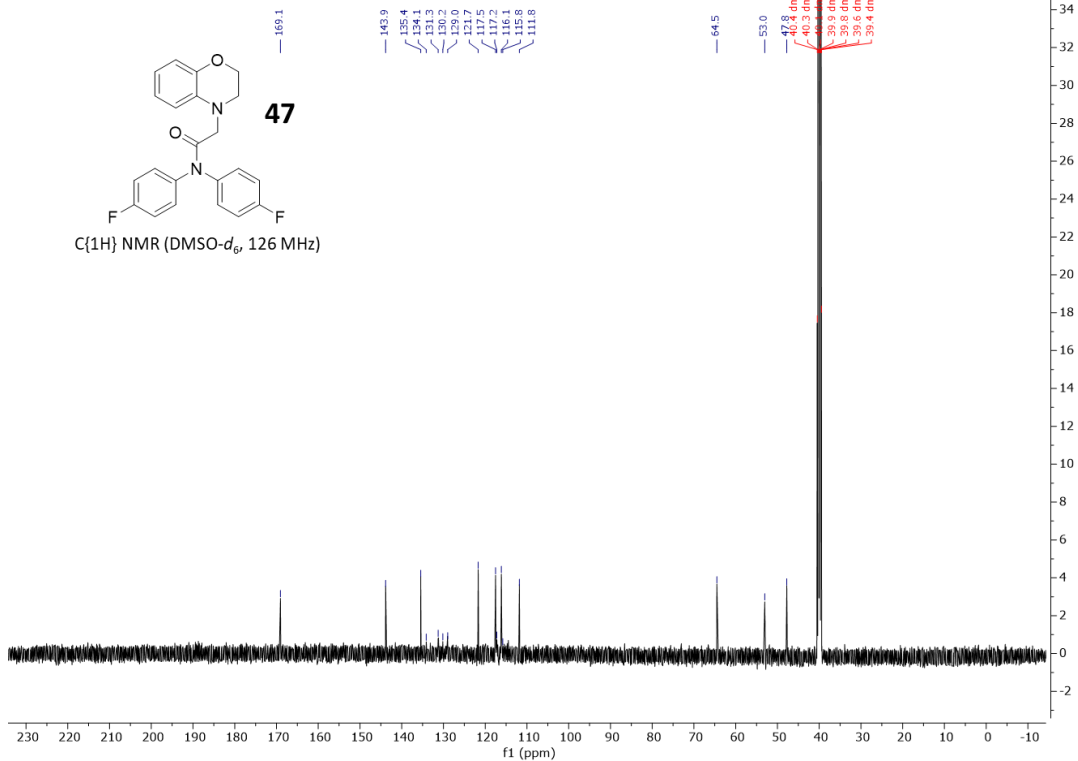
ss_4_14_PROTON_01



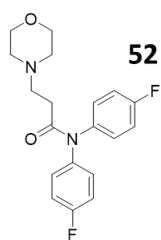
^1H NMR (DMSO- d_6 , 500 MHz)



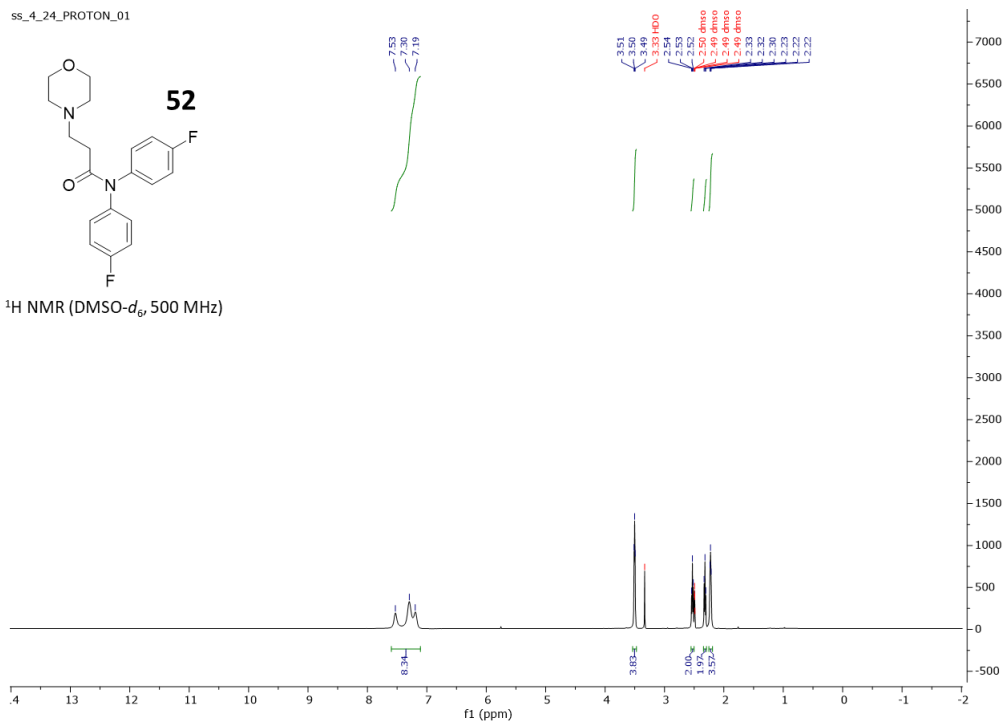
ss_4_14_CARBON_01

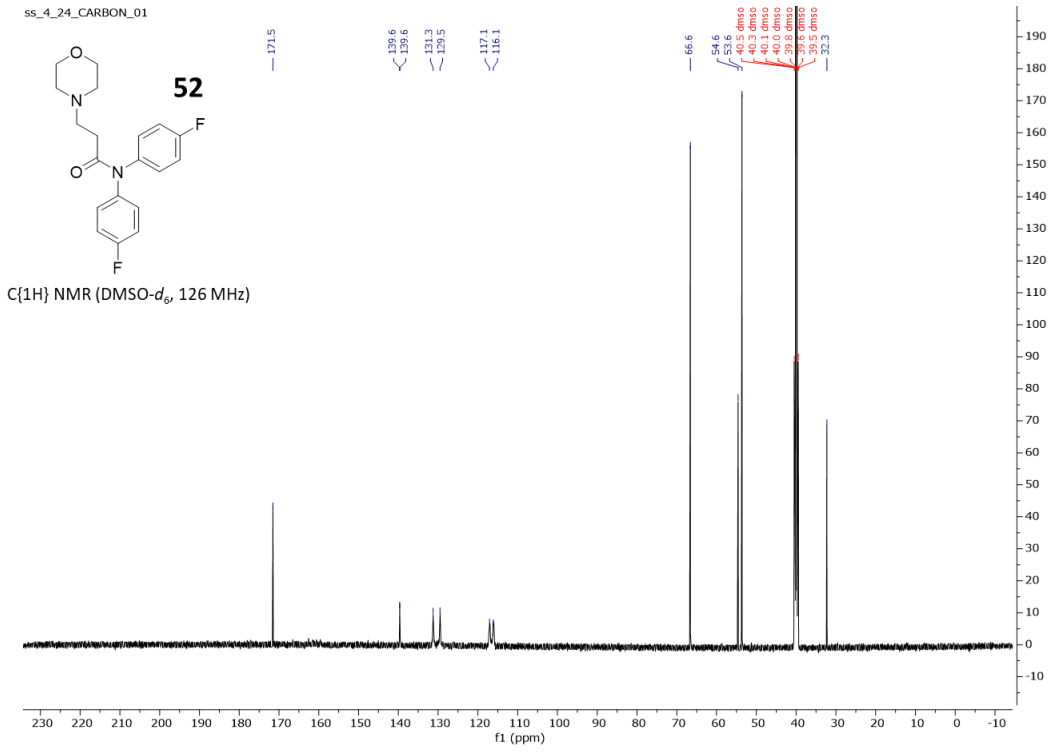


ss_4_24_PROTON_01

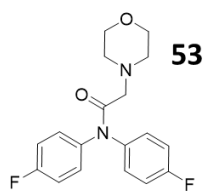


¹H NMR (DMSO-d₆, 500 MHz)

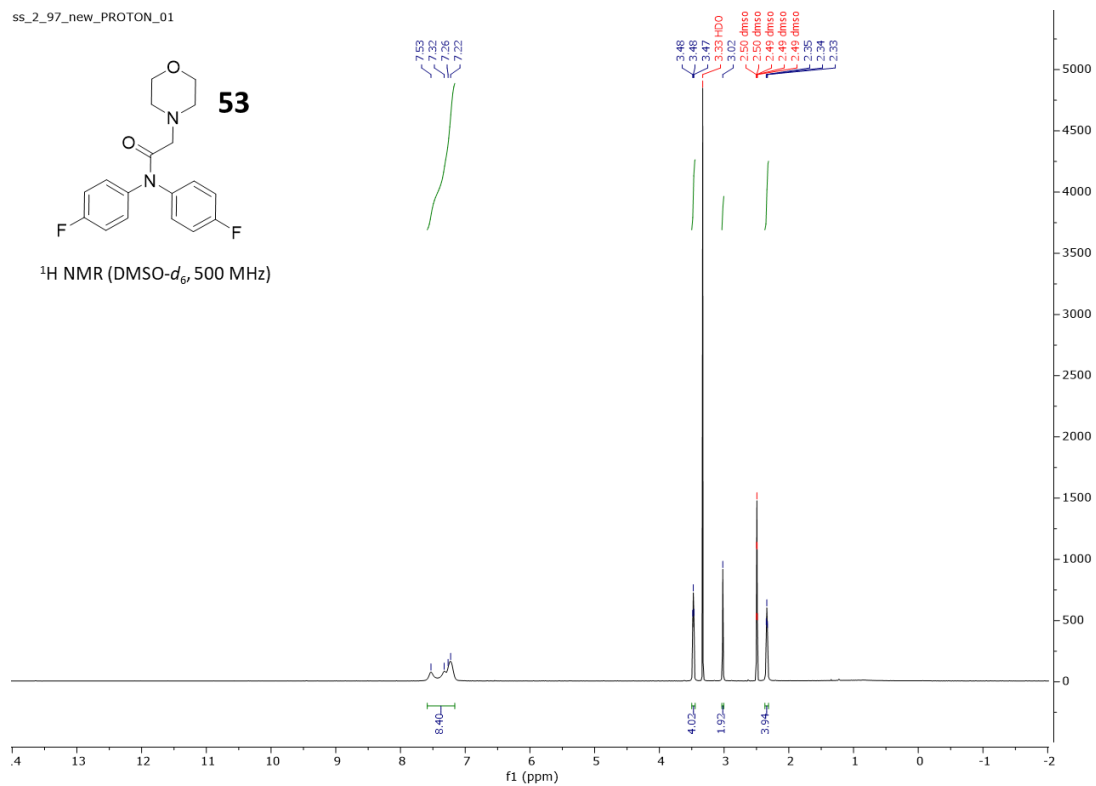




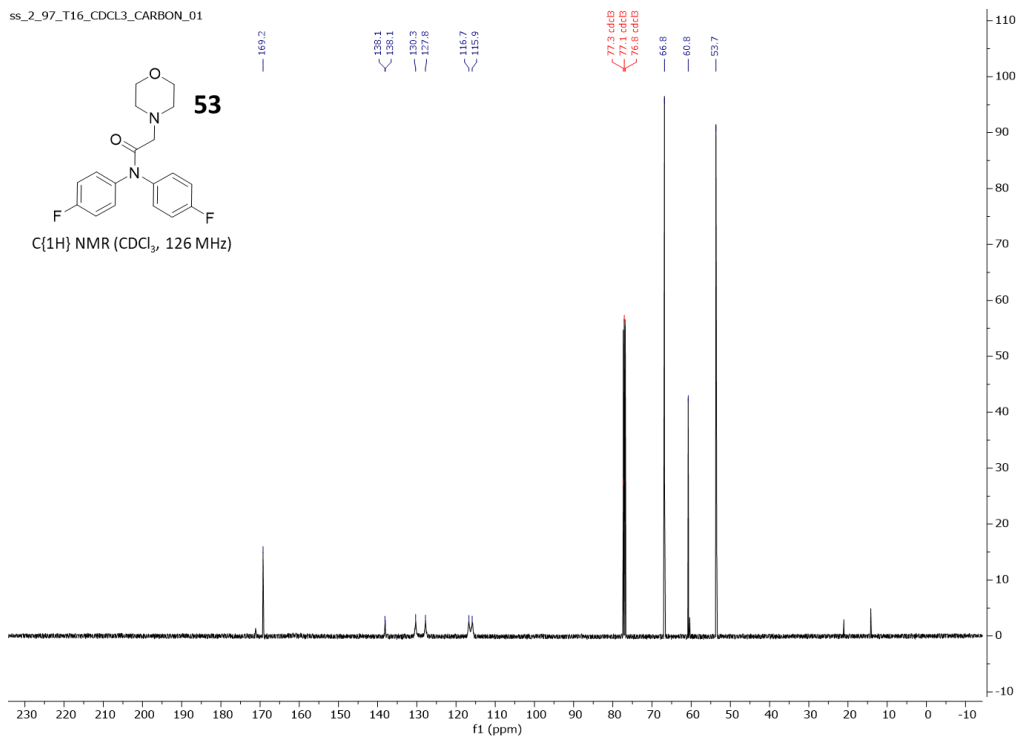
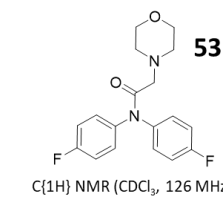
ss_2_97_new_PROTON_01



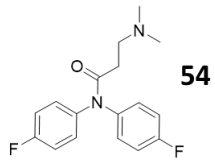
¹H NMR (DMSO-d₆, 500 MHz)



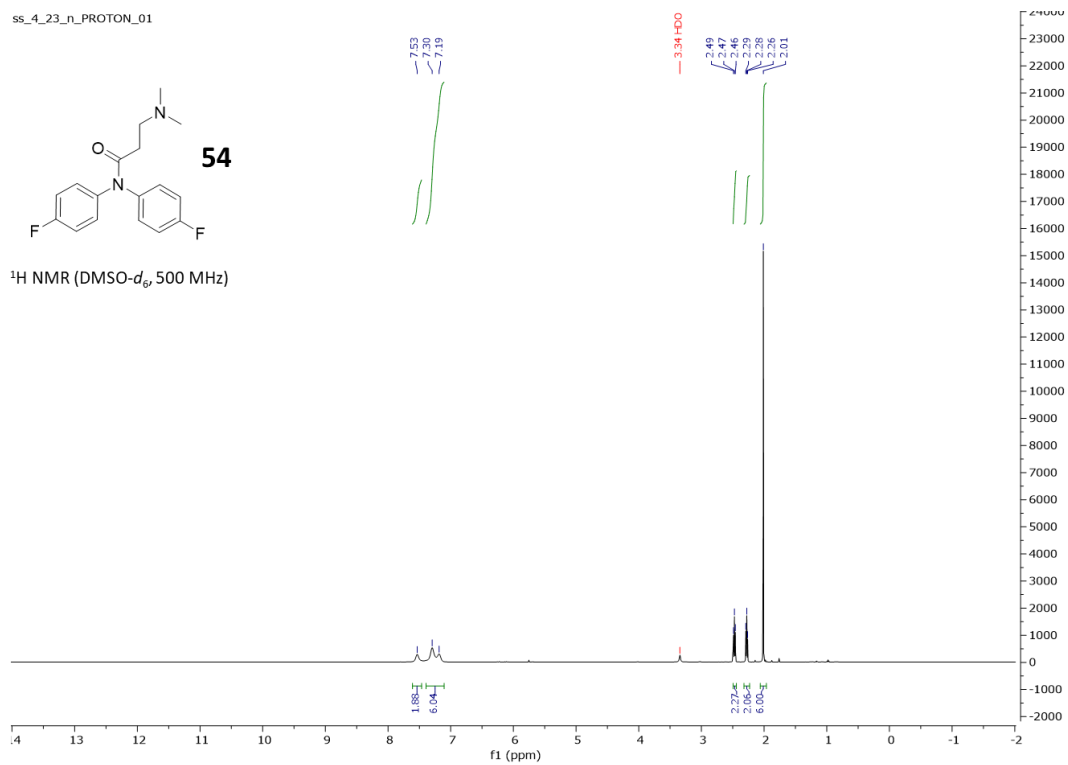
ss_2_97_T16_CDCL3_CARBON_01



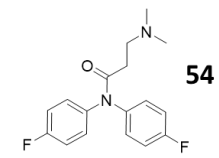
ss_4_23_n-PROTON_01



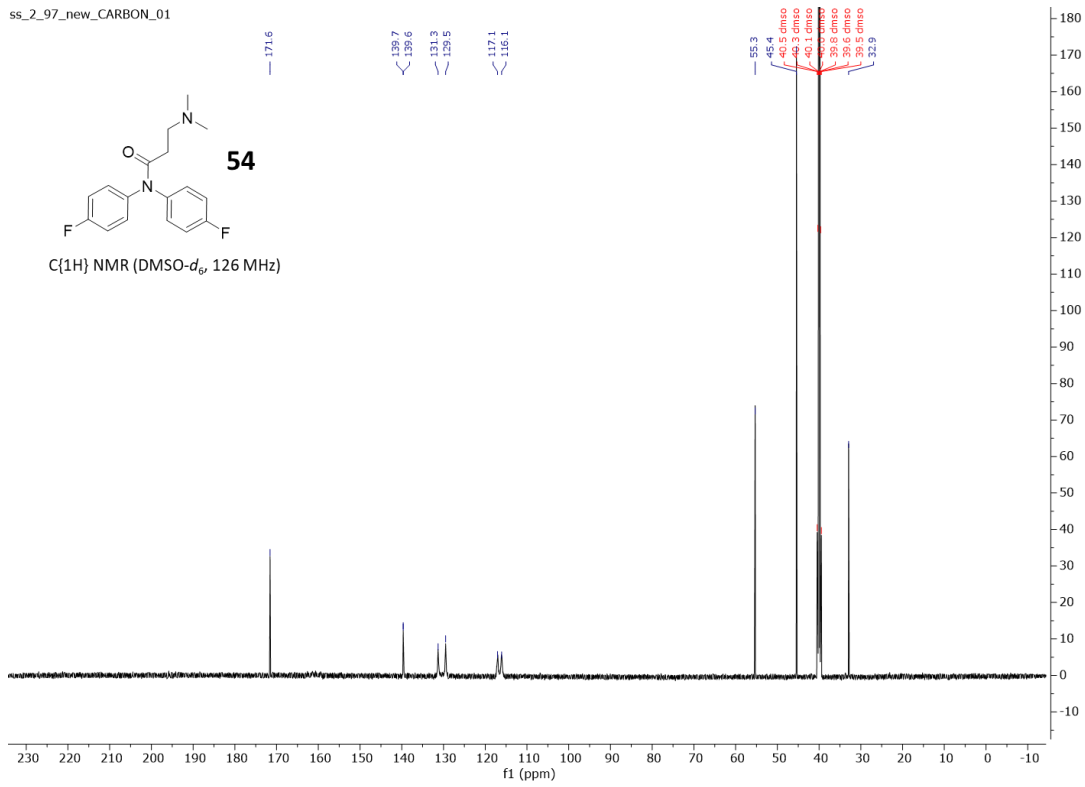
^1H NMR (DMSO- d_6 , 500 MHz)



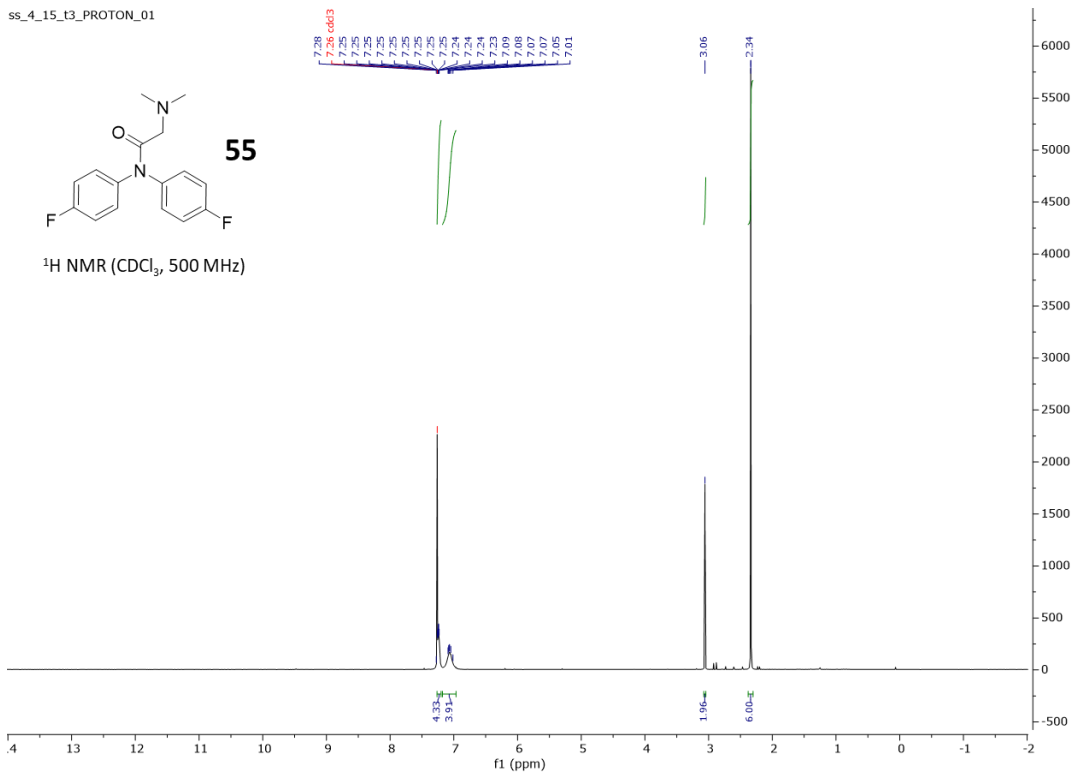
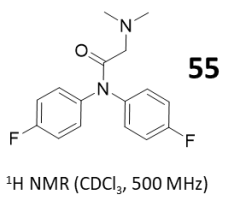
ss_2_97_new_CARBON_01



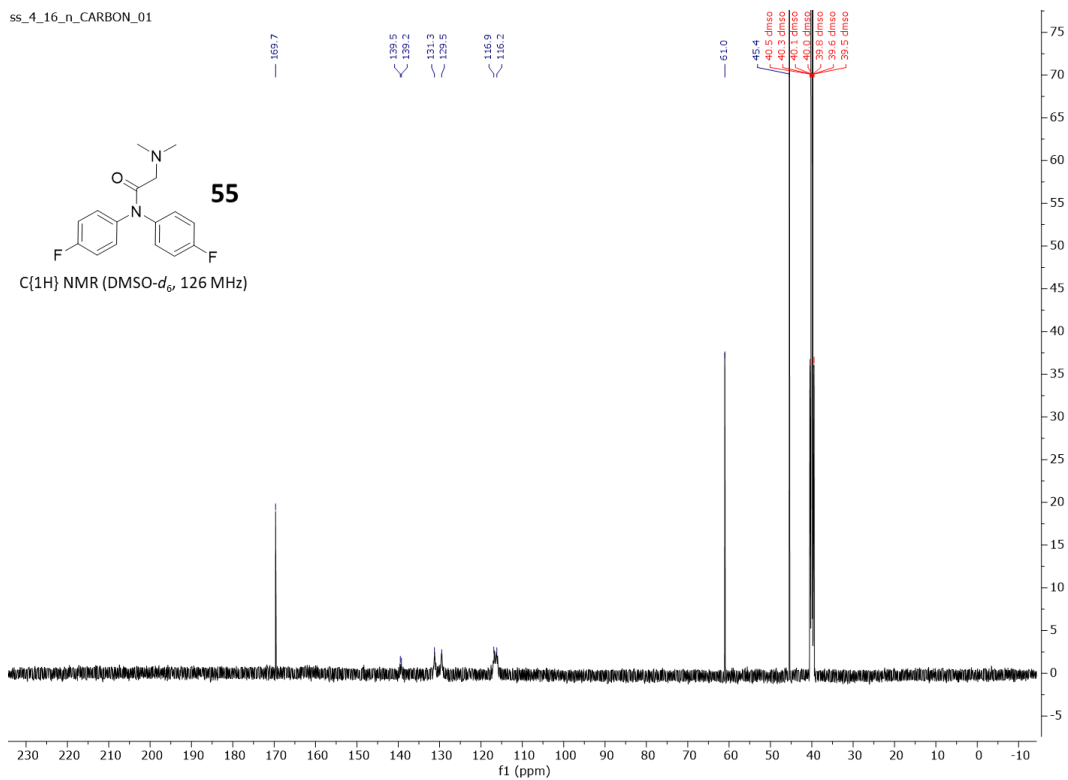
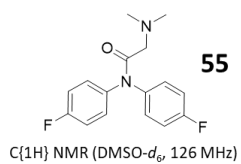
C{1H} NMR (DMSO-d₆, 126 MHz)



ss_4_15_t3_PROTON_01



ss_4_16_n_CARBON_01



Biological Protocols

Fluorogenic small peptide assay with purified 20S proteasome

The purified enzymatic activity assays were carried out in a black flat/clear bottom 96-well plate with a reaction volume of 100 μL . Different concentrations (3.75–30 μM or 0.16–30 μM) of test compounds were added to the wells containing 0.5 nM of human constitutive 20S proteasome diluted in a 38 mM Tris and 100 mM NaCl buffer with a pH of 7.8. The drug:proteasome mixture was incubated for 20 minutes at 37 $^{\circ}\text{C}$. Then, 10 μL of the fluorogenic substrates were added. The fluorogenic substrates used were a combination of Suc-LLVY-AMC, Z-LLE-AMC, and Boc-LRR-AMC with a final concentration of 6.67 μM of each. The activity was measured at 37 $^{\circ}\text{C}$ on a SpectraMax M5e spectrometer by measuring the change in fluorescence unit per minute for one hour at 380–460 nm. The rate of hydrolysis for the vehicle control was set at 100%, and the ratio of the treated sample over the vehicle control was used to calculate the fold change in rate of substrate hydrolysis by the proteasome.

Purified α -synuclein digestion with 20S proteasome

Proteolytic digestions of α -synuclein assays were carried out in a 25 μL reaction volume of 50 mM HEPES and 5 mM DTT buffer at a pH of 7.2, 300 nM of purified α -synuclein, and 10 nM purified human 20S proteasome. The 20S proteasome was first diluted to 11.1 nM in the HEPES buffer, and 0.5 μL of the test compounds in DMSO or DMSO alone were added. The drug:proteasome solution was incubated for 45 minutes at 37 $^{\circ}\text{C}$. After the incubation, 2.5 μL of a 3 μM stock of α -synuclein was added, and the mixture was incubated at 37 $^{\circ}\text{C}$ for an additional 3.5 hours. After the second incubation, 0.5 μM of GAPDH was added as a loading control. A concentrated SDS loading buffer

was also added, then the samples were boiled for 15 minutes to stop the digestion and immunoblotted.*For the evaluation of series II analogs, the concentration of α -synuclein was 1.5 μ M while the concentration of the 20S proteasome was 40 nM.

Cell Culture

HEK-293T cells were cultured in Dulbecco's modified Eagle's medium supplemented with 1% penicillin–streptomycin and 10% fetal bovine serum. All cell lines were maintained at 37 °C with 5% CO₂ in 10 cm tissue treated plates. Cell lines were routinely tested for mycoplasma contamination.

Cellular α -synuclein degradation

The HEK-293T cells were plated in 60 mm plates and grown to 80% confluency. The cells were then transiently transfected with Xtreme gene and the desired plasmid (5 μ g of DNA, TPPP and A53T α -synuclein, and 10 μ L of transfection reagent for a 1:2 dilution) diluted in 500 μ L Opti-mem. The expression of the target protein was conducted for 48 hours before treatment for an additional 16 hours. After the cells were treated with the test compounds or DMSO, the cells were scraped from the plate and washed with PBS. The plate was washed with PBS as well. The scraped cells in media and PBS were pelleted (300g for 5 minutes). The supernatant was removed, and the cell pellet was washed with ice cold PBS and once again pelleted (300g for 5 minutes). The PBS supernatant was removed, and the cell pellet was lysed with RIPA buffer with added protease inhibitors. The cell lysate was incubated for 15 minutes on ice. The lysate was centrifuged for 25 minutes at 500 g, then the supernatant was removed while the debris pellet was disposed of.

Immunoblotting

For all immunoblotting, a concentrated Laemmli sample buffer supplemented with 25% β -mercaptoethanol was added to all the samples and boiled for 10 minutes. The samples were then resolved on a 4-20% Tris-glycine SDS-PAGE gel and transferred onto a PVDF membrane using Mini Trans-Blot Electrophoretic Transfer Cell for 1 hour and 30 minutes. The membranes were blocked for 30 minutes with 5% Blocking Buffer at room temperature. The membrane was then incubated with the desired primary antibody (listed in the antibody section with dilution ratios) in 10 mL of Tris-buffered saline Tween 20 (TBST: 1x solution was made from a 10x TBS solution) at 4 °C for 16 hours. The immunoblots were washed with 1x TBST for 3x3 minutes before being incubated with the corresponding secondary antibody at room temperature for 1 hour. The immunoblots were developed with ECL Western reagent and imaged with an Azure Biosystems 300Q imager. If several proteins were probed for, the immunoblots were stripped using a mild stripping buffer (200 mM glycine, 3.5 mM SDS, and 8 mM Tween 20 with a pH of 2.2) for 20 minutes and then washed with TBST for 3x 5 minutes before re-probing. Immunoblots were then quantified using the Bio-Rad Image Lab software.

Replicates

Section 2.3 Replicates

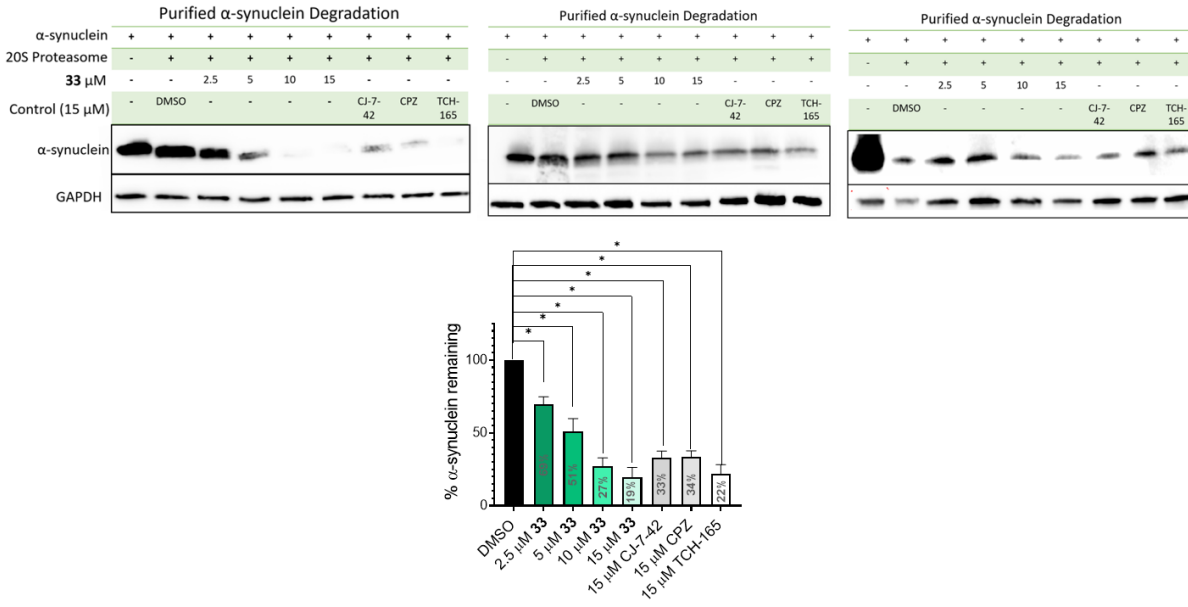


Figure 2.13: Westerns of α -synuclein degradation by purified 20S proteasome treated with compounds 33, CJ-7-42, CPZ, and TCH-165 (n=3).

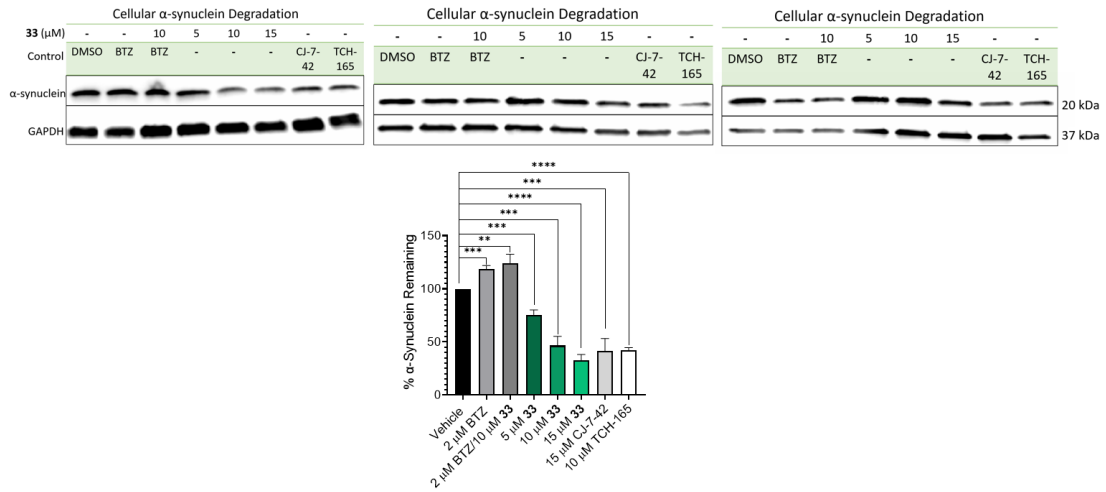
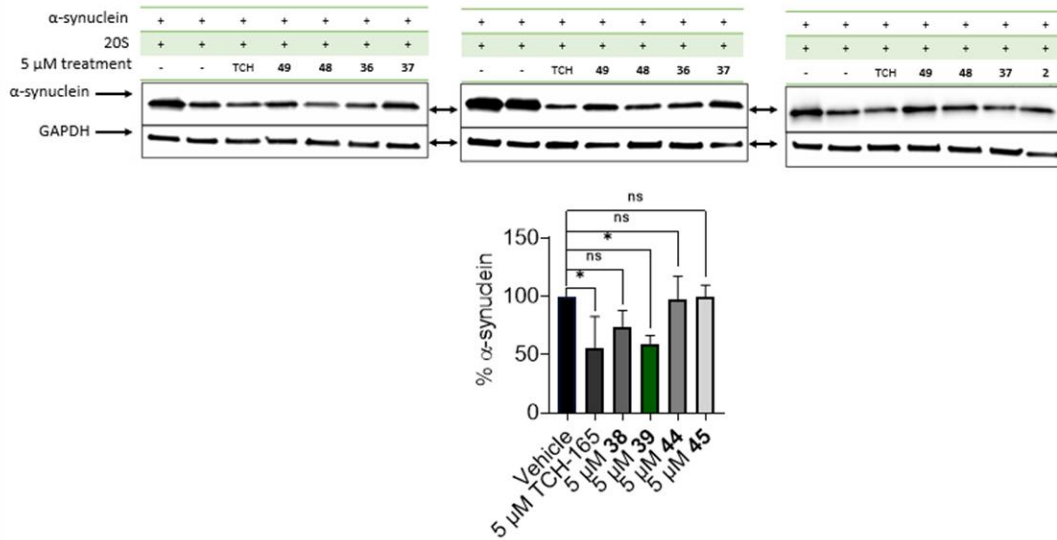


Figure 2.14: Western blots (n=3) of A53T mutated α -synuclein degradation in Hek293T cells treated with Vehicle (DMSO), BTZ, TCH-165, and compounds 33, and CJ-7-42.

Section 2.4 Replicates

A.



B.

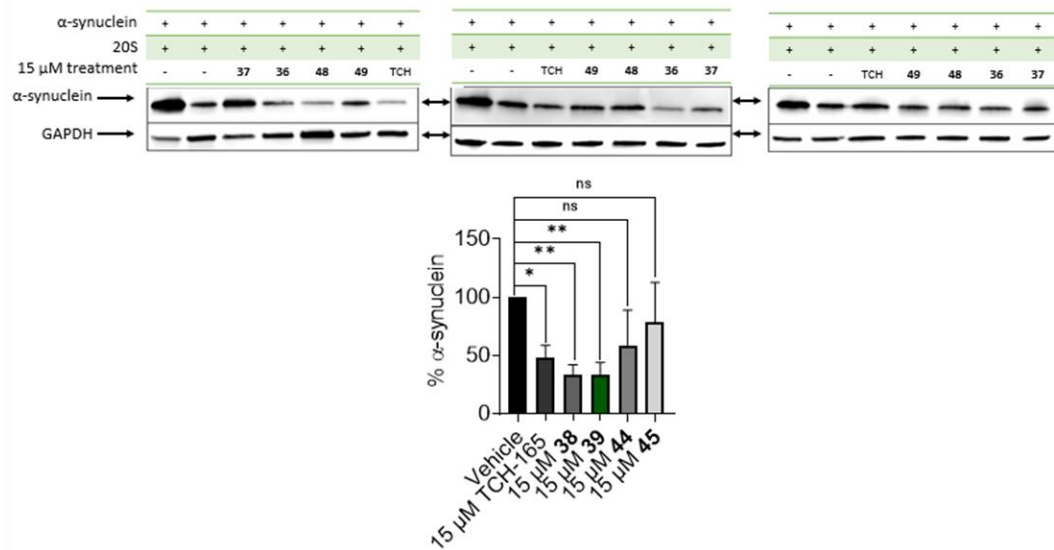
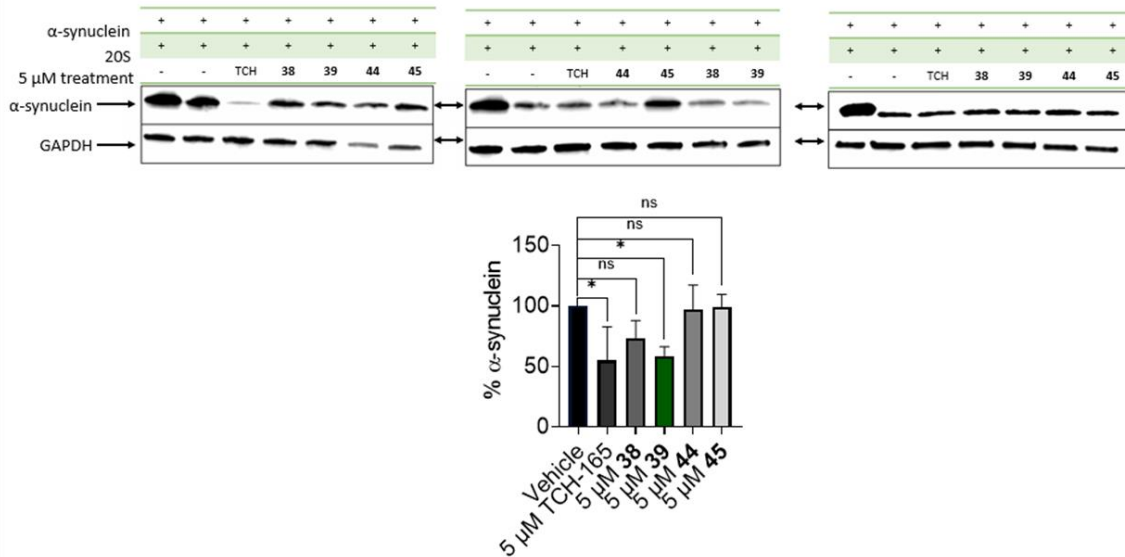


Figure 2.15: Westerns of α-synuclein degradation by purified 20S proteasome treated with (A) 5 μM and (B) 15 μM of compounds 36, 37, 48, 49, and TCH-165. The quantification values were all normalized to the GAPDH, and gels shown are indicative of n=3 independent experiments.

A.



B.

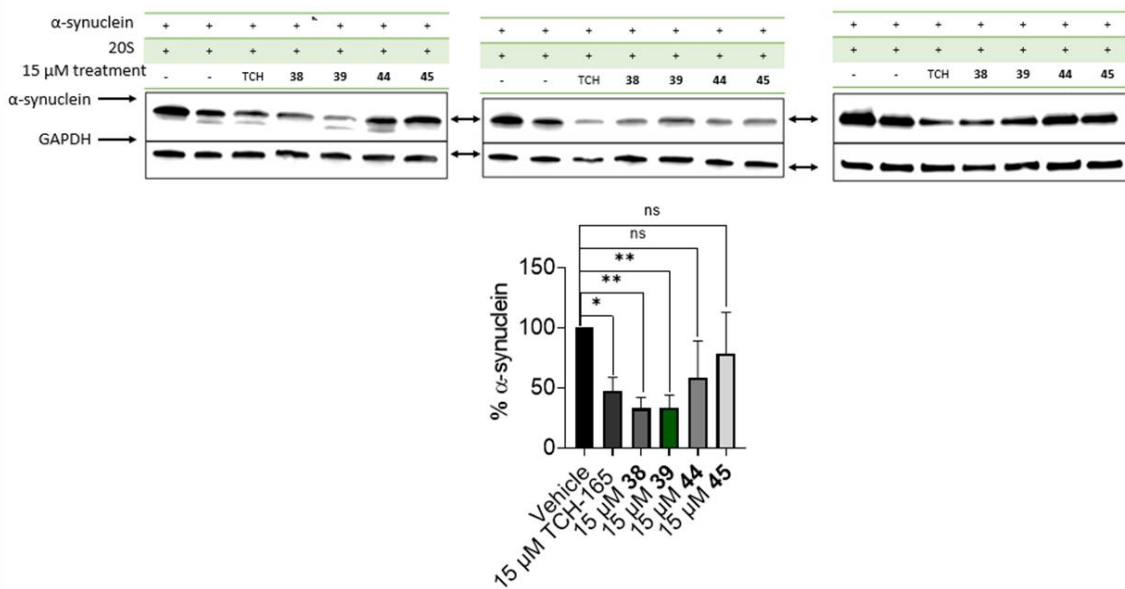


Figure 2.16: Westerns of α-synuclein degradation by purified 20S proteasome treated with (A) 5 μM and (B) 15 μM of compounds 38, 39, 44, 45, and TCH-165. The quantification values were all normalized to the GAPDH, and gels shown are indicative of n=3 independent experiments.

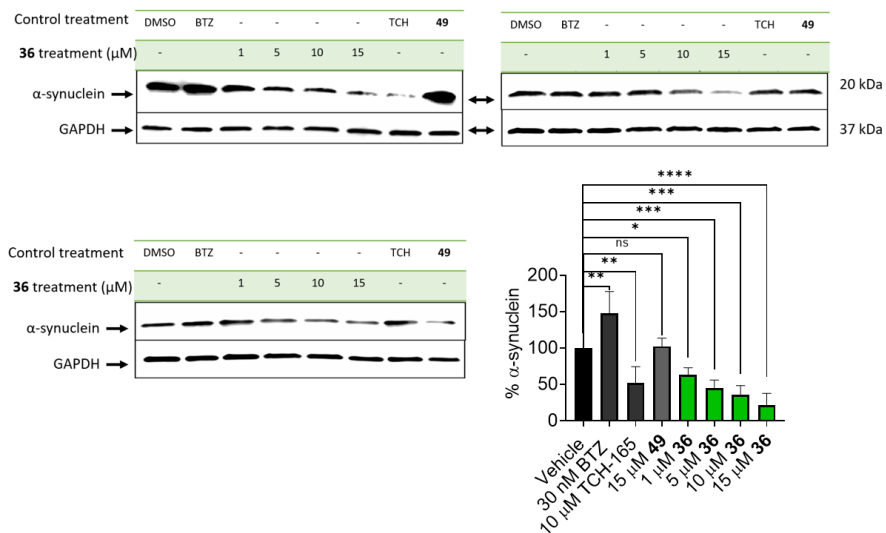


Figure 2.17: Western blots of A53T mutated α -synuclein degradation in HEK-293T cells treated with vehicle (DMSO), bortezomib (BTZ), TCH-165, and compounds 36 and 49. The quantification values were all normalized to the GAPDH, and gels shown are indicative of n=3 independent experiments. Error bars are based on standard deviation.

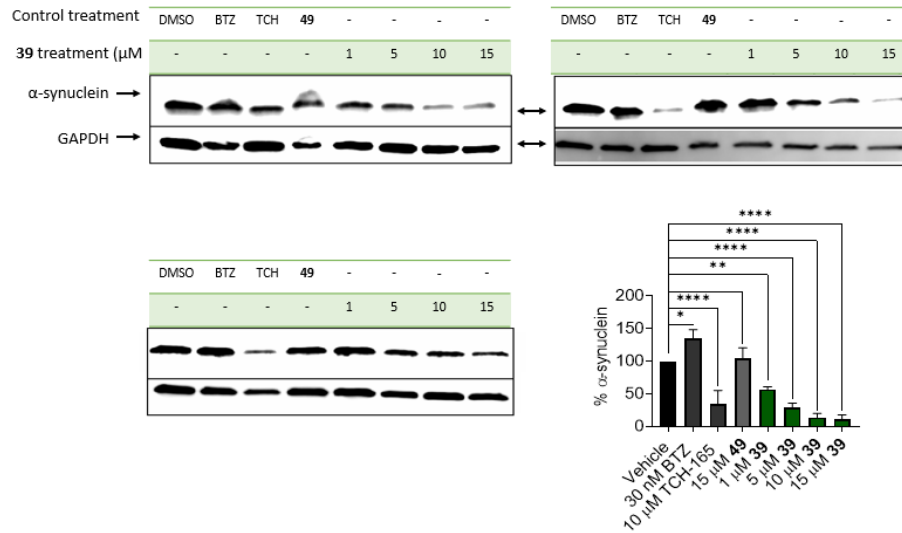


Figure 2.18: Western blots of A53T mutated α -synuclein degradation in HEK-293T cells treated with vehicle (DMSO), bortezomib (BTZ), TCH-165, and compounds 39 and 49. The quantification values were all normalized to the GAPDH, and gels shown are indicative of n=3 independent experiments. Error bars are based on standard deviation.

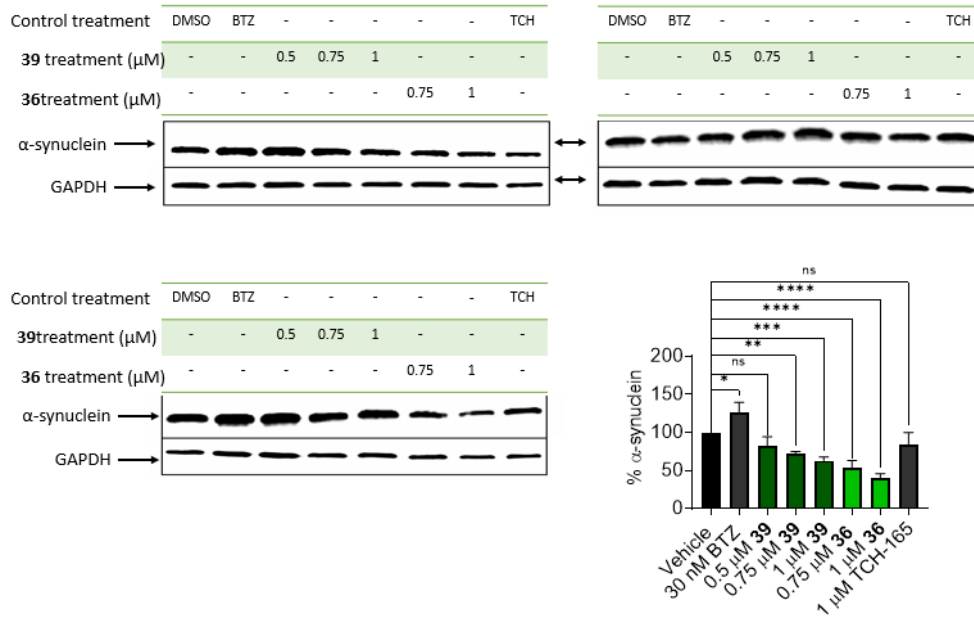


Figure 2.19: Western blots of A53T mutant α -synuclein degradation in HEK-293T cells treated with vehicle (DMSO), BTZ, TCH-165, and compounds 36 and 39 at lower concentrations. The quantification values were all normalized to the GAPDH, and gels shown are indicative of n=3 independent experiments. Error bars based on standard deviation.

CHAPTER THREE

Development of Cellular Models Recapitulating Proteasomal Impairment Seen in Synucleinopathies

3.1 Introduction

Multiple system atrophy (MSA), Parkinson's disease (PD), and dementia with Lewy Bodies (DLB) are members of a heterogeneous class of neurodegenerative diseases, termed synucleinopathies.¹ A pathological hallmark of synucleinopathies is the presence of α -synuclein.^{1, 2} α -synuclein is an intrinsically disordered protein highly expressed in neurons and comprises 1% of neuronal cytosolic proteins localized in presynaptic terminals.^{3, 4} While the exact physiological role of α -synuclein has not been elucidated, it has been proposed that α -synuclein regulates the release of neurotransmitters.^{5, 6} Due to the disordered nature of α -synuclein, it is prone to aggregation. To prevent α -synuclein aggregation, chaperones and nannies are expressed to interact with α -synuclein when it is not involved in the signaling pathway.⁷ In addition, the UPS plays a vital role in the clearance of monomeric α -synuclein. Under pathological conditions, either through aberrant expression of α -synuclein or impaired clearance, α -synuclein accumulates throughout the cell. The cause of α -synuclein accumulation is poorly understood, but it has been proposed that aging and genetic mutations are involved.⁸⁻⁹ Missense mutations of α -synuclein that increase the expression rate have been identified, such as the A53T mutation, often found in familial types of PD and has been observed to be prion-like when introduced to MSA aggregates.¹⁰⁻¹¹ Furthermore, in patients diagnosed with MSA and PD, 20S proteasome subunits are greatly diminished, which correlates to the decrease in proteasomal activity observed.¹² In both circumstances, the cellular proteostasis is perturbed, aiding in the accumulation of α -synuclein.

Once α -synuclein accumulates, aggregates can form, ultimately creating the characteristic α -synuclein deposits seen in synucleinopathies.^{13, 14, 16} The cell type bearing

the α -synuclein deposits is linked to the differing disease patterns of PD and MSA.¹⁵ Inclusions principally observed in neuronal cells are termed Lewy bodies and are associated with disorders like PD.^{13,14} α -synuclein inclusions localized in oligodendrocytes are termed glial cytoplasmic inclusions (GCIs) and are a hallmark of MSA.¹⁶ During the formation of these larger, insoluble aggregates, toxic oligomeric species of α -synuclein are created. The noxious oligomers have been identified to disrupt numerous cellular pathways, impairing the UPS activity.^{17,18,19} The impairment of the UPS then allows for the accumulation of α -synuclein, propagating a toxic cycle, ultimately leading to cell death (**Figure 3.1**). Preventing the propagation of this perturbed proteostasis cycle is required to produce viable therapeutics for neurodegenerative diseases, such as PD and MSA.

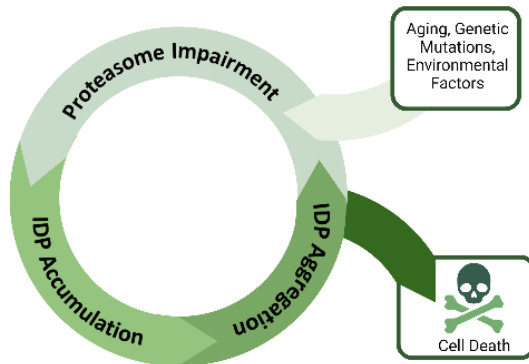


Figure 3.1: Schematic of the perturbed proteostasis cycle seen in neurodegenerative diseases, such as MSA and PD. *Created with BioRender

Proteasomal impairment models must be developed to evaluate further the potential of 20S proteasome enhancers as a therapeutic pathway to treat neurodegenerative diseases. While studies have successfully recapitulated the aggregation of α -synuclein in

cells, these experiments require primary cells and preformed α -synuclein fibrils (PFFs).²⁰⁻
²¹ To screen numerous molecules, the labor and cost required to use primary cells with PFFs would be significant. To overcome the limitations of previous methods, I developed an experimental method to induce α -synuclein aggregation in an immortalized cell line without using PFFs, described in **section 3.2**. Furthermore, a cellular model that directly evaluates the impact of diminished 20S proteasome levels on cellular proteostasis has yet to be developed. In **section 3.3**, the establishment of a cellular model to evaluate the impact of diminished proteasome levels on critical cellular pathways, such as the endoplasmic reticulum-mediated unfolded protein response, is detailed.

3.2 Proteasomal Impairment Induced by p25 α / α -synuclein Aggregates

3.2.1 Rational

Recently, it was identified that α -synuclein aggregates derived from PD and MSA patients structurally differ from one another.^{22, 23} The flexible nature of α -synuclein allows for the adoption of different conformations depending on the protein interacting with α -synuclein. The resulting differing conformations dictate the structure and the composition of the α -synuclein deposits, which play a significant role in the pathologies of the different synucleinopathies.^{22, 23} MSA-derived α -synuclein strains present a higher degree of β -sheet structures,²² and are significantly more toxic and resistant to protease degradation than their PD-derived counterparts.²⁴ *In vivo* studies established that MSA-derived fibrils induced more severe neurodegeneration, neuroinflammation, and motor impairment.²⁵ The more aggressive seeding and spreading behavior of the MSA α -synuclein fibrils

directly reflect the destructive nature of MSA.²⁵ The distinctive activity and structure of the MSA-derived α -synuclein strains have been associated with the co-localization of an oligodendrocyte-specific IDP, tubulin polymerization promoting protein (TPPP/p25 α), referred to as p25 α hereafter.^{26, 27, 28, 29} Physiologically, p25 α is solely expressed in oligodendrocytes and aids in neuronal myelination.^{28, 30} While the mechanism of α -synuclein entry into the oligodendrocytes is under debate, when present, p25 α migrates from the myelin sheaths to the cell body,²⁵ causing loss of neuronal myelination and induces the rapid co-aggregation with α -synuclein.^{31, 32} As a consequence, the newly formed p25 α / α -synuclein aggregates are excreted out of the oligodendrocytes and enter surrounding neurons in a prion-like fashion, aiding in the spread of GCI-like inclusions.^{33, 34} Exploiting the co-aggregative nature of α -synuclein and p25 α could lead to the development of a cellular model to evaluate the impact of 20S proteasome enhancement in the prevention of IDP aggregation.

3.2.2 *In Vitro* Evaluation of the Relationship Between p25 α / α -synuclein Aggregates and the 20S Proteasome

Before developing a cellular model that utilized the co-aggregative nature of p25 α and α -synuclein, the relationship between p25 α and the 20S proteasome had to be investigated. It was previously established that p25 α could be degraded through both autophagy and the UPS.^{35, 36, 37} To help elucidate the potential mechanism of proteasome enhancement in the intervention of synucleinopathies, the ability for purified 20S proteasome to degrade p25 α was therefore investigated in the following study. Purified 20S proteasome was suspended in a 120 mM NaCl, 50 mM Tris, and 0.1% β -mercaptoethanol buffer (pH 7.4) to a final concentration of 7.5 nM.³⁸ The proteasome was treated with either DMSO

(vehicle control) or 10 μ M of the following compounds: **36**, **39**, or inactive analog **54**, at 37 $^{\circ}$ C. In parallel, purified p25 α was separately incubated with 100 μ M of DTE at room temperature for 30 minutes. Subsequently, the purified p25 α (final concentration of 500 nM) was added to the proteasome:drug solution for 3 hours. As depicted in **Figure 3.2**, the DMSO-treated 20S proteasome decreased the amount of p25 α drastically. This observation suggested p25 α was indeed a 20S proteasome substrate. In addition, I found that compounds **36** and **39** increased the degradation rate of purified p25 α . Only 29% and 28% of p25 α remained, respectively, as compared to the DMSO treated samples (**Figure 3.2**). The inactive control, **54**, didn't significantly impact the rate of p25 α degradation.

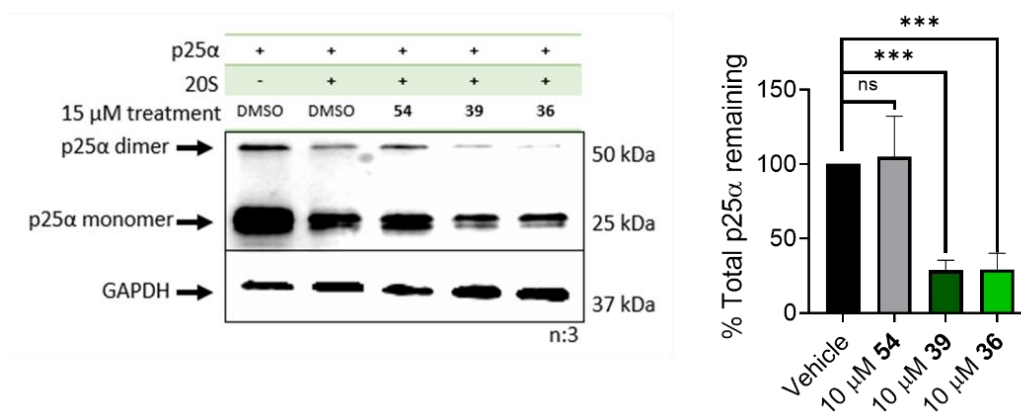


Figure 3.2: p25 α is a substrate of the 20S proteasome.

The degradation of purified p25 α with purified 20S proteasome that was treated with 15 μ M of compounds **36**, **39**, **54**, or DMSO. The assay was done in triplicate. Error bars denote standard deviation. One-way ANOVA statistical analysis was used to determine statistical significance (ns = not significant, * p < 0.05, ** p < 0.01, *** p < 0.001, **** p < 0.0001). Error bars based on standard deviation.

After establishing that p25 α is a 20S proteasome substrate, I moved to study whether the p25 α / α -synuclein interaction can cause weakened proteasome activity. It has been shown that IDP aggregates, such as α -synuclein only aggregates, impair the activity of the proteasome *in vitro*¹⁷ and in cells.³⁹ All samples were prepared in a similar manner; however, a primary incubation was performed for 45 minutes followed by a second incubation for 3-hours, and both occurred at 37 °C. After these incubation times, a covalent Me₄BodipyFL-Ahx₃Leu₃VS fluorescent probe was added, and the samples were further incubated at 37 °C for 15 minutes.⁴⁰ The probe was selected to visualize the activity of the 20S proteasome using a denaturing gel (as shown in **Figure 3.3**). The remaining levels of α -synuclein were then visualized through an immunoblot, and GAPDH was used as a loading control. Due to the low amounts of p25 α used in this study, I could not able to detect any of the remaining levels of p25 α on this gel. The activity of the 20S proteasome in each sample is depicted in **Figure 3.3**. Each lane represents a different combination and order of addition of 20S, PBS, p25 α , and α -synuclein. Lane 1 shows the activity of the 20S proteasome first treated with PBS for 45 minutes, then treated with PBS for the 3-hour incubation and used as the vehicle control. Lane 2 samples were first treated with 700 nM of α -synuclein, followed by adding PBS. The activity displayed by the sample in lane 2 had no significant difference compared to lane 1. The activity of the 20S proteasome in a sample that was first treated with 150 nM of p25 α , followed by the addition of PBS, is shown in lane 3. In this experiment, I saw a noticeable trend of reduced proteasome activity. However, this trend was identified as non-significant after the experiment was triplicated, using the one-way ANOVA statistical analysis (p-value of 0.4693). In lane 4, the 20S proteasome was treated first with 700 nM of α -synuclein,

followed by the addition of 150 nM of p25 α after the first incubation. After the 3-hour incubation, the activity of the 20S proteasome did not significantly differ from that observed in lane 1. Inversely, lane 5 represents the activity of the 20S proteasome when treated first with 150 nM of p25 α , followed by the addition of 700 nM of α -synuclein. The lane 5 samples showed a significant decrease (74%) in proteasome activity. The reduction in activity seen in the lane 5 sample was linked to the decline in α -synuclein degradation, with 197% α -synuclein remaining compared to lane 2 (**Figure 3.3**). In lane 6, 700 nM of α -synuclein and 150 nM of p25 α were added for the first 45-minute incubation, followed by the 20S proteasome and an additional 3-hour incubation. Like lane 5, the sample in lane 6 displayed impaired proteasome activity with a 59% decrease in proteasome activity. The degradation of α -synuclein was also prevented, with 175% α -

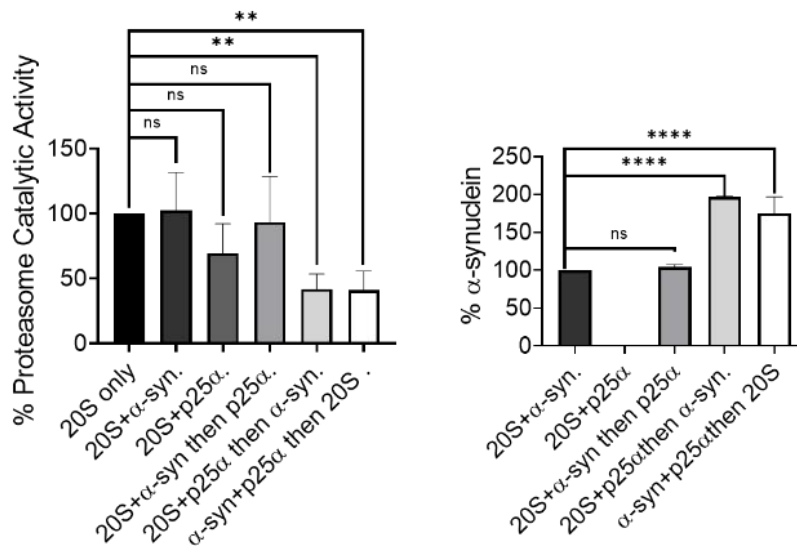
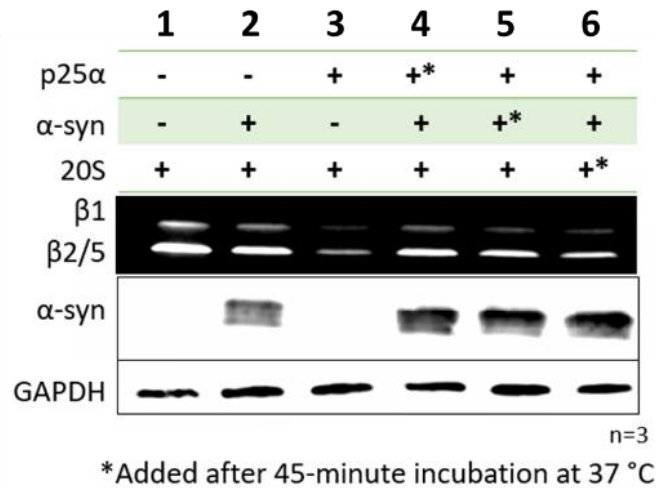


Figure 3.3: p25α/α-synuclein aggregates impair the activity of the proteasome.

Proteasomal impairment by p25α/α-synuclein aggregates, visualized using Me₄BodipyFL-Ahx₃Leu₃VS probe in an SDS-Page gel and levels of α-synuclein using immunoblotting. The assay was done in triplicate. Error bars denote standard deviation. One-way ANOVA statistical analysis was used to determine statistical significance (ns = not significant, *p < 0.05, **p < 0.01, ***p < 0.001, ****p < 0.0001). Error bars based on standard deviation.

synuclein remaining compared to samples treated with α -synuclein and PBS (lane 2) (**Figure 3.3**).

3.2.4 Identification of the Impact of p25 α / α -synuclein Aggregation on Proteasomal Function and Cell Viability

In the next set of studies, I moved to a cellular system to investigate the impact of 20S proteasome enhancement on p25 α levels. It has been reported that proteasome inhibitors, such as BTZ, can impair the clearance of p25 α in cells, implicating the role of the UPS in the degradation of p25 α .²⁹ I transiently transfected HEK-293T cells with a p25 α plasmid for 48 hours before treatment with 10 μ M of **36**, **39**, and **54** for 16 hours. In these studies, I substituted compound **54** for **49** as the inactive control due to the accessibility of compound **54**. Due to findings in previous studies,³¹ I also treated samples with 30 nM of BTZ (**Figure 3.4A**). While there was a slight decrease in p25 α levels in the HEK-293T cells treated with **54**; however, this decrease was identified as non-significant when triplicated. Samples treated with 10 μ M of compound **36** had a 45% reduction of p25 α , which contrasts the much more efficient 20S-mediated degradation of A53T α -synuclein induced by compound **36** (< 1 μ M). The samples treated with proteasome inhibitor, BTZ, displayed a modest 142% increase of p25 α as compared to the DMSO-treated samples (**Figure 3.4A**). When the degradation of p25 α was evaluated in PC12 cells, both compounds **36** and **39** were able to enhance the 20S proteasome-mediated degradation of p25 α at relatively high (10 μ M) concentrations (**Figure 3.4B**). Compound **36** outperformed compound **39** with 40% and 67% p25 α remaining.

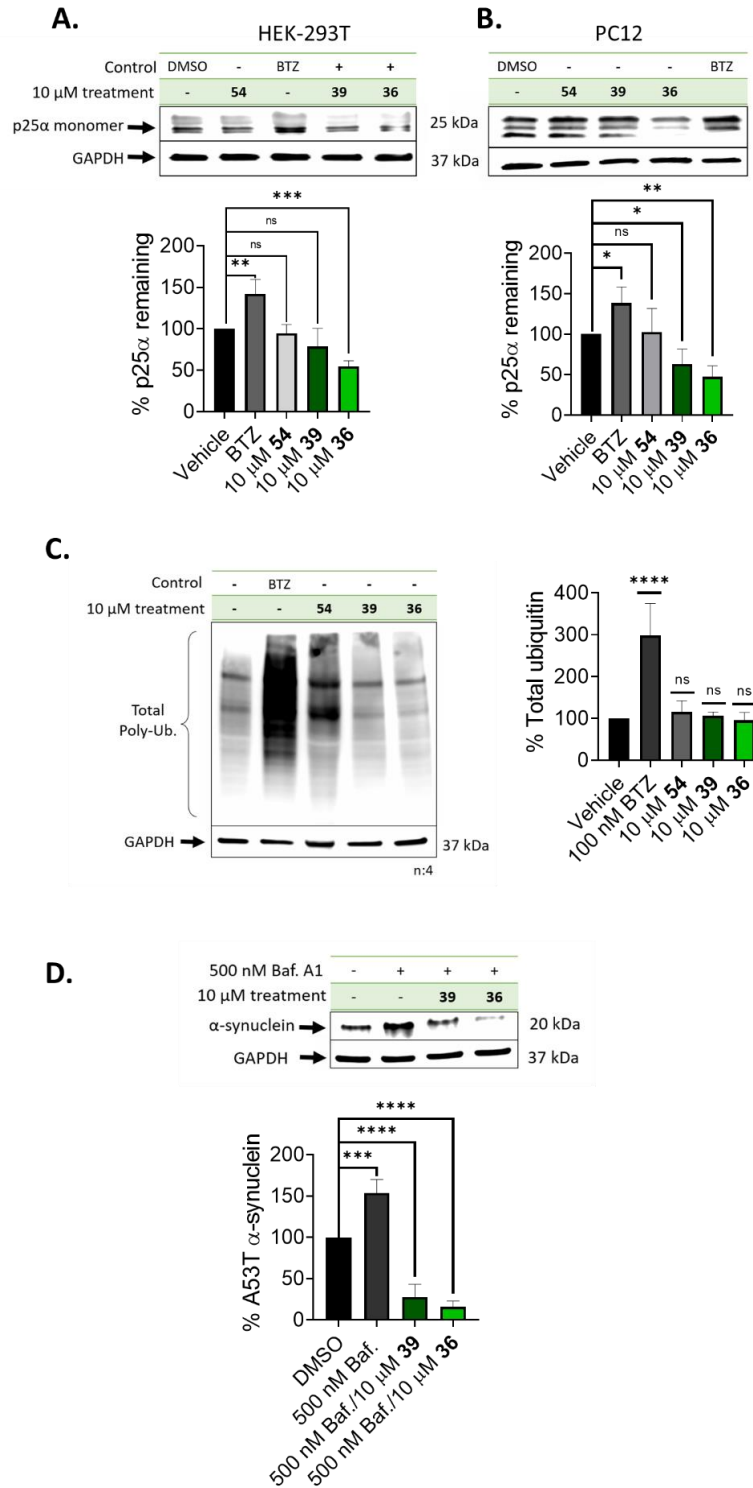


Figure 3.4: Compounds 36 can enhance the degradation of p25 α .

Figure 3.4 (cont'd)

The impact of 10 μ M of compounds 36, 39, and 54 on the 20S proteasome mediated degradation of p25 α in (A) HEK-293T cells and (B) PC12 cells. (C) Levels of A53T α -synuclein in HEK-293T cells that were pre-treated with 500 nM of Bafilomycin A1 and 10 μ M of either compound 36 or 39. (D) Levels of ubiquitin in HEK-293T cells treated with 10 μ M of compounds 36, 39, and 54. The quantification of the target protein remaining was normalized using the GAPDH levels, and compared to a DMSO treated control. Each set of assays were done in triplicate. Error bars denote standard deviation. One-way ANOVA statistical analysis was used to determine statistical significance (ns = not significant, *p < 0.05, **p < 0.01, ***p < 0.001, ****p < 0.0001). Error bars based on standard deviation.

It has been reported that p25 α / α -synuclein aggregates can be degraded through the autophagy pathway.³¹ To validate that compounds **36** and **39** prevent the accumulation of α -synuclein through the UPS, I again transfected HEK-293T cells with the A53T α -synuclein plasmid. Following the 48-hour protein expression period, I treated the cells with 500 nM of an autophagic flux inhibitor, Bafilomycin A1,⁴¹ for 1 hour. After the treatment with Bafilomycin A1, I treated the cells with 10 μ M of **36** and **39** (**Figure 3.4C**). Both compounds enhanced degradation the of A53T α -synuclein (16% and 28% remaining, respectively) despite the pretreatment with Bafilomycin A1, suggesting that the UPS is the main target of modulation for this class of small molecules. I next sought to identify if the modulation of the UPS was specific to the 20S proteasome or if the compounds were impacting the ubiquitin-dependent pathways. I treated unmodified

HEK-293T cells with 10 μ M of **36**, **39**, and **54** and 100 nM of BTZ, and the ubiquitin levels were visualized and quantified using immunoblotting (**Figure 3.4D**). Unsurprisingly, BTZ treated samples had 298% ubiquitin as compared to the vehicle, while **36**, **39**, and **54** didn't impact the levels of ubiquitin significantly, further supporting **36** and **39** as modulating the activity of the ubiquitin-independent pathway.

The co-enrichment of the α -synuclein and p25 α , by adding the purified IDPs directly into the cell culture media, leads to aggregation, mimicking the pathological state.^{31, 42, 43} The pheochromocytoma of the rat adrenal medulla cells, PC12, has been previously used to evaluate the impact of α -synuclein aggregates in cellular systems.^{44, 45} Furthermore, PC12 cells have been identified to take up IDPs from the media,⁴⁶ making them an ideal cell line to observe the impact of extracellular p25 α on cellular α -synuclein. Using PC12 cells transfected with the A53T α -synuclein plasmid, I investigated the effect of 20S proteasome enhancement on p25 α -induced α -synuclein aggregation. I transfected PC12 cells with the A53T mutant plasmid, and the protein was expressed for 48 hours. To investigate whether my small molecules assist in the prevention of p25 α /A53T α -synuclein aggregation, cells were treated with 10 μ M of **36**, **39**, and **54** for 2 hours. Then, I treated the transfected PC12 cells with purified p25 α (final concentration of 160 nM) for an additional 24 hours. PC12 cells that were either not transfected, only expressed A53T α -synuclein, or treated with purified p25 α were used as control samples. The PC12 cells were plated in a black opaque-bottom 96-well plate (10,000 cells/well).

To each well in the 96-well plate, I added 800 nM of the RB1 probe⁴⁷ to evaluate the degree of α -synuclein fibrillization. The change in fluorescence observed is attributed to the degree of aggregation and fibrillization of α -synuclein. PC12 cells that only expressed

A53T α -synuclein showed no significant increase in RB1 fluorescence compared to the unmodified vehicle. In contrast, cells treated with p25 α had a 234% increase in the observed fluorescence (**Figure 3.5A**). The fluorescence observed in the non-transfected cells was attributed to the basal levels of α -synuclein expressed in PC12 cells. However, this increase in α -synuclein fibrillization fluorescence was relatively mild compared to the samples expressing A53T α -synuclein with p25 α treatment, which showed an increase of 512%. When these cells were treated with **36** and **39**, there was a significant reduction in α -synuclein fibrillization with 157% and 173% fluorescent signal remaining, respectively. The inactive analog **54** showed no impact on fibrillization levels.

The degree of fibrillization was then related to proteasomal function by utilizing a luciferase-based assay, Proteasome Glo, to quantify the overall cellular proteasome activity. In contrast to the fibrillization studies, regular cells treated with p25 α didn't display a significant alteration of proteasome activity (**Figure 3.5B**). After treatment with purified p25 α , PC12 cells expressing A53T α -synuclein showed a 42% reduction in proteasome activity. Compounds **36** and **39** restored proteasomal activity to 86% and 70%, respectively. These results were further supported by the levels of A53T α -synuclein and ubiquitin present in each sample (**Figure 3.5C**). Lysed the remaining cells, and the A53T α -synuclein and ubiquitin levels were visualized and quantified via immunoblotting (**Figure 3.5C**). Samples containing both α -synuclein and p25 α displayed 155% of α -synuclein and 148% of ubiquitin as compared to the vehicle sample. Compounds **36** and **39** were again able to reduce the levels of both. Cells treated with **36** and **39** showed

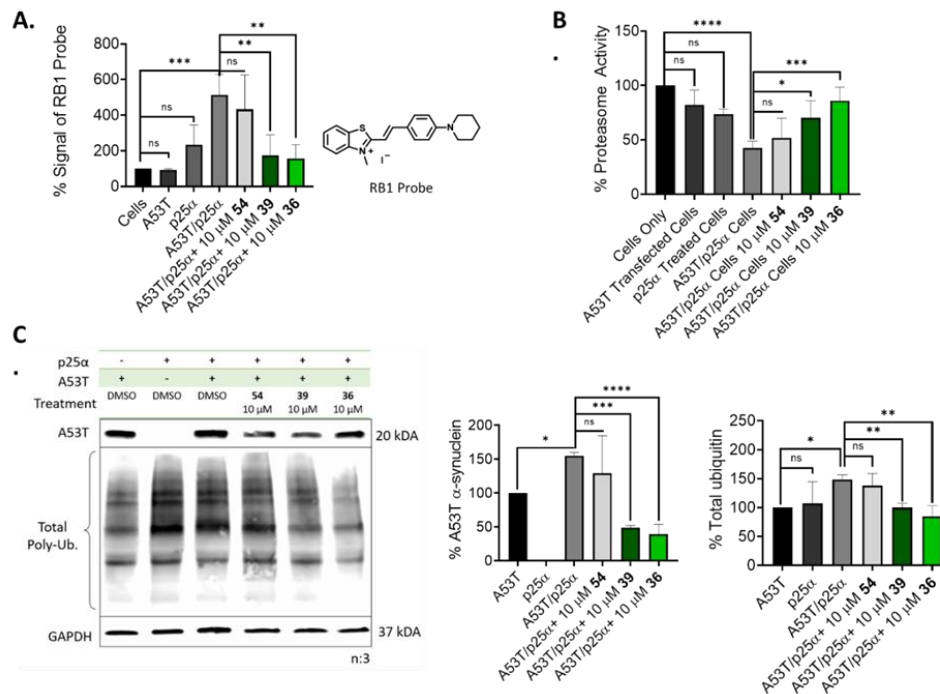


Figure 3.5: Compounds 36 and 39 combat p25 α / α -synuclein aggregates.

(A) The impact of 160 nM of purified p25 α addition on A53T α -synuclein RB1 fibrillization associate fluorescence in PC12 after a two hour incubation with 10 μ M of compounds 36, 39, and 54. (B) The proteasome activity in PC12 cells expressing A53T α -synuclein when cells treated with 10 μ M of compounds 36, 39, and 54 and then 160 nM of purified p25 α , quantified via Proteasome Glo based luminescence. (C) Immunoblots of A53T α -synuclein and ubiquitin in PC12 cells that were treated with 10 μ M of compounds 36, 39, or 54 for two hours before added 160 nM of purified p25 α . The quantification of the target protein remaining was normalized using the GAPDH levels, and compared to a DMSO treated control, in triplicate. Each set of assays were done in triplicate. Error bars denote standard deviation. One-way ANOVA statistical analysis was used to determine statistical significance (ns = not significant, *p < 0.05, **p < 0.01, ***p < 0.001, ****p < 0.0001).

reduced levels of α -synuclein (39% and 48% remaining, respectively) and a restoration in ubiquitin levels (**Figure 3.5C**).

Next, I evaluated the ability of compounds **36** and **39** to prevent p25 α -induced cell death in A53T α -synuclein expressing PC12 cells. PC12 cells were plated in a white 384 well-plate (2,500 cells/well) and then immediately transfected with the A53T α -synuclein plasmid for 24 hours. I treated the cells with 3 μ M of **36**, **39**, and **54**. The cells were also treated once every 24 hours with purified p25 α (160 nM daily concentration) for 72 hours. Cell Titer Glo was used to assess the cell viability. Cells solely expressing A53T α -synuclein had a cell viability of 61%, while cells repeatedly treated with p25 α showed significant cell death (28% cell viability) (**Figure 3.6A**). Only **36** prevented cell death in the PC12 cells, with 72% cell viability, while **39** and **54** could not rescue the cells systematically treated with p25 α (**Figure 3.6A**). The inability **39** to prevent cell death in this system can be related to compound **39**'s moderately enhanced 20S proteasome-mediated degradation of p25 α displayed in HEK-293T and PC12 cells.

With the observed impairment of the proteasome, I explored the cytotoxicity of these p25 α /A53T α -synuclein aggregates. Furthermore, I wanted to evaluate if proteasome enhancers could prevent the observed cytotoxicity. Previous studies have suggested MSA-like aggregates are cytotoxic through co-transfection of α -synuclein and p25 α plasmids.⁴⁸ Using a similar co-transfection protocol, I plated PC12 and HEK-293T cells in a white 384-well plate (2,500 cells/well) and then co-transfected with the two plasmids for 24 hours. I then treated these co-transfected cells with 3 μ M of **36**, **39**, and **54** for 72 hours. The cell viability was then observed using Cell Titer Glo (**Figure 3.6B**). In a second 384-well plate, I examined the overall proteasome activity, utilizing Proteasome Glo

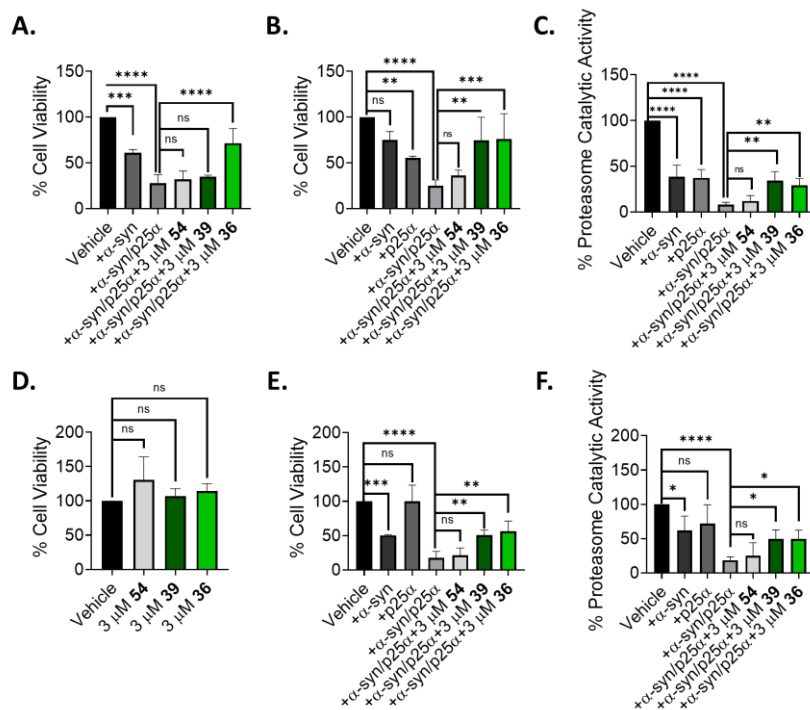


Figure 3.6: Compounds 36 and 39 protect cells from p25 α / α -synuclein aggregates toxicity.

(A) The cell viability of PC12 cells that were transfected with an A53T α -synuclein plasmid for 24 hours before the one-time treatment of 3 μ M of compounds **36**, **39**, and **54** and a daily treatment of 160 nM of purified p25 α for 3 days. (B) The cell viability and (C) proteasome activity of PC12 cells that were co-transfected with a p25 α and an A53T α -synuclein plasmid for 24 hours before treatment with 3 μ M of compounds **36**, **39**, and **54**. (D) The toxicity of the compounds in unmodified PC12 cells. (E) The cell viability and (F) proteasome activity of HEK-293T cells that were co-transfected with a p25 α and an A53T α -synuclein plasmid for 24 hours before treatment with 3 μ M of compounds **36**, **39**, and **54**. Error bars denote standard deviation, in triplicate. One-way ANOVA statistical analysis was used to determine statistical significance (ns = not significant, * $p < 0.05$, ** $p < 0.01$, *** $p < 0.001$, **** $p < 0.0001$).

(**Figure 3.6C**). The co-transfected PC12 cells displayed a 25% cell viability and 8% proteasome activity remaining, which was lower than the vehicle and cells transfected with either plasmid. The co-transfected cells treated with **36** and **39** increased the cell viability to 76% and 75%, respectively (**Figure 3.6B**). The proteasome activity in these samples increased, with **36** displaying 29% activity and **39** showing 34% activity remaining (**Figure 3.6C**). The impact of the compounds alone on un-modified cells is shown in **Figure 3.6D** with no observed cytotoxicity. The cytotoxicity was observed in HEK-293T cells as well; however, it became apparent that HEK-293T cells were much more sensitive to the co-expression of the two proteins with a 17% cell viability remaining, given a significantly reduced plasmid load and treatment time (**Figure 3.6E-3.6F**).

3.3 Proteasomal Impairment Model Through Interruption of 20S Assembly

3.3.1 Rational

As mentioned, the α -synuclein oligomeric species have been identified to impair several critical cellular pathways. Along with the UPS, the α -synuclein oligomers also alter the ER activity regarding protein trafficking,^{49, 50} synaptic vesicle transport,⁵¹ and Ca^{2+} homeostasis.^{52, 53} The ER is one of the biggest organelles in the cell and is a significant site of protein synthesis and folding,⁵⁴ carbohydrate metabolism,⁵⁵ lipids and steroid synthesis,⁵⁶ and calcium storage.⁵⁷ Thus, the disruption of the activity of the ER has devastating consequences.^{58, 59} Often, ER stress leads to the activation of what is known as the unfolded protein response (UPR).^{60, 61} The activation of the UPR is a commonality

seen across the synucleinopathy class of neurodegenerative diseases.^{62, 63, 64} The UPR is a series of complementary adaptive mechanisms that deal with the disruption of protein folding.^{60, 61} The early stages of the UPR are mediated through the activation of three major stress sensors.^{60, 61} The first is the attenuation of protein synthesis through inhibiting the translation of most proteins.⁶⁵ The inhibition of protein translation is achieved through the protein RNA-like ER kinase (PERK) mediated phosphorylation of a translation initiator factor 2 α (eIF2 α).⁶⁵ The second branch is the initiation of mRNA decay, which is regulated by inositol-requiring protein 1 (IRE1) dependent decay (RIDD).⁶⁶⁻⁶⁷ The last is the transformation of the activating transcription factor 6 cytosolic protein (ATF6) to its fragmented version, ATF6f (**Figure 3.7**).^{61, 68} Once these initial signaling pathways are underway, the final responses depend on the duration and intensity of the ER stress.⁶⁴ While the immediate result of activation of the UPR is the inhibition of the translation and folding of most proteins,⁶⁵ there is an upregulation of the expression of proteins that would aid in eliminating the accumulation of unfolded proteins. The expression of proteins involved in the ER-associated degradation (ERAD) machinery is typically upregulated, increasing their expression.^{69, 70} The proteasome is an essential ERAD component responsible for degrading misfolded or unfolded proteins that accumulate in the ER.^{69, 70} Proteasomal impairment has been linked to prolonged activation of the UPR, leading to irreversible ER stress.^{71, 72} Moreover, the long-term activation of the UPR leads to the induction of apoptosis⁷³ and is intertwined with chronic inflammation and numerous human diseases, including neurodegeneration.^{74, 75, 76} Activation of the UPR presents an excellent marker to identify an imbalance of proteostasis in cells, as it is a direct result of the accumulation of misfolded protein in the

ER.⁷⁷ Thus, a cellular model mirroring the activation of the UPR through proteasomal impairment presents a novel method for assessing the effect of enhancing the activity of the 20S proteasome on cellular proteostasis. Currently, the mainstay method of recapitulating impaired proteasome activity that induces UPR activation is through the direct inhibition of the proteasome using small molecules, such as BTZ.^{78, 79} The small molecule proteasome inhibitors are often covalent and bind directly to the catalytic sites, presenting a limitation to their use in models designed to evaluate the activation of the

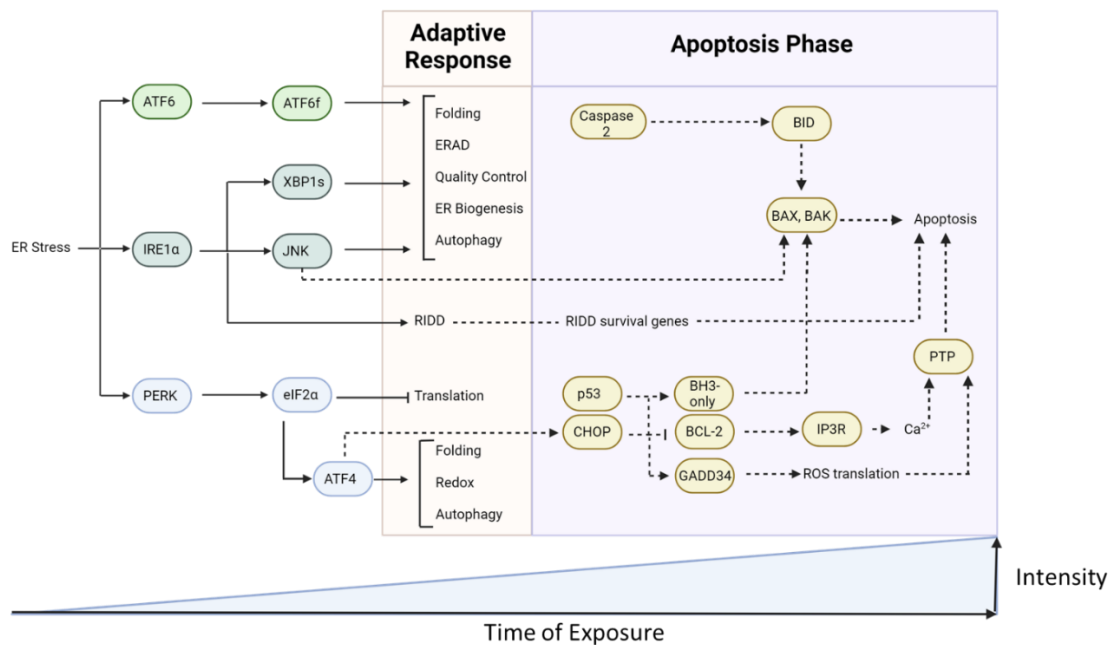


Figure 3.7: A schematic of the signaling cascades of the unfolded protein response and the outcome in relationship to the time and intensity of the ER stress. *Created with BioRender

20S proteasome.⁸⁰ Using siRNA to reduce cellular proteasome levels offers an alternative paradigm to recapitulate activation of the UPR through proteasomal impairment and

mimic the reduced concentration of proteasome seen in MSA and PD. siRNA, also known as silencing RNA, directly interacts with mRNA, causing its degradation and preventing the translation of the intended protein.⁸¹ As mentioned in **Chapter 1**, the assembly of the 20S proteasome is dependent on the formation of the α -ring.^{82, 83, 84, 85} The construction of the α -ring is subject to the stability of the $\alpha 4$ subunit⁸⁶ and the formation of the $\alpha 4$ - $\alpha 5$ - $\alpha 6$ - $\alpha 7$ intermediate.^{87, 88, 89, 90} In addition, $\alpha 4$ can insert into the precursor α -ring in place of $\alpha 3$, creating larger α -ring intermediates.^{91, 92} Thus, I wanted to evaluate siRNA that targets three α -ring subunits and its direct impact on proteasome assembly. Furthermore, the employment of siRNA presents a system to evaluate the impact of 20S proteasome enhancers on short- and long-term activation of the UPR and proteostasis.

3.3.2 Identification of siRNA to Lower Proteasome Abundance and Activity

To efficiently screen different α -subunit siRNA that would diminish proteasome levels and activity, I used the ZsGreen HEK-293T proteasome sensor cell line. The HEK-293T cells stably express ZsGreen, which is a green fluorescent protein, modified through the addition of a PEST region. The PEST region is a sequence of four amino acids, proline (P), glutamic acid (E), serine (S), and threonine (T), that significantly destabilizes proteins, ultimately decreasing the proteins half-life.⁹³ When the proteasome is fully functional, the modified ZsGreen protein will be rapidly degraded, providing a low baseline fluorescence.⁹⁴ However, if the activity of the proteasome is impaired, the ZsGreen protein will accumulate, increasing the cell's fluorescence. I first transfected the ZsGreen HEK-293T cells with siRNA that would silence PSMA7 ($\alpha 4$), PSMA1 ($\alpha 3$), or PSMA4 ($\alpha 6$). In addition, I treated the cells with a known proteasome inhibitor, BTZ, as a control to

visualize the accumulation of the ZsGreen protein in cells. Using a plate imager, the associated fluorescence after 24 hours (**Figure 3.8A**) and 48 hours (**Figure 3.8B**) was measured and quantified. The BTZ control had apparent fluorescence after 24 hours, but none of the siRNA transfected cells showed any marked change in fluorescence. However, after 48 hours, there was a significant increase in fluorescence in the cells transfected with the PSMA7 ($\alpha 4$) siRNA (**Figure 3.8B**), indicating that the silencing of the $\alpha 4$ subunit negatively impacts the activity of the proteasome.

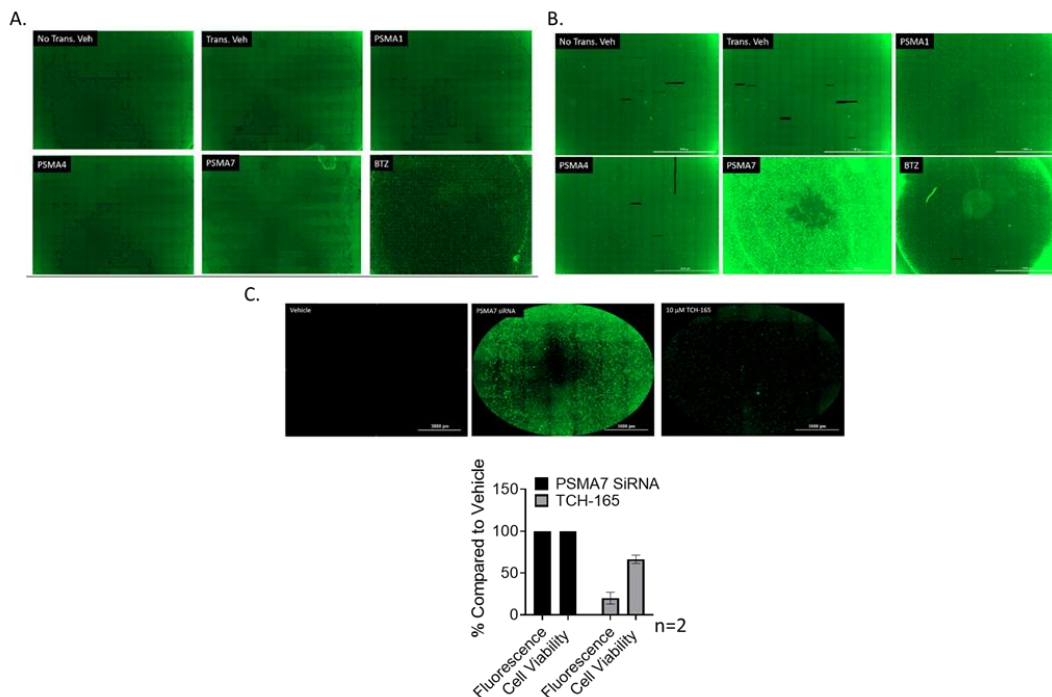


Figure 3.8: PSMA7 siRNA leads to impaired the activity of the proteasome.

Levels of ZsGreen fluorescence in ZsGreen HEK-293T cells transfected with either PSMA7 ($\alpha 4$), PSMA1 ($\alpha 6$), or PSMA4 ($\alpha 3$) siRNA at (A) 24 hours and (B) 48 hours. (C) The fluorescence of ZsGreen HEK-293T cells that were transfected with PSMA7 ($\alpha 4$) siRNA and then treated with either DMSO or 10 μ M of TCH-165. *Note n:2

With the proteasome impairment seen in cells transfected with the PSMA7 (α 4) siRNA, I moved forward with investigating if the 20S proteasome enhancer, TCH-165, could overcome the diminished proteasome levels by enhancing the 20S-mediated degradation of ZsGreen. The HEK-293T cells were transfected again with the PSMA7 (α 4) siRNA, and after 24 hours, I treated the cells with 10 μ M of TCH-165 for an additional 24 hours. In parallel, I also performed a cell viability assay to determine if the decrease in fluorescence was due to proteasome activation or cell death (**Figure 3.8C**). Samples were included that were transfected with the PSMA7 (α 4) siRNA, but then treated with DMSO in place of TCH-165 as the vehicle control and I included cells that were completely unmodified. TCH-165 decreased the fluorescence by 85% compared to the DMSO control and had a 63% cell viability. These results were exciting, demonstrating that proteasome activity can be impaired by silencing the α -subunits and that small molecule 20S proteasome enhancers can compensate for the diminished proteasome concentration. While these results were encouraging, I wanted to ensure that these findings were due to a decreased level of the proteasome and not through a separate mechanism.

The relationship between the increased ZsGreen fluorescence and diminished levels of the proteasome was investigated next. I transfected the ZsGreen HEK-293T cells with the PSMA7 (α 4) siRNA and conducted a weeklong time course to identify the time point with the lowest expression of PSMA7. The first time point was two days due to the fluorescence increase in my previous experiments, followed by four, five, and seven-day time points. I harvested the cells after each time point and lysed them with 20 mM Tris-HCl, 5 mM MgCl₂, 1 mM ATP, 0.5 mM EDTA, and 10% glycerol lysis buffer. Using

immunoblotting, the levels of the $\alpha 3$ subunit and total ubiquitin were quantified. Day four and day five had the lowest concentration of the $\alpha 3$ subunit. Interestingly, there was not a substantial impact on the overall concentration of ubiquitinated proteins (**Figure 3.9**), suggesting that the cells are maintaining proteostasis through alternative pathways. The minimal impact on the levels of ubiquitin may be due to the activation of the autophagy pathway, which can overcompensate when there is prolonged proteasomal dysfunction.^{75, 76} It is important to note that I evaluated the $\alpha 3$ subunit first, to identify the impact that silencing the $\alpha 4$ subunit had on other α -subunits. I did attempt to visualize the $\alpha 4$ subunit as well, however, the antibody we had at the time did not work well. In the future, this experiment should be redone to evaluate several proteasome subunits, particularly the $\alpha 4$ subunit.

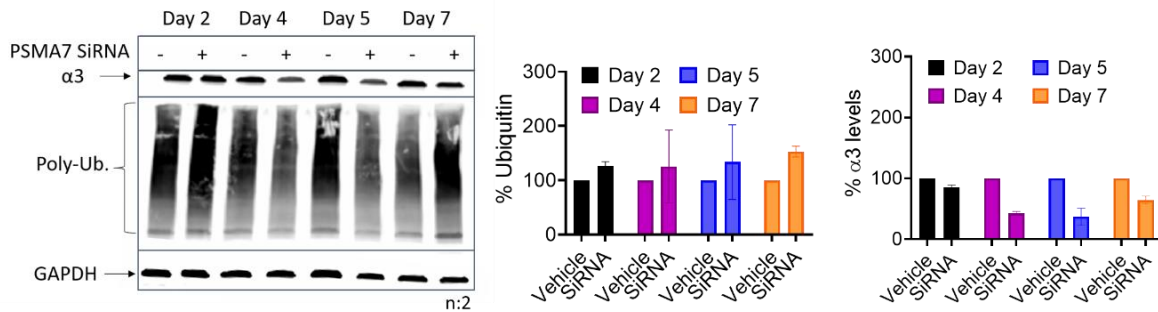


Figure 3.9: PSMA7 siRNA reduced the levels of the $\alpha 3$ subunit and leads to an increase in ubiquitin.

The levels of $\alpha 3$ and total ubiquitin in ZsGreen HEK-293T cells that were transfected with PSMA7 ($\alpha 4$) siRNA for 2, 4, 5, and 7 days as compared to cells that were not transfected. $\alpha 3$ subunit and ubiquitin were visualized using immunoblotting with GAPDH used as the loading control. *Note this is an n:2.

3.3.4 Evaluation of Lowered Proteasome Levels and the Unfolded Protein Response

With the results from the studies conducted with the ZsGreen HEK-293T cells, I was interested in evaluating if lowering proteasome concentrations would activate the UPR. I conducted the following assays with PC12 cells, which are suspension cells. The use of suspension cells is advantageous due to the ability to easily use the same sample of cells for several experiments, allowing for a direct comparison of the data obtained from each study with a high degree of continuity. For example, one could evaluate intact cells' proteasome activity and then directly compare its impact on specific protein levels using cell lysates. Thus, PC12 cells were transfected with the PSMA7 ($\alpha 4$) siRNA for zero, two, four, and six days. After each time point, I plated 15,000 cells/well in a white 384-well plate from the samples and quantified the proteasome activity using Proteasome Glo. The day zero time point acted as the vehicle control. It is important to note that this is preliminary data and only an n of 1 and that these studies must be replicated to identify if the trends are significant. Two days after transfecting the cells with the PSMA7 ($\alpha 4$) siRNA, 93% proteasome activity was observed compared to the zero day time point. However, the four and six day time points displayed 73% and 59% proteasome activity remaining, respectively (**Figure 3.10A**). The PC12 cells were lysed in a non-denaturing buffer (20 nM Tris-HCl, 5 mM MgCl₂, 1 mM ATP, 0.5 mM EDTA, and pH 8), and the cell lysate was first used to evaluate the levels of $\alpha 4$ and proteins ubiquitinated at the K48 position through western blot analysis. The decline in activity was closely mirrored by the levels of $\alpha 4$ remaining visualized through immunoblotting (**Figure 3.10B**). PC12 cells exposed to the PSMA7 ($\alpha 4$) siRNA for two days did not have an observable difference

compared to the zero day time point (**Figure 3.10B**). In contrast, the four and six day time points were observed to have 71% and 49% $\alpha 4$ present, respectively. Interestingly, the increase in K48 ubiquitin was only observed in the four day samples, with a 156% increase of K48 ubiquitinated proteins. Inversely, the six day sample had 80% total ubiquitin compared to the vehicle (**Figure 3.10B**). This trend could be associated with the synergetic relationship between the autophagy pathway and the UPS if reproducible. It has been identified that the autophagy pathway can compensate for the loss of proteasome activity.^{95, 96} Further studies should be conducted to evaluate if the activity of the autophagy pathway is enhanced during long periods of diminished proteasome levels.

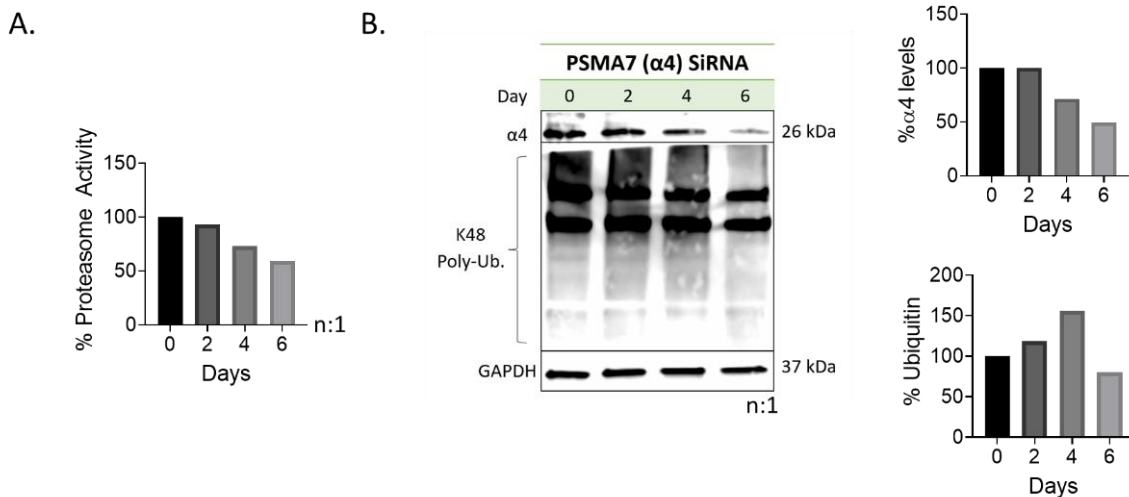


Figure 3.10: Silencing of the $\alpha 4$ subunit with siRNA leads to decreased proteasome activity.

(A) The activity of the proteasome and (B) $\alpha 4$ and total ubiquitin levels in PC12 cells that were transfected with PSMA7 ($\alpha 4$) siRNA for 0, 2, 4, and 6 days. GAPDH was used as the loading control. *Note n:1.

Next, I evaluated the level of unfolded proteins in PC12 cells that were exposed to the PSMA7 (α 4) siRNA. An increase in the mis and unfolded protein levels would indicate perturbed proteostasis and could be a marker for UPR activation. Typically, cysteine residues are protected through protein folding, preventing aberrant oxidation of cysteine residues exposed to the solvent.⁹⁷ However, in the case of the UPR activation, mis- or unfolded proteins accumulate, often exposing a free and reactive cysteine residue.⁹⁸ The TPE-MI probe can react with the exposed cysteine residues, and the conjugation enables a fluorescent emission, allowing for the relatively easy quantification of mis- and unfolded proteins in cell samples.⁹⁸ I hypothesized that the concentration of unfolded proteins would increase with the impaired activity of the proteasome (caused by reduced proteasome levels rather than direct inhibition). I tested my hypothesis by first transfecting PC12 cells with the PSMA7 (α 4) siRNA for five days. I included samples of unmodified PC12 cells, which were treated with 100 nM of 4 μ 8C, 2.5 μ M of Eeyarestatin I, or DMSO for 24 hours. The IRE α RNase inhibitor, 4 μ 8C, can partially inhibit the induction of the UPR through the inhibition of the most conserved UPR sensor, the IRE α branch,^{99, 100} The second molecule that was included as a control was an ERAD inhibitor, Eeyarestatin I.⁷⁹ While Eeyarestatin I is not a direct proteasome inhibitor, it does impair the activity of the ERAD, leading to the activation of the UPR.¹⁰¹ The samples treated with DMSO acted as the vehicle control.

After the treatment and transfection period, I plated 10,000 cells/well in 99 μ L of media in a black 96-well plate and added 1 μ L of TPE-MI in PBS (final concentration of 50 μ M). The cells and TPE-MI were incubated for 30 minutes at 37 °C before evaluating the fluorescent emission using a plate reader. The cells transfected with PSMA7 (α 4) siRNA

had a 297% increase in the unfolded protein-associated fluorescence compared to the vehicle control. The results of the two control compounds were as expected; there was a minor increase in fluorescence in the samples treated with 4 μ 8C (137%). In comparison, there was a 589% increase in cells treated with Eeyarestatin I (**Figure 3.11A**). The increase in the levels of unfolded proteins in the cells was then compared to the level and activity of the proteasome through immunoblotting. The PC12 cells were lysed using the non-denaturing lysis buffer, and the levels of α 4 and K48 ubiquitinated proteins were visualized through immunoblotting (**Figure 3.11B**). In agreement with my previous studies, cells transfected with the PSMA7 (α 4) siRNA for four days had 44% α 4 compared to the untreated and unmodified vehicle control. In addition, PSMA7 (α 4) siRNA transfected samples had a 186% increase in K48 ubiquitin. Interestingly, both the samples treated with 4 μ 8C and Eeyarestatin I slightly decreased the levels of α 4, with 79% and 87% compared to the vehicle control, respectively (**Figure 3.11B**). However, this trend may not be significant once replicated. Furthermore, the samples treated with 4 μ 8C showed a 48% decrease in the ubiquitin levels while samples treated with Eeyarestatin I displayed a 363% increase in ubiquitin (**Figure 3.11B**). The results from the sample treated with Eeyarestatin I was unsurprising due to the ubiquitin-dependent degradation that the ERAD of misfolded proteins conducts from the ER.¹⁰²

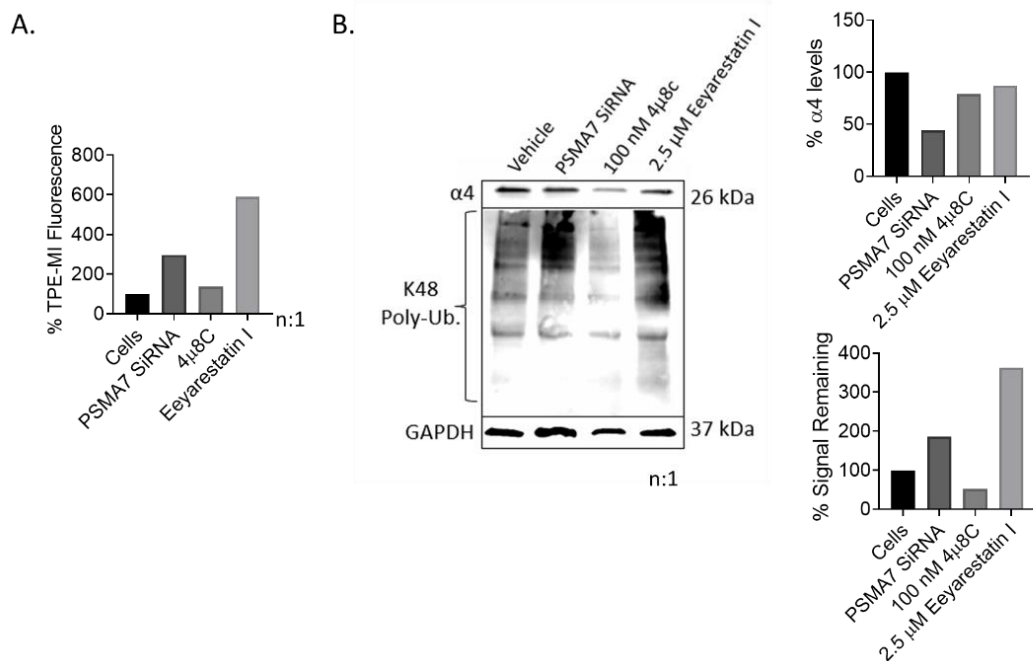


Figure 3.11: Silencing of PSMA7 (α 4) leads to increased levels of misfolded proteins.

(A) The level of unfolded associated fluorescence of the TPE-MI probe in PC12 cells that were transfected with PSMA7 siRNA or treated with 100 nM of 4 μ 8C or 2.5 μ M of Eeyarestatin I. (B) The levels of α 4 and ubiquitin in PC12 cells that were transfected with PSMA7 siRNA or treated with 100 nM of 4 μ 8C or 2.5 μ M of Eeyarestatin. GAPDH was used as the loading control. *Note n:1.

3.3.5 Future Work

While this project's preliminary data looks promising, several studies must be conducted to finish this story. The results must be replicated to ensure that the trends are significant and reproducible. Ideally, an inducible PSMA7 (α 4) siRNA cell line would be created to eliminate transfection-associated toxicity and allow for constant reduction of the α 4 subunit. This system would be great for evaluating the long-term induction of the UPR

and associated apoptosis. Furthermore, the activation of the three main UPR branches should be evaluated using immunoblotting. Once this model is firmly established, the impact of 20S proteasome enhancers on the activation and chronic induction of the UPR could be investigated. The TPE-MI probe could screen small molecules to reduce mis- and unfolded proteins within the system. Then, the levels of UPR markers could be evaluated using immunoblotting or ELISA.

3.4 Conclusion

A defining feature of the heterogeneous class of synucleinopathies is the formation of α -synuclein aggregates. However, other characteristics are standard in this class of neurodegenerative diseases, such as the diminished levels of proteasome subunits¹² and the activation of the UPR through ER stress.^{62, 63, 64} In developing therapeutics to treat complex neurodegenerative diseases, the ability to alleviate several cellular dysfunctions is needed. Thus, cellular models that recapitulate these cellular dysfunctions must be designed to identify the therapeutic potential of 20S proteasome enhancers. Using the co-aggregative nature of α -synuclein and p25 α , I developed a cellular model that recapitulated MSA-like aggregation and proteasomal impairment. With the addition of 20S proteasome enhancers, the aggregation between α -synuclein and p25 α can be disrupted, thus restoring proteasome activity, and preventing the associated cytotoxicity. Furthermore, using siRNA to reduce the levels of proteasome within the cell shows promise in developing a cellular model that mirrors the chronic activation of the UPR through constant stress to the ER. While this model is still in development, these two cellular models could be used to thoroughly evaluate the potential of 20S proteasome enhancement for treating neurodegenerative diseases such as MSA and PD.

REFERENCES

- (1) Koga, S.; Sekiya, H.; Kondru, N.; Ross, O. A.; Dickson, D. W. Neuropathology and molecular diagnosis of Synucleinopathies. *Mol. Neurodegener.* **2021**, *16*, 83-107.
- (2) Calabresi, P.; Mechelli, A.; Natale, G.; Volpicelli-Daley, L.; Di Lazzaro, G.; Ghiglieri, V. Alpha-synuclein in Parkinson's disease and other synucleinopathies: From overt neurodegeneration back to early synaptic dysfunction. *Cell Death Dis.* **2023**, *14*, 176-192.
- (3) Iwai, A. M., E.; Yoshimoto, M.; Ge, N.; Flanagan, L.; de Silva, H. A.; Kittel, A.; Saitoh, T. The precursor protein of non-A beta component of Alzheimer's disease amyloid is a presynaptic protein of the central nervous system. *Neuron* **1995**, 467-475.
- (4) Bendor, J. T.; Logan, T. P.; Edwards, R. H. The function of alpha-synuclein. *Neuron* **2013**, *79* (6), 1044-1087.
- (5) Bras, I. C.; Outeiro, T. F. Alpha-synuclein: Mechanisms of release and pathology progression in synucleinopathies. *Cells* **2021**, *10*, 375-394.
- (6) Lehtonen, S.; Sonninen, T. M.; Wojciechowski, S.; Goldsteins, G.; Koistinaho, J. Dysfunction of cellular proteostasis in Parkinson's Disease. *Front. Neurosci.* **2019**, *13*, 457-476.
- (7) Burmann, B. M.; Gerez, J. A.; Matecko-Burmann, I.; Campioni, S.; Kumari, P.; Ghosh, D.; Mazur, A.; Aspholm, E. E.; Sulskis, D.; Wawrzyński, M.; et al. Regulation of alpha-synuclein by chaperones in mammalian cells. *Nature* **2020**, *577* (7788), 127-132.
- (8) Tofaris, G. K. Initiation and progression of alpha-synuclein pathology in Parkinson's disease. *Cell Mol. Life Sci.* **2022**, *79* (4), 210-221.
- (9) Bobela, W.; Aebischer, P.; Schneider, B. L. Alpha-synuclein as a mediator in the interplay between aging and Parkinson's disease. *Biomolecules* **2015**, 2675-2700.
- (10) Prusiner, S. B.; Woerman, A. L.; Mordes, D. A.; Watts, J. C.; Rampersaud, R.; Berry, D. B.; Patel, S.; Oehler, A.; Lowe, J. K.; Kravitz, S. N.; et al. Evidence for alpha-synuclein prions causing multiple system atrophy in humans with parkinsonism. *Proc. Natl. Acad. Sci. U.S.A.* **2015**, 112-122.
- (11) Lee, H. J.; Ricarte, D.; Ortiz, D.; Lee, S. J. Models of multiple system atrophy. *Exp. Mol. Med.* **2019**, *51*, 1-10.
- (12) Bukhatwa, S.; Zeng, B. Y.; Rose, S.; Jenner, P. A comparison of changes in proteasomal subunit expression in the substantia nigra in Parkinson's disease, multiple system atrophy and progressive supranuclear palsy. *Brain Res.* **2010**, *1326*, 174-185.

- (13) Spillantini, M. G.; Schmidt, M. L.; Lee, V. M. Y.; Trojanowski, J. Q.; Jakes, R.; Goedert, M. α -Synuclein in Lewy bodies. *Nature* **1997**, *388*, 839-840.
- (14) Fares, M. B.; Jagannath, S.; Lashuel, H. A. Reverse engineering Lewy bodies: how far have we come and how far can we go? *Nat. Rev. Neurosci.* **2021**, *22*, 111-131.
- (15) Fouka, M.; Mavroeydi, P.; Tsaka, G.; Xilouri, M. In search of effective treatments targeting α -synuclein toxicity in synucleinopathies: pros and cons. *Front. Cell Dev. Biol.* **2020**, *8*, 559791-559823.
- (16) Heras-Garvin, A.; Stefanova, N. MSA: From basic mechanisms to experimental therapeutics. *Parkinsonism Relat. Disord.* **2020**, *73*, 94-104.
- (17) Thibaut, T. A.; Anderson, R. T.; Smith, D. M. A common mechanism of proteasome impairment by neurodegenerative disease-associated oligomers. *Nat. Commun.* **2018**, *9*, 1097-1111.
- (18) McKinnon, C.; De Snoo, M. L.; Gondard, E.; Neudorfer, C.; Chau, H.; Ngana, S. G.; O'Hara, D. M.; Brotchie, J. M.; Koprach, J. B.; Lozano, A. M.; et al. Early-onset impairment of the ubiquitin-proteasome system in dopaminergic neurons caused by α -synuclein. *Acta Neuropathol. Commun.* **2020**, *8* (1), 17-33.
- (19) Dantuma, N. P.; Bott, L. C. The ubiquitin-proteasome system in neurodegenerative diseases: Precipitating factor, yet part of the solution. *Front. Mol. Neurosci.* **2014**, *7*, 70-88.
- (20) Volpicelli-Daley, L. A.; Luk, K. C.; Patel, T. P.; Tanik, S. A.; Riddle, D. M.; Stieber, A.; Meaney, D. F.; Trojanowski, J. Q.; Lee, V. M. Exogenous α -synuclein fibrils induce Lewy body pathology leading to synaptic dysfunction and neuron death. *Neuron* **2011**, *72* (1), 57-71.
- (21) Tanik, S. A.; Schultheiss, C. E.; Volpicelli-Daley, L. A.; Brunden, K. R.; Lee, V. M. Lewy body-like α -synuclein aggregates resist degradation and impair macroautophagy. *J. Biol. Chem.* **2013**, *288* (21), 15194-15210.
- (22) Schweighauser, M.; Shi, Y.; Tarutani, A.; Kametani, F.; Murzin, A. G.; Ghetti, B.; Matsubara, T.; Tomita, T.; Ando, T.; Hasegawa, K.; et al. Structures of α -synuclein filaments from multiple system atrophy. *Nature* **2020**, *585*, 464-469.
- (23) Van der Perren, A.; Gelders, G.; Fenyi, A.; Bousset, L.; Brito, F.; Peelaerts, W.; Van den Haute, C.; Gentleman, S.; Melki, R.; Baekelandt, V. The structural differences between patient-derived α -synuclein strains dictate characteristics of Parkinson's disease, multiple system atrophy and dementia with Lewy bodies. *Acta Neuropathol.* **2020**, *139*, 977-1000.

- (24) Shahnawaz, M.; Mukherjee, A.; Pritzkow, S.; Mendez, N.; Rabadia, P.; Liu, X.; Hu, B.; Schmeichel, A.; Singer, W.; Wu, G.; et al. Discriminating alpha-synuclein strains in Parkinson's disease and multiple system atrophy. *Nature* **2020**, *578*, 273-277.
- (25) Ferreira, N.; Gram, H.; Sorrentino, Z. A.; Gregersen, E.; Schmidt, S. I.; Reimer, L.; Betzer, C.; Perez-Gozalbo, C.; Beltoja, M.; Nagaraj, M.; et al. Multiple system atrophy-associated oligodendroglial protein p25alpha stimulates formation of novel alpha-synuclein strain with enhanced neurodegenerative potential. *Acta Neuropathol.* **2021**, *142*, 87-115.
- (26) Stefanova, N. A mouse model of Multiple System Atrophy: Bench to bedside. *Neurother.* **2023**, *20*, 117-126.
- (27) Mavroeydi, P.; Arvanitaki, F.; Karakitsou, A. K.; Vetsi, M.; Kloukina, I.; Zweckstetter, M.; Giller, K.; Becker, S.; Sorrentino, Z. A.; Giasson, B. I.; et al. Endogenous oligodendroglial alpha-synuclein and TPPP/p25alpha orchestrate alpha-synuclein pathology in experimental multiple system atrophy models. *Acta Neuropathol.* **2019**, *138*, 415-441.
- (28) Olah, J.; Ovadi, J. Dual life of TPPP/p25 evolved in physiological and pathological conditions. *Biochem. Soc. Trans.* **2014**, *42*, 1762-1767.
- (29) Ota, K.; Obayashi, M.; Ozaki, K.; Ichinose, S.; Kakita, A.; Tada, M.; Takashi, H.; Ando, N.; Eishi, Y.; Mizusawa, H.; et al. Relocation of p25 α /tubulin polymerization promoting protein from the nucleus to the perinuclear cytoplasm in the oligodendroglia of sporadic and COQ2 mutant multiple system atrophy. *Acta Neuropathol. Commun.* **2014**, *2*, 136-155.
- (30) Ota, K.; Obayashi, M.; Ozaki, K.; Ichinose, S.; Kakita, A.; Tada, M.; Takashi, H.; Ando, N.; Eishi, Y.; Mizusawa, H.; et al. Relocation of p25 α /tubulin polymerization promoting protein from the nucleus to the perinuclear cytoplasm in the oligodendroglia of sporadic and COQ2 mutant multiple system atrophy. *Acta Neuropathol. Commun.* **2014**, *136*.
- (31) Lehotzky, A.; Olah, J.; Fekete, J. T.; Szenasi, T.; Szabo, E.; Gyorffy, B.; Varady, G.; Ovadi, J. Co-transmission of alpha-synuclein and TPPP/p25 inhibits their proteolytic degradation in human cell models. *Front. Mol. Biosci.* **2021**, *8*, 666026-666041.
- (32) Wong, J. H.; Halliday, G. M.; Kim, W. S. Exploring myelin dysfunction in multiple system atrophy. *Exp. Neurol.* **2014**, *23*, 337-344.
- (33) Krejciova, Z.; Carlson, G. A.; Giles, K.; Prusiner, S. B. Replication of multiple system atrophy prions in primary astrocyte cultures from transgenic mice expressing human alpha-synuclein. *Acta Neuropathol. Commun.* **2019**, *7*, 81-100.

- (34) Watts, J. C.; Giles, K.; Oehler, A.; Middleton, L.; Dexter, D. T.; Gentleman, S. M.; DeArmond, S. J.; Prusiner, S. B. Transmission of multiple system atrophy prions to transgenic mice. *Proc. Natl. Acad. Sci. U.S.A.* **2013**, *110*, 19555-19560.
- (35) Goldbaum, O.; Jensen, P. H.; Richter-Landsberg, C. The expression of tubulin polymerization promoting protein TPPP/p25alpha is developmentally regulated in cultured rat brain oligodendrocytes and affected by proteolytic stress. *Glia* **2008**, *56* (16), 1736-1746.
- (36) Olah, J.; Szenasi, T.; Szunyogh, S.; Szabo, A.; Lehotzky, A.; Ovadi, J. Further evidence for microtubule-independent dimerization of TPPP/p25. *Sci. Rep.* **2017**, *7*, 40594-40602.
- (37) Mavroepidi, P.; Arvanitaki, F.; Vetsi, M.; Becker, S.; Vlachakis, D.; Jensen, P. H.; Stefanis, L.; Xilouri, M. Autophagy mediates the clearance of oligodendroglial SNCA/alpha-synuclein and TPPP/p25A in multiple system atrophy models. *Autophagy* **2022**, *18* (9), 2104-2133.
- (38) Lindersson, E.; Lundvig, D.; Petersen, C.; Madsen, P.; Nyengaard, J. R.; Hojrup, P.; Moos, T.; Otzen, D.; Gai, W. P.; Blumbergs, P. C.; et al. p25alpha Stimulates alpha-synuclein aggregation and is co-localized with aggregated alpha-synuclein in alpha-synucleinopathies. *J. Biol. Chem.* **2005**, *280* (7), 5703-5715.
- (39) Vanecek, A. S.; Mojsilovic-Petrovic, J.; Kalb, R. G.; Tepe, J. J. Enhanced Degradation of Mutant C9ORF72-Derived Toxic Dipeptide Repeat Proteins by 20S Proteasome Activation Results in Restoration of Proteostasis and Neuroprotection. *ACS Chem. Neurosci.* **2023**, *14* (8), 1493-1448.
- (40) Leestemaker, Y.; de Jong, A.; Witting, K. F.; Penning, R.; Schuurman, K.; Rodenko, B.; Zaal, E. A.; van de Kooij, B.; Laufer, S.; Heck, A. J. R.; et al. Proteasome activation by small molecules. *Cell Chem. Biol.* **2017**, *24* (6), 725-736.
- (41) Mauvezin, C.; Neufeld, T. P. Bafilomycin A1 disrupts autophagic flux by inhibiting both V-ATPase-dependent acidification and Ca-P60A/SERCA-dependent autophagosome-lysosome fusion. *Autophagy* **2015**, *11* (8), 1437-1438.
- (42) Szenasi, T.; Olah, J.; Szabo, A.; Szunyogh, S.; Lang, A.; Perczel, A.; Lehotzky, A.; Uversky, V. N.; Ovadi, J. Challenging drug target for Parkinson's disease: Pathological complex of the chameleon TPPP/p25 and alpha-synuclein proteins. *Biochim. Biophys. Acta Mol. Basis Dis.* **2017**, *1863* (1), 310-323.
- (43) Lehotzky, A.; Tirian, L.; Tokesi, N.; Lenart, P.; Szabo, B.; Kovacs, J.; Ovadi, J. Dynamic targeting of microtubules by TPPP/p25 affects cell survival. *J. Cell Sci.* **2004**, *117*, 6249-6259.

- (44) Heravi, M.; Dargahi, L.; Parsafar, S.; Tayaranian Marvian, A.; Aliakbari, F.; Morshedi, D. The primary neuronal cells are more resistant than PC12 cells to alpha-synuclein toxic aggregates. *Neurosci. Lett.* **2019**, *701*, 38-47.
- (45) Ejlerskov, P.; Rasmussen, I.; Nielsen, T. T.; Bergstrom, A. L.; Tohyama, Y.; Jensen, P. H.; Vilhardt, F. Tubulin polymerization-promoting protein (TPPP/p25alpha) promotes unconventional secretion of alpha-synuclein through exophagy by impairing autophagosome-lysosome fusion. *J. Biol. Chem.* **2013**, *288* (24), 17313-17315.
- (46) Gassowska, M.; Czapski, G. A.; Pajak, B.; Cieslik, M.; Lenkiewicz, A. M.; Adamczyk, A. Extracellular alpha-synuclein leads to microtubule destabilization via GSK-3beta-dependent Tau phosphorylation in PC12 cells. *PLoS One* **2014**, *9* (4), 94259-94270.
- (47) Gaur, P.; Galkin, M.; Kurochka, A.; Ghosh, S.; Yushchenko, D. A.; Shvadchak, V. V. Fluorescent Probe for Selective Imaging of alpha-Synuclein Fibrils in Living Cells. *ACS Chem. Neurosci.* **2021**, *12* (8), 1293-1298.
- (48) Hasegawa, T.; Baba, T.; Kobayashi, M.; Konno, M.; Sugeno, N.; Kikuchi, A.; Itoyama, Y.; Takeda, A. Role of TPPP/p25 on alpha-synuclein-mediated oligodendroglial degeneration and the protective effect of SIRT2 inhibition in a cellular model of multiple system atrophy. *Neurochem. Int.* **2010**, *57* (8), 857-866.
- (49) Cooper, A. A.; Gitler, A. D.; Cashikar, A.; Haynes, C. M.; Hill, K. J.; Bhullar, B.; Liu, K.; Xu, K.; Strathearn, K. E.; Liu, F.; et al. Alpha-synuclein blocks ER-Golgi traffic and Rab1 rescues neuron loss in Parkinson's models. *Science* **2006**, *313* (5785), 324-328.
- (50) Mazzulli, J. R.; Zunke, F.; Isacson, O.; Studer, L.; Krainc, D. alpha-Synuclein-induced lysosomal dysfunction occurs through disruptions in protein trafficking in human midbrain synucleinopathy models. *Proc. Natl. Acad. Sci. U S A* **2016**, *113* (7), 1931-1936.
- (51) Nemani, V. M.; Lu, W.; Berge, V.; Nakamura, K.; Onoa, B.; Lee, M. K.; Chaudhry, F. A.; Nicoll, R. A.; Edwards, R. H. Increased expression of alpha-synuclein reduces neurotransmitter release by inhibiting synaptic vesicle reclustering after endocytosis. *Neuron* **2010**, *65* (1), 66-79.
- (52) Selvaraj, S.; Sun, Y.; Watt, J. A.; Wang, S.; Lei, S.; Birnbaumer, L.; Singh, B. B. Neurotoxin-induced ER stress in mouse dopaminergic neurons involves downregulation of TRPC1 and inhibition of AKT/mTOR signaling. *J. Clin. Invest.* **2012**, *122* (4), 1354-1367.
- (53) Belal, C.; Ameli, N. J.; El Kommos, A.; Bezalel, S.; Al'Khafaji, A. M.; Mughal, M. R.; Mattson, M. P.; Kyriazis, G. A.; Tyrberg, B.; Chan, S. L. The homocysteine-inducible endoplasmic reticulum (ER) stress protein Herp counteracts mutant alpha-synuclein-induced ER stress via the homeostatic regulation of ER-resident calcium release channel proteins. *Hum. Mol. Genet.* **2012**, *21* (5), 963-977.

- (54) Wang, M.; Kaufman, R. J. Protein misfolding in the endoplasmic reticulum as a conduit to human disease. *Nature* **2016**, *529* (7586), 326-335.
- (55) Hebert, D. N.; Garman, S. C.; Molinari, M. The glycan code of the endoplasmic reticulum: asparagine-linked carbohydrates as protein maturation and quality-control tags. *Trends Cell Biol.* **2005**, *15* (7), 364-370.
- (56) Fagone, P.; Jackowski, S. Membrane phospholipid synthesis and endoplasmic reticulum function. *J. Lipid Res.* **2009**, *50*, 311-316.
- (57) Clapham, D. E. Calcium signaling. *Cell* **2007**, *131* (6), 1047-1058.
- (58) Rao, R. V.; Ellerby, H. M.; Bredesen, D. E. Coupling endoplasmic reticulum stress to the cell death program. *Cell Death Differ.* **2004**, *11* (4), 372-380.
- (59) McGrath, E. P.; Centonze, F. G.; Chevet, E.; Avril, T.; Lafont, E. Death sentence: The tale of a fallen endoplasmic reticulum. *Biochim. Biophys. Acta Mol. Cell Res.* **2021**, *1868* (6), 119001-119009.
- (60) Ron, D.; Walter, P. Signal integration in the endoplasmic reticulum unfolded protein response. *Nat. Rev. Mol. Cell Biol.* **2007**, *8* (7), 519-529.
- (61) Hetz, C. The unfolded protein response: controlling cell fate decisions under ER stress and beyond. *Nat. Rev. Mol. Cell Biol.* **2012**, *13* (2), 89-102.
- (62) Martinez, A.; Lopez, N.; Gonzalez, C.; Hetz, C. Targeting of the unfolded protein response (UPR) as therapy for Parkinson's disease. *Biol. Cell.* **2019**, *111* (6), 161-168.
- (63) Makioka, K.; Yamazaki, T.; Fujita, Y.; Takatama, M.; Nakazato, Y.; Okamoto, K. Involvement of endoplasmic reticulum stress defined by activated unfolded protein response in multiple system atrophy. *J. Neurol. Sci.* **2010**, *297*, 60-65.
- (64) Hoozemans, J. J.; van Haastert, E. S.; Eikelenboom, P.; de Vos, R. A.; Rozemuller, J. M.; Scheper, W. Activation of the unfolded protein response in Parkinson's disease. *Biochem. Biophys. Res. Commun.* **2007**, *354* (3), 707-711.
- (65) Harding, H. P. N., I.; Zhang, Y.; Zeng, H.; Wek, R.; Schapira, M.; Ron, D. Regulated translation initiation controls stress-induced gene expression in mammalian cells. *Mol. Cell* **2000**, *6* (5), 1099-1108.
- (66) Han, D.; Lerner, A. G.; Vande Walle, L.; Upton, J. P.; Xu, W.; Hagen, A.; Backes, B. J.; Oakes, S. A.; Papa, F. R. IRE1 α kinase activation modes control alternate endoribonuclease outputs to determine divergent cell fates. *Cell* **2009**, *138* (3), 562-575.

- (67) Hollien, J.; Lin, J. H.; Li, H.; Stevens, N.; Walter, P.; Weissman, J. S. Regulated Ire1-dependent decay of messenger RNAs in mammalian cells. *J. Cell Biol.* **2009**, *186* (3), 323-331.
- (68) Ameri, K.; Harris, A. L. Activating transcription factor 4. *Int. J. Biochem. Cell Biol.* **2008**, *40* (1), 14-21.
- (69) Hoseki, J.; Ushioda, R.; Nagata, K. Mechanism and components of endoplasmic reticulum-associated degradation. *J. Biochem.* **2010**, *147* (1), 19-25.
- (70) Nunziante, M.; Ackermann, K.; Dietrich, K.; Wolf, H.; Gadtke, L.; Gilch, S.; Vorberg, I.; Groschup, M.; Schatzl, H. M. Proteasomal dysfunction and endoplasmic reticulum stress enhance trafficking of prion protein aggregates through the secretory pathway and increase accumulation of pathologic prion protein. *J. Biol. Chem.* **2011**, *286* (39), 33942-33953.
- (71) Lee, R. J.; Liu, C. W.; Harty, C.; McCracken, A. A.; Latterich, M.; Romisch, K.; DeMartino, G. N.; Thomas, P. J.; Brodsky, J. L. Uncoupling retro-translocation and degradation in the ER-associated degradation of a soluble protein. *EMBO J* **2004**, *23* (11), 2206-2215.
- (72) Hwang, J.; Qi, L. Quality control in the endoplasmic reticulum: Crosstalk between ERAD and UPR pathways. *Trends Biochem. Sci.* **2018**, *43* (8), 593-605.
- (73) Fribley, A.; Zhang, K.; Kaufman, R. J. Regulation of apoptosis by the unfolded protein response. *Methods Mol. Biol.* **2009**, *559*, 191-204.
- (74) Remondelli, P.; Renna, M. The endoplasmic reticulum unfolded protein response in neurodegenerative disorders and its potential therapeutic significance. *Front. Mol. Neurosci.* **2017**, *10*, 187.
- (75) Matus, S.; Glimcher, L. H.; Hetz, C. Protein folding stress in neurodegenerative diseases: a glimpse into the ER. *Curr. Opin. Cell Biol.* **2011**, *23* (2), 239-252.
- (76) Ajoalabady, A.; Lindholm, D.; Ren, J.; Pratico, D. ER stress and UPR in Alzheimer's disease: mechanisms, pathogenesis, treatments. *Cell Death Dis* **2022**, *13* (8), 706-720.
- (77) Hetz, C.; Chevet, E.; Oakes, S. A. Proteostasis control by the unfolded protein response. *Nat. Cell Biol.* **2015**, *17* (7), 829-838.
- (78) Spaan, I.; van Nieuwenhuijzen, N.; Kimman, T.; Rockx-Brouwer, D.; Tieland, R. G.; Maurice, M. M.; Minnema, M. C.; Raymakers, R. A.; Peperzak, V. Wnt inhibitors reduce the unfolded protein response and enhance bortezomib-induced cell death in multiple myeloma. *Blood Adv.* **2023**, *7* (7), 1103-1107.

- (79) Ri, M. Endoplasmic-reticulum stress pathway-associated mechanisms of action of proteasome inhibitors in multiple myeloma. *Int. J. Hematol.* **2016**, *104* (3), 273-280.
- (80) Nunes, A. T.; Annunziata, C. M. Proteasome inhibitors: structure and function. *Semin. Oncol.* **2017**, *44* (6), 377-380.
- (81) Hu, B.; Zhong, L.; Weng, Y.; Peng, L.; Huang, Y.; Zhao, Y.; Liang, X. J. Therapeutic siRNA: state of the art. *Signal Transduct. Target Ther.* **2020**, *5* (1), 101-126.
- (82) Schnell, H. M.; Walsh, R. M., Jr.; Rawson, S.; Kaur, M.; Bhanu, M. K.; Tian, G.; Prado, M. A.; Guerra-Moreno, A.; Paulo, J. A.; Gygi, S. P.; et al. Structures of chaperone-associated assembly intermediates reveal coordinated mechanisms of proteasome biogenesis. *Nat. Struct. Mol. Biol.* **2021**, *28* (5), 418-425.
- (83) Rousseau, A.; Bertolotti, A. Regulation of proteasome assembly and activity in health and disease. *Nat. Rev. Mol. Cell Biol.* **2018**, *19* (11), 697-712.
- (84) Hirano, Y.; Hendil, K. B.; Yashiroda, H.; Iemura, S.; Nagane, R.; Hioki, Y.; Natsume, T.; Tanaka, K.; Murata, S. A heterodimeric complex that promotes the assembly of mammalian 20S proteasomes. *Nature* **2005**, *437* (7063), 1381-1385.
- (85) La Tallec, B., Barrault, M. B., Courbeyrette, R., Guerois, R., Marsolier-Kergoat, M. C., Peyroche, A. 20S proteasome assembly is orchestrated by two distinct pairs of chaperones in yeast and in mammals. *Cell* **2007**, *27*, 660-674.
- (86) Li, D.; Dong, Q.; Tao, Q.; Gu, J.; Cui, Y.; Jiang, X.; Yuan, J.; Li, W.; Xu, R.; Jin, Y.; et al. c-Abl regulates proteasome abundance by controlling the ubiquitin-proteasomal degradation of PSMA7 subunit. *Cell* **2015**, *10* (4), 484-496.
- (87) Wu, W.; Sahara, K.; Hirayama, S.; Zhao, X.; Watanabe, A.; Hamazaki, J.; Yashiroda, H.; Murata, S. PAC1-PAC2 proteasome assembly chaperone retains the core alpha4-alpha7 assembly intermediates in the cytoplasm. *Genes Cells* **2018**, *23* (10), 839-848.
- (88) Hirano, Y.; Kaneko, T.; Okamoto, K.; Bai, M.; Yashiroda, H.; Furuyama, K.; Kato, K.; Tanaka, K.; Murata, S. Dissecting beta-ring assembly pathway of the mammalian 20S proteasome. *EMBO J.* **2008**, *27* (16), 2204-2213.
- (89) Sekiguchi, T.; Satoh, T.; Kurimoto, E.; Song, C.; Kozai, T.; Watanabe, H.; Ishii, K.; Yagi, H.; Yanaka, S.; Uchiyama, S.; et al. Mutational and combinatorial control of self-assembling and disassembling of human proteasome alpha subunits. *Int. J. Mol. Sci.* **2019**, *20* (9), 2308-2321.
- (90) Apcher, G. S.; Maitland, J.; Dawson, S.; Sheppard, P.; Mayer, R. J. The alpha4 and alpha7 subunits and assembly of the 20S proteasome. *FEBS Lett.* **2004**, *569* (1), 211-216.

- (91) Le Tallec, B.; Barrault, M. B.; Courbeyrette, R.; Guerois, R.; Marsolier-Kergoat, M. C.; Peyroche, A. 20S proteasome assembly is orchestrated by two distinct pairs of chaperones in yeast and in mammals. *Mol. Cell* **2007**, *27* (4), 660-674.
- (92) Padmanabhan, A.; Vuong, S. A.; Hochstrasser, M. Assembly of an evolutionarily conserved alternative proteasome isoform in human cells. *Cell Rep.* **2016**, *14* (12), 2962.
- (93) Rogers, S. W., R.; Rechsteiner, M. Amino acid sequences common to rapidly degraded proteins: the PEST hypothesis. *Science* **1986**, *234*, 364-368.
- (94) Rickardson, L.; Wickstrom, M.; Larsson, R.; Lovborg, H. Image-based screening for the identification of novel proteasome inhibitors. *J. Biomol. Screen* **2007**, *12* (2), 203-210.
- (95) Demishtein, A.; Fraiberg, M.; Berko, D.; Tirosh, B.; Elazar, Z.; Navon, A. SQSTM1/p62-mediated autophagy compensates for loss of proteasome polyubiquitin recruiting capacity. *Autophagy* **2017**, *13* (10), 1697-1708.
- (96) Wang, C.; Wang, X. The interplay between autophagy and the ubiquitin-proteasome system in cardiac proteotoxicity. *Biochim. Biophys. Acta* **2015**, *1852* (2), 188-194.
- (97) Requejo, R.; Hurd, T. R.; Costa, N. J.; Murphy, M. P. Cysteine residues exposed on protein surfaces are the dominant intramitochondrial thiol and may protect against oxidative damage. *FEBS J.* **2010**, *277* (6), 1465-1480.
- (98) Chen, M. Z.; Moily, N. S.; Bridgford, J. L.; Wood, R. J.; Radwan, M.; Smith, T. A.; Song, Z.; Tang, B. Z.; Tilley, L.; Xu, X.; et al. A thiol probe for measuring unfolded protein load and proteostasis in cells. *Nat. Commun.* **2017**, *8* (1), 474.
- (99) Stewart, C.; Estrada, A.; Kim, P.; Wang, D.; Wei, Y.; Gentile, C.; Pagliassotti, M. Regulation of IRE1alpha by the small molecule inhibitor 4mu8c in hepatoma cells. *Endoplasmic Reticulum Stress Dis.* **2017**, *4* (1), 1-10.
- (100) Cross, B. C.; Bond, P. J.; Sadowski, P. G.; Jha, B. K.; Zak, J.; Goodman, J. M.; Silverman, R. H.; Neubert, T. A.; Baxendale, I. R.; Ron, D.; et al. The molecular basis for selective inhibition of unconventional mRNA splicing by an IRE1-binding small molecule. *Proc. Natl. Acad. Sci. U S A* **2012**, *109* (15), 869-878.
- (101) Wang, Q.; Shinkre, B. A.; Lee, J. G.; Weniger, M. A.; Liu, Y.; Chen, W.; Wiestner, A.; Trenkle, W. C.; Ye, Y. The ERAD inhibitor Eeyarestatin I is a bifunctional compound with a membrane-binding domain and a p97/VCP inhibitory group. *PLoS One* **2010**, *5* (11), 15479-15491.
- (102) Mehrtash, A. B.; Hochstrasser, M. Ubiquitin-dependent protein degradation at the endoplasmic reticulum and nuclear envelope. *Semin. Cell Dev. Biol.* **2019**, *93*, 111-124.

APPENDIX

Methods

Cell Culture

HEK-293T cells were cultured in Dulbecco's modified Eagle's medium supplemented with 1% penicillin–streptomycin and 10% fetal bovine serum. PC12 cells were cultured in RPMI 1640 supplemented with 1% penicillin–streptomycin, 5% fetal bovine serum and 10% horse serum. All cell lines were maintained at 37 °C with 5% CO₂ in 10 cm tissue treated plates. Cell lines were routinely tested for mycoplasma contamination.

Section 3.2 Associated Methods

Antibodies

Primary antibodies used for the immunoblotting of the purified α -synuclein degradation, *in vitro* proteasome impairment, and the HEK-293T cellular studies were mouse monoclonal anti- α -synuclein IgG (1:1333) and anti-mouse HRP-linked IgG (1:1000). For the *in vitro* degradation of p25 α , rabbit monoclonal anti-p25 α IgG (1:1000) and anti-rabbit HRP-linked IgG (1:1000), were used. The PC12 cellular studies utilized rabbit anti- α -synuclein IgG (1:1000) and HRP tagged anti-ubiquitin (1:1000). For all studies the HRP tagged anti-GAPDH (1:1333) was used.

DNA transfection and immunoblotting

The HEK-293T cells were plated in 60 mm plates and grown to 80% confluency. The cells were then transiently transfected with Xtreme gene and the desired plasmid (5 μ g of DNA, TPPP and A53T α -synuclein, and 10 μ L of transfection reagent for a 1:2 dilution) diluted in 500 μ L Opti-mem. The expression of the target protein was conducted for 48 hours before treatment for an additional 16 hours. After the cells were treated with the test

compounds or DMSO, the cells were scraped from the plate and washed with PBS. The plate was washed with PBS as well. The scraped cells in media and PBS were pelleted (300g for 5 minutes). The supernatant was removed, and the cell pellet was washed with ice cold PBS and once again pelleted (300g for 5 minutes). The PBS supernatant was removed, and the cell pellet was lysed with RIPA buffer with added protease inhibitors. The cell lysate was incubated for 15 minutes on ice. The lysate was centrifuged for 25 minutes at 500 g, then the supernatant was removed while the debris pellet was disposed of. Like the experiments with the HEK-293T cells, the PC12 were plated in 60 mm plates after being strained with Flowmi[®] Cell Strainers. The PC12 cells were then transfected in the same manner as the HEK-293T cells, using the same protein expression and treatment period. After the treatments, the cells were collected with media and pelleted (300g for 5 minutes). The supernatant was removed, and the cell pellet was washed with ice cold PBS and pelleted again (300g for 5 minutes). The PBS supernatant was removed, and the cell pellet was resuspended with PBS that contained protease inhibitors and lysed using sonication. The lysate was centrifuged for 25 minutes at 1000 g, then the supernatant was removed while the debris pellet was disposed. The concentration of total protein in each sample was calculated using the Pierce BCA Protein Analysis Kit, and lysates were standardized to the lowest total protein concentration.

For all immunoblotting, a concentrated Laemmli sample buffer supplemented with 25% β -mercaptoethanol was added to all the samples and boiled for 10 minutes. The samples were then resolved on a 4-20% Tris-glycine SDS-PAGE gel and transferred onto a PVDF membrane using Mini Trans-Blot Electrophoretic Transfer Cell for 1 hour and 30 minutes. The membranes were blocked for 30 minutes with 5% Blocking Buffer at room

temperature. The membrane was then incubated with the desired primary antibody (listed in the antibody section with dilution ratios) in 10 mL of Tris-buffered saline Tween 20 (TBST: 1x solution was made from a 10x TBS solution) at 4 °C for 16 hours. The immunoblots were washed with 1x TBST for 3x3 minutes before being incubated with the corresponding secondary antibody at room temperature for 1 hour. The immunoblots were developed with ECL Western reagent and imaged with an Azure Biosystems 300Q imager. If several proteins were probed for, the immunoblots were stripped using a mild stripping buffer (200 mM glycine, 3.5 mM SDS, and 8 mM Tween 20 with a pH of 2.2) for 20 minutes and then washed with TBST for 3x 5 minutes before re-probing. Immunoblots were then quantified using the Bio-Rad Image Lab software.

Purified p25 α digestion with 20S proteasome

The degradation of p25 α was carried out in a total reaction volume of 25 μ L. A solution of an 8.5 nM proteasome stock was made in 120 mM NaCl, 50 mM Tris, and 0.1% β -mercaptoethanol buffer with a pH of 7.2. A final concentration of 7.5 nM of 20S proteasome was treated with 0.5 μ L of either DMSO or 10 μ M of **36**, **39**, or **54** for 30 minutes at 37 °C. During this 30-minute incubation, a 5,000 nM stock of purified p25 α was incubated with 100 μ M of DTE for 30 minutes at room temperature. After incubation, the purified 2.5 μ L p25 α (final concentration of 500 nM) was added to the drug:proteasome solution for an additional 3 hours. Then, 0.5 μ M of GAPDH was added as a loading control. A concentrated SDS loading buffer was also added, then the samples were boiled for 15 minutes to stop the digestion and immunoblotted.

Purified 20S proteasome impairment by p25 α / α -synuclein aggregates

Proteasome impairment was evaluated in a 50 μ L reaction volume, and a stock solution of 18.75 nM of 20S proteasome was made in a 120 mM NaCl, 50 mM Tris, and 0.1% β -mercaptoethanol buffer with a pH of 7.2. Samples were then made with 40 μ L of a 20S proteasome solution (final concentration of 15 nM) and then 5 μ L of either PBS, α -synuclein (final concentration of 700 nM), or p25 α (final concentration of 150 nM) for 45 minutes at 37 °C. An additional sample of 700 nM α -synuclein and 150 nM p25 α were incubated for 45 minutes at 37 °C. After this incubation, 1 μ L of Me4BodipyFL-Ahx3Leu3VS fluorescent probe was added to a final concentration of 1.5 μ M. Then, 0.5 μ M of GAPDH was added as a loading control. A concentrated SDS loading buffer was also added, then the samples were boiled for 15 minutes to stop the digestion. The samples were then resolved on a 4-20% Tris-glycine SDS-PAGE gel, and the fluorescence was visualized using Azure Biosystems 300Q imager at an excitation of 524 nm and emission of 572 nm. The samples were then immunoblotted.

P25 α induced α -synuclein fibrillization and proteasome impairment in PC12 cells

The PC12 cells transiently transfected with the A53T α -synuclein plasmid were treated with either DMSO or 10 μ M of compounds **36**, **39**, or **54** for 2 hours, or cells were treated with purified p25 α (final concentration of 160 nM, diluted in PBS) for 2 hours (after the 48-hour expression period). After this incubation, the cells treated with the compounds first were treated with purified p25 α . The cells treated with p25 α first were then treated with DMSO or 10 μ M of compounds **36**, **39**, or **54** (0.1 % final DMSO concentration). After this second treatment, cells were incubated for an additional 24 hours.

RB1 Probe Fibrillization

Prior to being lysed, PC12 cells were once again strained with the tip cell strainer and plated to 10,000 cells/well (100 μ L volume) in a black opaque bottom 96-well plate. Then, 1 μ L of the RB1 probe (final concentration of 800 nM, synthesized following reported protocol)⁶⁴ were added to each plate and incubated for 45 minutes at 37 °C. After this incubation, the fluorescence of each well was evaluated using a microplate reader at an excitation of 561 nm and emission of 589 nm.

Proteasome Glo

Like the RB1 probe assay, prior to lysis, the PC12 cells were strained and plated to 3,000 cells/well in a white 384-well plate at a 20 μ L volume. Then, 10 μ L of the Proteasome Glo reagent was added and incubated at room temperature for 20 minutes. The luminescence for each well was identified using the microplate reader.

Cytotoxicity

The PC12 cells were plated in a white 384-well plate (2,500 cells/well at a 15 μ L total volume) after being strained with a cell strainer. Each well was either transfected with no plasmid, 0.5 μ g of an A53T α -synuclein plasmid, 0.1 μ g of a p25 α plasmid, or a combination of the A53T α -synuclein and p25 α plasmids and 1.2 μ L of the transfection reagent (diluted in a final volume of 15 μ L in the Opti-mem). After a 24-hour transfection, DMSO and 3 μ M of **36**, **39**, and **54** were added (DMSO samples of each treatment were diluted in Opti-mem to a final DMSO concentration of 0.03%) for an additional 72 hours. Then, 10 μ L of the Cell Titer Glo reagent or 10 μ L of the Proteasome Glo reagent were added, and the luminescence per well was recorded. The cell viability and proteasome activity assays for the HEK-293T cells were conducted in the same manner, but with the

following alterations. The A53T α -synuclein plasmid was lowered to 0.1 μ g with 0.02 μ g of the p25 α plasmid. The treatment time was lowered to 48 hours from 72 hours.

Systematic treatment with purified p25 α .

PC12 cells were plated at 2,500 cells/well in a white 384-well plate to a volume of 15 μ L. Cells were then transfected with either no plasmid or 0.5 μ g of the A53T α -synuclein plasmid and 1 μ L of the transfection reagent (diluted up to 15 μ L of Opti-mem). After 24 hours, cells were treated with DMSO or 3 μ M of compounds **36**, **39**, and **54**. The cells were also treated with 160 nM of p25 α , which was done every 24 hours for 3 days. Then, 10 μ L of the Cell Titer Glo reagent was added, and the luminescence per well was recorded.

Section 3.3 Associated Methods

Antibodies

Primary antibodies used for the immunoblotting of the cell-based assays were a rabbit monoclonal anti ZsGreen IgG (1:2000), HRP tagged anti-ubiquitin (1:1000), mouse anti- α 3 (1:1000), mouse anti- α 4 (1:1000), anti-mouse HRP-linked IgG (1:1000), and an anti-rabbit HRP-linked IgG (1:1000). For all studies the HRP tagged anti-GAPDH (1:1333) was used.

siRNA transfection and immunoblotting

The HEK-293T cells were plated in 60 mm plates and grown to 30% confluency. The cells were then transiently transfected with Xtreme gene and the desired plasmid. 0.5 μ g of PSMA7, PSMA1, or PSMA4 siRNA was diluted in 50 μ L Opti-mem. Then 2.5 μ L of the transfection reagent was diluted in 50 μ L Opti-mem. The transfection reagent dilution was then added to the siRNA dilution. The silencing of the target protein was conducted for

24 and 48 hours or for 2, 4, 6, and 8 days for the time trials. 24 hours before the time point was finished, the compound of interest was added. For immunoblotting the cells were scraped from the plate and washed with PBS. The plate was washed with PBS as well. The scraped cells in media and PBS were pelleted (300g for 5 minutes). The supernatant was removed, and the cell pellet was washed with ice cold PBS and once again pelleted (300g for 5 minutes). The PBS supernatant was removed, and the cell pellet was lysed with RIPA buffer with added protease inhibitors. The cell lysate was incubated for 15 minutes on ice. The lysate was centrifuged for 25 minutes at 500 g, then the supernatant was removed while the debris pellet was disposed of. Like the experiments with the HEK-293T cells, the PC12 were plated in 60 mm plates after being strained with Flowmi[®] Cell Strainers. The PC12 cells were then transfected in the same manner as the HEK-293T cells, silencing the PSMA7 gene for 2, 4, and 6 days. Then the cells were collected with media and pelleted (300g for 5 minutes). The supernatant was removed, and the cell pellet was washed with ice cold PBS and pelleted again (300g for 5 minutes). The PBS supernatant was removed, and the cell pellet was resuspended with PBS that contained protease inhibitors and lysed using sonication. The lysate was centrifuged for 25 minutes at 1000 g, then the supernatant was removed while the debris pellet was disposed. The concentration of total protein in each sample was calculated using the Pierce BCA Protein Analysis Kit, and lysates were standardized to the lowest total protein concentration.

For all immunoblotting, a concentrated Laemmli sample buffer supplemented with 25% β -mercaptoethanol was added to all the samples and boiled for 10 minutes. The samples were then resolved on a 4-20% Tris-glycine SDS-PAGE gel and transferred onto a PVDF

membrane using Mini Trans-Blot Electrophoretic Transfer Cell for 1 hour and 30 minutes. The membranes were blocked for 30 minutes with 5% Blocking Buffer at room temperature. The membrane was then incubated with the desired primary antibody (listed in the antibody section with dilution ratios) in 10 mL of Tris-buffered saline Tween 20 (TBST: 1x solution was made from a 10x TBS solution) at 4 °C for 16 hours. The immunoblots were washed with 1x TBST for 3x3 minutes before being incubated with the corresponding secondary antibody at room temperature for 1 hour. The immunoblots were developed with ECL Western reagent and imaged with an Azure Biosystems 300Q imager. If several proteins were probed for, the immunoblots were stripped using a mild stripping buffer (200 mM glycine, 3.5 mM SDS, and 8 mM Tween 20 with a pH of 2.2) for 20 minutes and then washed with TBST for 3x 5 minutes before re-probing. Immunoblots were then quantified using the Bio-Rad Image Lab software.

ZsGreen HEK-293T siRNA screening

In a 6 well plate, Hek-293T cells that stably express ZsGreen protein were plated and grown to 30% confluency. Then following the siRNA transfection protocol, the cells were transfected with PSMA7, PSMA1, and PSM4 siRNA or treated with 500 nM of BTZ. The fluorescent signal of the cells was evaluated 24 and 48 hours after the transfection using a Biotek Cytation 3 plate imager. Using PSMA7 as the ideal siRNA to lower proteasome activity, the cells plated on a 24 well plate and grown to a 30% confluency, were transfected using the transfection protocol. After 24 hours, the cells were treated with 10 μ M of TCH-165. Then using the Biotek Cytation 3 plate imager, the fluorescence of each well was recorded. Then samples of each cell were analyzed for cell viability using 10 μ L

of the cell culture and 10 μ L of the Cell Titer Glo reagent. The fluorescent signal observed in cells that were transfected with the PSMA7 siRNA acted as the vehicle control.

Proteasome Glo

Following the transfection protocol, PC12 cells were transfected with the PSMA7 siRNA for 0, 2, 4, and 6 days. To ensure that the studies were finished at the same time, the 6-day time point were the first samples transfected and then the 4-day followed by the 2-day time point. The transfected PC12 cells were plated on a white 384 well plate and 15,000 cells/well in 25 μ L of media. Then 25 μ L of the proteasome glo reagent was added. The plate was incubated for 15 minutes at room temperature and then read using the plate reader. The cells that were transfected for the 0-day time point was used as the vehicle control.

UPR evaluation in PC12 with PSMA7 siRNA

Following the transfection protocol, PC12 cells were transfected with the PSMA7, the PSMA7 gene was silenced for 5 days. At day 4, cells were treated with 100 nM of 4 μ 8C and 2.5 μ M of Eeyarestatin I for 24 hours. Then 10,000 cells/well were added to black 96-well plates in 99 μ L of media. Then 1 μ L of TPE-MI (final concentration of 50 μ M) is added. The cells were then incubated for 45 minutes at 37 $^{\circ}$ C and then read using a plate reader, with excitation of 350 nm and emission of 470 nm. The cells that were unmodified acted as the vehicle control.

Replicates

Section 3.2

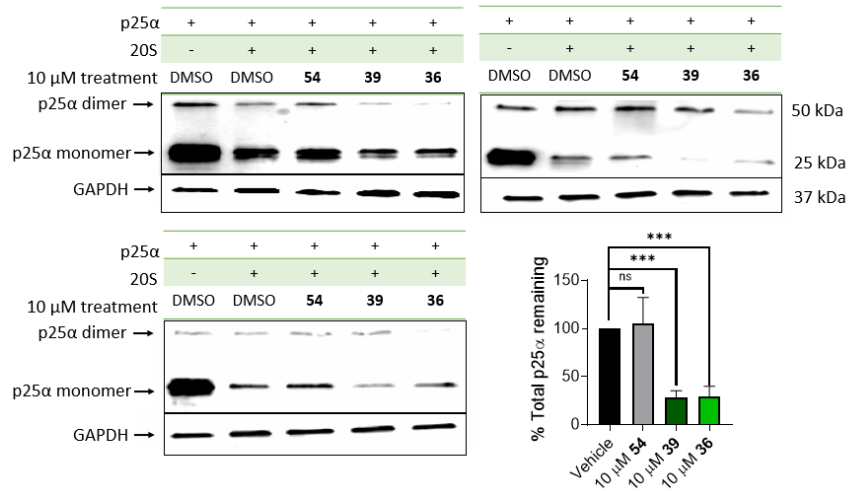


Figure 3.12: Westerns of p25α degradation by purified 20S proteasome treated 10 μM of compounds 36, 39, and 54. The quantification values were all normalized to the GAPDH, and gels shown are indicative of n=3 independent experiments.

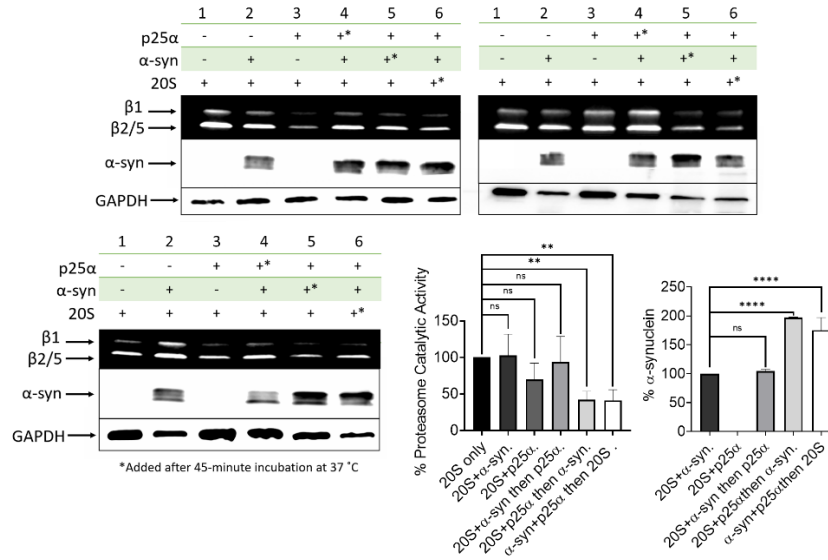


Figure 3.13: Activity gel of the 20S proteasome when treated with different orders of addition of purified p25α and α-synuclein compared to the remaining levels of α-synuclein. The quantification values were all normalized to the GAPDH, and gels shown are indicative of n=3 independent experiments.

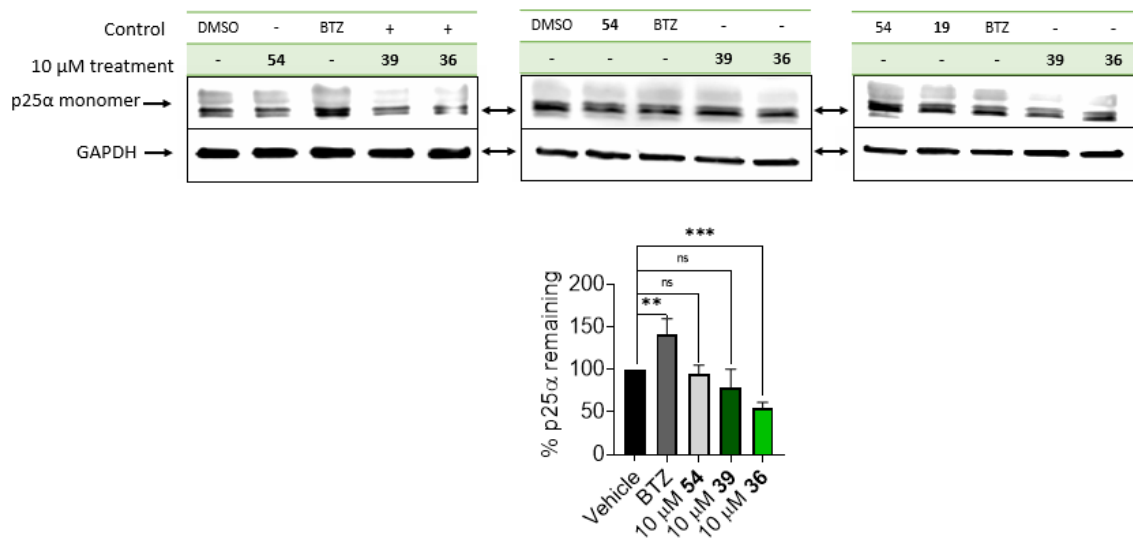


Figure 3.14: Western blots of p25 α degradation in HEK-293T cells treated with vehicle (DMSO), BTZ, and 10 μ M of compounds 36, 39, and 54. The quantification values were all normalized to the GAPDH, and gels shown are indicative of n=3 independent experiments. Error bars based on standard deviation.

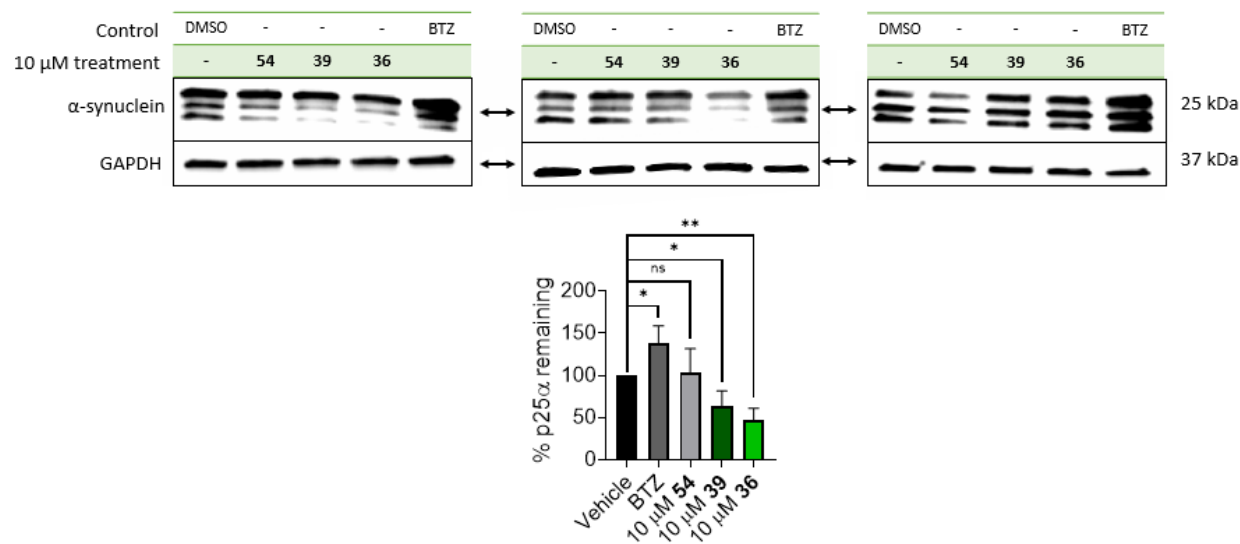


Figure 3.15: Western blots of p25α degradation in PC12 cells treated with vehicle (DMSO), BTZ, and 10 μM of compounds 36, 39, and 54. The quantification values were all normalized to the GAPDH, and gels shown are indicative of n=3 independent experiments. Error bars based on standard deviation.

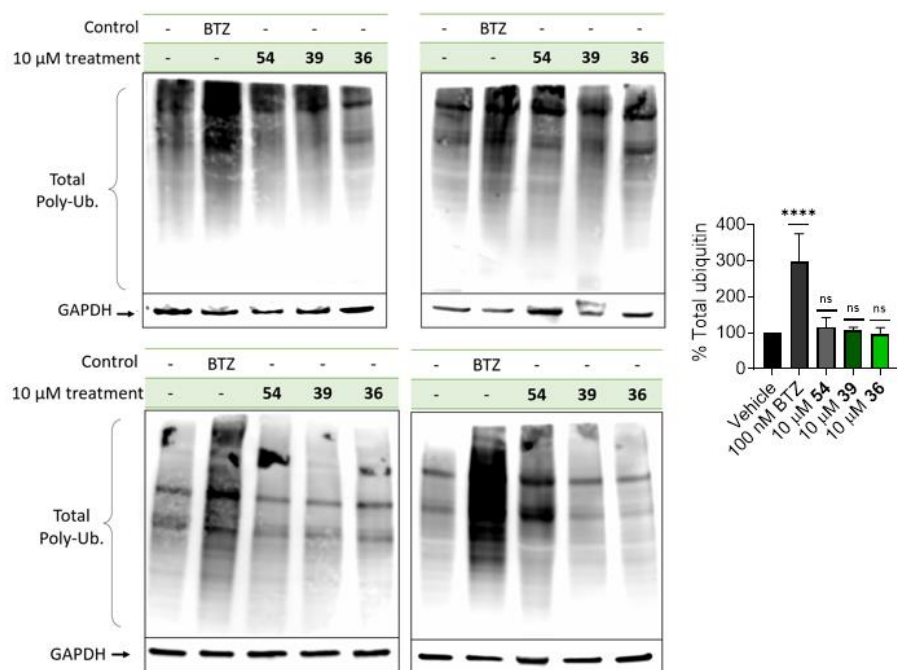


Figure 3.16: Western blots of ubiquitin levels in HEK-293T cells that were treated with DMSO and 10 μM of compounds 36, 39, and 54. The quantification values were all normalized to the GAPDH, and gels shown are indicative of n=3 independent experiments. Error bars based on standard deviation.

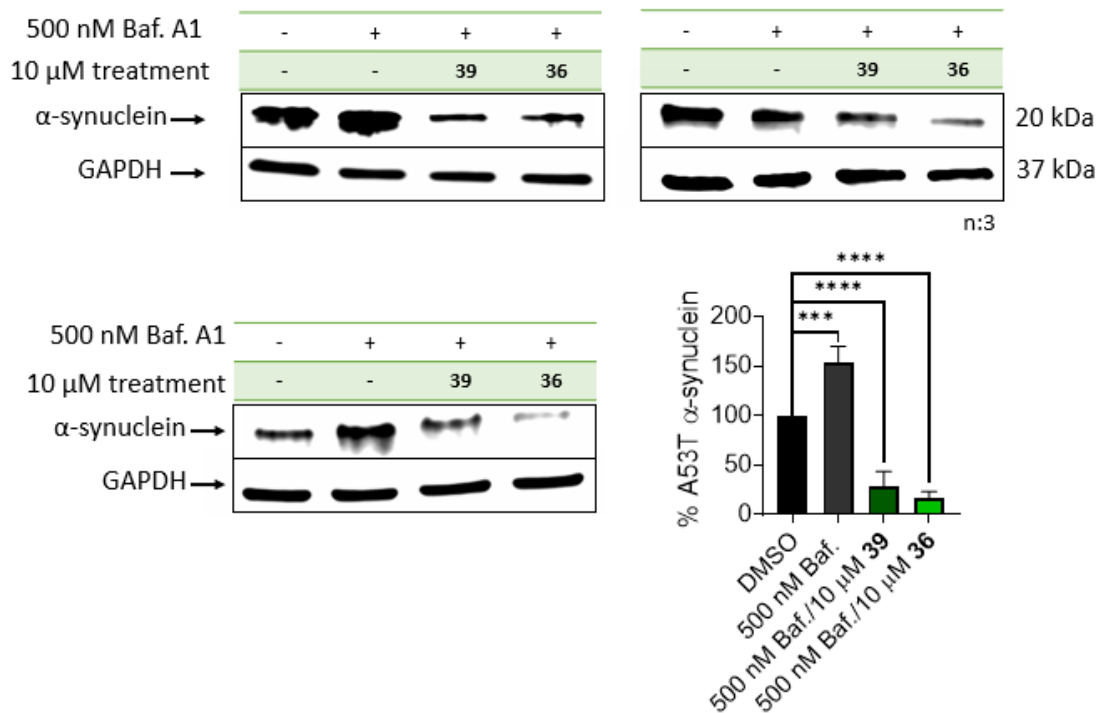


Figure 3.17: Western blots of A53T mutated α -synuclein degradation in HEK-293T cells that were pretreated with 500 nM Bafilomycin A1 and then treated with DMSO and 10 μ M of compounds 36 and 39. The quantification values were all normalized to the GAPDH, and gels shown are indicative of n=3 independent experiments. Error bars based on standard deviation.

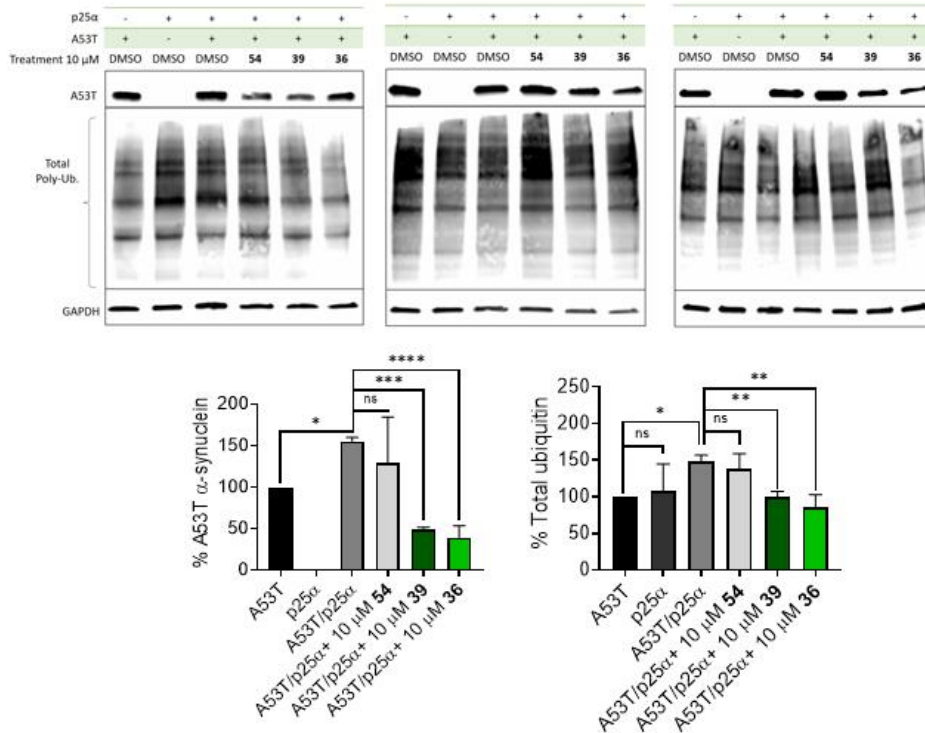


Figure 3.18: Western blots of A53T α -synuclein and ubiquitin levels in PC12 cells that were treated with DMSO and 10 μ M of compounds 36, 39, and 54 for two hours before the addition of 160 nM purified p25 α . The quantification values were all normalized to the GAPDH, and gels shown are indicative of n=3 independent experiments. Error bars based on standard deviation.

Section 3.3 Replicates

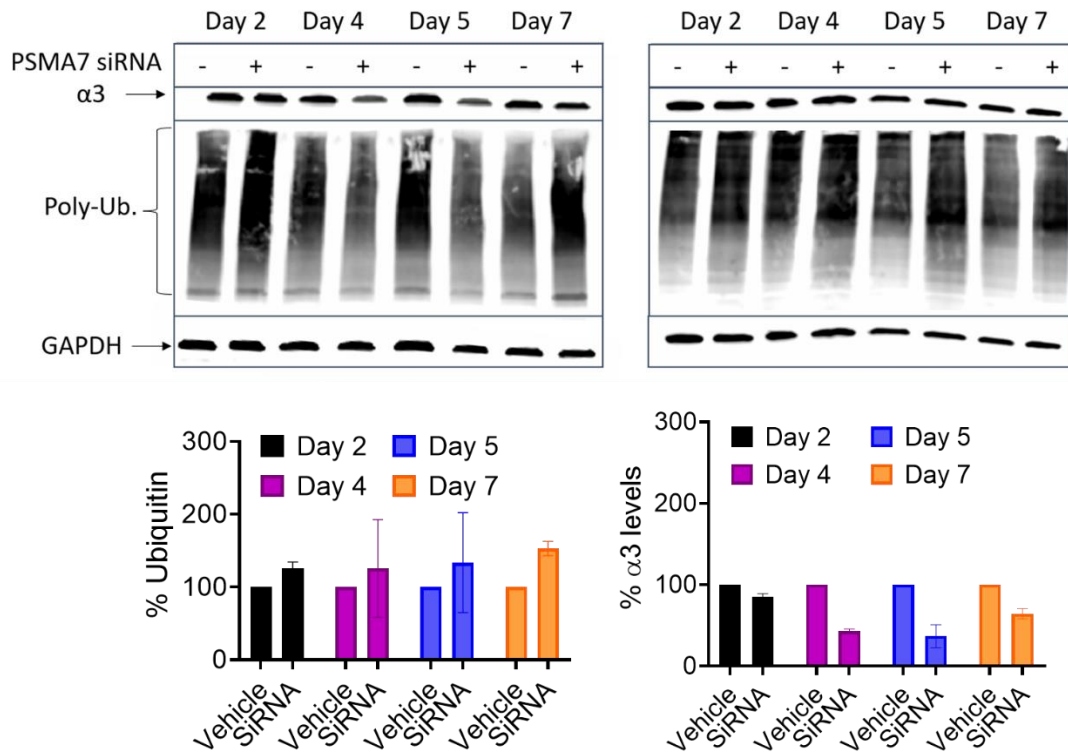


Figure 3.19: Western blots of ZsGreen HEK-293T cells that were transfected with PSMA7 (α4) siRNA for 2, 4, 5, and 7 days as compared to cells that were not transfected. α3 subunit and ubiquitin were visualized using immunoblotting with GAPDH used as the loading control. *Note this is an n:2.

CHAPTER FOUR

Development and Utilization of the First Cell-Based High-Throughput Screen for 20S Proteasome Enhancers

4.1 Introduction

IDPs have become a focus in the development of therapeutics for a range of diseases, yet the innate flexibility of IDPs poses a significant obstacle in the development of direct small molecule modulators.^{1, 2} Preventing IDP accumulation by enhancing the proteolytic activity of the 20S proteasome using small molecules and peptides is therefore considered a promising alternative.^{3, 4, 5, 6, 7} While there has been significant progress in the development of small molecule and peptide 20S proteasome enhancers, the chemical space is limited, and few molecules display potent cellular activity. Novel classes of 20S proteasome enhancers must be identified to evaluate this new therapeutic strategy further in cell models and *in vivo*. To address this need, cellular activity assays must be developed to meet the demands of high-throughput screening.

Standard proteasome activity measurement assays utilize a modified small peptide substrate conjugated to a 4-amino-7-methylcoumarin (AMC) probe.⁸ Although the AMC probes are valuable tools, their small size allows them to enter the 20S proteasome core without the gate being fully open, leading to poor sensitivity.⁹ Furthermore, the AMC-based small peptide probes are not cell permeable, limiting their use to cell lysates or purified enzymatic assays.¹⁰ With the limitations in mind, Förster Resonance Energy Transfer (FRET) based probes were designed to evaluate proteasome activity *in vitro*.¹¹ The sensitivity of the FRET probes makes them an ideal choice for high-throughput assays when using purified 20S proteasome.¹² However, similarly to the AMC probes, the FRET probes are not cell permeable, limiting their use to examining non-cellular or cell lysate proteasomal activity.^{10, 12} In addition, small peptide probes are designed to mimic the preferred cleavage site of each proteasomal catalytic site.⁹ Moreover, all three

probes must be combined to evaluate the overall proteasome activity. The protocols of proteasome inhibition and enhancement often differ drastically. For example, the proteasome must be artificially activated with a detergent, like sodium dodecyl sulfate (SDS), to test for proteasome inhibition.¹³ Furthermore, the proteolytic degradation of the small peptide probes (with 3-5 amino acids) doesn't necessarily recapitulate the endogenous proteasome-mediated degradation of full-size proteins. To address the shortcomings, we sought to develop a cellular high-throughput assay capable of detecting small molecules that induce 20S proteasome-mediated degradation of intact intrinsically disordered proteins.

The two-bead assay, known as an AlphaLISA (Amplified Luminescent Proximity Homogeneous Assay Linked Immunosorbent Assay), provides an ideal platform to evaluate the total concentration of the full-length GFP-ODC protein due to its high sensitivity and ease of modification. Herein, we describe the development of a cell-based AlphaLISA designed to measure the proteolytic degradation of a well-known IDP, ornithine decarboxylase (ODC), that is tagged with a green fluorescent protein (GFPSpark) on its N-terminus (**Figure 3.1A**).⁷ Compared to other GFP types, GFPSpark folds more quickly and maintains its exceptionally stable β -barrel structure, resulting in a high degree of stability that proves difficult for even the 19S cap's unfolding abilities to overcome.¹⁴ ODC is a homodimeric enzyme that plays a vital role in the biosynthesis of polyamines. In its monomeric form, ODC is inactive, intrinsically disordered, and can be degraded by the 20S proteasome.^{7, 15} The opposing structural characteristics of GFPSpark and ODC make their conjugated protein combination an ideal substrate for the evaluation of 20S proteasome modulation by small molecules. Utilization of the cell based

AlphaLISA enabled us to screen the NIH Clinical Library and the Prestwick Library, identifying erlotinib as a new 20S proteasome enhancer.

4.2 Development and Utilization of AlphaLISA Based High-Throughput Screen

4.2.1 Rational

AlphaLISA assays rely on an electron transfer between two beads: a donor and an acceptor bead.^{16, 17} When the donor bead is excited with 680 nm of light, a singlet oxygen species is produced.^{16, 17} The oxygen species can travel approximately 200 nm and add across an alkene double bond of a thioxene derivative on the acceptor bead.¹⁸ The energy released during this reaction then excites a Europium chelate, ultimately emitting a signal around 615 nm.^{16, 17, 19} However, if the acceptor bead is not within 200 nm, the reaction will not occur, and no signal will be emitted at 615 nm (**Figure 3.1B**).

The distance dependency of the AlphaLISA is advantageous in developing a proteasome activity assay. Here, the donor bead was coated with streptavidin and conjugated with a biotinylated anti-ODC antibody, while the acceptor bead was coated with an anti-GFP antibody. When the full-length conjugated protein is present, the two beads are brought together, causing the AlphaLISA signal observed at 615 nm. In a cellular setting, the proteasome can readily degrade the ODC portion of the conjugated protein, lowering the concentration of the full-length GFP-ODC in the cell lysate. The degradation of the GFP-ODC protein prevents the beads from being kept within 200 nm, decreasing the emission signal at 615 nm. Thus, when introducing a proteasome modulator, the degree to which ODC is proteolytically degraded will be readily altered. If a proteasome inhibitor is present,

the AlphaLISA signal should be increased compared to the signal resulting from the basal degradation of untreated proteasomes. Inversely, if a proteasome enhancer is in the system, the signal should decrease compared to the untreated control due to enhanced proteolysis of ODC.

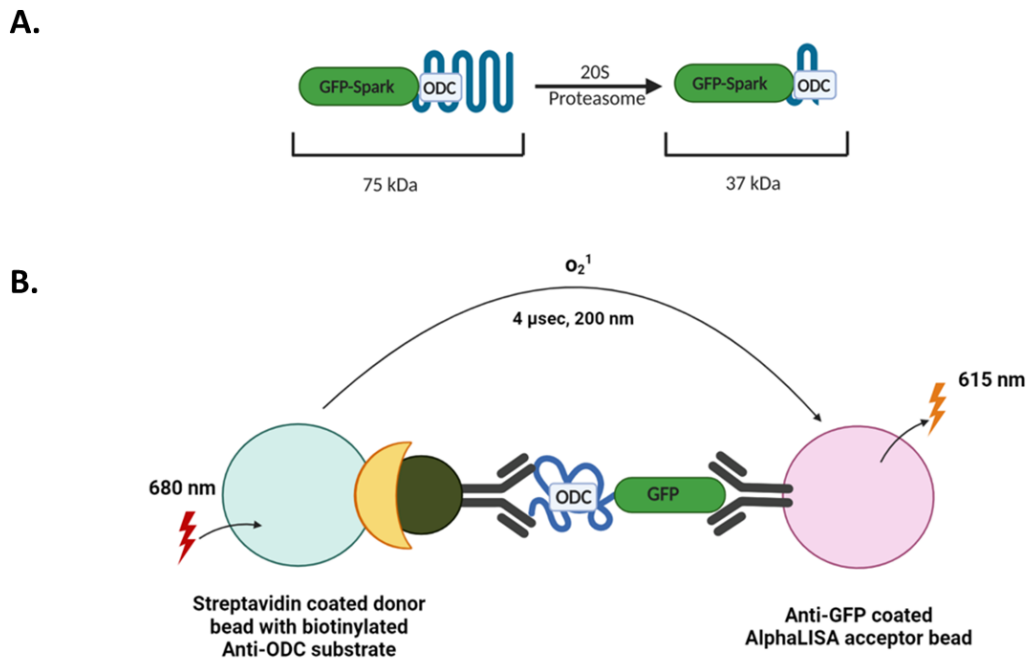


Figure 3.1: Schematic of the GFP-ODC AlphaLISA.

(A) Schematic of theorized cleavage pattern of the GFP-ODC conjugated protein by the 20S proteasome and (B) the interaction between the donor and acceptor beads when brought together by the GFP-ODC conjugated protein.

*Created with BioRender

4.2.2 Assay Development

Before evaluating proteasome modulators, the AlphaLISA assay was optimized to ensure the signal is stable and reproducible. To screen the concentrations of both beads and the

antibodies needed for the highest and most consistent AlphaLISA signal, HEK-293T cells transiently expressing GFP-ODC were used. Cells were seeded at 1,000 cells/well in white, opaque bottom, 384-well plates. The cells were incubated for 12 hours for cellular adherence and recovery from the plating process. The cells were then directly lysed in the assay plate, and eight different combinations of concentrations of the acceptor bead (10 µg/mL or 5 µg/mL), streptavidin donor bead (40 µg/mL or 20 µg/mL), and the biotinylated anti-ODC antibody (1 nM or 3 nM) were screened. Cell lysates not treated with the biotinylated anti-ODC antibody served as the negative control.²⁰ The AlphaLISA signal of each condition was then compared to the negative control. All the combinations produced a significant signal-to-noise ratio over the negative control; however, cell lysates treated with 10 µg/mL anti-GFP acceptor bead, 40 µg/mL Streptavidin donor bead, and 3 nM of the biotinylated anti-ODC antibody displayed the highest signal-to-noise ratio of 41 over the negative control. The 10 µg/mL anti-GFP acceptor bead, 40 µg/mL Streptavidin donor bead, and 3 nM of the biotinylated anti-ODC antibody conditions were carried forward to optimize cell type and number.²⁰

While the transiently transfected cell line produced a high signal-to-noise ratio, a stable cell line would ensure signal stability and reproducibility. Furthermore, a stable cell line would be needed to adapt our assay for high-throughput screening. Using flow cytometry, a pool of HEK-293T cells that were stably transfected with the GFP-ODC construct were sorted into medium (light green box) and high GFP (dark green box) expressors (**Figure 4.2A**). The resulting cell populations were seeded at 2,500 cells/well in the white 384-well plates. The AlphaLISA was performed using the previously optimized bead concentration. Interestingly, the cells that expressed high levels of GFP did not produce any AlphaLISA

signal (**Figure 4.2B**), while the medium expressors displayed a significant signal-to-noise ratio of 15. At substantially high concentrations of the analyte (GFP-ODC), non-productive complexes can be formed i.e., GFP-bound beads or ODC-bound beads only, but not the ternary complex, which is known as the Hook effect.

Using the “pool of medium expressors,” the optimal number of cells/well was determined (**Figure 4.2C-E**). The HEK-293T cells were seeded at 2,500 cells/well, 5,000 cells/well, and 10,000 cells/well in a white 384-well plate. As the cells were plated, samples from each seeding condition were also treated with a proteasome inhibitor, Bortezomib (BTZ), and a known 20S proteasome enhancer, TCH-165⁷ to identify which cell number would produce the most significant signal difference between the two proteasome modulators and the untreated vehicle. In parallel, we conducted the assay with and without cycloheximide (CHX) to visualize whether halting protein production is needed to observe a significant effect by proteasome modulators (**Figure 4.2C-E**).²⁰

While all three seeding conditions displayed a high AlphaLISA signal, the non-CHX treated samples seeded at 10,000 cells/well displayed a signal-to-noise ratio of 23 over the negative control, making the 10,000 cells/well seeding conditions optimal (**Figure 4.4E**). The CHX-treated samples seeded at 10,000 cells/well only had a signal-to-noise ratio of 6. The percent change observed with the proteasome inhibitor, BTZ, and the proteasome activator, TCH-165,⁷ were comparable between the CHX-treated and non-treated cells. Therefore, eliminating the addition of CHX streamlines the assay workflow without affecting the magnitude difference that the proteasome modulators have on the AlphaLISA signal.²⁰

Upon optimization of the AlphaLISA, we executed a Z' test to evaluate the robustness of the assay, allowing for validation that the AlphaLISA could be employed in a high-throughput screen. A Z' test measures the Z' factor which is a function of assay quality. The Z' factor describes the separation between the positive and negative control, giving an indication of the likelihood of false negatives or positives.²¹ Assays that have a Z' factor of 0.5 or higher are considered to be excellent candidates for high-throughput screening. The AlphaLISA assay was carried out in a white 384-well plate, and half of the wells were not treated with the biotinylated anti-ODC antibody to act as our negative control. The Z' factor was determined using the data collected from these experiments (**Figure 4.2F**). Using the median values and median absolute deviation, the Z' robust factor was calculated to be 0.69, indicating the high reproducibility and robustness of the assay. The robust Z' factor reduces the influence of outliers, while the standard Z' factor equation would have to be manually manipulated to account for them.²² While the Z' factor was excellent, we still needed to validate a dose-response signal decrease with a proteasome activator, TCH-165 (**Figure 4.2G**). Using optimized conditions, the assay produced a clear dose-response decrease when subjected to a range of TCH-165 concentrations, resulting in an IC₅₀ of 10 μM (**Figure 4.2G**), deeming the assay optimized and ready to use in a 2,000-compound screen.²⁰

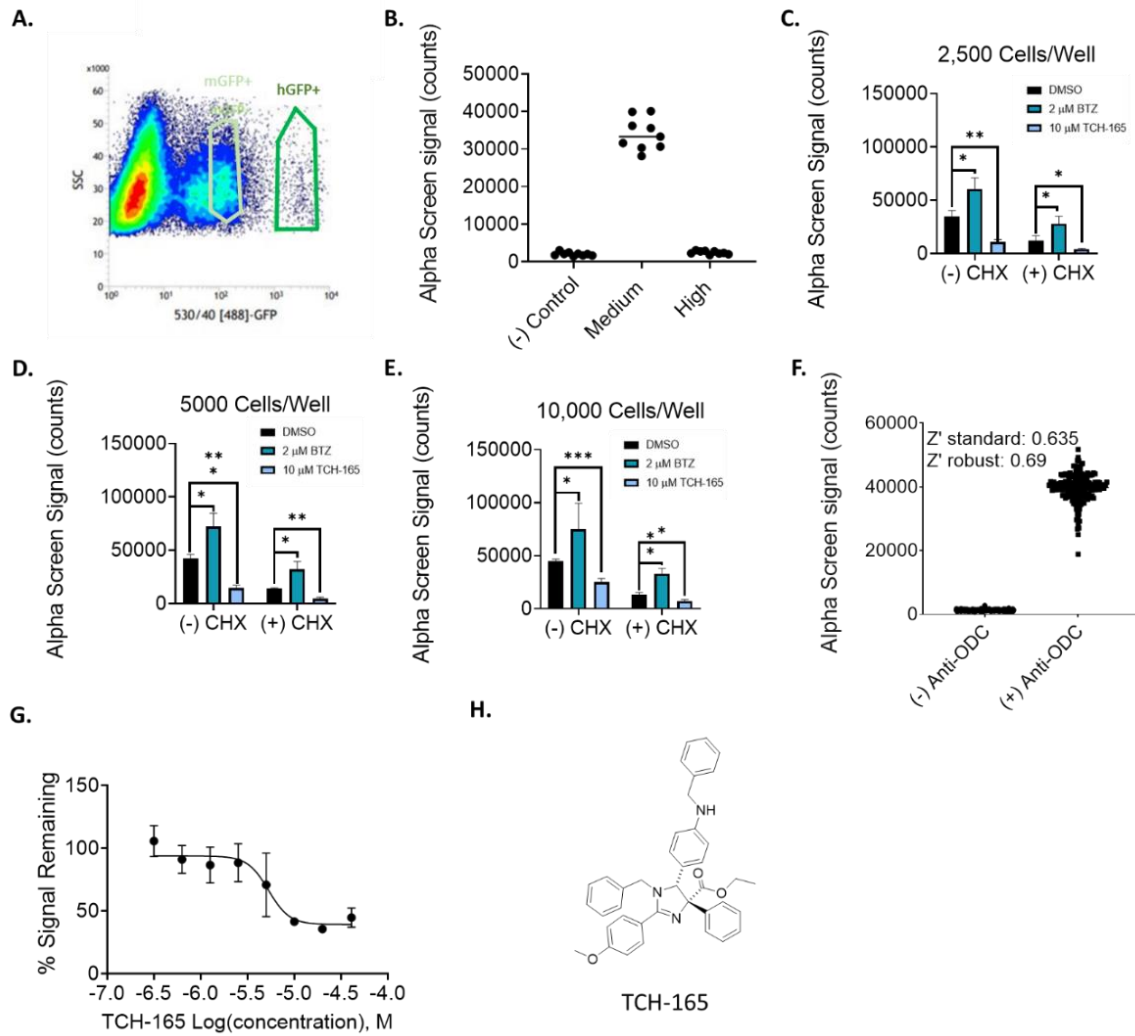


Figure 4.2: Optimization of the GFP-ODC AlphaLISA.

(A) Distribution of GFP expressors sorted using Flow Cytometry. The lighter green box represents cells that display a “medium” GFP signal (mGFP⁺), while the dark green box are the cells that display a “high” GFP signal (hGFP⁺). (B) The AlphaLISA signal of each of the cell populations. AlphaLISA signal of (C) 2,500 cells/well, (D) 5,000 cells/well, and (E) 10,000 cells/well when treated with DMSO, 10 μM TCH-165, and 2 μM of BTZ in two conditions, with and without cycloheximide (CHX).

Figure 4.2 (cont'd)

(One-way ANOVA statistical analysis was used to determine statistically significant. (ns = not significant, * $p < 0.05$, ** $p < 0.01$, *** $p < 0.001$, **** $p < 0.0001$). (F) The sample distribution from a full 384 well plate to examine the Z'-score, which was calculated to be 0.635. (G) The dose-response inhibition of the AlphaLISA signal by TCH-165. (H) Structure of TCH-165.

4.2.3 Prestwick and NIH Clinical Compound Library Screening

With the successful development of the AlphaLISA and the validation of its reproducibility and robustness, the Prestwick and the NIH Clinical compound libraries were screened. Prior to beginning the screen, we established the criteria required for a molecule to be considered a hit: compounds that reduced the AlphaLISA signal by >35% with >90% cell viability in a parallel Cell Titer Glo assay. We also established the orthogonal assays needed to evaluate the hit compounds and the activity that they must exhibit to be considered a lead compound (**Figure 4.3**). The AlphaLISA was performed using the optimized conditions, and once the cells were plated in a white 384-well plate, we immediately treated samples with 15 μM of each of the test compounds for 16 hours. Of the 2,000 compounds screened from the two libraries, 62 compounds lowered the AlphaLISA signal by 35% while maintaining at least 90% cell viability and were carried forward.

To eliminate false positives, we used a TrueHits assay to evaluate the interaction of the 62 compounds with the AlphaLISA signal itself. Compounds that inhibited the AlphaLISA signal by 25% or more were removed, leaving 36 compounds. The 36 compounds were

then evaluated in a GFP-ODC AlphaLISA using an 8-point titration (80 μ M-0.625 μ M) using solutions made from the original library compound plates.

Of the 36 compounds, 11 displayed a 35% inhibition of the GFP-ODC AlphaLISA signal at 15 μ M. Fresh powder stocks of the 11 compounds and a 20S activator identified in our 2017 screen,⁶ chlorpromazine (CPZ), were re-evaluated again in an 8-point GFP-ODC AlphaLISA (**Figure 4.4**). CPZ was used as a direct way to compare a successful lead identified in the 2017 high-throughput screen and our novel cell-based high-throughput

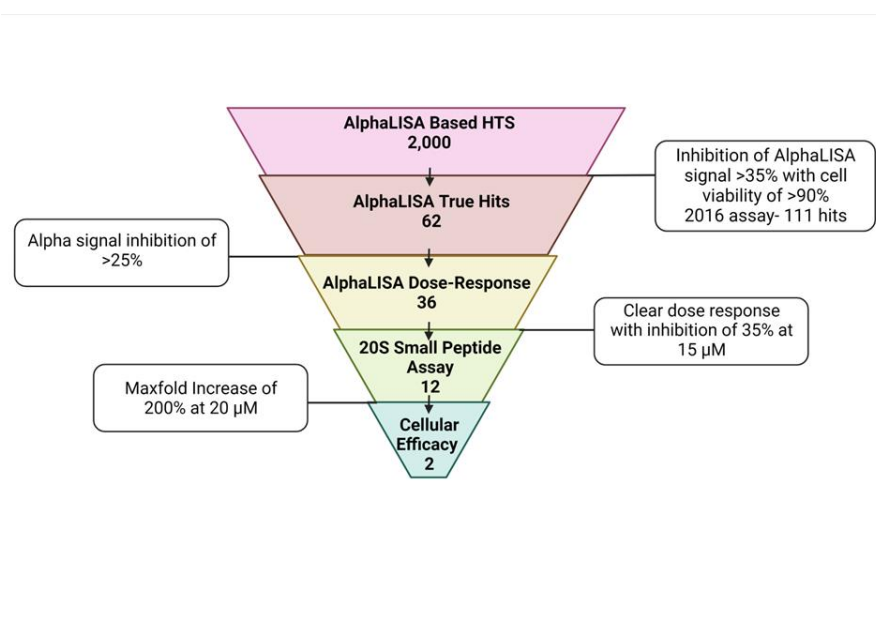


Figure 4.3: Screening funnel for the screening of the Prestwick and NIH Clinical Libraries, which consist of 2,000 compounds, using the optimized AlphaLISA.

screen.⁶ As mentioned, ODC can exist as a disordered monomer or as a structure homodimer.^{15, 23} The structural alterations between the two states may explain the inability for the signal to rarely decrease below 50%. The 20S proteasome is responsible for the degradation of the disordered monomeric ODC species, but would be unable to degrade the larger, structured ODC homodimers.^{6, 7, 24} Thus, enhancing the activity of the

20S proteasome is limited to the enhanced degradation of one of the two ODC species present, causing the AlphaLISA signal to never reach baseline in samples treated with small molecule 20S proteasome enhancers.

Of the 11 compounds and CPZ, only five compounds displayed a reduction in the GFP-ODC AlphaLISA signal that could not be directly attributed to decrease in cell number (**Figure 4.4**). Hycanthone, a frame-shift mutagen used to treat schistosomiasis,²⁵ displayed an IC₅₀ of the AlphaLISA signal of 15.1 μ M with a CC₅₀, or the concentration at which there is 50% cell death, of 69.7 μ M (**Figure 4.4A**). The EGFR kinase inhibitor,²⁶ erlotinib, displayed a promising dose response in the AlphaLISA, with no significant cell cytotoxicity (**Figure 4.4B**), but did display poor solubility at the higher concentrations. Quinacrine, an antimalarial medication,²⁷ was more cytotoxic with a CC₅₀ of 16.0 μ M but showed similar potency in the AlphaLISA as erlotinib (IC₅₀ of 4.8 μ M, **Figure 4.4C**). The last two compounds, a commonly used mineralocorticoid and androgen receptor antagonist, spironolactone,²⁸ and an antibiotic, nifuroxazide,²⁹ showed a decrease in the AlphaLISA signal with low cytotoxicity values. However, they did not reduce the signal by 50% (**Figure 4.4D-E**). The 8-point titration curves of the remaining six compounds and CPZ are displayed in **Figure 4.4F**. Two compounds, homoharringtonine and triptolide, significantly decreased the AlphaLISA signal but not in a dose-dependent manner. Homoharringtonine and triptolide are both natural products that have been evaluated for treating a variety of cancers, and both natural products inhibit the expression of proteins.^{30, 31} Homoharringtonine inhibits protein translation by preventing the initial elongation step through the interaction with the ribosomal A-site,³⁰ while triptolide inhibits RNA polymerase II-mediated transcription (**Figure 4.4G-H**).³¹ Although the two

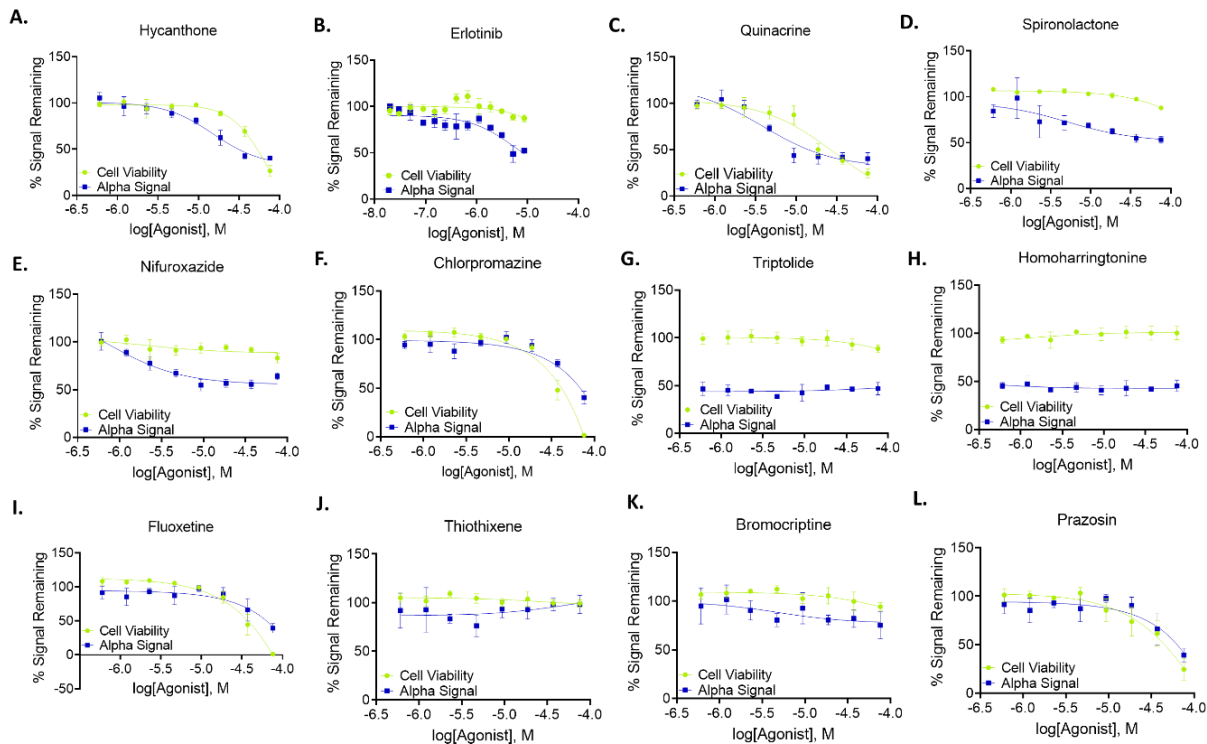


Figure 4.4: The 8-point dose response curves of lead compounds.

Dose response curves of (A) hycanthone, (B) erlotinib (C) quinacrine, (D) spironolactone, (E) nifuroxazide, (F) chlorpromazine, (G) triptolide, (H) homoharringtonine, (I) fluoxetine, (J) thiothixene, (K) bromocriptine, (L) prazosin. The green line represents cell viability, and the blue line represents percent of the AlphaLISA signal, data was graphed with GraphPad Prism 9 [Nonlinear regression: Log agonist vs. response-variable slope (3parameters)]

compounds will not become lead compounds, they represent great controls for our screen and emphasize the importance of orthogonal assays to validate our lead compounds. The remaining compounds, prazosin, thiothixene, bromocriptine, and fluoxetine, either did not reduce the AlphaLISA signal below 50% (**Figure 4.4I-L**) or did not reduce the AlphaLISA signal without significant cell death.²⁰

4.2.4 Hit Validation

To ensure direct activation of the 20S proteasome was occurring, the 20S proteasome activities of all five compounds and CPZ (as a control) were assessed by utilizing the standard fluorogenic 7-amino-methylcoumarin (AMC) in a purified proteasome assay. The conjugated small peptide substrates that correspond to each one of the catalytic sites in the 20S proteasome were used: chymotrypsin-like site (Suc-LLVY-AMC), caspase-like site (Z-LLE-AMC), and trypsin-like site (Boc-LRR-AMC).³² The 20S proteasome was treated with a range of concentrations of the compounds and a vehicle control and subsequently incubated at 37 °C for 20 minutes. After incubation, an equimolar mixture of the three fluorogenic peptide probes (13.3 μ M of each) was added, and the fluorescent output was recorded every 5 minutes for an hour. The rate of 20S proteasome-mediated proteolysis induced by the small molecules was evaluated at varying concentrations to determine the EC₂₀₀. Compounds were added to wells that contained 1 nM of purified human 20S proteasome in an 8-point titration with concentrations ranging from 1.25 μ M to 80 μ M. The compounds deemed active were retested at a 10-point concentration titration of 0.32 μ M to 80 μ M.²⁰

Of the 5 compounds evaluated for purified 20S proteasome activation, only erlotinib satisfied our final screening funnel criteria (**Figure 4.5A**, EC₂₀₀ < 20 μ M). Prazosin was also evaluated for the 20S proteasome enhancement due to its structural similarity to erlotinib (**Figure 4.5A**). The 20S proteasome treated with erlotinib and prazosin displayed a max-fold increase of 5.7 and 4.5, respectively. Of the three catalytic sites in the 20S proteasome, CPZ only activated the chymotrypsin-like site while having an overall max-fold increase of 6.3.⁶ The three catalytic sites in the 20S proteasome allosterically

communicate with one another.⁸ CPZ's selective activation of a single-site may interfere with its ability to effectively cleave the GFP-ODC substrate. Unlike CPZ, both prazosin and erlotinib were observed to activate more than one catalytic site. Prazosin activated two catalytic sites: the caspase-like site (max fold increase of 5.8) and the chymotrypsin-like site (max fold increase of 4.5) (**Figure 4.5B-D**). Erlotinib, however, activated the trypsin-like, chymotrypsin-like, and caspase-like sites, with max fold increases of 5.9, 5.1, and 3.1, respectively (**Figure 4.5B-D**). The activities of the remaining 4 compounds are depicted in **Figure 4.5E**.²⁰

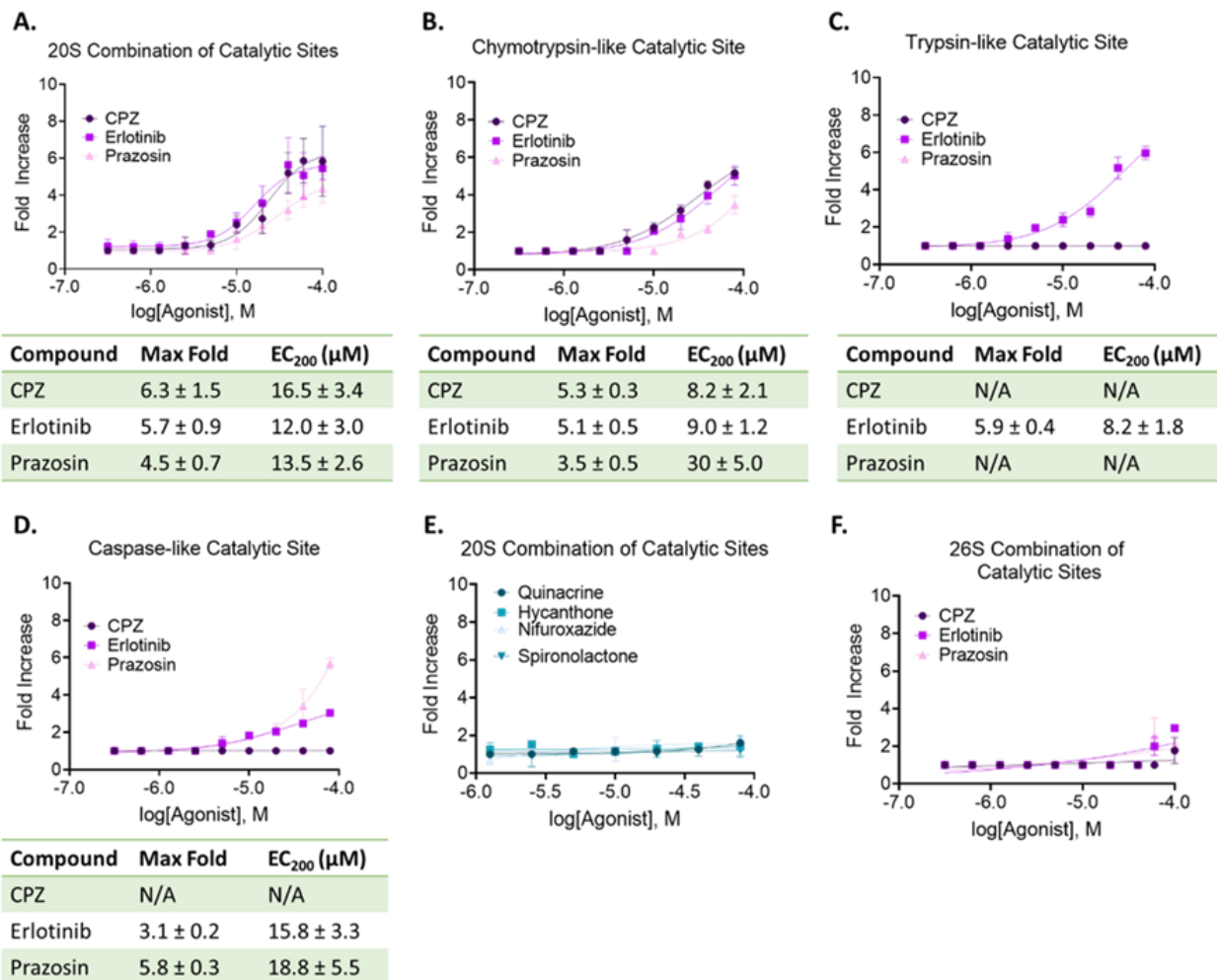


Figure 4.5: Erlotinib and prazosin enhance the activity of the 20S proteasome.

The activation of the overall 20S proteasome through substrates that evaluate the (A) combination catalytic, (B) chymotrypsin-like catalytic site, (C) trypsin-like catalytic site, and (D) caspase-like catalytic site by CPZ, erlotinib, and prazosin. (E) The activity of quinacrine, hycanthone, nifuroxazide, and spironolactone towards the 20S proteasome. (F) Activation of the 26S proteasome when treated with erlotinib, prazosin, and CPZ.

The selectivity of the three compounds for purified 20S proteasome over purified 26S proteasome was then evaluated using the same fluorogenic small peptide assay. Only at

the highest concentration, erlotinib and prazosin were able to modestly activate the 26S proteasome between 2.5 to 3-fold, with CPZ only enhanced the 26S proteasome 2-fold (**Figure 4.5F**), indicating that the primary enhanced proteolytic activity resides with the 20S proteasome.

Due to its efficient proteasome enhancement *in vitro*, erlotinib was the most promising novel proteasome enhancer. To determine if the proteasome activity displayed by erlotinib translates to a full-length and pathologically relevant protein, we evaluated if erlotinib-treated 20S proteasome enhanced α -synuclein degradation *in vitro*. We treated purified 20S proteasome with two concentrations of erlotinib (10 μ M and 20 μ M) and a DMSO control. After a 45-minute incubation at 37 °C, purified α -synuclein was added, and the mixture was incubated for an additional three hours. The levels of α -synuclein were visualized and quantified using a western blot, and the level of GAPDH was used as the loading control. As compared to the untreated proteasome, the samples treated with 10 μ M of erlotinib had 68% α -synuclein remaining(**Figure 4.6B-C**). The proteasome incubated with 20 μ M of erlotinib had 48% α -synuclein remaining, indicating erlotinib's ability to enhance the proteolytic activity of the proteasome translates to full-length IDPs other than ODC.²⁰

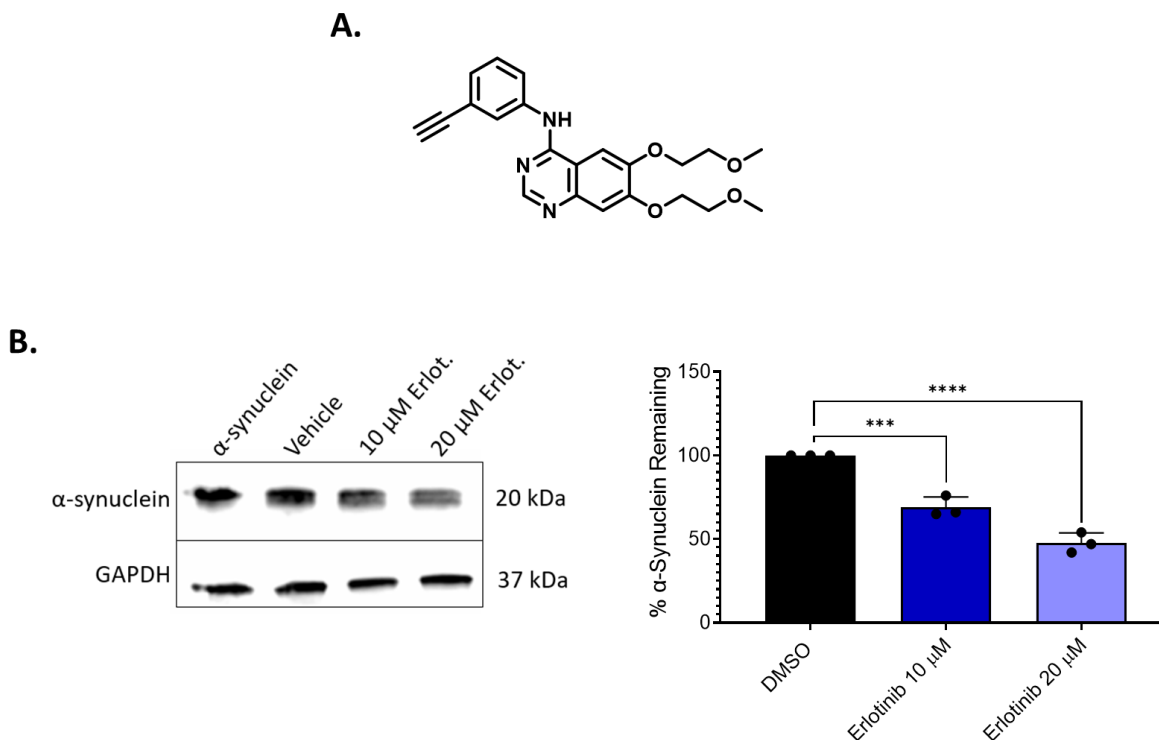


Figure 4.6: Erlotinib enhances the 20S proteasome mediated degradation of purified α -synuclein.

(A) The structure of erlotinib. (B) The proteolytic degradation of purified α -synuclein by the 20S proteasome when treated with DMSO or erlotinib (10 μ M or 20 μ M). One-way ANOVA statistical analysis was used to determine statistically significant. (ns = not significant, * $p < 0.05$, ** $p < 0.01$, *** $p < 0.001$, **** $p < 0.0001$) with error bars denoting SD.

Finally, the ability of erlotinib to enhance the degradation of ODC in an assay orthogonal to the AlphaLISA was evaluated to verify the mechanism of the reduction of the AlphaLISA signal seen by the lead compounds. The HEK-293T cells that stably expressed the conjugated GFP-ODC used in the high-throughput screen were treated with two concentrations of erlotinib and prazosin (10 and 20 μ M), 20 μ M of CPZ, and 5 μ M of a

proteasome inhibitor, Bortezomib (BTZ). CPZ was used again to directly compare the hits from the two screens while BTZ was used as a negative control. The levels of GFP-ODC were visualized and quantified using a western blot with the band at 75 kDa representing the full-length conjugated protein and the band at 35 kDa a fragment of GFP-ODC (**Figure 4.7A**), but only the full-length protein band was quantified. Both concentrations of prazosin and the CPZ control did very little in enhancing the degradation of ODC. CPZ had 97% of the full length GFP-ODC remaining, and prazosin at the same concentration had 84% of ODC remaining. Erlotinib, in contrast, showed a significant enhancement in the degradation of the full length GFP-ODC. At 10 μ M, only 34% of the intact conjugated protein remained, while at 20 μ M, only 16% remained (**Figure 4.7A**). To ensure we were solely observing 20S proteasome activation, we evaluated ubiquitin levels in the same cell lysates (**Figure 4.7B**). None of the compounds had any effect on K48 ubiquitin except for the proteasome inhibitor, BTZ, supporting that erlotinib does not impact the ubiquitin-dependent pathway and rather enhances degradation through the ubiquitin-independent pathway.

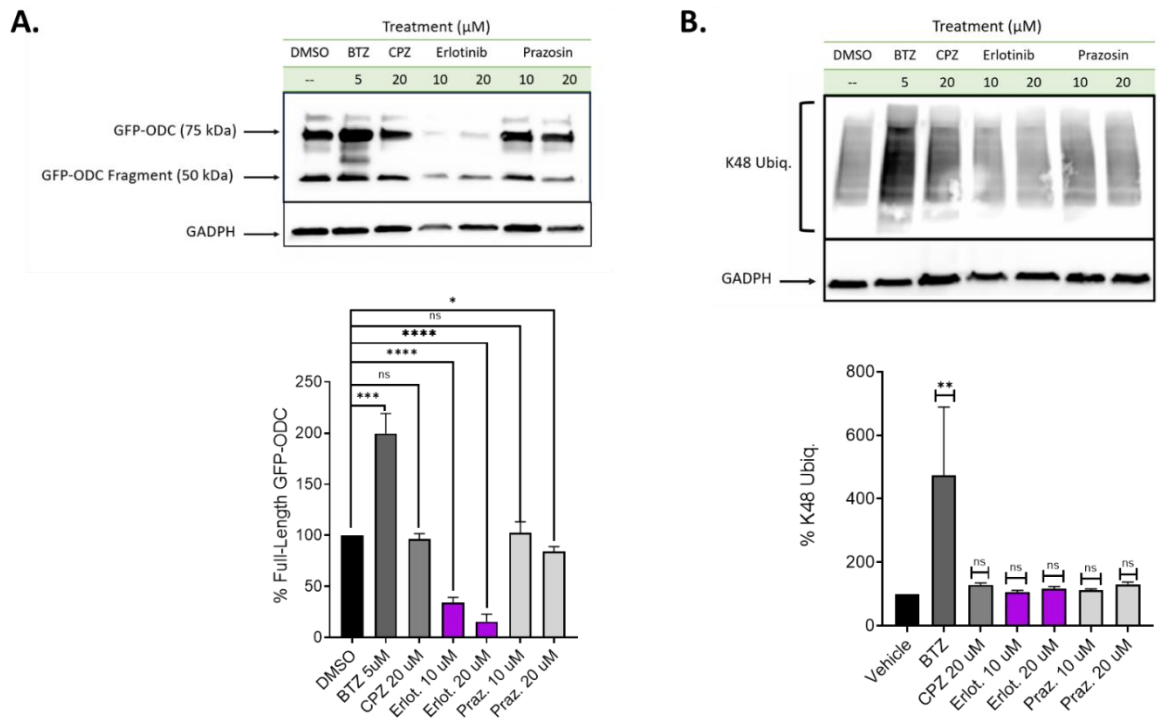


Figure 4.7: Erlotinib reduces the GFP-ODC AlphaLISA signal through the degradation of full-length GFP-ODC.

(A) The degradation of GFP-ODC by the lead hits, visualized and quantified using a western blot. There were two significant bands identified. The band at 75 kDa was identified as the full-length GFP-ODC and the band at 35 kDa is predominantly GFP, with a small fragment of ODC remaining. Cells were treated with 10 μM or 20 μM of erlotinib and prazosin. As controls, 5 μM of a proteasome inhibitor, Bortezomib (BTZ), was used and 20 μM of CPZ was added. Quantification of the full length GFP-ODC was done in triplicate. (B) The effects of overall ubiquitinylation in cells that are treated with erlotinib, prazosin, and CPZ. Quantification of α -synuclein degradation by each compound was done in triplicate. One-way ANOVA statistical analysis was used to determine statistically significant. (ns = not significant, * $p < 0.05$, ** $p < 0.01$, *** $p < 0.001$, **** $p < 0.0001$) with error bars denoting SD.

4.3 Screening of 25,000 Compounds

4.3.1 Rational

Using the GFP-ODC AlphaLISA assay to screen the Prestwick and NIH Clinical library, a novel 20S proteasome enhancer, erlotinib, was identified. While erlotinib's *in vitro* activity is comparable to the lead compound CPZ, erlotinib is a more efficient cellular 20S proteasome enhancer. The identification of erlotinib signifies that the cell-based nature of the GFP-ODC AlphaLISA aids in identifying non-cytotoxic molecules that can efficiently enhance the proteasome-mediated degradation of proteins in cells. With this success, we felt confident to begin screening more extensive libraries. Dr. Lisabeth and I moved to screen 25,000 compounds and validate the lead molecules. Screening a large and diverse set of chemical libraries can expand the chemical space of 20S proteasome enhancers.

4.3.2 Re-Optimization Through Antibody Screening

Dr. Lisabeth and I prepared to screen the 25,000 compounds in batches of around 3,000 compounds daily. Sadly, on the first day of screening, only one plate out of ten plates tested displayed any AlphaLISA signal, which was an unexpected result due to the consistent AlphaLISA signal we had obtained in the previous screen. While analyzing what could account for this disparity between the plates, we identified that we had used different batches of the anti-ODC antibody purchased from the same vendor. With the purchase of a large quantity of the anti-ODC antibody, the efficiency of the antibody to recognize the ODC epitope may have decreased, diminishing the AlphaLISA signal. To investigate our theory, we conducted an AlphaLISA to compare the negative control with

a titration of increasing concentration of the anti-ODC antibody (ranging from 0.06 $\mu\text{g/mL}$ to 16 $\mu\text{g/mL}$) (**Figure 4.8A**). We expected an increase in the AlphaLISA signal with the increasing antibody concentrations; however, this was not the case. The AlphaLISA signal with or without the anti-ODC antibody was the same, signifying that the anti-ODC antibody was either not interacting with the donor bead through the binding of the biotin to the streptavidin, or the antibody was unable to recognize the ODC portion of the conjugate protein. In either case, we had to pivot and identify an alternative path forward. To solve the abolished AlphaLISA signal problem, I first obtained anti-ODC antibodies through different vendors to identify if altering the anti-ODC antibody all together would restore the AlphaLISA signal. We screened three concentrations (0.12 $\mu\text{g/mL}$, 0.24 $\mu\text{g/mL}$, and 0.47 $\mu\text{g/mL}$) of the new anti-ODC antibody (labeled antibody A) and compared the AlphaLISA signal to that of the original anti-ODC antibody, labeled antibody B. The antibody that was used for the 2,000-compound screen, labeled antibody C, was included at the highest concentration (0.47 $\mu\text{g/mL}$) to directly compare the difference in activity of the different batches of anti-ODC antibody from the same vendor. With the addition of antibody A, the AlphaLISA signal was over 600,000 counts at all three concentrations. In comparison, antibody C displayed an AlphaLISA signal of 40,000 counts, which is consistent with the AlphaLISA signal we observed in the 2,000-compound screen. In contrast, at every concentration, antibody B had an AlphaLISA signal comparable to that of the negative control, or 4,000 counts (**Figure 4.8B**). Thus, with the replacement of the anti-ODC antibody we were able to restore the AlphaLISA signal and further support that the original anti-ODC antibody was the cause of the decreased AlphaLISA signal. In addition, with the efficiency of antibody A, we needed to decrease the concentration

significantly. The slight increase of AlphaLISA signal with the reduced antibody concentrations suggests that the system may be over-saturated with anti-ODC antibodies and could negatively impact the efficacy of the assay (**Figure 4.8B**). To ensure that we used the optimal concentration of antibody A, we further screened three lower concentrations (0.12 $\mu\text{g/mL}$, 0.06 $\mu\text{g/mL}$, and 0.03 $\mu\text{g/mL}$) of the antibody in the AlphaLISA assay. With the lower concentrations of antibody A, there was a dose-dependent decrease in the AlphaLISA signal, with 0.12 $\mu\text{g/mL}$ providing the highest AlphaLISA signal of over 150,000 counts.

We wanted to reassess the Z' factor at three cell seeding conditions before moving onto the final screen. Using the 0.12 $\mu\text{g/mL}$ concentration of antibody A, we evaluated the Z' factor for the AlphaLISA when 10,000 cells/well, 5,000 cells/well, and 2,500 cells/well were used (**Figure 4.8C**). The original seeding condition, 10,000 cells/well, performed the best, with a Z' robust factor of 0.726 and an AlphaLISA signal of over 300,000 counts. However, with the reduced cell number, the screening time would be significantly shortened due to the decreased time needed to grow an adequate number of cells. Additionally, the seeding condition of 5,000 cells/well still provided an excellent Z' robust factor of 0.617 and a high signal-to-noise ratio (83). The excellent Z' factor gave us the confidence to begin screening the 25,000 compound libraries with 0.12 $\mu\text{g/mL}$ of antibody A and reduced the cell seeding number from 10,000 cells/well to 5,000 cells/well.

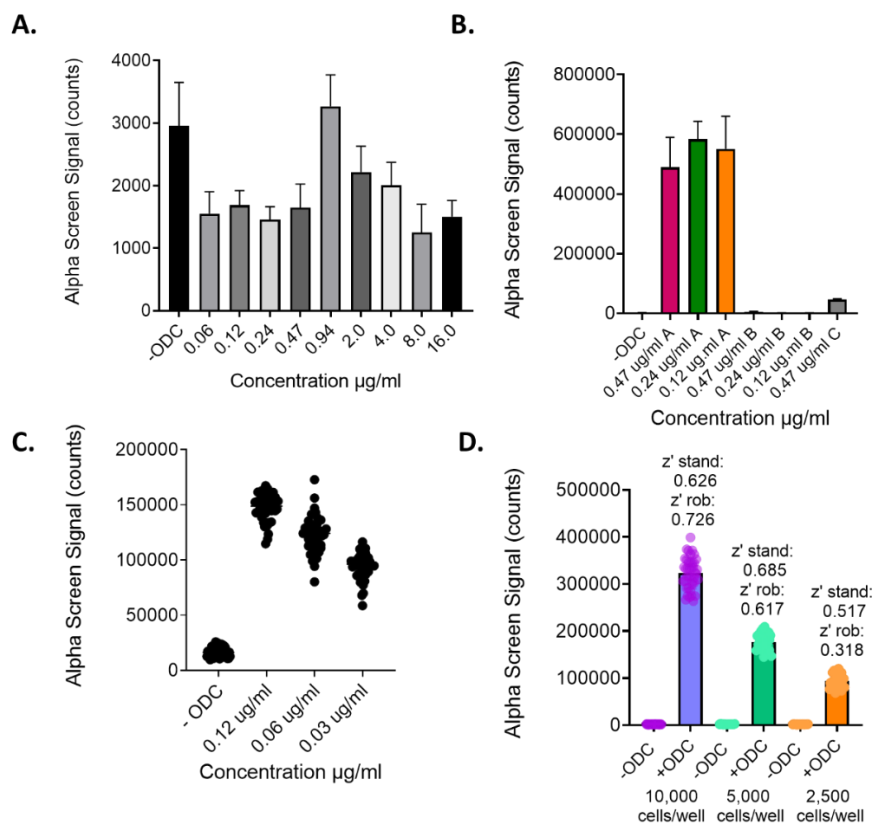


Figure 4.8: AlphaLISA signal is extremely dependent on the efficiency of the anti-ODC antibody.

(A) Evaluating AlphaLISA signal with the use of a concentration titration of antibody A.

(B) The comparison of the AlphaLISA signal with the use of antibody A vs the response with antibody B and C.

(C) The AlphaLISA signal response with decreasing concentrations of antibody A.

(D) The Z' test with 10,000 cells/well, 5,000 cells/well, and 2,500 cells/well seeding conditions with the use of 0.12 µg/mL of antibody A.

4.3.3 Screening Funnel

Once the re-optimized conditions were identified, 25,000 compounds were screened utilizing the GFP-ODC AlphaLISA. A similar screening funnel as the 2,000-compound screen was used (**Figure 4.9**). Of the original 25,000 compounds, 305 compounds

displayed 35% reduction in the AlphaLISA signal, while maintaining over 90% cell viability. The remaining compounds were then evaluated in a True Hits assay that would test the compound's ability to interfere with interaction of the donor and acceptor beads or the AlphaLISA signal itself, reducing the number of compounds to 64. The GFP-ODC AlphaLISA was utilized again to evaluate the 64 compounds in a dose-response assay. Those molecules that had a dose-dependent decrease in the AlphaLISA signal with a reduction of at least 35% at 15 μM were carried forward. The ability of the remaining 13 compounds to enhance the activity of the 20S proteasome was then determined. Of the 13 compounds, five compounds had an EC_{200} of 20 μM or below. The compounds identified in the 25,000 screen have now become new projects for the Tepe lab and ongoing SAR studies are being conducted to further expand the chemical space of small molecule 20S proteasome enhancers.

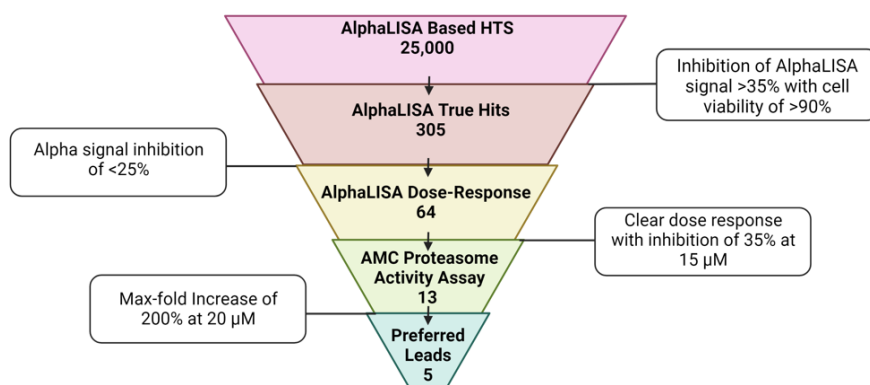


Figure 4.9: Screening funnel for the screening of a variety of compound libraries, which totaled 25,000 compounds, using the optimized AlphaLISA.

4.4 Conclusion

The UPS is responsible for the degradation of most intracellular and soluble proteins.³³ Dysregulation of the expression or degradation of proteins, including IDPs, can cause fatal cellular system failures.³⁴ Recently, enhancement of the 20S proteasome has provided a promising therapeutic pathway for diseases such as neurodegeneration and cancers such as multiple myeloma.^{3-6, 35} Despite the potential of the innovative therapeutic pathway, limited cell-based high-throughput assays are available to identify novel proteasome modulators. Herein, we describe the successful optimization of a cell-based AlphaLISA assay that evaluates the increased or decreased degradation of ODC, a model IDP. We readily modified the AlphaLISA assay to meet the demands of a high-throughput screen and successfully screened two compound libraries: the Prestwick and NIH Clinical Libraries. From screening of the two libraries, we identified 11 hit compounds. Of the 11 compounds, only erlotinib was identified as a new 20S proteasome enhancer. While erlotinib is an EGFR tyrosine kinase inhibitor, the reported IC₅₀ for this activity is 2 nM,³⁹ which is drastically lower than the IC₅₀ of 9.4 μM in the AlphaLISA. The μM concentration range of erlotinib's IC₅₀ suggests that the increased proteolytic degradation of ODC is not through its EGFR activity. Furthermore, erlotinib's ability to enhance the activity of the proteasome was confirmed through the fluorogenic small peptide assay. Erlotinib was able to enhance all three catalytic sites of the 20S proteasome with an overall max fold increase of 5.7, which translated to the enhanced proteolytic degradation of purified full-length α-synuclein with 68% α-synuclein remaining in samples treated with 10 μM of erlotinib and only 48% remaining when treated with 20 μM of erlotinib. The proteasome enhancement by erlotinib was selective for the 20S proteasome as displayed

both in the purified small peptide assay and in the HEK-293T cells expressing GFP-ODC. While both 10 μ M and 20 μ M of erlotinib readily enhanced the degradation of ODC (34% and 16% remaining, respectively), it had no impact on the levels of ubiquitinated proteins, making erlotinib the only lead compound identified. The development of the GFP-ODC AlphaLISA assay will readily allow for the identification of novel proteasome modulators, such as erlotinib. The newly identified compounds can now be further developed to diminish any non-proteasome related biological activity and allow for the synthesis of more potent and efficient 20S proteasome enhancers.

REFERENCES

- (1) Zhang, Y.; Cao, H.; Liu, Z. Binding cavities and druggability of intrinsically disordered proteins. *Protein Sci.* **2015**, *24*, 688-705.
- (2) Bhattarai, A.; Emerson, I. A. Dynamic conformational flexibility and molecular interactions of intrinsically disordered proteins. *Journal of Biosciences* **2020**, *45* (1). DOI: 10.1007/s12038-020-0010-4.
- (3) Fiolek, T. J.; Keel, K. L.; Tepe, J. J. Fluspirilene analogs activate the 20S proteasome and overcome proteasome impairment by intrinsically disordered protein oligomers. *ACS Chem. Neurosci.* **2021**, *12*, 1438-1448.
- (4) Fiolek, T. J.; Magyar, C. L.; Wall, T. J.; Davies, S. B.; Campbell, M. V.; Savich, C. J.; Tepe, J. J.; Mosey, R. A. Dihydroquinazolines enhance 20S proteasome activity and induce degradation of alpha-synuclein, an intrinsically disordered protein associated with neurodegeneration. *Bioorg. Med. Chem. Lett.* **2021**, *36*, 127821-127826.
- (5) Staerz, S. D.; Jones, C. L.; Tepe, J. J. Design, synthesis, and biological evaluation of potent 20S proteasome activators for the potential treatment of alpha-synucleinopathies. *J. Med. Chem.* **2022**, *65*, 6631-6642.
- (6) Jones, C. L.; Njomen, E.; Sjogren, B.; Dexheimer, T. S.; Tepe, J. J. Small molecule enhancement of 20S proteasome activity targets intrinsically disordered proteins. *ACS Chem. Biol.* **2017**, *12*, 2240-2247.
- (7) Njomen, E.; Osmulski, P. A.; Jones, C. L.; Gaczynska, M.; Tepe, J. J. Small molecule modulation of proteasome assembly. *Biochemistry* **2018**, *57* (28), 4214-4224.
- (8) Kisselev, A. F.; Goldberg, A. L. Monitoring activity and inhibition of 26S proteasomes with fluorogenic peptide substrates. *Methods Enzym.* **2005**, 364-378.
- (9) Zerfas, B. L.; Coleman, R. A.; Salazar-Chaparro, A. F.; Macatangay, N. J.; Trader, D. J. Fluorescent probes with unnatural amino acids to monitor proteasome activity in real-time. *ACS Chem. Biol.* **2020**, *15* (9), 2588-2596.
- (10) Gan, J.; Leestemaker, Y.; Sapmaz, A.; Ovaa, H. Highlighting the proteasome: Using fluorescence to visualize proteasome activity and distribution. *Front. Mol. Biosci.* **2019**, *6*, 14-22.
- (11) Coleman, R. A.; Trader, D. J. Development and application of a sensitive peptide reporter to discover 20S proteasome stimulators. *ACS Comb. Sci.* **2018**, *20* (5), 269-276.
- (12) Coleman, R. A.; Trader, D. J. A sensitive high-throughput screening method for identifying small molecule stimulators of the core particle of the proteasome. *Curr. Protoc. Chem. Biol.* **2018**, *10* (4), e52-e66.

- (13) Meng, L. M., R.; Kwok, B. H. B.; Elofsson, M.; Sin, N.; Crews, C. M. . Epoxomicin, a potent and selective proteasome inhibitor, exhibiting in vivo anti inflammatory activity. *Proc. Natl. Acad. Sci. USA* **1999**, *96*, 10403-10408.
- (14) Braganca, C. E.; Kraut, D. A. Mode of targeting to the proteasome determines GFP fate. *J. Biol. Chem.* **2020**, *295* (47), 15892-15901.
- (15) Kahana, C.; Asher, G.; Shaul, Y. Mechanisms of protein degradation: an odyssey with ODC. *Cell Cycle* **2005**, *4* (11), 1461-1464.
- (16) Bielefeld-Sevigny, M. AlphaLISA immunoassay platform- the "no-wash" high-throughput alternative to ELISA. *Assay Drug Dev. Technol.* **2009**, *7*, 90-92.
- (17) Prabhu, L.; Chen, L.; Wei, H.; Demir, O.; Safa, A.; Zeng, L.; Amaro, R. E.; O'Neil, B. H.; Zhang, Z. Y.; Lu, T. Development of an AlphaLISA high throughput technique to screen for small molecule inhibitors targeting protein arginine methyltransferases. *Mol. Biosyst.* **2017**, *13* (12), 2509-2520.
- (18) Ishii, K. Functional singlet oxygen generators based on phthalocyanines. *Coord. Chem. Rev.* **2012**, *256*, 1556-1568.
- (19) Mai, E., Wong, W. L., Bennett, G., Billeci, K. Comparison of ELISA and Alphascreen Assay Technologies for Measurement of Protein Expression Levels. *PerkinElmer Application Note* **2002**.
- (20) Staerz, S. D.; Lisabeth, E. M.; Njomen, E.; Dexheimer, T. S.; Neubig, R. R.; Tepe, J. J. Development of a cell-based AlphaLISA assay for high-throughput screening for small molecule proteasome modulators. *ACS Omega* **2023**, *8*, 15650-15659.
- (21) Asli, N.; Sergio, C.; Taosheg, C. Data analysis approaches in high throughput screening. *Drug Discovery* **2013**, 201-226.
- (22) Zhang, J. H.; Chung, T. D.; Oldenburg, K. R. A simple statistical parameter for use in evaluation and validation of high throughput screening assays. *J. Biomol. Screen* **1999**, *4* (2), 67-73.
- (23) Mamroud-Kidron, E.; Omer-Itsicovich, M.; Bercovich, Z.; Tobias, K. E.; Rom, E.; Kahana, C. A unified pathway for the degradation of ornithine decarboxylase in reticulocyte lysate requires interaction with the polyamine induced protein, ornithine decarboxylase antizyme. *Eur. J. Biochem.* **1994**, *226*, 547-554.
- (24) Asher, G.; Bercovich, Z.; Tsvetkov, P.; Shaul, Y.; Kahana, C. 20S proteasomal degradation of ornithine decarboxylase is regulated by NQO1. *Mol. Cell* **2005**, *17* (5), 645-655.

- (25) Hartman, P. E.; Levine, K.; Hartman, Z.; Berger, H. Hycanthone: A frameshift mutagen. *Science* **1971**, *172*, 1058-1060.
- (26) Moyer, J. D.; Barbacci, E. G.; Iwata, K. K.; Arnold, L.; Boman, B.; Cunningham, A.; DiOrio, C.; Doty, J.; Reynolds, M. M.; Sloan, D.; Theleman, A.; Miller, P. Induction of apoptosis and cell cycle arrest by CP-358,774, an inhibitor of epidermal growth factor receptor tyrosine kinase. *Cancer Res.* **1997**, *57*, 4838-4848.
- (27) Van Dyke, K.; Lantz, C.; Szustkiewicz, C. Quinacrine: Mechanisms of antimalarial action. *Science* **1970**, *169*, 492-493.
- (28) Gabbard, R. D.; Hoopes, R. R.; Kemp, M. G. Spironolactone and XPB: An old drug with a new molecular target. *Biomolecules* **2020**, *10* (5), 756-770.
- (29) Covaci, O.-I.; Mitran, R.-A.; Buhalteanu, L.; Dumitrescu, D. G.; Shova, S.; Manta, C.-M. Bringing new life into old drugs: a case study on nifuroxazide polymorphism. *CrystEngComm* **2017**, *19* (26), 3584-3591.
- (30) Lü, S.; Wang, J. Homoharringtonine and omacetaxine for myeloid hematological malignancies. *J. Hematol. Oncol.* **2014**, *7*, 1-10.
- (31) Titov, D. V.; Gilman, B.; He, Q. L.; Bhat, S.; Low, W. K.; Dang, Y.; Smeaton, M.; Demain, A. L.; Miller, P. S.; Kugel, J. F.; et al. XPB, a subunit of TFIIH, is a target of the natural product triptolide. *Nat. Chem. Biol.* **2011**, *7* (3), 182-1888.
- (32) Trader, D. J.; Simanski, S.; Dickson, P.; Kodadek, T. Establishment of a suite of assays that support the discovery of proteasome stimulators. *Biochim. Biophys. Acta. Gen. Subj.* **2017**, *1861* (4), 892-899.
- (33) Thibaudeau, T. A.; Smith, D. M. A practical review of proteasome pharmacology. *Pharmacol. Rev.* **2019**, *71*, 170-197. Tanaka, K. The proteasome: overview of structure and functions. *Proc. Jpn. Acad. Ser. B Phys. Biol. Sci.* **2009**, *85* (1), 12-36. George, D. E.; Tepe, J. J. Advances in proteasome enhancement by small molecules. *Biomolecules* **2021**, *11* (12), 1789-1816. From NLM Medline.
- (34) Thibaudeau, T. A.; Anderson, R. T.; Smith, D. M. A common mechanism of proteasome impairment by neurodegenerative disease-associated oligomers. *Nat. Commun.* **2018**, *9*, 1097-1111.
- (35) Njomen, E.; Vanecek, A.; Lansdell, T. A.; Yang, Y. T.; Schall, P. Z.; Harris, C. M.; Bernard, M. P.; Isaac, D.; Alkharabsheh, O.; Al-Janadi, A.; et al. Small molecule 20S proteasome enhancer regulates MYC protein stability and exhibits antitumor activity in multiple myeloma. *Biomedicines* **2022**, *10* (5), 756-770.

APPENDIX

Methods

GFP-ODC Transfection

HEK-293T cells were seeded at a density of 1×10^5 cells/mL in a 24-well plate overnight. DNA (1ug of GFPSpark-ODC plasmid) was mixed with 250 μ L of serum free-DMEM medium. Sinofection transfection reagent (5 μ L) was mixed with 250 μ L of serum free-DMEM medium in a separate vial. The two vials were then combined and incubated at room temperature for 15 minutes. The mixture was then added to the HEK-293T cells in the 24-well plate and incubated for 4 hours at 37 °C with 5% CO₂. After this incubation, the media was replaced with fresh DMEM. After three days, cells were removed from the plate with trypsin (0.25%) and resuspended in hygromycin selection media (100 μ g/mL). The surviving clones were picked and expanded in the selection media for six weeks. After three passages, stable expression was confirmed by confocal fluorescent imaging, using standard GFP filters. The stable clones were then further sorted using Flow Cytometry, using the standard GFP filters to make pools of “high” and “medium” GFP expressors.

Bead Concentration Optimization

HEK-293T cells that transiently expressed GFP-ODC were seeded at 500 cells/well in a solid bottom white 384-well plate in 20 μ L of DMEM media for 12 hours. The cells were then lysed with 5 μ L of the AlphaLISA lysis buffer. The lysate was then diluted in the 1x AlphaLISA immunoassay buffer to the desired 10x final concentration. 5 μ L of each sample was transferred into a solid-bottom white 384 well plate. Then, 10 μ L of the anti-GFP acceptor bead and biotinylated anti-ODC were added in different ratios and

incubated for one hour at room temperature. After this incubation, 25 μ L of the donor beads were added for each of the screened concentrations and incubated for a further 30 minutes. The AlphaLISA signal was measured using the BioTek plate reader equipped with an Alpha filter.

AlphaLISA

HEK-293T cells that stably expressed GFP-ODC were plated 10,000 cells/well in a 384-well plate in 20 μ L of phenol red free DMEM. The cells were then immediately treated with either DMSO or TCH-165. After 18 hours, 5 μ L of the 5x AlphaLISA Surefire lysis buffer was added to each well, then the plate was incubated on a shaker (400 rpm) at room temperature for 30 minutes. During this first incubation, a 10x mix of either a mixture of biotinylated anti-ODC (4.7 μ g/mL) and anti-GFP (100 μ g/mL) in 1x AlphaLISA immunoassay buffer or just anti-GFP (100 μ g/mL) in 1x AlphaLISA immunoassay buffer was made under limited light conditions. After the lysis was complete, 5 μ L of either mixture was added to each well using an automated dispenser. After this addition, the plate was incubated at room temperature and in the dark for one hour. Then, a 2.5x mix was made with the streptavidin donor bead (100 μ g/mL) in 1x AlphaLISA immunoassay buffer in a limited fluorescent light setting. From this 2.5x mix, 20 μ L was added to each well using the automated dispenser, and the plate was incubated again at room temperature in the dark for 30 minutes. The AlphaLISA signal was measured using BioTek plate reader equipped with Alpha filter. *Note the assay is very sensitive to light. However, one can use filtered light, such as seen in **Figure 4.10**.



Figure 4.10: Lamp used to conduct the GFP-ODC AlphaLISA.

TrueHits Screen

In the white 384-well assay plate, 20 μL of clear DMEM was added. Then, a 1.7x stock solution of Biotin (final concentration of 10 μM) was added. The desired drugs were then added at the same concentration that the screen was run (15 μM). 5x of the AlphaLISA donor bead stock was then added (for a final concentration of 10 $\mu\text{g}/\text{mL}$) and incubated for one hour at room temperature. Then, a 5x solution of the AlphaLISA acceptor bead was added (final concentration of 10 $\mu\text{g}/\text{mL}$), and the mixture was incubated in the dark for 30 minutes at room temperature. The AlphaLISA signal was measured using BioTek plate reader equipped with Alpha filter.

Small Peptide Assay

Activity assays were carried out in a 100 μL reaction volume using a black flat/clear bottom 96-well plate. Different concentrations (1.25–80 μM) of test compounds were added to the wells containing 1 nM of human constitutive 20S proteasome in a 38 mM

Tris-HCl and 100 mM NaCl buffer at a pH of 7.8. The mixture was allowed to incubate for 15 min at 37 °C. After this incubation, 5 µL of the fluorogenic substrates were added. The fluorogenic substrates used were either one of the following or a combination of all three (final concentration of 6.67 µM of each): Suc-LLVY-AMC (CT-L activity, final concentration of 20 µM), Z-LLE-AMC (Casp-L activity, final concentration of 20 µM), Boc-LRR-AMC (T-L activity, final concentration of 40 µM). The activity was measured at 37 °C on a SpectraMax M5e spectrometer by measuring the change in fluorescence unit per minute for 1 hour at 380–460 nm. The rate of hydrolysis for the vehicle control was set at a 100%, and the ratio of the treated sample over the vehicle control was used to calculate the fold change in rate of substrate hydrolysis by the proteasome. The same protocol was used for the activity assays involving the 26S proteasome, but 2.5 mM ATP and 5 mM Magnesium chloride were added to the assay buffer in the place of NaCl.

***In Vitro* Degradation of α -synuclein**

Degradation assays were carried out in a 25 µL reaction volume using a 50 mM HEPES and 5 mM DTT buffer at a pH of 7.2, 0.3 µM of purified α -synuclein, and 10 nM of purified human 20S proteasome. The 20S proteasome was first diluted to 45.5 nM in the HEPES buffer, and 0.5 µL of the test compounds or DMSO was added. This mixture was incubated for 45 minutes at 37 °C. After this incubation, 2.5 µL of a 15 µM stock of α -synuclein was added. The degradation mixture was incubated at 37 °C for 3 hours, then, 0.5 µM of GAPDH was added as a loading control. The reaction was stopped with the addition of concentrated SDS loading buffer and boiled for 20 minutes. The samples were then resolved on a 4-20% Tris-glycine SDS-PAGE gel and immunoblotted with mouse monoclonal anti- α -synuclein IgG (1:2000) and anti-mouse HRP-linked IgG (1:2000). The

immunoblots were developed with ECL Western reagent and imaged with an Azure Biosystems 300Q imager.

Cellular Degradation of GFP-ODC

In 60 mm plates, HEK-293T cells that stably expressed GFP-ODC were grown to 80% confluency. Then, the cells were treated with 3 μ L of either DMSO or the test compound at the desired concentration. The cells were treated for 16 hours and then scraped and pelleted (300g for 5 minutes). The supernatant was taken off, and the cell pellet was washed with ice cold PBS then lysed with the addition of RIPA buffer containing protease inhibitors. The cell lysate was incubated for 20 minutes on ice. The lysate was centrifuged for 15 minutes at 500g, and then the supernatant was collected. A concentrated SDS loading buffer was added, and the samples were boiled for 10 minutes. The samples were then resolved on a 4-20% Tris-glycine SDS-PAGE gel and immunoblotted with mouse monoclonal anti-ODC IgG (1:2000) and anti-mouse HRP-linked IgG (1:2000). The immunoblots were developed with ECL Western reagent and imaged with an Azure Biosystems 300Q imager.

Replicates

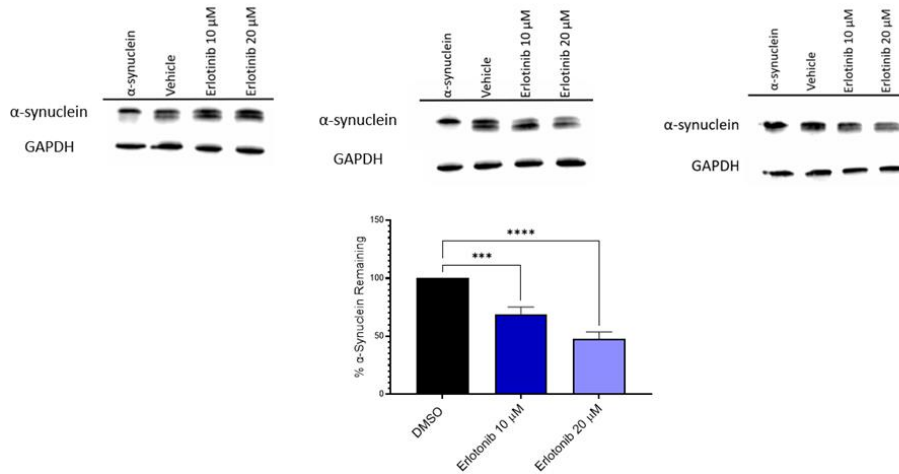


Figure 4.11: Westerns of α -synuclein degradation by purified 20S proteasome treated with 10 μ M and 15 μ M of Erlotinib (n=3). One-way ANOVA statistical analysis was used to determine statistically significant. (ns = not significant, * p < 0.05, ** p < 0.01, * p < 0.001, **** p < 0.0001) with error bars denoting SD.**

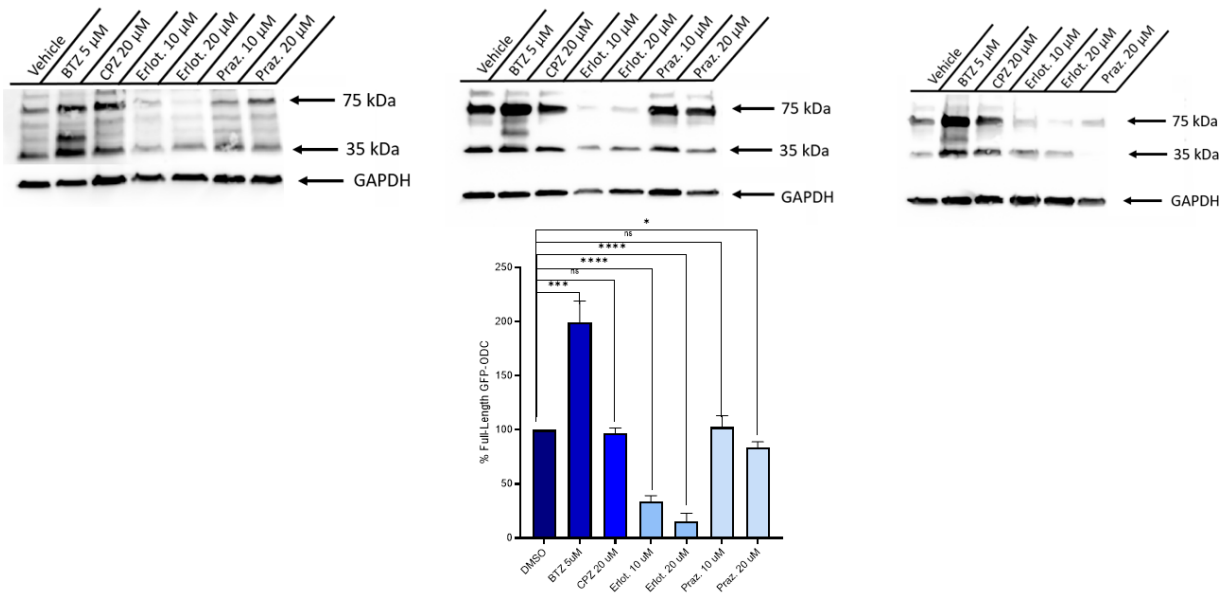


Figure 4.12: Westerns of the cellular degradation of GFP-ODC in HEK293T cells when treated with either BTZ (5 μM), CPZ (20 μM), Erlotinib (10 μM and 20 μM), or Prazosin (10 μM and 20 μM) (n=3 except 10 μM of Prazosin). One-way ANOVA statistical analysis was used to determine statistically significant. (ns = not significant, *p < 0.05, **p < 0.01, *p < 0.001, ****p < 0.0001) with error bars denoting SD.**

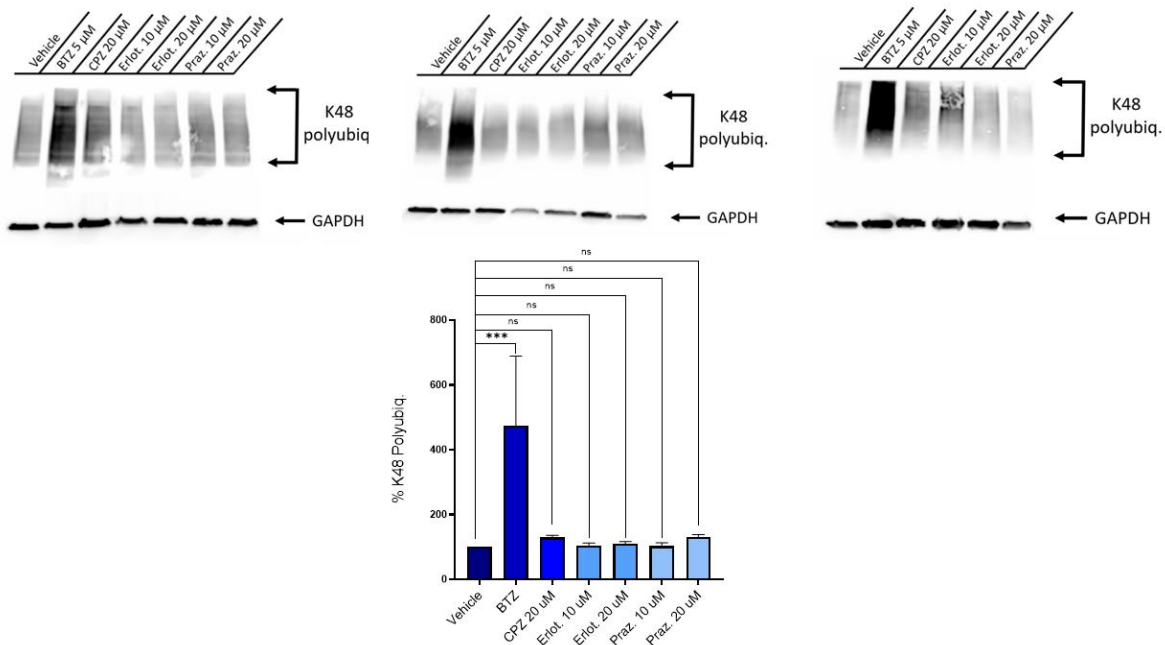


Figure 4.13: Westerns on Ubiquitin build-up in HEK293T cells when treated with either BTZ (5 μM), CPZ (20 μM), Erlotinib (10 μM and 20 μM), or Prazosin (10 μM and 20 μM) (n=3 except 10 μM of Prazosin). One-way ANOVA statistical analysis was used to determine statistically significant. (ns = not significant, *p < 0.05, **p < 0.01, *p < 0.001, ****p < 0.0001) with error bars denoting SD.**

CHAPTER FIVE

Materials and Miscellaneous

5.1 Materials

5.1.1 Antibodies

Reagent Antibodies	Source	Identifier
Mouse Monoclonal Anti- α -synuclein	Novus Biologics	NBP2-15365
Anti-Alpha-synuclein antibody [EPR20535]	Abcam	ab212184
Rabbit Monoclonal Anti-p25 α	Novus Biologics	NBP1-91613
Mouse HRP Tagged Anti-GAPDH	Novus Biologics	NBP2-27103H
Mouse Monoclonal Anti- α 3	Santa Cruz	sc-166205
Mouse Monoclonal Anti- α 4	Santa Cruz	sc-271297
Rabbit Monoclonal Anti-ZsGreen	Takara	632474
Biotin Conjugated ODC1 pAb	Epigentek	A56670-050
Biotin Conjugated ODC1/485	Novus Biologics	NBP2-34700B
Anti-Rabbit HRP-Linked	Cell Signaling	7074S
Anti-Mouse HRP-Linked	Cell Signaling	70745
Rabbit Anti- α -ynuclein	Abcam	ab212184
Mouse HRP Tagged Anti-Ubiquitin	Santa Cruz	sc-8017

Table 5.1 Antibodies used within this work.

5.1.2 Recombinant DNA/Oligonucleotides

Reagent	Source	Identifier
Recombinant DNA/Oligonucleotides		
Human Tppp cDNA Clone	genomics online	ABIN4629840
Tubulin Polymerization Promoting Protein (TPPP) (NM_007030) Human Tagged ORF Clone	Origene	RC213142
pHM6- α -synuclein-A53T	Addgene	40825
Ornithine Decarboxylase/ODC1 cDNA ORF Clone, Human, N-GFPSpark® tag	Sino Biological	HG18052-ANG
ESIRNA HUMAN PSMA4	Sigma-Aldrich	EHU057861
ESIRNA HUMAN PSMA7	Sigma-Aldrich	EHU099921
ESIRNA HUMAN PSMA1	Sigma-Aldrich	EHU140871

Table 5.2 Recombinant used herein.

5.1.3 Recombinant Proteins and Peptides

Reagent	Source	Identifier
Recombinant Proteins and Peptides		
Human 20S Proteasome Protein, CF	R&D Systems	E-360-050
Suc-Leu-Leu-Val-Tyr-AMC (Suc-LLVY-AMC)	R&D Systems	S-280-05M
Z-Leu-Leu-Glu-AMC (Z-LLE-AMC)	Cayman Chemicals	10008117
Boc-LRR-AMC (trifluoroacetate salt)	Cayman Chemicals	26642
Recombinant Human alpha-Synuclein Protein, CF	R&D Systems	SP-485-500
Recombinant Human GAPDH Protein	R&D Systems	NBP2-52615
Recombinant Human Tppp	Purified	N/A

Table 5.3 Recombinant proteins and peptides used.

5.1.4 Bacterial Strains

Reagent	Source	Identifier
Bacterial Strains		
DH5 α Chemically Competent E. coli	ThermoFisher Scientific	18265017
BL21(DE3) Chemically Competent E. Coli	ThermoFisher Scientific	EC0114

Table 5.4 Bacterial strains utilized.

5.1.5 Mammalian Cell Lines

Reagent	Source	Identifier
Mammalian Cell Lines		
HEK-293T	ATCC	CRL-3216
PC12	ATCC	CRL-1721
Living Color ZsGreen HEK	N/A	No longer sold

Table 5.5 Mammalian cell lines utilized herein.

5.1.6 Reagents and Chemicals

Reagent	Source	Identifier
Reagents and Chemicals		
Dulbecco's Modified Eagle's Medium	Gibco	11995-065
Penicillin–Streptomycin	Gibco	15140-122
Fetal Bovine Serum	Gibco	26140-079
RPMI 1640	Gibco	11875-093
Horse Serum Donor Herd	Sigma-Aldrich	H1270
Opti-mem	Gibco	31985-070
0.25% Trypsin-EDTA (1x)	Gibco	25200-056
DMEM, high glucose, no glutamine, no phenol red	ThermoFisher Scientific	31053036
Hgromycin B	Sigma-Aldrich	H3274
SOC Medium	Sigma-Aldrich	S1797
Kanamycin Sulfate	Sigma-Aldrich	K1377
Lysogeny broth	Neogen	NGM0088A
IPTG	Sigma-Aldrich	I6758
Plasmid Maxi kit	QIAGEN	12163
cOmplete™, Mini, EDTA-free Protease Inhibitor Cocktail	Sigma-Aldrich	11836170001
X-tremeGENE siRNA Transfection Reagent	Sigma-Aldrich	4476093001
X-tremeGENE HP DNA Transfection Reagent	Sigma-Aldrich	6366236001
Sinofection transfection reagent	Sino Biological	STF02
PBS	Sigma-Aldrich	D8537
RIPA Buffer	Sigma-Aldrich	R0278
Pierce BCA Protein Analysis Kit	ThermoFisher Scientific	23225
Laemmli Sample Buffer	Bio-Rad	1610747
2-Mercaptoethanol	Sigma-Aldrich	M6250
4-20% Tris-glycine SDS-PAGE gel	Bio-Rad	4561096
PVDF membrane	Bio-Rad	1620177
Blotting Grade Blocker	Bio-Rad	1706404
Radiance plus	Azure Biosystems	AC2103
Me4BodipyFL-Ahx3Leu3VS Fluorescent probe	R&D Systems	I-190
RP1 Probe	Gaur, P.; et al. ⁶⁴	N/A
TPE-MI	MedChemExpress	HY-143218
Proteasome Glo Reagent	Promega	G8660
Cell Titer Glo Reagent	Promega	G3580

Table 5.6 Reagents and chemical used.

Reagent	Source	Identifier
Reagents and Chemicals (cont.)		
TCH-165	Njomen, E.; et al. ⁴²	N/A
Bortezomib	Cayman Chemicals	10008822
HisTrap HP His tag protein purification columns	Cytiva	29051021
Amicon ultra-15 10 K filters	Millipore Sigma	UFC901008
Flowmi® Cell Strainers (with a porosity of 40 µm)	Sigma-Aldrich	BAH136800040
AlphaLISA Surefire Ultra Lysis Buffer	Perkin-Elmer	ALSU-LB
AlphaLISA Anti-GFP Acceptor Beads	Perkin-Elmer	AL133C
AlphaLISA Streptavidin Donor Bead	Perkin-Elmer	6760002
AlphaLISA Biotin-Free TruHits Detection Kit, 1,000 Assay Points	Perkin-Elmer	AL901D

Table 5.7 Further reagents utilized.

5.1.7 Instrumentation

Reagent	Source	Identifier
Instrumentation		
ÄKTA go protein purification system	Cytiva	29383015
Bio-Rad Gene Pulser II electroporation system	Bio-Rad	165-2105
Q500 Sonicator	Qsonica	Q500-110
Mini Trans-Blot Electrophoretic Transfer Cell	Bio-Rad	1703930
Azure Biosystems 300Q imager	Azure Biosystems	AZI300-01
SpectraMax® M5e Microplate Reader	Molecular Devices	Refurbished
BioTek Synergy Neo	Agilent	N/A

Table 5.8 Instrumentation utilized in this work.

5.1.8 Software

Reagent	Source	Identifier
Software		
Bio-Rad Image Lab software	Bio-Rad	Bio-Rad: https://www.bio-rad.com/en-us/product/image-lab-software?ID=KRE6P5E8Z
GraphPad Prism 8	GraphPad	GraphPad: https://www.graphpad.com/scientific-software/prism/
Softmax Pro 7.1	Molecular Devices	Molecular Devices: https://support.moleculardevices.com/s/article/SoftMax-Pro-7-1-software-Download-page

Table 5.9 Software used within this work.

5.2 Miscellaneous

5.2.1 Quantification and Statistical Analysis

Data are presented as mean \pm standard deviation (SD). For each figure, the number of replicates is indicated in the figure legends. Statistical analysis was only performed on experiments with three or more replications or “n”s. Western blot quantifications were performed with Bio-Rad Image Lab software. Statistical analysis was performed with GraphPad Prism 8 software. One-way ANOVA analysis with appropriate post-hoc analysis was used for multiple comparisons of means. Effect was considered significant for * $p < 0.05$, ** $p < 0.01$, *** $p < 0.001$, **** $p < 0.0001$.

5.2.2 Note

Section 2.3 of chapter 2 is reprinted with permission from J. Med. Chem. 2022, 65, 9, 6631-6642 Publication Date: April 27, 2022. Copyright 2023 American Chemical Society.

<https://doi.org/10.1021/acs.jmedchem.1c02158> Sections 2.4 of chapter 2 and section 3.2 of chapter 3 are a part of a paper submitted and under revision to *iScience*.

Section 4.2 of chapter 4 is reprinted with permission from *ACS Omega* 2023, 8, 17, 15650–15659 Publication Date: April 21, 2023. Copyright 2023 American Chemical Society. <https://doi.org/10.1021/acsomea.3c01158>